Integration of 4D Seismic Data in Reservoir Characterization with Facies Parameter Uncertainty

by

Mostafa Hadavandsiri

A thesis submitted in partial fulfillment of the requirements for the degree of

Doctor of Philosophy

in

Mining Engineering

Department of Civil and Environmental Engineering
University of Alberta

Abstract

Reservoir exploration and production are always conducted in presence of geological uncertainty that is an inevitable result of incomplete data and heterogeneity at all scales. Modeling subsurface geology based on limited data is subject to uncertainty and its accurate assessment plays a key role in resource estimation and reservoir management decision making. Canadian oil sand reservoirs are the third largest oil reserves in the world and play a key role in the economy of Canada. There are many challenges and technical details associated with the enhanced oil recovery (EOR) technologies that are required to produce high-viscosity oil. This increases the importance of an accurate model of geological uncertainty as a necessary input for the exploration planning and reservoir management. An accurate assessment of geological uncertainty requires the modeling workflow to consider (1) all available sources of data to be reproduced and (2) model parameter uncertainty to be included. The geological uncertainty is then represented by multiple geostatistical realizations that can be used simultaneously for optimal reservoir management decision making. In this thesis, a practical framework is developed to improve the model of geological uncertainty. A realistic model of geological uncertainty requires parameter uncertainty associated with the input statistical parameters to be considered. Limited well data does not permit unambiguous specification of the required parameters. These parameters often have a global and widespread influence on the resources and reserves. One of the main contributions of this research is to quantify prior proportion uncertainty for categorical variables such as facies in presence of a trend. The trend model provides additional information about the subsurface geological setting. Facies modeling is of great significance for reservoir characterization as it explains a major aspect of spatial heterogeneity and geological uncertainty. Large-scale flow patterns are often controlled by the spatial arrangement and continuity of facies because, the variability of permeability in between facies is more significant compared to that within facies.

Each source of data provides information about the reservoir with different scales and levels of precision. Although there are well-established geostatistical techniques for stochastic simulation of the reservoir conditioned to static data, practical integration of information obtained from dynamic data remains a major challenge. The changes in reservoir properties including fluid saturation, pressure and temperature can be monitored by dynamic data to obtain information about the large scale connectivity and quality of fluid flow within the reservoir. A novel methodology is proposed for effective integration of dynamic data into the geological modeling workflow. This methodology is based on geostatistical enforcement of anomalies identified from dynamic sources of data such as four dimensional (4D) seismic. All geostatistical realizations are updated to honor the information obtained from the dynamic data that become available during the reservoir life cycle.

Preface

Parts of this thesis have been previously published, or are in the publication process.

Chapters 2 and 3 are composed in part by Hadavand, M. and Deutsch , C. V. (2017). Facies Proportion Uncertainty in Presence of a Trend, published by Journal of Petroleum Science and Engineering.

Chapter 4 is composed in part by Hadavand, M. and Deutsch , C. V. (2016). A Practical Methodology for Integration of 4D seismic in Steam Assisted Gravity Drainage Reservoir Characterization, published by SPE Journal of Reservoir Evaluation and Engineering.

Chapter 5 is composed in part by Hadavand, M., Carmichael, P., Dalir, A., Rodriguez, M., Silva, D., and Deutsch, C. V. (2017). Integration of 4D seismic in SAGD Reservoir Characterization, submitted to SPE Reservoir Evaluation and Engineering.

In memory of my grandparents

Acknowledgments

I would like to thank my supervisor, Dr. Clayton V. Deutsch for his support, invaluable advice and enthusiasm for sharing his knowledge in geostatistics. The opportunity to learn from Clayton has been one the greatest fortunes in my life. Thank you to everyone at the Centre for Computational Geostatistics, specifically Dr. Johnathan Manchuk for his advice and help during my research.

Financial support from sponsors of the Centre for Computational Geostatistics and the Natural Sciences and Engineering Research Council of Canada is gratefully acknowledged.

I wish to thank my parents Ahmad and Shahnaz for their love and encouragement, without whom I would never have enjoyed so many opportunities. Last but not least, I would like to thank my wife and my best friend Samira for her support, patience and love.

Table of Contents

List of Figures

List of Tables

List of Symbols

Symbol	Description
$^\circ$	degrees as a unit of measurement of angles
$\forall$	for all
A	modeling or geologic domain
F	cumulative distribution function of a random function
γ	variogram
G^{-1}	standard normal quantile function
$\mathbf{h}$	separation vector
x_{50}	median value of a random function
μ	mean of a random function
n	number of observations
x_{25}	first quantile value of a random function
x_{75}	third quantile value of a random function
ϕ	porosity
ρ	correlation coefficient
σ	standard deviation of a random function
S_w	water saturation
B_o	formation volume factor
τ	probability tuning parameter
$\mathbf{u}$	coordinate vector
x_{max}	maximum value of a random function
x_{min}	minimum value of a random function

List of Abbreviations

Abbreviation	Description
2D	two dimensional
3D	three dimensional
4D	four dimensional
AER	Alberta Energy Regulator
ART	Anomaly Recognition Tool
CCDF	conditional cumulative distribution function
CDF	cumulative density function
CMG	Computer Modeling Group
CSS	cyclic steam stimulation
DA	Drainage Area
EOR	enhanced oil recovery
GSLIB	Geostatistical Software Library
HTPG	hierarchical truncated pluri-Gaussian
km	kilometer
LHS	Latin hypercube sampling
LMC	linear model of coregionalization
m	meter
MCS	Monte Carlo sampling
MIHS	muddy inclined heterolithic strata
MPS	multiple point statistics
NDF	normalized difference factor
OOIP	Original Oil in Place
PCA	principal component analysis
PCSD	pressure cyclic steam drive
PCT	proportion calibration tool
PPMT	projection pursuit multivariate transform
RF	random function
RV	random variable

Abbreviation	Description
SAGD	steam assisted gravity drainage
SD	steam drive
SGS	sequential Gaussian simulation
SIHS	sandy inclined heterolithic strata
SIS	sequential indicator simulation
SS	steam stimulation
TBA	trend building algorithm
TG	truncated Gaussian
TPG	truncated pluri-Gaussian
VPC	vertical proportion curve

Chapter 1

Introduction

Petroleum exploration and production are inherently risky activities and decisions are always made in presence of geological uncertainty (Pyrcz and Deutsch, 2014). The uncertainty originates from incomplete data and is a measure of our lack of knowledge about the true spatial and statistical distribution of rock and fluid properties. Successful reservoir management decision making relies on an accurate assessment of uncertainty in recoverable resources (Bratvold and Begg, 2006; Hanea et al., 2015). This becomes more critical for heavy oil reservoir management as they are more marginal and small changes in the reservoir can change the economics significantly. The world's heavy oil resources are more than twice those of conventional light crude oil (Le Ravalec et al., 2009). According to the Canadian association of petroleum producers, Canada has the third largest oil reserves with large quantities of heavy crude found in oil sand reservoirs. Canadian oil sands are found in the Athabasca, Peace River and Cold Lake deposits in the provinces of Alberta and Saskatchewan (Figure 1.1).

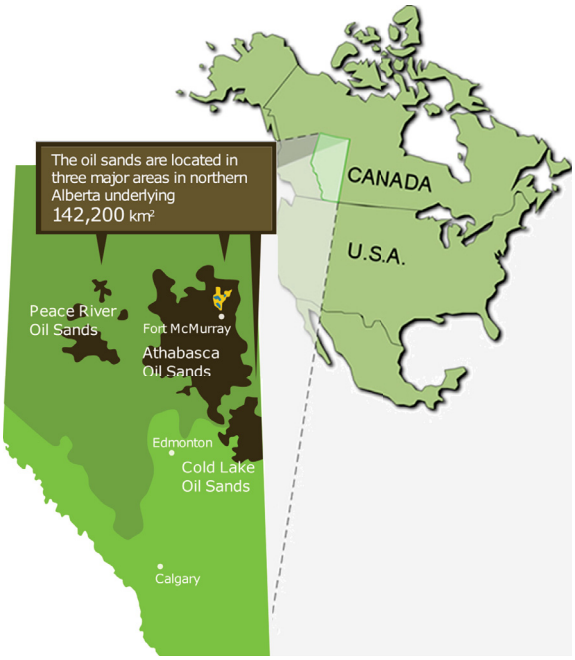

Figure 1.1: Alberta oil sand deposits (obtained from www.aer.com & www.history.alberta.ca).

Oil sands are unconsolidated deposits held together with a naturally occurring mixture of sand, water, clay and an extremely viscous form of hydrocarbons referred to as bitumen (Hein, 2006). Heavy oil production plays a key role in the economy of Canada. According to the Government of Alberta, as of 2014, Alberta's oil sands proven reserves are 166 billion barrels. Only 3% of the oil sand reserves are close enough to the surface to be mined and rest may be recovered by in-situ methods. Due to very high viscosity of bitumen, enhanced oil

recovery (EOR) approaches including thermal recovery are employed for heavy oil production. Such recovery approaches are expensive and technically challenging compared to conventional recovery methods (Kokal and Al-Kaabi, 2010). Thus, careful and rational reservoir management decision making is of great significance at all stages of heavy oil exploration and production.

Steam assisted gravity drainage (SAGD) is a common thermal recovery method for heavy oil production in Canada. According to Alberta Energy, projects using SAGD technology have increased from 5 projects in 2000 to 16 projects in 2013. In SAGD, two horizontal wells are drilled close to each other as shown in Figure 1.2. The top well is the injector that injects steam (energy) into the reservoir to increase the temperature while the lower one (the producer) benefits from gravity to produce heated bitumen (Butler, 1985). The length of each well pair is around 1 kilometer and the vertical spacing between the producer and injector is commonly between 5 to 10 meters. SAGD is more efficient and economic compared to other in-situ recovery alternatives such as cyclic steaming. SAGD yields higher recovery with a lower number of wells and less required water and energy. Also, since steam is injected at relatively lower pressure, the environmental effects are reduced (Butler, 1998).

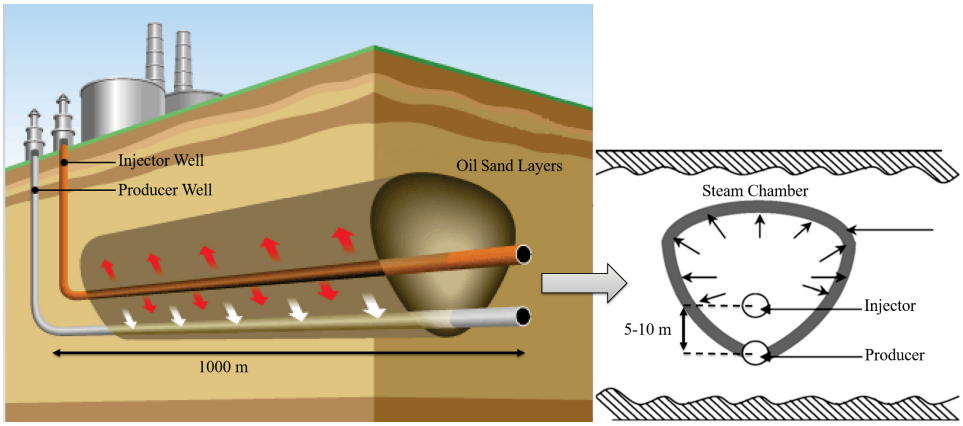

Figure 1.2: Heavy oil production by SAGD (obtained from www.japex.co.jp).

It has been realized that an accurate assessment of uncertainty is a necessary starting point for reservoir management as it helps to increase monetary value and/or mitigate loss in utility (risk) (Bickel and Bratvold, 2008; Bratvold and Begg, 2006). Geostatistics provide a numerical modelling framework to quantify the geological uncertainty. A geostatistical reservoir model is a set of spatially distributed variables including: the structure of each stratigraphic layer, facies at each location within each layer, petrophysical properties such as porosity, permeability, fluid saturations and often thermal properties within facies (Pyrcz and Deutsch, 2014). Such a model should reproduce the input data and local geological concepts. In order to quantify the uncertainty due to incomplete data, multiple models are generated and each model consists of one realization of each variable. Stochastic simulation based on Monte Carlo sampling is employed to generate realizations of reservoir properties that should be treated as if they were equally probable (Isaaks, 1991).

The current practice of reservoir management lacks aspects of geological uncertainty in the decision making

process. Thus, a practical framework is required to accurately define the geological uncertainty and transfer it into production uncertainty. This framework requires geostatistical tools to integrate all available data and first order sources of uncertainty. The geological uncertainty is then characterized by multiple equally-probable geostatistical realizations. Many realizations must be considered in order to transfer this uncertainty to production forecasts and obtain an accurate distribution of recoverable reserves or any other economic measure (i.e., utility). Based on expected utility hypothesis (Friedman and Savage, 1952), the optimal decision is defined as the one that maximizes the expected utility (profit) or minimizes the expected loss over all realizations.

Geostatistical realizations represent a realistic space of uncertainty when the input statistics and geological concepts are well known. However, reservoirs are large and data is sparse; therefore, these parameters are subject to uncertainty. Thus, the uncertainty may be more than what is represented by geostatistical realizations generated based on the same underlying statistical and geological parameters (Khan and Deutsch, 2015; Pyrcz and Deutsch, 2014). The uncertainty in input statistical parameters is referred to as parameter uncertainty and is of great significance for resource/reserve estimation. In order to obtain an accurate assessment of geological uncertainty, the prior parameter uncertainty for both categorical (i.e., facies) and continuous variables (i.e., petrophysical properties) must be quantified and integrated into the geostatistical reservoir modelling.

During the life cycle of a reservoir, as time passes, more information and additional data become available. Integration of time-varying or dynamic data into the reservoir modelling constrains uncertainty and improves subsequent decisions. Using geostatistical techniques for reservoir modelling with static data such as local measurements from wells and two dimensional (2D)/three dimensional (3D) seismic data has become well-established. However, the effective integration of dynamic data in a practical reservoir-modelling workflow remains a major challenge. Each source of data provides information about the reservoir with different scales and levels of precision. The main challenge is the effective integration of all available information to correctly quantify the uncertainty in reservoir properties. The integration of different sources of data cannot be addressed through a hierarchical workflow because, the final reservoir model needs to honor all available data simultaneously (Castro et al., 2006). Many approaches and methodologies have been proposed and implemented for the integration of dynamic data in geological modelling (Alfi and Hosseini, 2016; Andersen et al., 2006; Bhakta et al., 2016; Chakra and Saraf, 2016; Negash et al., 2017; Ouenes and Bhagavan, 1994). For industrial applications, it is necessary to follow a practical and yet effective methodology to integrate information inferred from the available dynamic data.

Time-lapse three-dimensional or four dimensional (4D) seismic is one of the main dynamic data for heavy oil reservoir monitoring and management. This data contains valuable information about fluid movement, pressure build up and quality of fluid flow within the reservoir during recovery (Gosselin et al., 2001; Lumley and Behrens, 1998). Seismic attributes are sensitive to the spatial distribution of two types of reservoir properties: static (time invariant) such as porosity, permeability and lithology; and dynamic (time variant) such as changes in fluid saturation, pore pressure and temperature (Arenas et al., 2001). A 3D seismic survey that is a single snapshot

of the reservoir does not differentiate between static and dynamic properties. 4D seismic analysis with repeated 3D seismic surveys provides the differences in seismic attributes to inform on time varying processes during production (Lumley and Behrens, 1998). Figure 1.3 shows an example 4D seismic data related to a SAGD drainage area that is pad 101S from Surmont project.

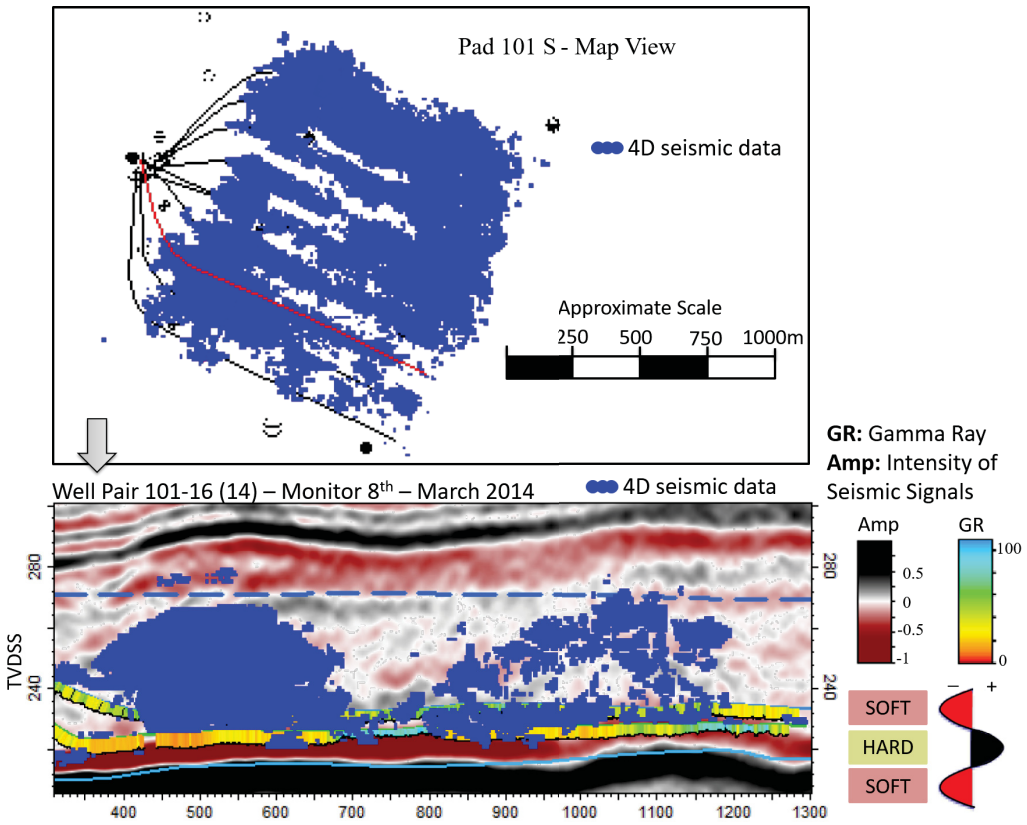

Figure 1.3: An example 4D seismic data. Obtained form Alberta Energy Regulator (AER), annual Surmont SAGD performance review (http://www.aer.ca/).

In Figure 1.3, GR denotes gamma ray logs acquired along the horizontal wells and Amp represents the the amplitude or intensity of seismic signals. TVDSS is true vertical depth sub-sea level that is equivalent to elevation. The map view shows the result of 4D seismic analysis for the entire pad. The scattered dark blue points represent areas of the reservoir within which the changes in seismic attributes is beyond a certain threshold. Also, Figure 1.3 includes a cross section along one of the well pairs (highlighted in red) that shows how 4D seismic data can be used to monitor the effect of recovery process and changes in fluid saturations. 4D seismic is often used in a qualitative sense to infer some information that can be used for reservoir management (MacBeth et al., 2006; Stalder, 2013). Seismic surveys are expensive and there is a limited time window to benefit from this information. Effective integration of 4D seismic in the geostatistical reservoir modelling can improve the geological uncertainty and provides a better estimation of recoverable resources. However, 4D seismic images can be noisy, hard to interpret and sometimes misleading (Lumley et al., 2003; MacBeth et al., 2006). This is the main reason that in

practice, qualitative assessment of 4D seismic data based on professional judgment is preferred over mathematical methods such as inverse modelling. A practical methodology is required to update all geostatistical realizations to reproduce the information obtained from 4D seismic data. The updated realizations can be used for reservoir management decisions including areal or vertical realignment of wells, modifying well patterns and rates and targeting significant bypassed oil by well workovers, sidetracks or new wells (Lumley and Behrens, 1998). Figure 1.4 depicts incremental 4D seismic images for a SAGD project with 9 well pairs plotted in red. The blue points represent the result of 4D seismic analysis and highlights ares of the reservoir where the differences in a seismic attribute over time is bigger than a threshold. As can be seen in Figure 1.4, the evolution of steam chamber around a well pair over time can be monitored using incremental 4D seismic data. Updated realizations of the geological model based on what is learned from historical data can be used to plan for expedient field actions.

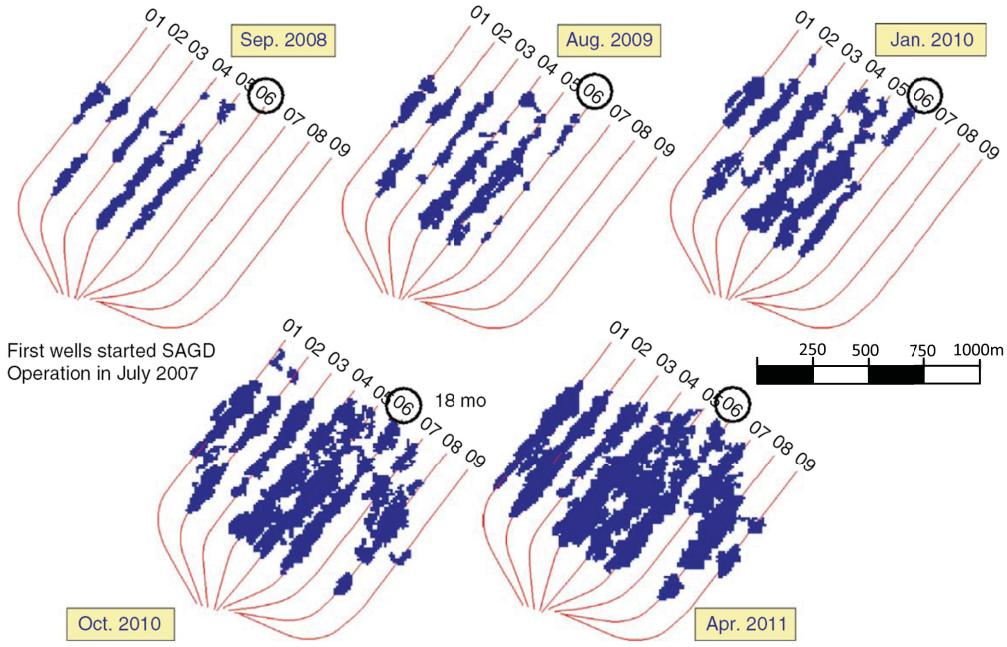

Figure 1.4: Incremental 4D seismic data for pad 102N of Surmont SAGD project (obtaind from (Stalder, 2013)).

In this research, SAGD is the main focus of case studies to evaluate the implementation of the proposed framework for heavy oil reservoir characterization. However, the same principles and methodologies can be extended into other recovery approaches for heavy oil production such as steam stimulation (steam stimulation (SS)) cyclic steam stimulation (cyclic steam stimulation (CSS)), steam drive (steam drive (SD)) and pressure cyclic steam drive (pressure cyclic steam drive (PCSD)). During SAGD, as the heated bitumen moves downward and get produced, it is replaced by injected steam. This forms a steam chamber that primarily moves upward during a rising phase until reaching impermeable barriers at the top of the reservoir where it starts to move laterally during a spreading phase. The amount of produced oil is in direct relation with propagation of the steam chamber. The heating and replacement of high viscosity bitumen with steam together with changes in

pressure and temperature makes it possible to study the steam chamber evolution using 4D seismic analysis. Figure 1.5 shows an example of processed 4D seismic data for a SAGD project represented by blue surfaces. Horizontal wells are colored based on their inclination angle. 4D seismic images along with surveillance wells and other historic data can be used to evaluate the large scale flow patterns within the reservoir based on steam chamber propagation.

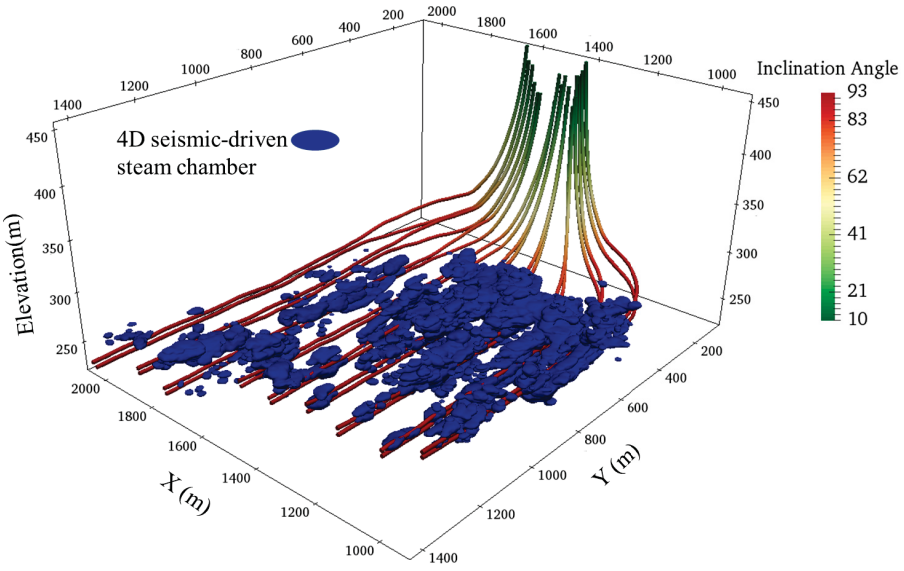

Figure 1.5: An example of 4D seismic data for a SAGD drainage area in Surmont project (Hadavand et al., 2017).

Reservoir management decisions are always made in the face of uncertainty. A geostatistical framework provides the required tools to develop a quantitative model that delineates our lack of knowledge about the true subsurface geology. This model is referred to as model of geological uncertainty that is represented by an ensemble of geostatistical realizations.

1.1 Space of Uncertainty

1.1.1 Model of Geological Uncertainty

For any reservoir there is a single true distribution of petrophysical properties. It is not possible to establish this true spatial distribution of properties based on sparse well data. There is uncertainty that is not an inherent feature of the reservoir, but comes from our lack of knowledge. An accurate model of uncertainty is a necessary element in reservoir management to minimize loss (Begg et al., 2001). Application of deterministic (or scenario-based) models followed by sensitivity analysis is one approach to quantify the space of uncertainty (Amudo et al., 2009; Damsleth et al., 1992; Ehinola and Akinbodewa, 2014; Gohari et al., 2015). This gives some information regarding the uncertainty; however, does not always quantify a realistic space of uncertainty (Alshehri, 2009). On the other hand, the use of probabilistic reservoir modelling to capture the spatial model of uncertainty has

significantly increased (Bickel and Bratvold, 2008; Rose, 2007). Geostatistics is a branch of applied statistics focused on probabilistic study of spatial phenomena. Although it was initially developed for mining, it has been applied to many other fields including petroleum, geography, meteorology, hydrology, oceanography and environmental sciences. Geostatistics uses spatial features inferred from data and employs stochastic simulation (Goovaerts, 1997; Journel and Huijbregts, 1978) to generate numerical models of the reservoir also known as realizations that jointly represent the model of uncertainty. The realizations reproduce sampled data along with the inferred model of spatial variability and the geological framework. Unlike conventional mapping algorithms that were designed to create smooth maps of large scale geological features, geostatistical simulation techniques are developed to introduce the full variability. The small scale variability introduced by the resulting realizations may mask the large-scale trends but, stochastic simulation is more appropriate for predicting flow performance (Pyrcz and Deutsch, 2014). Figure 1.6 compares a conventional map of porosity based on linear estimation (1.6a) against a conditional geostatistical realization (1.6b).

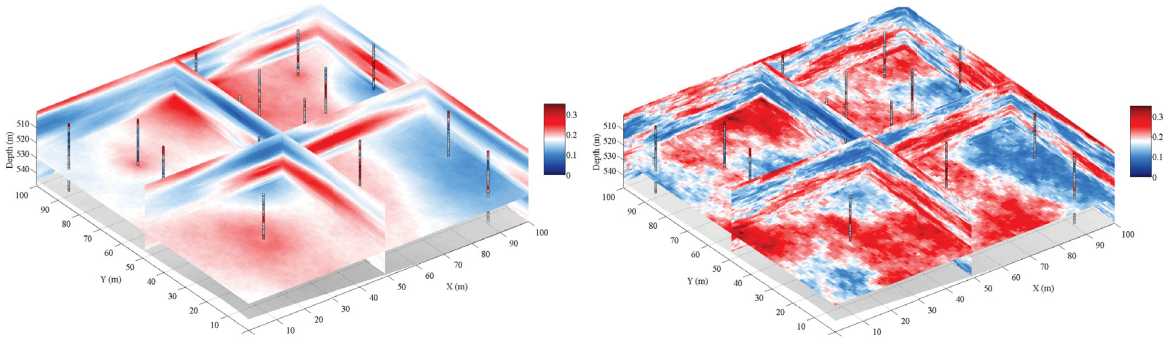

(a) Linear estimate of porosity.

(b) Simulated realization of porosity.

Figure 1.6: An example updated datafile containing the original data file and the sampled enforcing data for one realization.

In geostatistical modelling, a reservoir property at an unsampled (unknown) location is characterized by a random variable (RV) that is traditionally denoted by a capital letter, say Z, while an outcome is denoted by the corresponding lower case letter z. The RV follows a probability distribution ($F(\mathbf{u}; z)$) that is often location dependent and may be denoted as $Z(\mathbf{u})$ where $\mathbf{u}$ is a location coordinate vector. The collection of all possible random variables ($Z(\mathbf{u})$) for many locations in the domain of interest A is called a random function (RF).

$$Z(\mathbf{u}) \qquad \forall\, \mathbf{u} \in A \tag{1.1}$$
$$F(\mathbf{u}; z) = Prob\{Z \leq z\}$$

Probability is a central concept in geostatistics and many techniques have been developed to quantify local probability distribution for a random variable conditioned to multiple available sources of data (Pyrcz and Deutsch, 2014). This is followed by Monte Carlo sampling to populate all variables in the entire domain of

interest and generate a geostatistical realization. Figure 1.7 shows an example 3D map of uncertainty that is characterized by the conditioning well data.

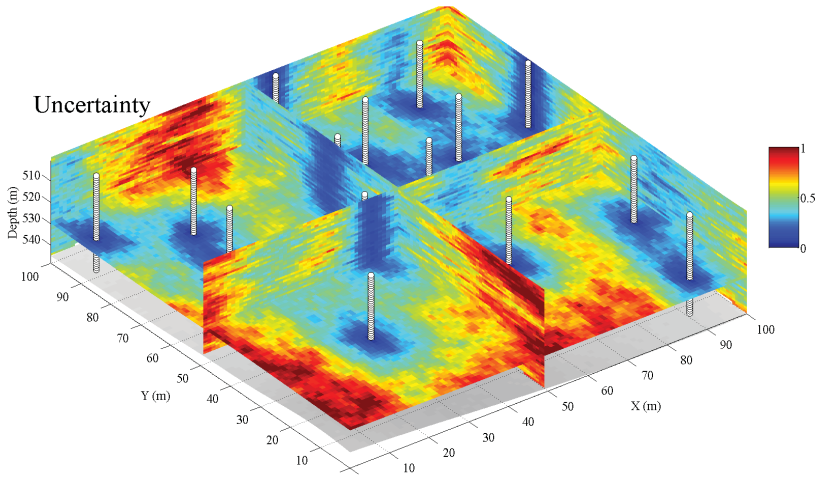

Figure 1.7: Local uncertainty represneted by variance of a variable being modeled in standard Gaussian units.

Sequential indicator simulation (SIS) (Journel, 1983), multiple point statistics (MPS) (Guardiano and Srivastava, 1993) and truncated pluri-Gaussian (TPG) (Armstrong et al., 2003) are some of the geostatistical techniques for simulation of categorical variables such as facies. Multivariate geostatistical techniques are employed for simulation of continuous petrophysical properties within facies. Current best practice may be based on using multivariate transformation techniques such as projection pursuit multivariate transform (PPMT) (Barnett et al., 2014) to a provide a multivariate Gaussian framework for independent simulation of each variable. This is followed by joint back-transformation of the Gaussian variables to original units to restore the multivariate relationships between different petrophysical properties.

PPMT is an established technique that transforms data with complex relationships to an uncorrelated multivariate Gaussian distribution (Barnett and Deutsch, 2015a). The transformation is applied in steps. The first step is univariate normal score transformation based on matching probabilities between univariate cumulative density function (CDF) of each variable (F_i) and standard univariate Gaussian CDF (G) as presented in Equation 1.2.

$$y_i(\mathbf{u}_\alpha) = G^{-1}(F_i(z_i(\mathbf{u}_\alpha))), \;\; \forall i \in \{1 \dots K\}, \;\; \forall \alpha \in \{1 \dots n\} \tag{1.2}$$

where K is number of variables and n is the number of homotopic observations of them. Each of the K variables are transformed according to Equation 1.2, yielding an $n \times K$ data matrix of marginally/univariate Gaussian, $Y_{n \times K}$.

The second step is data sphering that transfers Y to be uncorrelated with unit variance according to:

$$X = YVD^{-\frac{1}{2}}V^T \tag{1.3}$$

Step 1: $Y \times V$

Step 2: $Y \times V \times D^{-\frac{1}{2}}$

Step 3: $Y \times V \times D^{-\frac{1}{2}} \times V^T$

where the spectral decomposition of the covariance matrix, C $(\frac{1}{n}Y^TY)$ gives the eigenvector matrix, $V_{K\times K}$ and the diagonal eigenvalue matrix, $D_{K\times K}$. Equation 1.3 contains three main steps including: 1) principal component analysis (PCA) that is rotating variables to an orthogonal principal axes of variability (Hotelling, 1933), 2) normalizing variables to have a variance of one and 3) projecting the orthogonal variables back to the basis of the original variables. The third step helps to minimize the loading of each original variable (i.e., Y_i) onto its corresponding transformed variable (i.e., X_i). As a result, the mixing of variables is reduced and the transformed variables are more likely to be similar to the original ones in terms of marginal features (Barnett and Deutsch, 2015a). After data sphering, projection pursuit algorithm is implemented to transform the pre-processed data, X to an uncorrelated multivariate Gaussian distribution. The algorithm is based on a projection index, $I(\theta)$ that measures univariate non-Gaussianity for a projection of data, $p = X\theta$ that is associated with a unit length vector, θ. If X is multivariate Gaussian, any θ leads to a projection that is univariate Gaussian with $I(\theta)$ equal to zero. The iterative projection pursuit algorithm finds the projection with maximum non-Gaussianity and applies univariate normal score transformation until reaching to a multivariate Gaussian distribution based on a relevant stopping criteria (Barnett, 2015; Barnett and Deutsch, 2015a). Figure 1.8 compares univariate normal score transformation with PPMT for two petrophysical properties including porosity (Z_1) and permeability (Z_2) log data from a real datasets (DV_Well.dat). Figure 1.8 illustrates how PPMT provides an uncorrelated multivariate Gaussian distribution along with marginal univariate Gaussian distributions. Following the PPMT transformation, each transformed variable can be modeled independently in a Gaussian framework. The final models of transformed variables are then back-transformed to original units. This approach facilitates multivariate modelling of continuous variables and also enables the geostatistical models to reproduce complex multivariate relationships.

1.1.2 Parameter Uncertainty

The ensemble of geostatistical realizations represents the spatial heterogeneity and can quantify a realistic space of uncertainty if the input statistics and the geological framework are well known (Pyrcz and Deutsch, 2014). However, early in the reservoir's life cycle these parameters are uncertain. This is often referred to as model parameter uncertainty and its integration in geostatistical modelling is of great significance especially for early

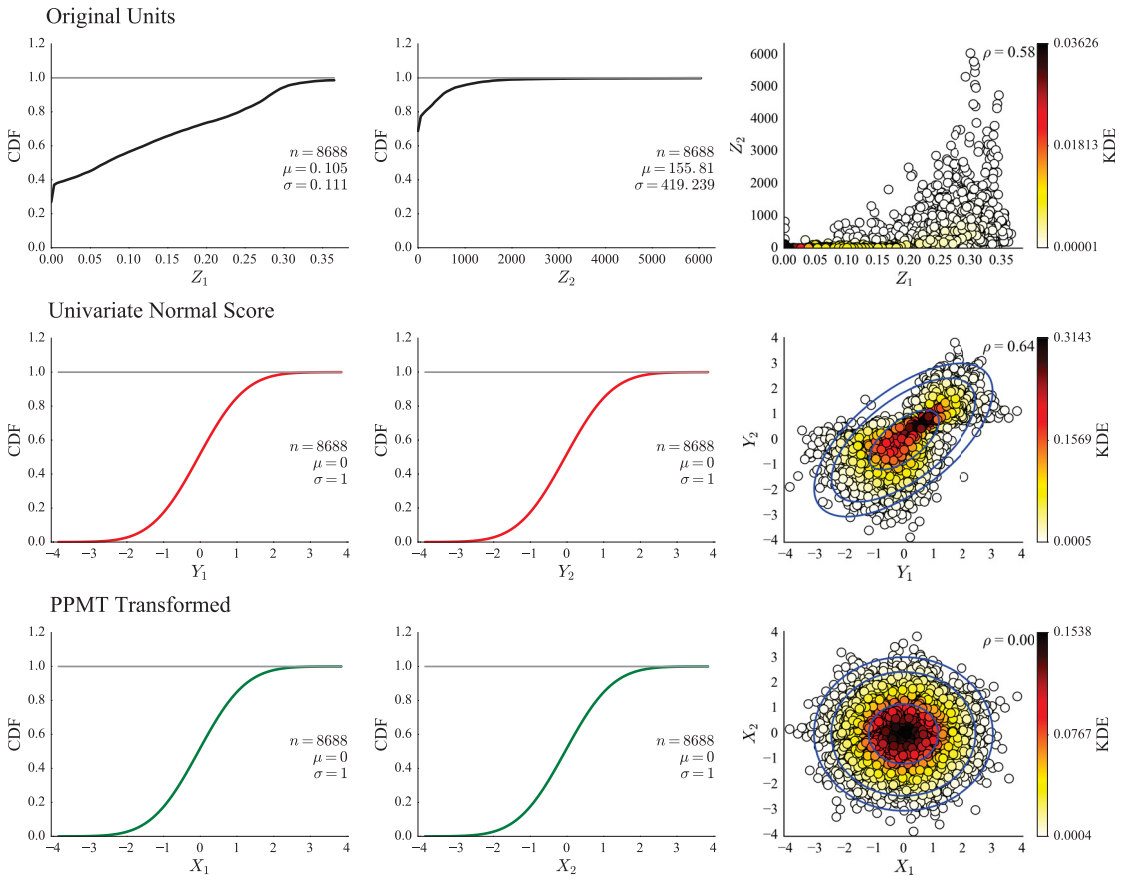

Figure 1.8: PPMT transformation compared to univariate normal score transformation.

reservoir assessment and decision-making (Khan and Deutsch, 2015; Khan et al., 2014; Rezvandehy, 2016). The current practice of reservoir modelling does not account for this uncertainty in a consistent and robust manner.

The bootstrap (Efron and Tibshirani, 1986) refers to a technique based on Monte Carlo statistical resampling that can be used to quantify the prior parameter uncertainty in global statistics. In the bootstrap, data are assumed to be independent and representative of the entire domain. The spatial bootstrap is an extension of the bootstrap technique that accounts for correlation between data using a covariance function (Solow, 1985). However, the effect of conditioning data and the finite reservoir domain are ignored in the spatial bootstrap. The conditional finite domain (CFD) technique is an alternative technique that considers the size of the domain being studied and also the effect of conditioning data (Babak and Deutsch, 2009) but, its implementation in practice is difficult and often results in low uncertainty. The global kriging variance is another option that can be used to quantify the uncertainty in the first order moment of the input statistics (i.e., the mean). However, the kriging variance decreases as the size of the domain increase which does not comply with the reality of parameter uncertainty associated with the mean (Deutsch and Deutsch, 2010).

A recent approach proposed by Khan and Deutsch (2015) and later implemented by (Rezvandehy, 2016) is based on two steps for integration of parameter uncertainty in geostatistical modelling. The first step quantifies

the prior uncertainty in input statistics using the spatial bootstrap followed by the second step that transfers it through the geostatistical modelling process that narrows the uncertainty by adding the effect of conditioning data and accounting for the finite domain limits. This approach can be used in a multivariate framework that transfers the joint parameter uncertainty through the geostatistical modelling. However, the assumption of multivariate Gaussianity and developing a model of co-regionalization are the main issues associated with this method. In this context, using joint multivariate distribution of prior parameter uncertainty in geostatistical modelling is another unexplored practical issue. Rezvandehy (2016) developed a framework for quantification of multivariate histogram uncertainty for continuous variables based on multivariate transformation and independent statistical resampling. Accounting for uncertainty related to proportions of categorical variables (i.e., facies) in presence of a trend is another missing element in quantifying the space of uncertainty.

1.2 Dynamic Data and Reservoir Characterization

Reservoir properties that change over time can be monitored by dynamic data that provide valuable information about the large-scale subsurface geology. As time passes and dynamic data become available, the model of uncertainty should be updated with such information. Although there are well-established geostatistical techniques for reservoir modelling based on available static data, effective integration of dynamic data in a practical workflow remains a challenge (Kulahci, 2015; Oliver and Chen, 2011). Each type of data provides information about the subsurface geological heterogeneity with different scale and level of precision. The integration of different sources of data cannot be addressed through a hierarchical workflow because, the final reservoir model needs to honor all available data simultaneously (Castro et al., 2006). In a geostatistical framework, static data such as local measurements from wells and 2D/3D seismic data can be used to quantify the local uncertainty in the reservoir properties being modeled. Such local uncertainty is presented by a conditional distribution of the reservoir property that can be used in Monte Carlo simulation to generate realizations of reservoir properties conditioned to all available static data (Isaaks, 1991). On the other hand, the dynamic data reflect changes in reservoir properties that are controlled by large scale variations in reservoir properties and specifically the connectivity and quality of fluid flow within the reservoir. Often, dynamic data cannot be directly integrated into the calculation of the local conditional distributions at each location.

4D seismic, surveillance well and production data are the main dynamic data for petroleum reservoir characterization that provide some insight into large-scale quality of fluid flow within the reservoir. One general approach for integration of dynamic data is based on conditioning the geological/statistic model to reproduce the observations of dynamic data with minimum interference with the underlying geological concepts and static data (Abdollahzadeh et al., 2013; Andersen et al., 2006; Chakra and Saraf, 2015; Deutsch and Journel, 1994; Likanapaisal and Tchelepi, 2015; Mezghani et al., 2004; RamaRao et al., 1995; Rwechungura et al., 2011; Wen et al., 2000). This is called history matching or inverse modelling and is a parameter estimation problem. In this context, the application of inverse modelling to match 4D seismic images is often called seismic history

matching (Rwechungura et al., 2011).

A common ground of almost all inverse modelling techniques is building a mismatch function on which some minimization algorithm is imposed (Rwechungura et al., 2011; Wen et al., 2005). The mismatch function comes from the difference between the actual observation of dynamic data (i.e., production data or seismic) and the response of the geological model that is simulated by a mathematical/forward model. For instance, seismic history matching requires time-lapse forward rock-physics modelling that is coupled with flow simulation in order to generate synthetic 4D seismic data based on variations in fluid content, pressure and temperature during the recovery process (Tolstukhin et al., 2012). Minimizing the mismatch between the actual observations of 4D seismic attributes and generated synthetic ones within the reservoir is required for inverse modelling (Rajput et al., 2016). The challenge of conditioning geological models to reproduce observations of dynamic data has motivated development of many inverse modelling techniques. Some of the main ones are discussed here.

Simulated Annealing (SA) is a multi-objective optimization technique that can be employed for integration of different sources of data in reservoir characterization (Deutsch and Journel, 1994; Ouenes and Bhagavan, 1994; Vasco and Datta-Gupta, 1997). SA relies on applying reasonable perturbations into an initial model of the reservoir while checking the effect of them on a comprehensive objective function. It benefits from a flexible decision making rule that accepts perturbations that decrease the objective function while imposing a descending probability control parameter called cooling temperature on perturbations that increase the objective function. This is similar to the mutation mechanism in evolutionary optimization algorithms like Genetic algorithms to avoid trapping in local optimal solutions. Using SA as a post-processing tool to condition the geostatistical models into the dynamic data can improve its efficiency (Deutsch and Journel, 1994). However, SA is an optimization technique and its performance highly depends on the number of parameters, consistency between data types, and the most important factor, an annealing schedule that specifies how to lower the "cooling temperature" to obtain convergence (Geman and Geman, 1984).

Castro et al. (2006) proposed another approach for integration of dynamic data based on mixing conditional probabilities. This approach is mainly developed for facies modelling and is based on calculating conditional probabilities for different sources of data including well log data, 3D/4D seismic and historical production data at each location. In this context, suppose that A is the event of interest at a certain location $u = (x, y, z)$. D_1 represents hard geological data, D_2 and D_3 represent 3D and 4D seismic data respectively and D_4 is related to historical production data. The first challenge is to properly determine the prior conditional probabilities based on each source of data. In this regard, the probability model $P(A|D_1)$ can be computed based on geostatistical modelling techniques such as indicator kriging and multiple point statistics. $P(A|D_2)$ is often obtained using calibration between well logs and 3D seismic data. However, in this approach, $P(A|D_2, D_3)$ is obtained based on inferring a model of local facies proportions. An iterative procedure based on probability perturbation is used to obtain a model for $P(A|D_4)$ based on mismatch between flow simulation results and field production data. The conditional probabilities are combined based on an alternative for Bayesian analysis that account for

dependence in between different events using a tuning parameter τ (Journel, 2002). Equation 1.4 is obtained from (Castro et al., 2006) to explain the probability mixing method.

$$\frac{x}{d_1} = \left(\frac{d_2}{a}\right)^{\tau_1} \left(\frac{d_3}{a}\right)^{\tau_2} \left(\frac{d_4}{a}\right)^{\tau_3} \tag{1.4}$$

where

$$x = \frac{1 - P(A|D1, D2, D3, D4)}{P(A|D1, D2, D3, D4)}$$

$$a = \frac{1 - P(A)}{P(A)}$$

$$d_1 = \frac{1 - P(A|D_1)}{P(A|D_1)} \qquad d_2 = \frac{1 - P(A|D_2)}{P(A|D_2)}$$

$$d_3 = \frac{1 - P(A|D_3)}{P(A|D_3)} \qquad d_4 = \frac{1 - P(A|D_4)}{P(A|D_4)}$$

Determining τ is another challenge to properly capture the conditional dependence or redundancy between different sources of data. However, in this approach, the tuning parameter (τ) is set to 1 for all conditional probabilities and a very simplistic combination scheme is implemented. In order to implement any probability mixing method including Bayesian analysis, considering simplifying assumptions is often required to gain reasonable mathematical derivation. These assumptions can cause biases in estimation of the joint conditional probability that needs to be addressed. On the other hand, it is still required to consider iterative perturbations and optimization process to tune the conditional probabilities of dynamic data in order to match the actual observations of them. Translating dynamic data into conditional probabilities at all locations is not an efficient approach. Dynamic data reflect complex and non-linear changes in the reservoir affected by the recovery process.

Zonation or re-parameterization techniques can improve the efficiency of inverse modelling by reducing the number of parameters (or degrees of freedom) involved in the optimization process. In this regard, locations or zones within the geological model that have highest correlation with the objective function (mismatch) are identified and included in the inverse modelling process to mitigate the computational burden. Pilot points (Avansi and Schiozer, 2015; Jiménez et al., 2016; LaVenue et al., 1995), sequential self calibration (Gómez-Hernánez et al., 1997; Wen et al., 2002), and principal component analysis (PCA) are some of the main re-parametrization methods (Rwechungura et al., 2011; Wen et al., 2005). The implementation of these techniques can improve the overall efficiency of the inverse modelling problem and also minimize the changes that are made to static model during its conditioning to observations of dynamic data. The process of conditioning a reservoir model with static and dynamic data must be simultaneous; it cannot be done sequentially or hierarchically.

The Ensemble Kalman filter (EnKF) is another data assimilation technique that has gained popularity due to its simple conceptual structure and ability to handle large-scale problems (Chen and Oliver, 2010; Gu and Oliver, 2005; Oliver and Chen, 2011; Shuai et al., 2016). EnkF was first introduced by Evensen (Evensen, 1994). EnKF

uses multiple realizations of reservoir properties (an ensemble of realizations) to form an empirical covariance function. Then, all realizations are conditioned to the available measurements of static data and also observations of dynamic data simultaneously during each iteration or ensemble step (Hadavand and Deutsch, 2014). In this context, EnKF can be regarded as a gradient-based optimization technique with a convenient formulation. An example formulation of EnKF is summarized below.

$$\begin{aligned}
\text{Ensemble Mean: } & \bar{U_t^f} = \frac{(U_t^f.e).e^T}{N_e} \\
\text{Sample Covariance: } & \hat{C}^f = \frac{(U_t^f - \bar{U_t^f}).(U_t^f - \bar{U_t^f})^T}{N_e - 1} \\
\text{Nonlinear Forecast Step: } & U_t^f = F(U_{t-1}^a) + EM \\
\text{Linear Analysis Step: } & U_t^a = U_t^f + K_t.(D_t - H_t.U_t^f) \\
\text{Kalman Gain: } & K_t = \hat{C}^f.H_t^T.(H_t.\hat{C}^f.H_t^T + \Sigma_t)^{-1}
\end{aligned} \tag{1.5}$$

where U is the $(N_m.N_b + N_s.N_b) \times N_e$ augmented matrix consist of static and dynamic variables. In this context, N_m is the number of static variables, N_s is the number of dynamic variables, N_b is the number of grid cells (i.e., locations within a gridded space) and N_e is the number of ensemble realizations. As shown in Equation 1.5, the EnKF consists of a nonlinear forecasting step using a model operator F (i.e., flow simulator) and a linear analysis step that updates the augmented matrix based on the available data. EM is the model error matrix related to the model operator (usually set to zero). The subscript (t) refers to time or assimilation step, the superscript (f) is related to the forecast step and the superscript (a) shows the result of the analysis step. K_t is the Kalman gain matrix, D_t is the $N_{d,t} \times N_e$ matrix consisting of available measurements of static data and observations of dynamic data at the time step t. H_t is the $N_{d,t} \times (N_m.N_b + N_s.N_b)$ observation matrix that determines which variables have been measured or observed. $\hat{C}^f$ is the $(N_m.N_b + N_s.N_b) \times (N_m.N_b + N_s.N_b)$ sample covariance matrix which is calculated based on ensemble realizations. Finally, Σ_t is the $N_{d,t} \times N_{d,t}$ diagonal measurement/observation error matrix that assumes the errors of measurement/observations are not correlated which is a reasonable assumption.

The final result of EnKF is limited by the variability within the ensemble of realizations which reduces with each iteration of EnKF. Updating all realizations towards a single optimum response causes this loss of variability (also known as ensemble collapse). Also, EnKF cannot reproduce complex measures of dependence (multiple point relationships) that may be required for complex spatial features.

A common challenge associated with any inverse modelling technique is the ability to handle the computational cost of running forward/mathematical models that simulate the physics of the reservoir (Rwechungura et al., 2011). Thermal flow simulators and petro-elastic models are two examples of such forward models that provide a connection between the static reservoir properties and the observations of dynamic data. These models

are often highly nonlinear without a simple analytical solution. Both gradient-based and non-gradient optimization algorithms require some kind of sensitivity analysis or running the forward model iteratively. In addition, it should be noted that history matching/inverse modelling problems are almost always ill-posed meaning that there are many realizations that honor all the static and dynamic data simultaneously (Oliver and Chen, 2011). Observations of dynamic data are affected by large scale patterns in the spatial distribution of reservoir properties and there are multiple geologically plausible patterns that honor these observations. In order to integrate information obtained from dynamic data, it is required to update all geostatistical realizations independently. This applies more constraints on the model of geological uncertainty as more information becomes available.

Although automatic history matching based on different techniques has been regarded as a possible solution for integration of dynamic data, its implementation in practice may not be possible. The success of this approach is strongly dependent on the quality of dynamic data and the reliability of forward models (Castro et al., 2006; Tolstukhin et al., 2012). The computational cost of automatic history matching may not allow consideration of all geostatistical realizations to update the space of uncertainty based on the dynamic data.

1.3 Decision Making in Presence of Uncertainty

Reservoir exploration and production involves making critical decisions related to an uncertain future. Assigning the number and locations of exploratory wells, selecting an optimum development plan and deciding whether to invest in a project are examples of such decisions (Pyrcz and Deutsch, 2014). The conventional decision making process does not completely consider uncertainty and relies on deterministic models with a few scenarios of the future of the reservoir (Pyrcz and Deutsch, 2014; Rose, 2007). The economic under-performance of many oil recovery projects has been tied to poor decision making without accurate evaluation of uncertainty (Begg et al., 2002; Bratvold and Begg, 2006; Sazonov et al., 2015).

The geological uncertainty can be effectively quantified by multiple geostatistical realizations. However, transferring geological uncertainty into production results is incomplete when choosing one or several realizations based on a specific ranking criteria (Fenik et al., 2009; McLennan and Deutsch, 2005; Pyrcz and Deutsch, 2014). Many reservoir studies choose a $P50$ realization (the one that ranks in the middle) based on a simple resource calculation. Many petroleum production projects do not return the predicted technical and economical expectations and the main cause of failure in many cases may be the lack of an accurate model of uncertainty in recoverable resources for decision making analysis (Babin et al., 2016; Bratvold and Begg, 2006). Choosing the optimal development plan or any other critical reservoir management decision should considered all realizations that represent the space of uncertainty (da Cruz, 2000). Based on this framework, all geostatistical realizations of the geological model are used to transfer uncertainty into production responses to calculate a measure of profit/utility. The optimal decision maximizes the expected utility over all realizations (Arnold et al., 2016; da Cruz, 2000; Friedman and Savage, 1952). Furthermore, the concept of a loss function can be used to consider different consequences for under- and over-estimation (Srivastava, 1987). This allows the decision maker to incorporate

relevant economic parameters that affect heavy oil recovery (Srivastava, 1990). This approach is regarded as full uncertainty integration in decision making and its implementation calls for execution of a forward model (i.e., flow simulation) many times (da Cruz, 2000). This research motivates the idea of using all realizations all the time for accurate transfer of geological uncertainty to heavy oil reservoir management.

1.4 Research Plan

In this thesis, a framework is developed for practical integration of geological uncertainty into heavy oil reservoir management. This framework provides the required geostatistical tools to generate numerical geological models that account for parameter uncertainty and reproduce information obtained from dynamic sources of data. In this context, an accurate model of parameter uncertainty is developed for both categorical and continuous variables. Prior proportion uncertainty associated with categorical variables (i.e., facies) is quantified in presence of a trend that is a model of locally varying proportions. Stochastic indicator simulation at data locations is employed to quantify the prior proportion uncertainty based on statistical resampling. Multiple realizations of the trend model represent the prior proportion uncertainty and can be integrated into any geostatistical modelling technique. Figure 1.9 shows an example of prior proportion uncertainty quantified based on well data for five facies: Breccia, Sand, sandy inclined heterolithic strata (SIHS), muddy inclined heterolithic strata (MIHS) and Mud. Figure 1.9a summarizes the prior uncertainty in global facies proportions while 1.9b depicts corresponding realizations of the trend model. In Figure 1.9b, colored lines represent the cumulative proportions and the space between them shows the proportion of each facies. For instance, red line represents proportion of Breccia while the gold lines shows the proportion of Sand and Breccia and so on. The integration of prior parameter uncertainty into the stochastic facies simulation provides a realistic and accurate posterior model of proportion uncertainty.

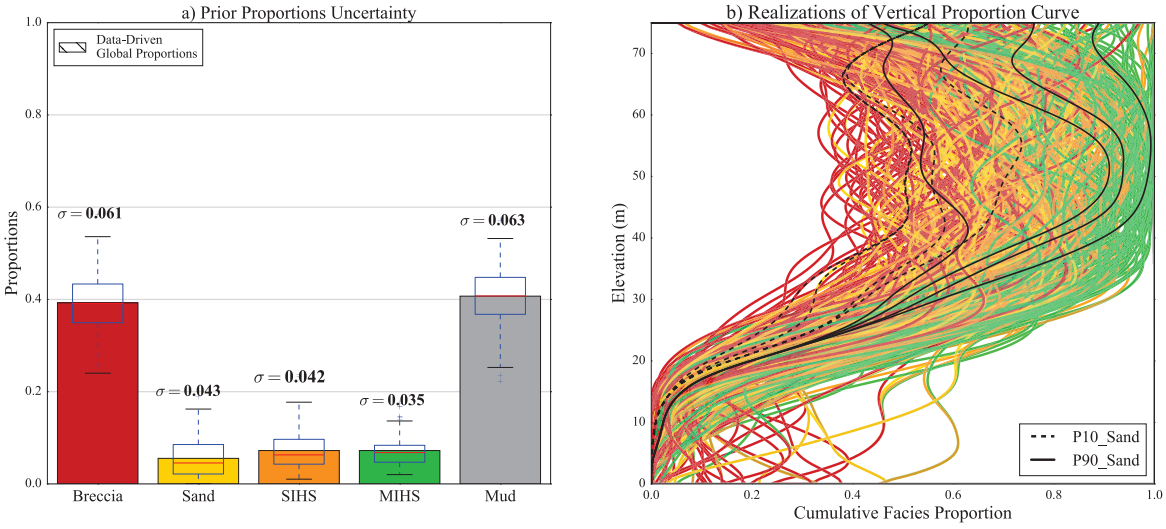

Figure 1.9: An example showing the prior facies proportion uncertainty.

In reservoir modelling, facies often provide the stationary domains for continuous variables (i.e., petrophysi-

cal properties). Sampled properties such as shale volume, porosity, permeability and fluid saturation often show complex multivariate relationships. Figure 1.10 shows an example of relationships between different petrophysical properties observed from well data within a net facies (i.e., sand). The geostatistical simulation must reproduce such relationships that characterize the geological process. The same constraint applies to the parameter uncertainty associated with input statistics of petrophysical properties. A geostatistical tool is developed to quantify the multivariate parameter uncertainty associated with petrophysical properties within each facies. Also, a practical workflow is proposed to integrate the multivariate parameter uncertainty in geostatistical reservoir modelling.

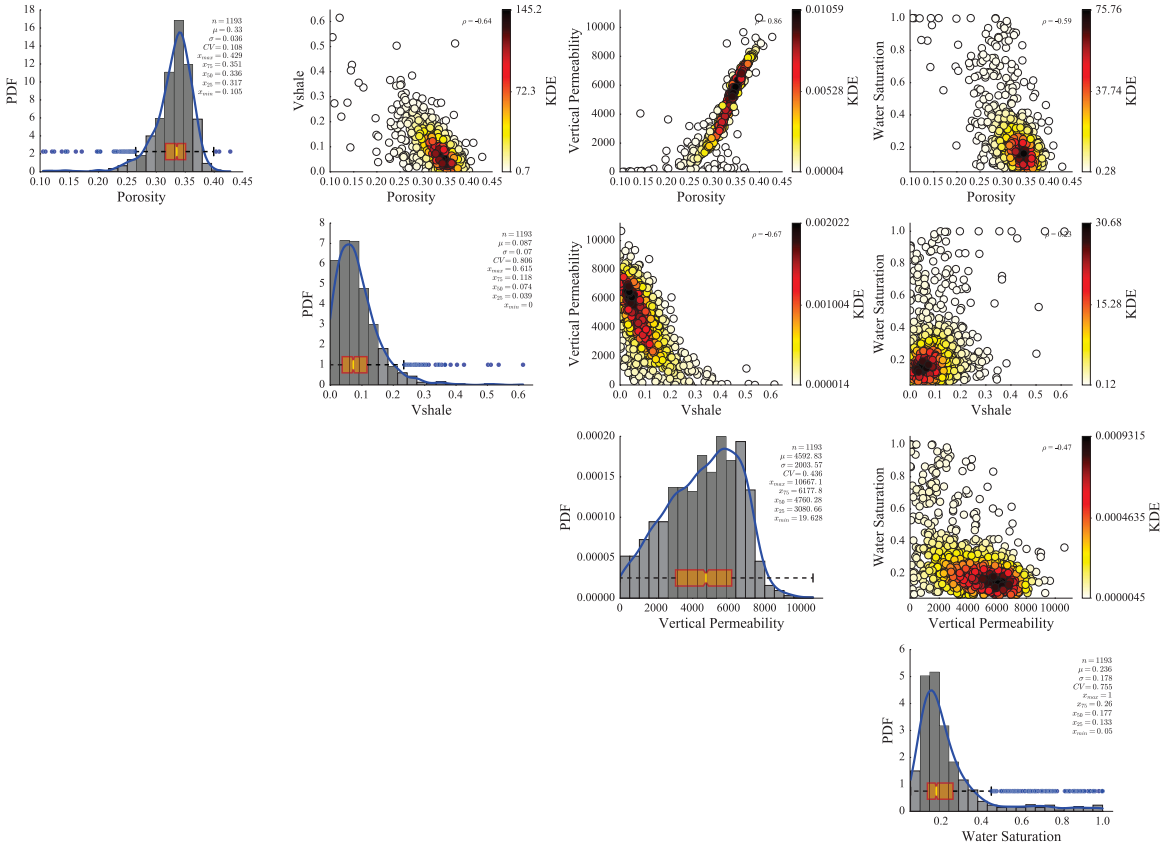

Figure 1.10: An example of multivariate relationships between petrophysical properties.

The model of geological uncertainty can be constrained based on what is learned from dynamic data as the recovery process carries on. A practical methodology is developed, implemented and tested for integration of information inferred form dynamic data such as 4D seismic images into the reservoir modelling workflow (Hadavand and Deutsch, 2016). This is done based on geostatistical enforcement of anomalies identified by visual inspection of 4D seismic images along with other sources of information obtained over the time. As was mentioned above, 4D-seismic images contain valuable information about large-scale fluid flow within the reservoir. Such information may be best described by anomalies in fluid flow that can be inferred from the

unusual patterns in variations of a seismic attribute, such as travel time or acoustic impedance. Considering the quality and scale of 4D-seismic data, these anomalies are sources of information that can be identified with a high level of confidence. In this context, an anomaly is where flow occurs unexpectedly or where there is no flow when it is expected. There are two main types of anomalies: flow barriers and conduits. Since an anomaly is associated with the quality of fluid flow, its effective directional permeability is a suitable measure to evaluate its existence in a geostatistical realization. A fidelity analysis determines what percentage of realizations reproduce each anomaly and also specifies the missing anomalies for each realization. Geostatistical anomaly enforcement is implemented based on sampling admissible enforcing data and generating updated data files for each realization that contain the original well data along with the unique enforcing data sampled for the missing anomalies. The last step is to repeat geostatistical modelling workflow with separate data file for each realization. This results in updated realizations that represent a more accurate model of geological uncertainty that is constrained by information obtained form 4D seismic images and other dynamic sources of data.

1.5 Dissertation Outline

Chapter 2 presents the theory of quantifying parameter uncertainty for categorical and continuous variables based on statistical resampling. Accurate quantification of prior proportion uncertainty for categorical variables in presence of a trend and its integration in geostatistical reservoir modelling is the main focus of this chapter. In addition, a methodology is proposed to improve sampling of multivariate proportion uncertainty with a limited number of realizations. Continuous petrophysical properties are often modeled within facies. The parameter uncertainty associated with distribution of continuous properties is another important source of uncertainty that is quantified based on multivariate spatial bootstrap. A workflow is proposed for integration of facies proportion uncertainty along with joint multivariate parameter uncertainty associated with statistical distribution of petrophysical properties into the geostatistical reservoir modelling.

Chapter 3 presents a case study based on real well data from a petroleum reservoir to explain the quantification and integration of parameter uncertainty into reservoir characterization. Facies proportion uncertainty is quantified in presence of a trend and multiple realizations of the trend model is generated that represent the prior proportion uncertainty. The geostatistical facies simulation is conducted by considering a separate realization of the trend model for each final facies realizations. This results in practical integration of proportion uncertainty in geostatistical facies modelling. Also, multivariate histogram uncertainty is quantified within facies and integrated in multivariate geostatistical modleing of petrophysical properties.

Chapter 4 introduces a practical methodology for integration of 4D seismic data in geostatistical reservoir modeling. Visual inspection and professional judgment are employed to infer information from 4D seismic data. Such information are represneted by anomalies in flow patterns. An automated fidelity analysis evaluates the reproduction of identified anomalies by geostatistical realizations. Realizations are updated to enforce the missing anomalies and integrate what has been learned from 4D seismic data. This is based on sampling enforcing data

for the missing anomalies that is done independently for each realization. The last step is to repeat the geostatistical modelling workflow considering the new data files that contain original well data along with the sampled enforicng data for each realization. An example is presented in this chapter to explain the implementation of the prosed methodology.

Chapter 5 presents a real case study considering 4D seismic data from a SAGD drainage area in Surmont project. The proposed methodology in Chapter 4 is implemented to integrate 4D seismic data in geostatistical modeling of the drainage area. A collection of guidelines and best practices for anomaly identification is presented in this chapter. Comprehensive fidelity analysis before and after geostatistical anomaly enforcement is considered to evaluate the proposed methodology. In addition, thermal flow simulation is executed for an isolated part of the drainage area that is affected by an anomaly to study the effect of geostatistical anomaly enforcement. Finally, an algorithm is introduced for facies proportion calibration if a target proportion is required to be honored by geostatistical realizations.

Chapter 6 presents a comprehensive case study that employs all the methodologies and geostatistical tools developed in this thesis to establish a workflow for improved reservoir characterization. The prior facies proportion uncertainty and multivariate histogram uncertainty are quantified based on hard data. Information obtained from 4D data is integrated into the geostatistical reservoir modelling along with the prior parameter uncertainty. Finally, the posterior uncertainty in facies proportions and distribution of petrophysical properties are studied before and after integration of 4D seismic data.

Chapter 7 wraps up the thesis with a summary of contributions and discusses the potential limitations. A number of suggestion are provided to improve the methodologies and geostatistical tools developed in this thesis.

Appendix A describes the computer programs developed to implement proposed methodologies and also provides a user manual for each program.

Chapter 2

Proportion Uncertainty in Presence of a Trend

2.1 Introduction

Geostatistical modelling of regionalized variables requires input statistical parameters (Babak and Deutsch, 2009). For instance, in order to simulate a petrophysical property, say porosity, its representative probability distribution (i.e., histogram) is required while, for facies modelling, proportions of different categories are the main input statistics. These parameters are inferred based on available data. Economic and environmental constraints result in limited data compared to the size of the reservoir. Thus, the inference of statistical parameters is subject to uncertainty. Stochastic simulation based on kriging or a multivariate Gaussian framework quantifies the local uncertainty at specific locations conditioned to different sources of data (Khan and Deutsch, 2015). Parameter uncertainty is at a higher level of consideration and is often referred to as global uncertainty to differentiate it from local uncertainty. Apart from possible ergodic fluctuations associated with stochastic simulation (Pyrcz and Deutsch, 2014), geostatistical realizations reproduce the input statistical parameters. Thus, if the same underlying input parameters are used for all realizations, there is an underestimation of global uncertainty (Khan and Deutsch, 2015; Wang and Wall, 2003). Parameter uncertainty should be integrated in the geostatistical modelling to obtain an accurate model of geological uncertainty (Khan and Deutsch, 2015; Rezvandehy, 2016). There are many input parameters including distributions of continuous and categorical variables, models of spatial variability (i.e., variograms), structural surfaces and domain size. This thesis is focused on providing a framework to integrate proportion uncertainty into geostatistical modelling. A methodology is proposed for quantification of facies proportion uncertainty in presence of a trend (Hadavand and Deutsch, 2017). Section 2.2 explains the methodology and presents an experimental setup that is developed to validate the proposed methodology based on reference proportion uncertainty. In Section 2.3, a geostatistical tool is introduced to quantify the multivariate parameter uncertainty associated with distribution of continuous petrophysical properties within facies. Also, the seamless integration of the parameter uncertainty into facies and multivariate petrophysical property modelling is presented.

2.2 Proportion Uncertainty

A reservoir property that can assume a continuum of values between two given ranges is called a continuous variable; otherwise it is a categorical variable. Modelling categorical variables such as facies is of great significance for resource estimation and strongly affects reservoir flow responses (Pyrcz and Deutsch, 2014). In geostatistical reservoir modelling, the spatial distribution of facies defines the stationary domains for continuous

properties such as porosity and permeability and explains a major aspect of spatial heterogeneity and geological uncertainty (Falivene et al., 2006; Pyrcz and Deutsch, 2014). For heavy oil production, the spatial arrangement of facies determines the large-scale flow patterns. The variability of permeability between facies is more significant than within facies. Facies proportions are the main input statistical parameter for facies modelling. However, limited well data does not permit unambiguous calculation of proportions (Babak and Deutsch, 2009; Dowd and Pardo-Igúzquiza, 2002). In this research, a methodology is proposed for quantification of proportion uncertainty using the spatial bootstrap. Facies are often modeled in presence of a trend that characterizes the local geological conditions. Thus, apart form a model of spatial variability (i.e., variogram), a trend model is used in the statistical resampling of the data (spatial bootstrap). As explained in Chapter 1, there are two main steps for integration of parameter uncertainty into a realistic model of geological uncertainty. The first step is to quantify the prior proportion uncertainty that is based on statistical resampling and is represented by multiple realizations of the global proportions or the trend model. The proposed statistical resampling accounts for data configuration, spatial correlation and the underlying trend model. The second step is to transfer the prior proportion uncertainty through the geostatistical facies modelling. This narrows the uncertainty by considering the effect of conditioning data and accounting for the reservoir limits.

2.2.1 Quantifying Prior Proportion Uncertainty in Presence of a Trend

In ideal circumstances, exhaustive measurements may be collected to find the true distribution of a reservoir property. In practice, the reservoir is sampled with a very limited number of data. Thus, the calculated distribution differs from the true distribution. For a categorical variable such as facies, proportions are subject to uncertainty. The spatial bootstrap is the process of resampling the available data while respecting the data configuration and the model of spatial correlation. This provides multiple realizations of sampled data that are treated as equally-probable and can be used to quantify the prior proportion uncertainty. The spatial bootstrap for categorical variables is implemented using unconditional SIS at data locations. SIS is a well-established stochastic technique for categorical variable modelling (Journel and Alabert, 1989; Journel and Isaaks, 1984; Journel, 1983). There are some concerns about indicator simulation. The indicator variograms only consider two-point statistical measures and there is no explicit control over the cross correlation between the simulated categories (Deutsch, 2006). However, there are some good features of SIS that makes it a reasonable technique for the spatial bootstrap. For one thing, the required modelling parameters can be easily inferred from limited well data. Also, indicator kriging is a robust algorithm to quantify local conditional probabilities and the sequential simulation provides a straightforward way to model the uncertainty in the spatial distribution of categorical variables (Deutsch, 2006).

A base-case trend model inferred from the available data provides a model of locally varying proportions for the indicator kriging. This is necessary for the spatial bootstrap in presence of a trend. In this context, a trend building algorithm (TBA) is used to generate the base-case trend based on available facies data. The

trend building algorithm is also used to generate realizations of the trend model based on the spatial bootstrap realizations of facies data. The prior uncertainty in facies proportions is then represented by multiple realizations of the trend model that accounts for the configuration and the spatial correlation in presence of a trend.

2.2.1.1 Unconditional Indicator Simulation at Data Locations

The spatial bootstrap sampling is implemented by unconditional indicator simulation. This provides the ability to consider large data sets with high resolution sampling down wells. Consider a regionalized categorical variable $Z(\mathbf{u})$ at locations $\mathbf{u}$ within a stationary domain A and with K different categories or facies. The facies are mutually exclusive meaning that at each location only one category exists. Also, one of the categories must exist at all locations. In this context, categorical variables can be expressed as a series of indicator variables:

$$I(\mathbf{u},k)=\begin{cases}1, & \text{if } Z(\mathbf{u})=k\\ 0, & \text{otherwise}\end{cases}, \quad k=1,...,K, \quad \forall\ \mathbf{u}\in A \tag{2.1}$$

An indicator variable can be interpreted as the probability of a category to prevail at a particular location: the probability is 1 if it prevails and 0 if it does not. Indicator variography is used to quantify the transition probability for each category as a function of vector Euclidean distance. This quantifies the spatial continuity for each of the K indicator variables. The indicator variogram is calculated, interpreted and modeled to represent the two-point statistical spatial variability and is expressed as:

$$\gamma_I(\mathbf{h};k)=\frac{1}{2}\,E\{\,[I(\mathbf{u};k)-I(\mathbf{u}+\mathbf{h};k)]^2\,\}, \quad k=1,...,K \tag{2.2}$$

where $E\{\}$ is the expected value or probability weighted average and $\mathbf{h}$ is the distance vector between the two points. Indicator kriging is used to estimate the local distribution of uncertainty conditioned to local indicator data. In presence of n nearby local data, the kriging estimator is written:

$$I^*(\mathbf{u};k)-P(\mathbf{u};k)=\sum_{\alpha=1}^{n}\lambda_\alpha(\mathbf{u};k)[I(\mathbf{u}_\alpha;k)-P(\mathbf{u}_\alpha;k)], \quad k=1,...,K \tag{2.3}$$

where $P(\mathbf{u};k)$ is the prior model of local proportions provided by the trend model that is inferred based on local data and represents the subsurface geological formation. The kriging weights are assigned to minimize the error variance providing the following system of linear equations:

$$\sum_{\beta=1}^{n}\lambda_\beta(\mathbf{u};k)C(\mathbf{u}_\alpha-\mathbf{u}_\beta;k)=C(\mathbf{u}_\alpha-\mathbf{u};k), \quad \alpha=1,...,n \ \ \&\ k=1,...,K \tag{2.4}$$

$$C(\mathbf{h};k)=C(0,k)-\gamma_I(\mathbf{h};k)$$

where $C(\mathbf{h}; k)$ is the covariance function calculated based on the corresponding indicator variogram (Journel, 1983). In this context, $C(0, k)$ denotes the indicator variance. Indicator kriging for each category provides the local conditional probability at an unsampled location that can be integrated to infer a conditional cumulative distribution function (CCDF). These estimated probabilities are post processed to ensure they are non negative and that they sum to 1. Indicator simulation is then implemented by Monte Carlo sampling of the CCDF. Figure 2.1 summarizes how a CCDF is formed and used for simulation based on Monte Carlo sampling.

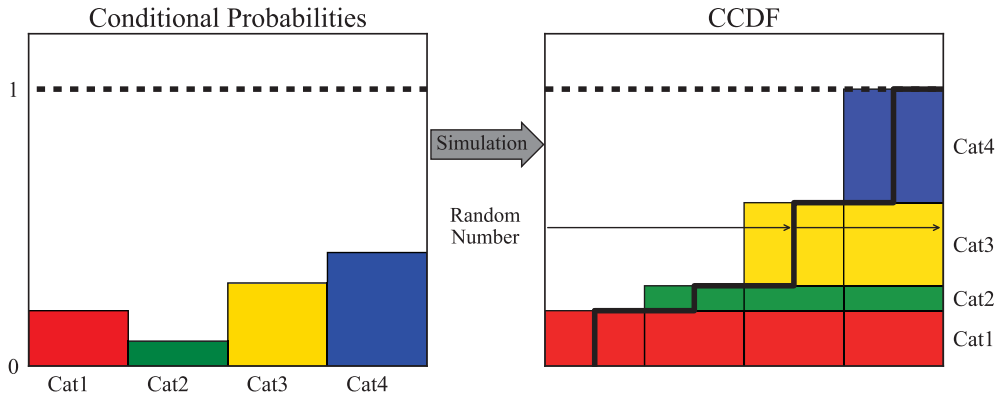

Figure 2.1: Indicator simulation by Monte Carlo sampling of the conditional cumulative distribution function.

2.2.1.2 Trend Building Algorithm (TBA)

Categorical variables such as facies often follow a trend, that is, a locally varying model of proportions. A trend modelling tool is required. The resulting trend can be integrated into the geostatistical facies modelling as an input parameter. The prior proportion uncertainty may be presented by multiple realizations of the trend model. The trend modelling is based on kernel-weighted distances that provide a smooth map of facies proportions. The indicator data within a user-defined bandwidth are identified and are weighted based on their distance to the target location. The declustering weights are considered to obtain a representative trend model. There are alternatives for the kernel function; Figure 2.2 shows some of them. Epanechnikov and quartic spline kernels are considered as options for the TBA. Although the kernel shape has a minimal effect on trend modelling, the kernel bandwidth and anisotropy in the principal directions can strongly affect the trend calculation. The bandwidth is usually assigned based on the range of spatial continuity and professional discretion. However, it is possible to determine the optimal trend modelling bandwidth by minimizing the correlation between trend values and the residuals (Qu and Deutsch, 2015).

There are different options for trend modelling including: vertical, aerial and 3D. The vertical trend is calculated by weighting data based on their vertical position. The result is sometimes referred to as a vertical proportion curve (VPC). Vertical variations in proportions are very common. The aerial trend is calculated based on averaging data along the vertical direction followed by kernel density weighting in the 2D horizontal plane. Finally, a 3D trend modelling is implemented based on 3D kernel density weighting and there is an ad-

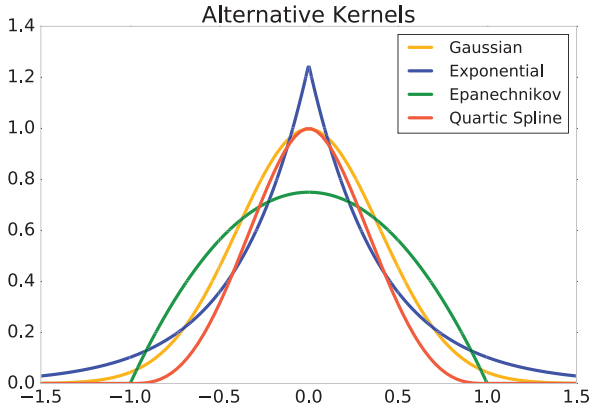

Figure 2.2: Some kernel functions.

ditional option to calibrate the 3D calculated trend to match the vertical trend model. The principal directions and corresponding bandwidths of the kernel define spatial anisotropy in trend calculation. This is considered by a transformation that rotates the data coordinates to the principal coordinates and also scales them based on the major bandwidth.

$$\begin{bmatrix} M_1 \\ M_2 \\ M_3 \end{bmatrix} = \begin{bmatrix} cos(\alpha)cos(\beta) & sin(\alpha)cos(\beta) & -sin(\beta) \\ -\frac{R_1}{R_2}sin(\alpha) & \frac{R_1}{R_2}cos(\alpha) & 0 \\ \frac{R_1}{R_3}sin(\beta)cos(\alpha) & \frac{R_1}{R_3}sin(\beta)sin(\alpha) & \frac{R_1}{R_3}cos(\beta) \end{bmatrix} \times \begin{bmatrix} X \\ Y \\ Z \end{bmatrix} \tag{2.5}$$

where β is the angle between major axis and the horizontal plane that is dip angle measure positive down. α is the angle of the major axis from the East-West (i.e., X) measured counter clockwise.

In Equation 2.5, R_1, R_2, R_3 are the kernel radii (half of the bandwidth) along the principal directions i.e., major (M_1), minor (M_2) and vertical (M_3), respectively. Figure 2.3 shows an example of using the TBA to get the trend model based on limited well data for 3 facies: Shale, Mixed and Sand. In this example, the TBA is used to get a 3D trend model that is calibrated based on the vertical trend calculation. A base-case trend model is used to provide the local proportions for the indicator kriging. In this way, the spatial bootstrap implemented by unconditional SIS accounts for the existing trend in local variations of proportions within the domain of interest.

The statistical resampling results in multiple realizations of the sampled data. The TBA is also employed to generate the corresponding realizations of the trend model based on the spatial bootstrap realizations of sampled data. As a result, the prior proportion uncertainty is represented by multiple realizations of the trend model that will be integrated into the geostatistical modelling workflow to obtain a realistic posterior uncertainty. In order to visualize the prior uncertainty in the 3D trend model, realizations of the VPC are plotted in Figure 2.4. The $P10$ and $P90$ realizations based on the global proportion of Sand (the most important net facies) are plotted to provide a better understanding of the space of uncertainty. The colored lines in Figure 2.4 represent the cumulative proportions and the space in between them determines the proportion of each category. In this

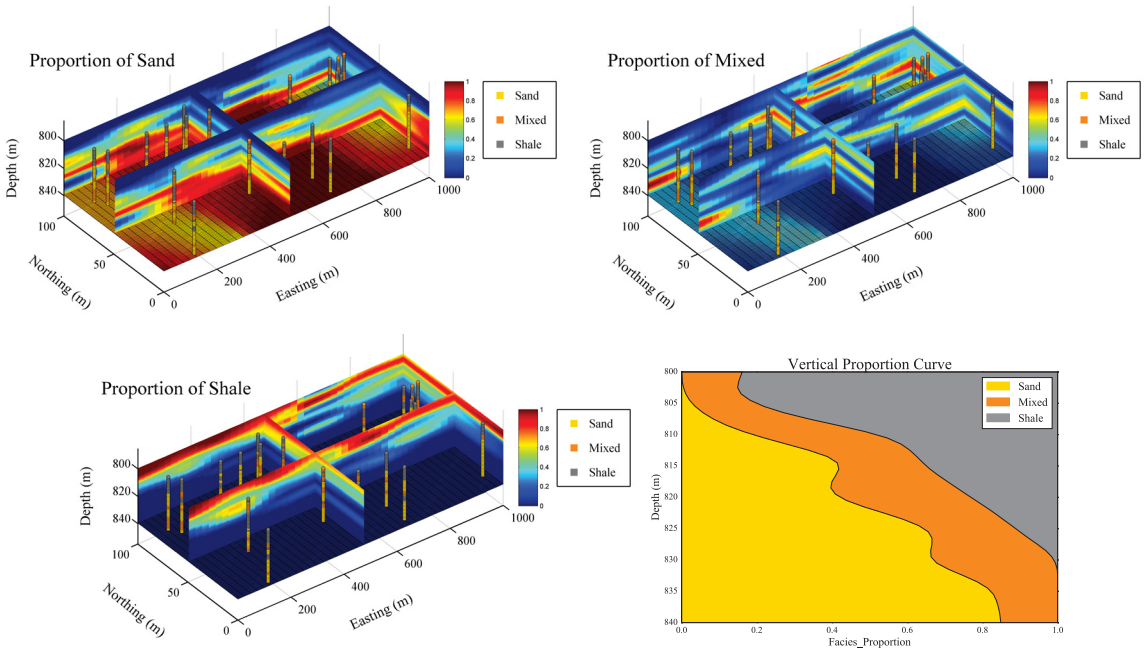

Figure 2.3: An example of using the TBA to infer a trend model based on sampled data.

context, the gold line shows the proportion of Sand while the orange represents proportion of Sand plus Mixed.

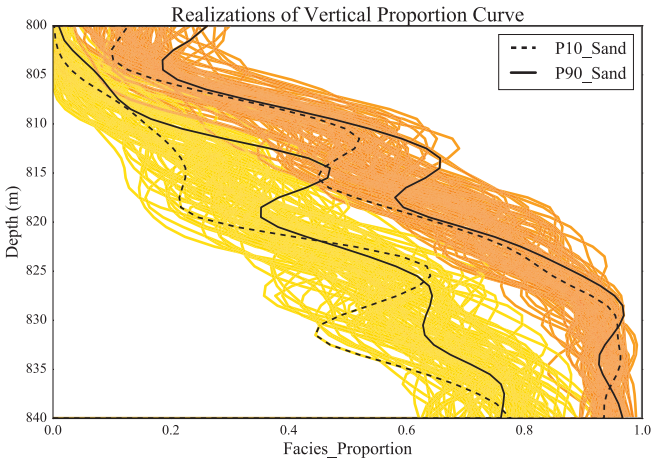

Figure 2.4: Multiple realizations of a vertical proportion curve.

2.2.2 Posterior Proportion Uncertainty

Realistic posterior uncertainty for a categorical variable is obtained by considering the prior proportion uncertainty in the geostatistical modelling workflow. The prior proportion uncertainty does not consider the effect of the conditioning data and domain size. The spatial bootstrap only accounts for the data configuration and the spatial correlation between data locations. In case of having a stationary covariance function/variogram, the

variance in the proportions of a categorical variable based on statistical resampling can be derived as:

$$P_k = E\{I(k)\} = \frac{1}{n}\sum_{\alpha=1}^{n} I(\mathbf{u}_\alpha; k), \quad k = 1, ..., K \tag{2.6}$$

$$E\{P_k\} = P_k, \quad k = 1, ..., K$$

$$Var\{P_k\} = E\{P_k^2\} - P_k^2 = E\{\frac{1}{n^2}\sum_{\alpha=1}^{n}\sum_{\beta=1}^{n} I(\mathbf{u}_\alpha; k)I(\mathbf{u}_\beta; k)\} - P_k^2$$

$$= \frac{1}{n^2}\sum_{\alpha=1}^{n}\sum_{\beta=1}^{n} E\{I(\mathbf{u}_\alpha; k)I(\mathbf{u}_\beta; k)\} - P_k^2 = \frac{1}{n^2}\sum_{\alpha=1}^{n}\sum_{\beta=1}^{n} C(\mathbf{u}_\alpha - \mathbf{u}_\beta; k)$$

$$= \frac{C(0;k)}{n} + \frac{1}{n^2}\sum_{\alpha=1}^{n}\sum_{\beta=1}^{n} C(\mathbf{u}_\alpha - \mathbf{u}_\beta; k), \quad \alpha \neq \beta$$

where $C(0;k) = Var\{I(\mathbf{u};k)\} = P_k(1-P_k)$

$$= \frac{P_k(1-P_k)}{n} + \frac{1}{n^2}\sum_{\alpha=1}^{n}\sum_{\beta=1}^{n} C(\mathbf{u}_\alpha - \mathbf{u}_\beta; k), \quad \alpha \neq \beta$$

Considering independent data: $n = n_{eff}$

$$\Rightarrow Var\{P_k\} = \frac{P_k(1-P_k)}{n_{eff}}, \quad k = 1, ..., K$$

where n is the number of sampled data, P_k is the proportion of category k, $I(\mathbf{u}_\alpha; k)$ is the indicator variable for category k at data location $\mathbf{u}_\alpha$ and $C(\mathbf{u}_\alpha, \mathbf{u}_\beta; k)$ is the covariance between two data locations for the k category. Based on Equation 2.6, n_{eff} refers to the number of independent data that are separated by distances larger than variogram ranges. The number of effective data depends on the spatial configuration of data and the spatial continuity.

$$Var\{P_k\} = \frac{P_k(1-P_k)}{n_{eff}} = \frac{1}{n^2}\sum_{\alpha=1}^{n}\sum_{\beta=1}^{n} C(\mathbf{u}_\alpha - \mathbf{u}_\beta; k) \tag{2.7}$$

$$n_{eff} = \frac{n^2}{\sum_{\alpha=1}^{n}\sum_{\beta=1}^{n}\frac{C(\mathbf{u}_\alpha - \mathbf{u}_\beta; k)}{P_k(1-P_k)}}$$

$$\Rightarrow n_{eff} = \frac{n^2}{\sum_{\alpha=1}^{n}\sum_{\beta=1}^{n}\rho(\mathbf{u}_\alpha - \mathbf{u}_\beta; k)}$$

where $\rho(\mathbf{u}_\alpha - \mathbf{u}_\beta; k)$ is the indicator correlation function. As shown in Equation 2.7 and also from experimental results, the prior parameter uncertainty associated with proportions increases as the variogram range increases and in turn the number of independent or effective data reduces. This is not the real space of uncertainty because the effect of conditioning data and finite domain limits are not considered. Passing the prior proportion uncertainty through a geostatistical modelling workflow provides posterior uncertainty that is narrower and more realistic by applying the conditioning data and domain size. Realizations of the trend model can be integrated into the geostatistical modelling workflow as an input parameter to obtain the posterior uncertainty.

The trend realizations are used one at a time for each realization of the final facies model. The quantified prior parameter uncertainty based on the proposed methodology could also be integrated into other categorical variable modelling techniques including object based, multiple point statistics (MPS) and truncated pluri-Gaussian (Armstrong et al., 2003).

2.2.3 Checking the Proposed Methodology for Facies Proportion Uncertainty

An experimental setup is developed to check the methodology proposed above. This setup measures the uncertainty in global proportions of a categorical variable by searching a library of reference images for a comparable situation of conditioning data. The experimental setup includes the following steps:

I Generating a library of reference images for a categorical variable with different trend models.

II Considering a set of sampled data at limited locations and searching through the images to find matching data.

III Sampling a defined domain of interest around each matching pattern and calculating the actual uncertainty in global proportions.

IV Implementing the proposed methodology to quantify prior parameter uncertainty that is represented as multiple realizations of the trend model.

V Integrating the prior parameter uncertainty into the categorical modelling workflow to get conditional realizations of the domain of interest and posterior uncertainty.

VI Comparing the measured uncertainty against the posterior uncertainty from the proposed methodology.

As the number of sampled data (n) and the number of categories (K) increases the chance of finding sufficient matching patterns within a library of reference images goes down. In this context, there are K^n possible patterns for the sampled data. In order to make it computationally plausible, 16 sampled data for a categorical variable with two categories (i.e., a binary case) are considered. A repository of reference images is generated based on multiple trend models because it is possible to find matched patterns in different reference images with different underlying trend models. Using a range of trend models provides a more realistic space of uncertainty. Figure 2.5 shows four examples of the reference images and their corresponding trend models.

In this experiment, a binary categorical variable with two facies of Sand and Shale is considered. As can be seen in Figure 2.5, the trend models are vertical proportion curves and the challenge for is to infer a representative VPC based on limited sampled data. All the reference 2D images are considered to be cross sections with a total height of 16 m and a vertical resolution of 1 m. The number of sampled data is limited to 16 from a single vertical well that samples the entire elevation (Figure 2.6). Also, the trend models are considered to represent

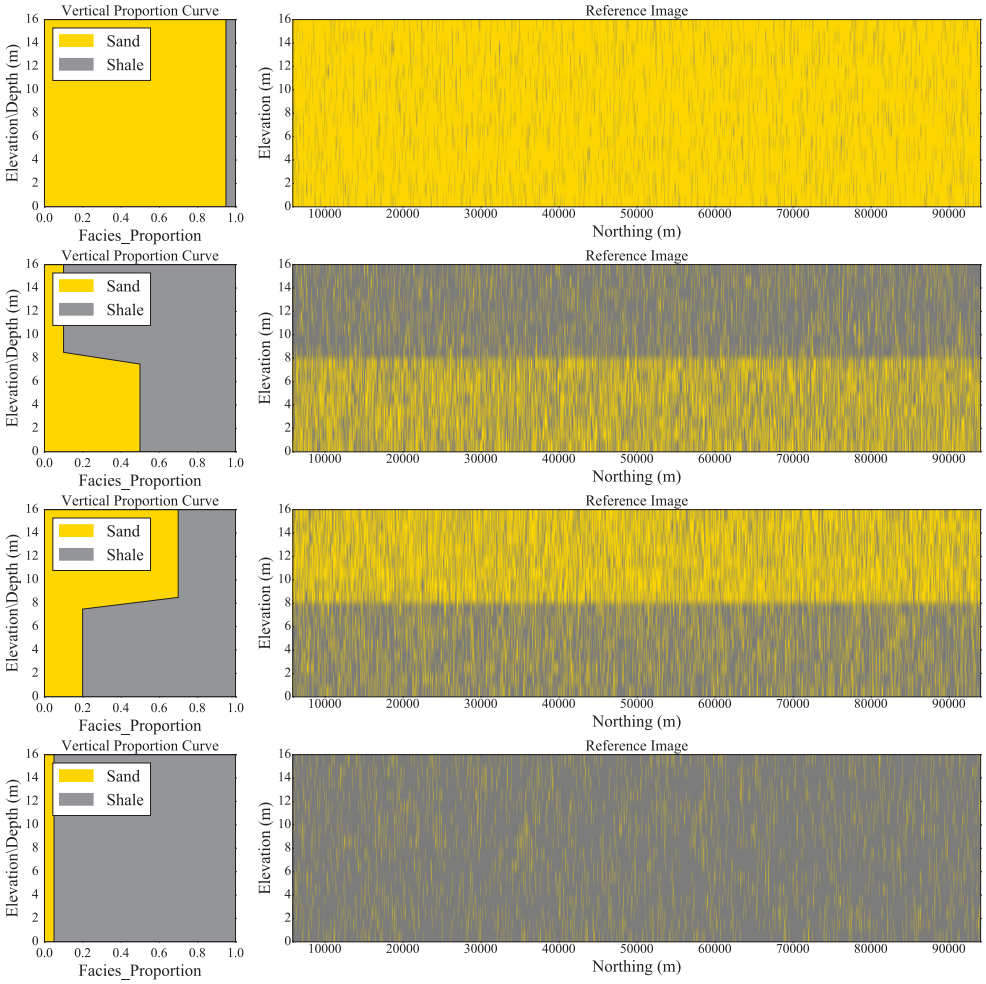

Figure 2.5: Some of the reference images and their corresponding trend models.

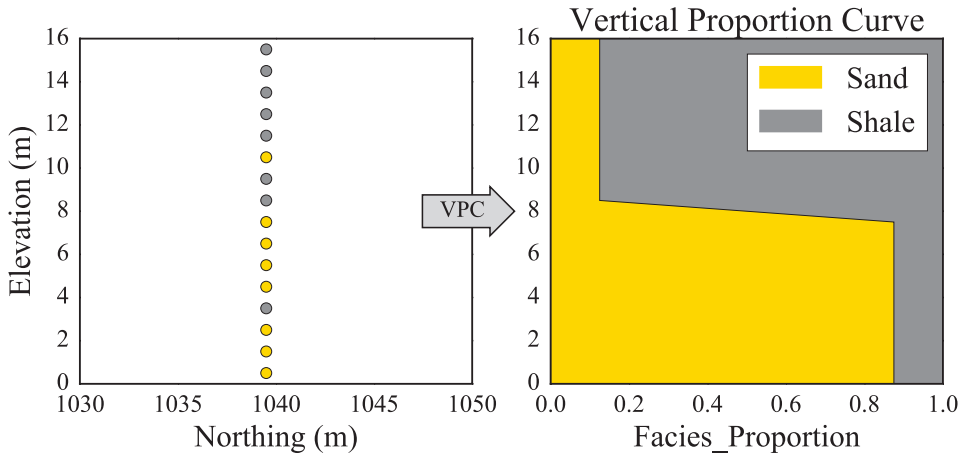

Figure 2.6: Sample data and inference of a representative VPC.

different proportions for the top and bottom half of the elevation. This makes it possible to infer a VPC even with one well. Figure 2.6 shows an example of sampled data and the VPC inferred based on the sampled data.

The proportions of facies for the top and bottom half of the VPC model vary from 5% to 95%. Each reference VPC model is generated by considering different proportions for the top and bottom half. A repository of 121 reference images based on different VPC models are generated. Figure 2.5 shows four examples of these reference images. Also, in order to remove the uncertainty associated with the spatial continuity, the same indicator variogram model is used for all the reference images. Figure 2.7 shows the standardized indicator variogram used for the experimental setup.

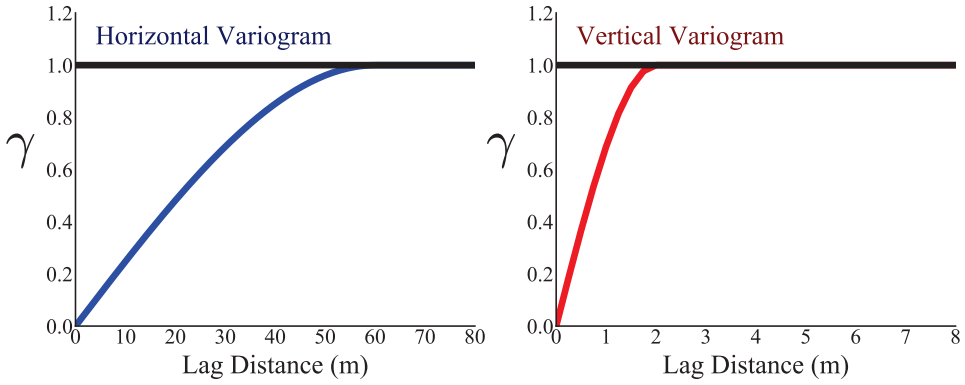

Figure 2.7: Indicator variogram used for the experimental setup.

The next step is to consider a set of sampled data and scan through the ensemble of reference images to find matching patterns. Then, consider a domain of interest around the patterns and calculate the global proportion for the categorical variable. This provides multiple possible domains that include the same data patterns. Thus, it is possible to calculate the global proportion and find the overall uncertainty in its distribution. Figure 2.8 shows an example of sampled data and some of the matched cases found by scanning through the ensemble of reference images. A domain of interest can be defined and the proportion calculated to define the distribution of uncertainty. For the sampled data shown in Figure 2.8, the distribution of global proportions based on scanning reference images is shown in Figure 2.9.

The next step is to implement the proposed methodology to estimate proportion uncertainty for the sampled data. First, the prior parameter uncertainty in presence of trends is quantified. This is automated with software that utilizes the proposed methodology of spatial bootstrap based on unconditional indicator simulation at data locations. The trend model is a VPC based on a simple averaging window because of the simplicity of the experimental setup. Figure 2.10 represents the prior parameter uncertainty for the sampled data shown in Figure 2.8 based on 1000 spatial bootstrap realizations.

As seen in the summary statistics in Figures 2.9 and 2.10, the prior uncertainty is higher than the one calculated by scanning the reference images. This is expected because the spatial bootstrap does not account for the conditioning of the data and the finite limits of the domain of interest. Thus, it is required to integrate the prior

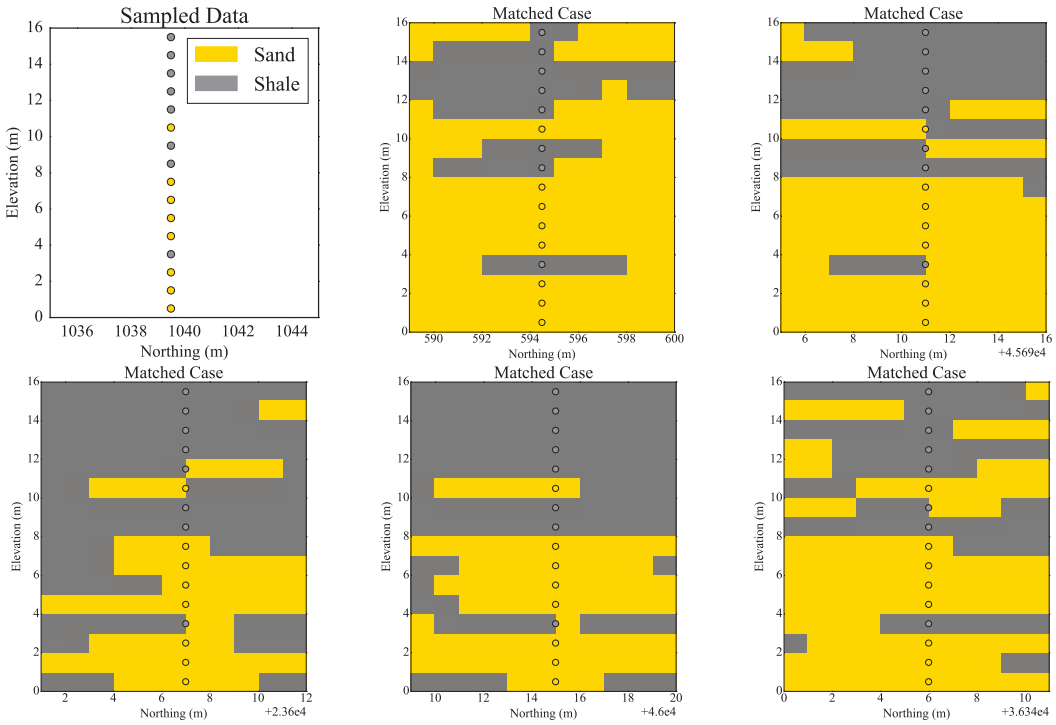

Figure 2.8: An example of sampled data and some of the matched cases found by scanning through the library of reference images.

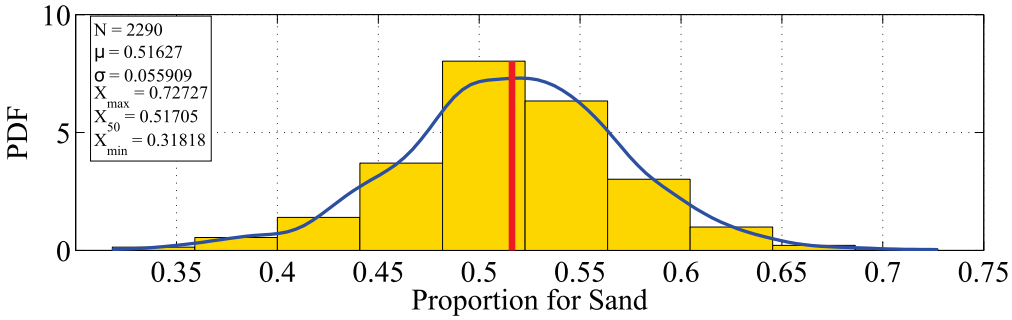

Figure 2.9: Uncertainty in proportions through scanning library of reference images.

parameter uncertainty into the geostatistical modelling in order to obtain the posterior uncertainty. Geostatistical simulation of the categorical variable for the domain of interest is executed for each realization of the trend model. In this context, each realization of the prior parameter uncertainty corresponds to one final realization of the categorical model for the domain of interest. Figure 2.11 shows an example final simulated realization of the categorical variable for the domain of interest.

Figure 2.12 shows the posterior proportion uncertainty for the sampled data (Figure 2.8). As can be seen in Figure 2.12, the uncertainty is reduced and close to the result of image scanning. This is due to the effect of conditioning and finite domain limit. This process is repeated for many cases with different sampled data

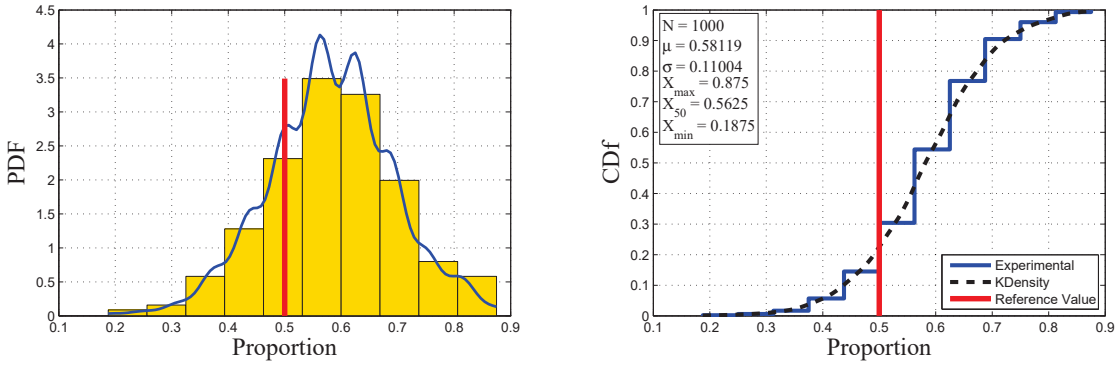

Figure 2.10: Prior proportion uncertainty for Sand quantified by the proposed implementation of the spatial bootstrap (2290 matches were found).

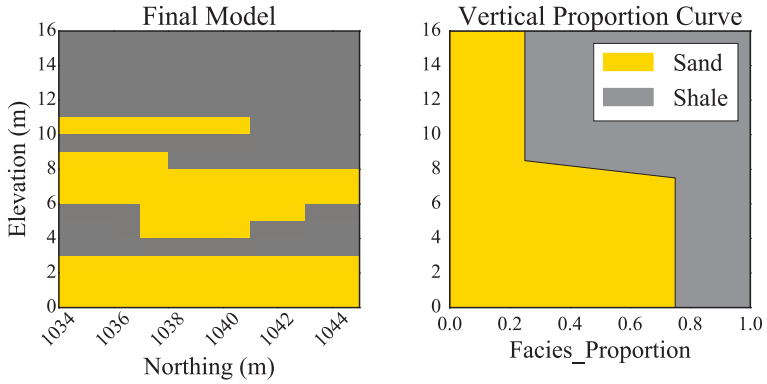

Figure 2.11: An example final realization after geostatistical modelling and the corresponding realization of VPC.

patterns and also domain size. This provides more experimental results to evaluate the proposed methodology by comparing the quantified posterior uncertainty with the one measured through scanning the reference images. Figure 2.13 shows this comparison. The quantified uncertainty in proportions of the categorical variable is highly correlated with the experimental results. Based on the findings of the experimental setup, it is concluded that the overall framework is reasonable.

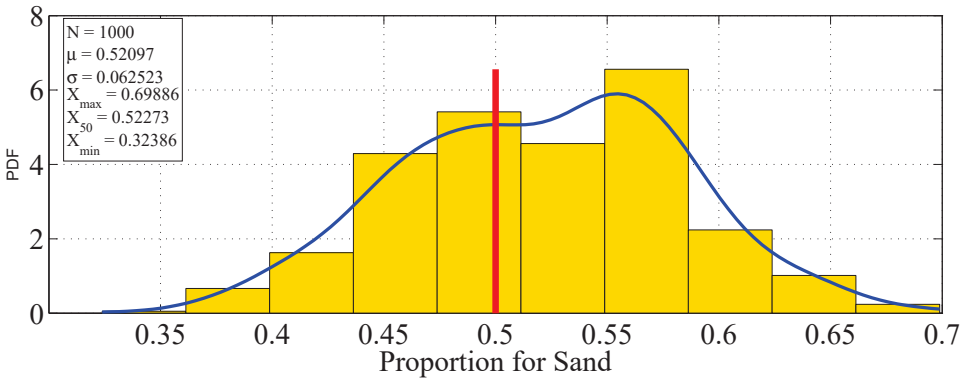

Figure 2.12: Posterior proportion uncertainty.

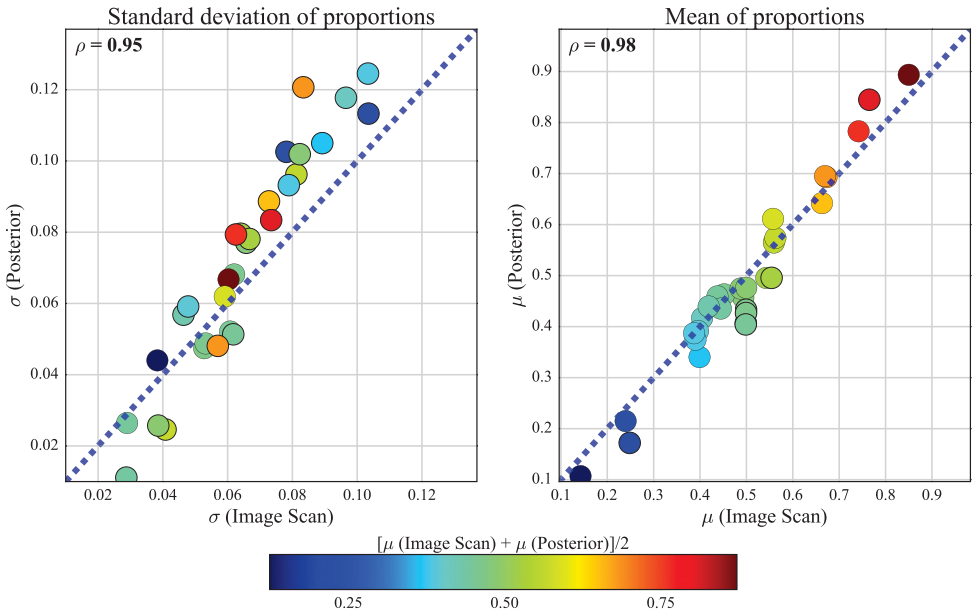

Figure 2.13: Checking the result of multiple experiments.

Considering Figure 2.13, on the right hand side plot, the proportions are very close to the 45 degree line; however, there is a minor conditional bias where high proportions in the image are even higher in the posterior model. The points on the left hand side showing the standard deviations are colored by their proportions. There are low and high proportions for all ranges of standard deviation. It is clear that the posterior standard deviation is slightly higher than image scan results in most cases. This is a conservative result, that is, higher uncertainty. It is believed that this is due to model boundaries where the image scan considers a larger domain; therefore, leading to slightly lower uncertainty.

The proposed methodology for quantifying prior proportion uncertainty is implemented by a computer program. The main input parameters are the indicator variogram models along with the sampled facies/categorical data. The result is represented either as realizations of the global proportions or realizations of the trend model based on modelling preferences. This can be easily implemented into any facies simulation technique to transfer the prior proportion uncertainty to the geostatistical models and the posterior uncertainty.

2.2.4 Improved Sampling of Proportion Uncertainty

Geostatistical simulation is based on Monte Carlo sampling (MCS) of the space of uncertainty and generating multiple realizations. The question of how many realizations depends on the aspect of uncertainty being quantified and the required precision (Pyrcz and Deutsch, 2014). For proportion uncertainty, the spatial bootstrap is based on MCS of a joint multivariate space of uncertainty characterized by proportions of categories/facies. In order to have a uniform sampling of the proportion uncertainty at limited data locations, it is required to generate many realizations. This becomes more critical in case of having sparse sampled data. The spatial bootstrap is

implemented by unconditional simulation at data locations. Thus, generating a large number of them is not computationally expensive. However, only a limited number of realizations can be processed through subsequent geostatistical modelling for resource estimation and performance evaluation. The challenge is to uniformly sample the multivariate parameter uncertainty with a limited number of realizations. Thus, it is required to improve sampling of the proportion uncertainty with limited number of spatial bootstrap realizations. Latin hypercube sampling (LHS) is a technique that improves uniform sampling of univariate distributions based on stratifying the CDF (McKay, 1992). Because true randomness is not perfectly uniform and stratification improves uniform sampling of the univariate distribution (Deutsch and Deutsch, 2012). Neither MCS nor LHS consider multivariate uniformity in the sampling process. Deutsch and Deutsch (2012) proposed an extension of LHS for multivariate models based on a realization elimination algorithm that increases multidimensional uniformity (LHSMDU). This methodology is based on generating a sampling matrix for a large number of realizations and removing close ones until reaching the required number of realizations. Consider N variables that are to be realized L times. The sampling matrix required for the stochastic simulation is an $L \times N$ matrix consisting of uniform random numbers in [0, 1]. The CDF for each variable ($F(x_i)$) is then sampled by the random numbers to generate L realizations. LHSMDU is based on generating an $ML \times N$ sampling matrix that is M times bigger than required, then eliminate the realizations with the smallest average Euclidean distance (D_{ij}).

$$\text{Sampling Matrix} = \begin{bmatrix} F(x_1)_1 & \dots & F(x_N)_1 \\ . & . & . \\ . & . & . \\ . & . & . \\ F(x_1)_L & \dots & F(x_N)_L \end{bmatrix} \quad F(x_n)_l \in [0,1] \tag{2.8}$$

$$D_{ij} = \sqrt{\sum_{n=1}^{N} (F(x_n)_i - F(x_n)_j)^2} \quad i,j = 1, ..., L$$

where $x_n, \quad n \in [1, N]$ is a variable that needs to be realized, $l \in [1, L]$ denotes the realization number and D_{ij} is the multivariate statistical distance between two realizations. The Euclidean distance provides a measure of similarity for realizations and is commonly used in multivariate statistics (Johnson and Wichern, 2002). In order to impose multidimensional uniformity for correlated variables, LHSMDU uses Cholesky LU decomposition (Tanabe and Sagae, 1992) of the covariance matrix between variables in Gaussian units. However, a covariance function that is a measure of linear relationship is not capable of characterizing complex multivariate relationships. A methodology is proposed based on post-processing of stochastic realizations to improve multidimensional uniformity and in turn realization efficiency. PPMT (Barnett et al., 2014) is used to transfer realizations of different variables/properties into a multivariate uncorrelated Gaussian framework. The Euclidean distance between realizations in Gaussian units is affected by the distribution density. Thus, realizations located in high density regions of the multivariate distribution are deemed to be more similar to each other. To

address this problem, after PPMT transformation, each realization is transformed to the [0, 1] uniform distribution using the standard Gaussian CDF. Afterwards, Euclidean distances can be used to form a licit dissimilarity matrix and eliminate realizations with the smallest mean Euclidean distance. The objective here is to improve uniform sampling of a multivariate space of uncertainty with a limited number of realizations. In this context, the prior proportion uncertainty is sampled with a large number of spatial bootstrap realizations and then they are post-processed and a limited number of them are selected that efficiently represent the multidimensional space of uncertainty. The proposed methodology can be used in the geostatistical simulation workflow as a post-processing tool to improve the selection of realizations going forward to more expensive geostatistical modeling and post-processing.

To implement the improved sampling, the first step is to generate a large number of spatial bootstrap realizations, say $B = M \times L$, where L is the final number of realizations selected from B number of realizations that is M times more than L. The next step is to calculate the multidimensional statistical distances between each realization and others (i.e., D_{ij}). For proportion uncertainty, the proportions of different categories/facies define the dimensions of the space of uncertainty and the statistical distances are calculated as:

$$D_{ij} = \sqrt{\sum_{k=1}^{K} (P(k)_i - P(k)_j)^2} \quad i, j = 1, \ldots, B \tag{2.9}$$

where $P(k)$ is the proportion of each category and K is the number of categories. This yields a symmetric $B \times B$ matrix of statistical distances that may be interpreted as a dissimilarity matrix. An iterative elimination algorithm removes realizations with smallest average distance from others. The initial large number of realizations are assumed to provide a reasonably uniform sampling of the space of uncertainty and the elimination process aims to keep a limited number of realizations with large minimum statistical distances. However, the distances must be calculated in a uniform multidimensional space. This is achieved by PPMT followed by standard Gaussian CDF transformation. Figure 2.14 shows an example of 1000 realizations characterized by two variables (i.e., two dimensions) in original units. As can be seen in Figure 2.14c, the uniform bivariate/bi-dimensional space can be used to calculate the statistical distances and implement the elimination process to keep a limited number of realizations.

Consider the example shown in Figure 2.14. The initial pool of 1000 realizations are characterized by the two variables and the corresponding bivariate relationship. The proposed smart selection transfers realizations into a uniform space where the statistical distance can be used to select a limited number of realizations. However, if the statistical distance is calculated in original units (naive approach), the elimination process is biased due to nonuniform probability distribution. Figure 2.15 compares the proposed smart selection method versus the naive approach for selecting a limited number of realization (100) from an initial pool of realizations (1000).

As can be seen in Figure 2.15, the smart selection method preserves the bivariate relationships and effective sampling of the initial pool of realizations with a limited number of realizations. The proposed smart selection

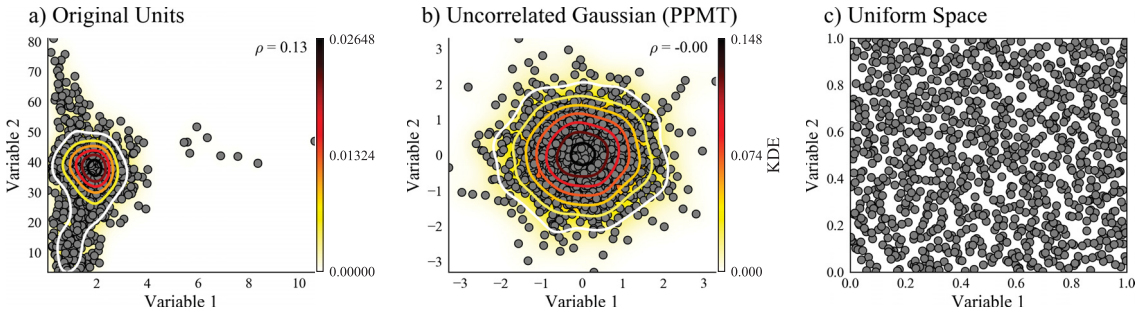

Figure 2.14: Improved selection of realizations in a uniform multidimensional space.

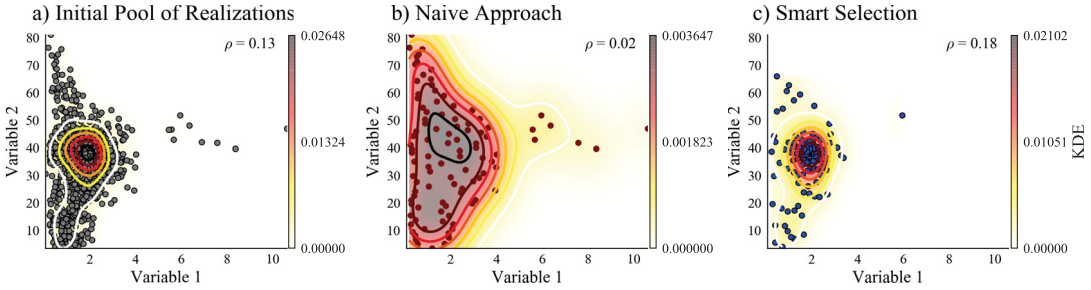

Figure 2.15: A comparison between naive approach and the proposed smart selection method.

methodology for realization elimination is as follows:

- Step 1: Generate $B = M \times L$ realizations based on the multivariate spatial bootstrap where L is the target number of limited realizations and M is a multiplier.
- Step 2: Identify variables that characterize the multivariate parameter uncertainty.
- Step 3: Transform the realizations to remove the complex relationships between variables. PPMT can be used to transfer realizations to an uncorrelated standard Gaussian framework.
- Step 4: Transfer each variable independently to $[0, 1]$ distribution using the standard Gaussian CDF.
- Step 5: For each realization, calculate the Euclidean distance (D_{ij}) to all other realizations in the uniformly distributed framework. This provides a symmetric $B \times B$ distance matrix.
- Step 6: For each realization, find the two smallest calculated distances (i.e., two nearest neighbour realizations) and calculate the average of the two distances.
- Step 7: Eliminate the realization with smallest average distance calculated in step 6.
- Step 8: Return to step 6 and iteratively eliminate realizations until only L realizations remain.

In step 6, the two nearest neighbors are considered to decide which realization needs to be eliminated. Considering only the nearest neighbor results in identifying pairs of realizations for elimination. Figure 2.16

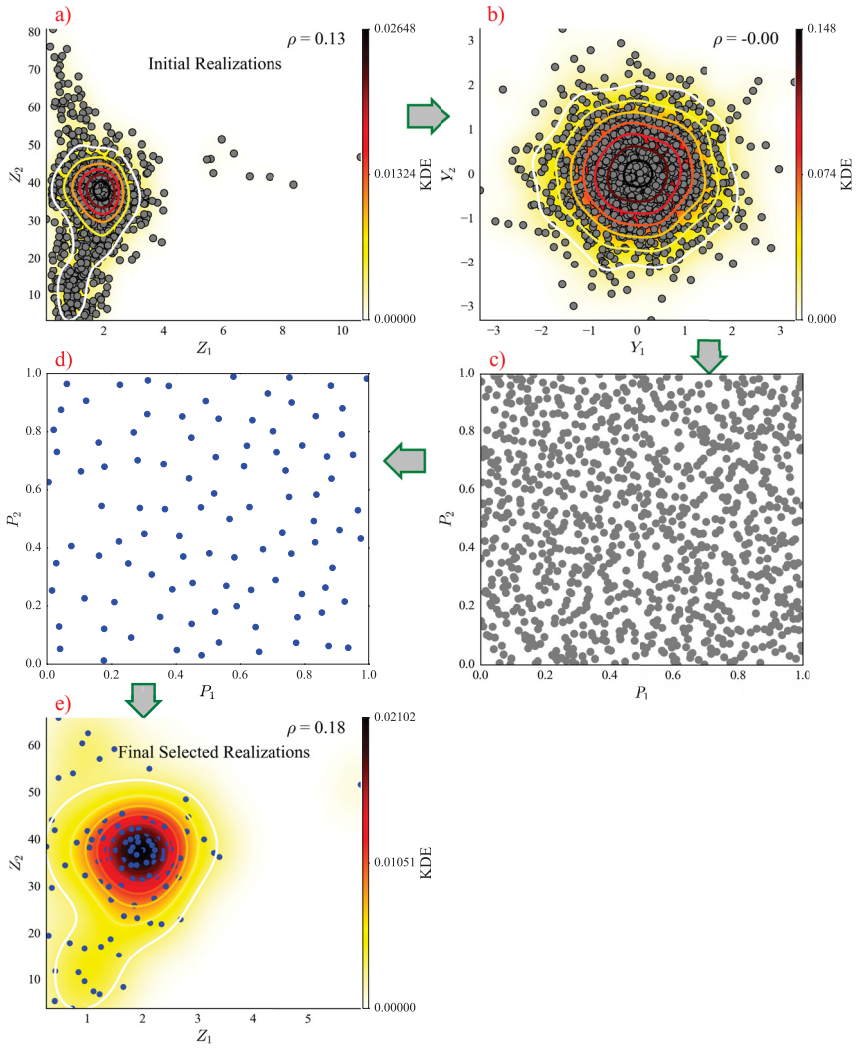

Figure 2.16: Steps of the proposed methodology to improve uniform sampling of a space of uncertainty.

demonstrates how the proposed elimination algorithm is implemented to uniformly sample a bivariate space of uncertainty. As mentioned above, this methodology is employed as a post-processing tool to improve multi-dimensional uniform sampling. Figure 2.16 shows 1000 initial realizations of two variables that characterize the bivariate distribution. PPMT transfers realizations into an uncorrelated bivariate standard Gaussian frame work (Figure 2.16b). After PPMT, the transformed variables are independent and have standard Gaussian marginal distribution. For the iterative elimination process, it is required to transfer the realizations into a uniform multivariate distribution; otherwise, the sampling process is biased. This is done by independent transformation of each variable to the [0,1] uniform distribution using the standard Gaussian CDF as is shown in Figure 2.16c. Afterwards, the elimination process is implemented until reaching to the desired number of realizations.

The proposed methodology for multi-dimensional uniform sampling was checked by a simple case study that employs this methodology for uniform sampling of multivariate parameter uncertainty. In this regard, four

synthetic wells are generated to provide data for three facies including Sand, Mixed and Shale as shown in Figure 2.17. The objective of this case study is to compare the proposed methodology of selecting a limited number of spatial bootstrap realizations (i.e., smart selection) with random generation (i.e., random selection). The spatial bootstrap quantifies the prior parameter uncertainty by considering data configuration and the spatial correlation. This is done by unconditional sequential indicator simulation at data locations based on indicator variogram inferred from available data and a base-case trend model that is a VPC for this case study as shown in Figure 2.18.

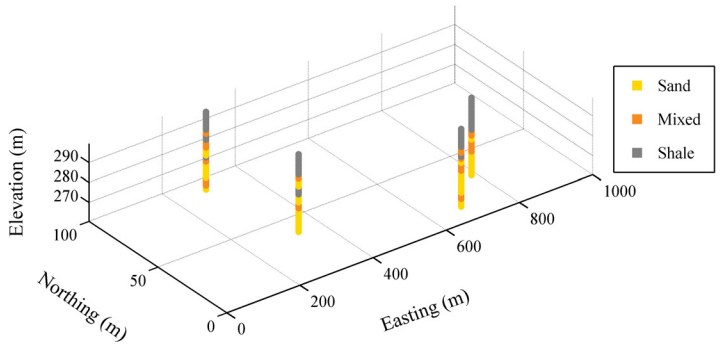

Figure 2.17: Synthetic well data for the first case study.

In this case study, each realization is characterized by the global proportions of the three facies. Although the proportions sum to 1, it is required to consider all three proportions as the components/dimensions of the multivariate parameter uncertainty. The constraint is removed after PPMT and transformation to the Gaussian CDF values. A reference model of multivariate parameter uncertainty is quantified by generating 100000 SBS realizations of the global proportions. Both the smart and random selection method are applied to generate limited number of realizations ranging from $L = 10$ to 1000. For each number of realizations the experiment was repeated for 500 trials to make the comparison over the average/expected results. In this case study, the smart selection was done by generating $B = M \times L$ realizations where M was taken to be 10. For instance, if the target is to select 100 final spatial bootstrap realizations, 1000 realizations are generated and the elimination algorithm is employed to select the final 100 realizations with maximized minimum statistical distance.

$$D_{ij} = \sqrt{\sum_{n=1}^{3} (P(n)_i - P(n)_j)^2} \quad i,j = 1,\ldots,10L \tag{2.10}$$

$P(1) =$ Proportion of Sand

$P(2) =$ Proportion of Mixed

$P(3) =$ Proportion of Shale

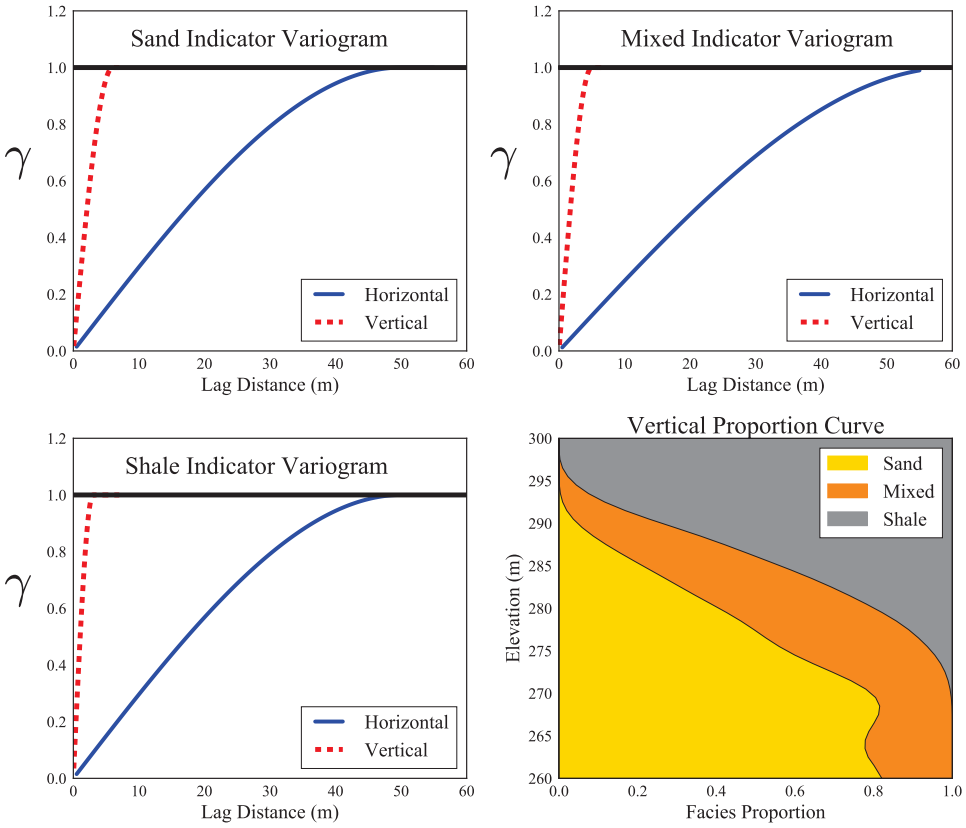

Figure 2.18: Indicator variograms and base-case trend model for the case study.

The spatial bootstrap is based on stochastic simulation and the reference model of the parameter uncertainty was generated independently by considering a different seed for the pseudo random number generator. However, both smart selection and random selection cases share the same seed or sequence of random numbers for each trial. This provides a reliable framework for the comparison. Figure 2.19 shows the multivariate parameter uncertainty for the reference case that is characterized by proportions of Sand, Mixed and Shale facies.

In order to study the sampling of the multivariate proportion uncertainty, a scaler parameter was defined that is a function of all three proportions. The scaler parameter is similar to original oil in place ($OIIP$) that provides a measure of resources.

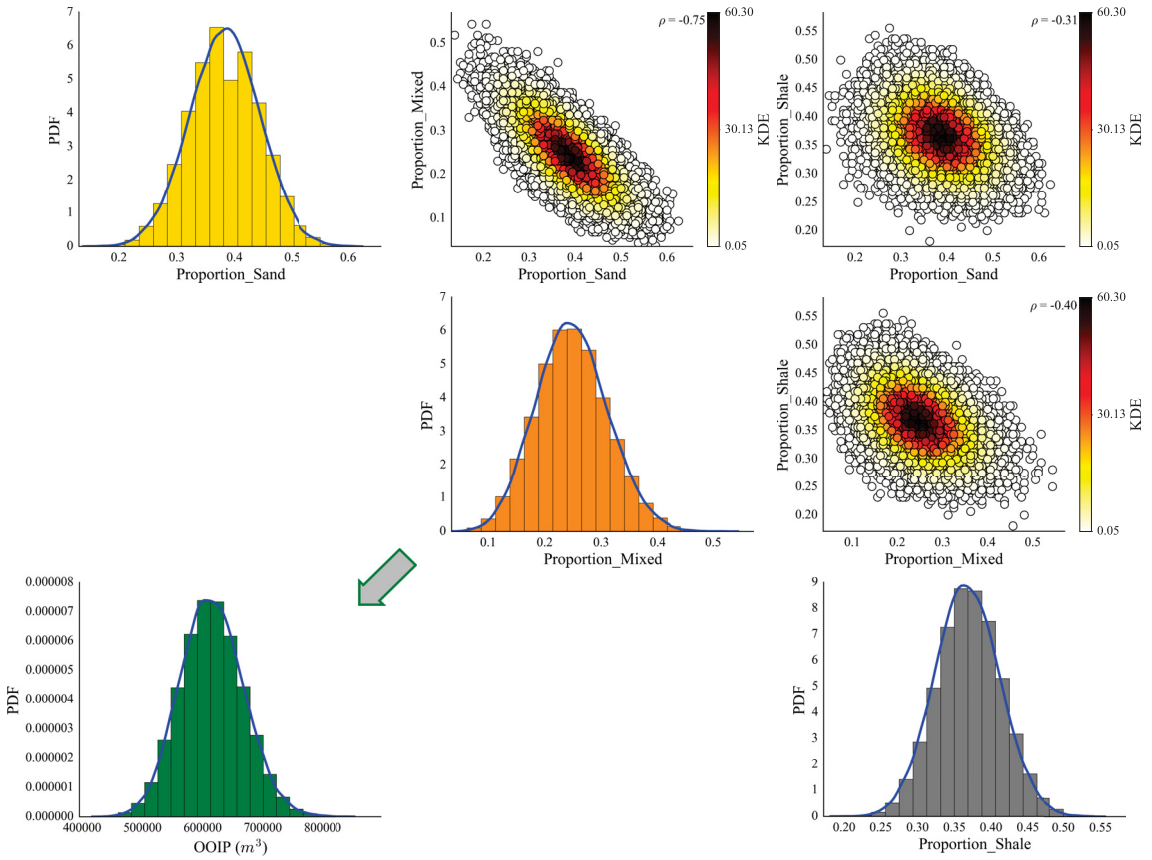

Figure 2.19: The multivariate space of proportion uncertainty and the distribution of the scaler parameter ($OOIP$) for the first case study.

$$\phi = P(1)\phi_{Sand} + P(2)\phi_{Mixed} + P(3)\phi_{Shale} \tag{2.11}$$
$$Sw = P(1)Sw_{Sand} + P(2)Sw_{Mixed} + P(3)Sw_{Shale}$$
$$OOIP = AT \times (1 - Sw)\phi$$

where ϕ and Sw are the equivalent porosity and water saturation calculated based on the proportions of facies. In this context, porosity and water saturation within each facies were considered to be $\phi_{Sand} = 0.35$, $\phi_{Mixed} = 0.2$, $\phi_{Shale} = 0.05$, $Sw_{Sand} = 0.05$, $Sw_{Mixed} = 0.3$ and $Sw_{Shale} = 0.4$. $OOIP$ is calculated for a reservoir with the given thickness and area of the deposit, $T = 40\ m$ and $A = 100000\ m^2$ respectively. The multivariate space of proportion uncertainty can be translated into a univariate distribution of $OOIP$. The SBS realizations of $OOIP$ generated by both approaches are compared against the reference 100000 realizations. In order to evaluate the relative power of the proposed approach, a statistical measure similar to Kolmogrov-Smirnov D (KSD) statistic was used (Deutsch and Deutsch, 2012). This measure, e is given by:

$$e = max|F^{-1}_{Reference}(q) - F^{-1}_{Selected}(q)| \quad q = 0.1, 0.2, \ldots, 0.9 \tag{2.12}$$

where q is the quantile value and F is the cumulative distribution function. The measure e is not dimensionless like the D statistic, but is useful for comparing the two sampling methods. The lower the e, the higher the probability that the two distributions are sampled from the same pool. The statistical measure was calculated for 500 trials and the expected/average values was considered to compare the smart selection versus random selection. Figure 2.20 shows how the proposed smart selection and the random selection perform in light of being compared to a reference distribution of $OOIP$ that was quantified by exhaustive spatial bootstrap realizations. As can be seen in Figure 2.20, the proposed selection of realizations performs better compared to the conventional random selection. 100 smartly selected realizations are equivalent to more than 200 randomly selected realizations.

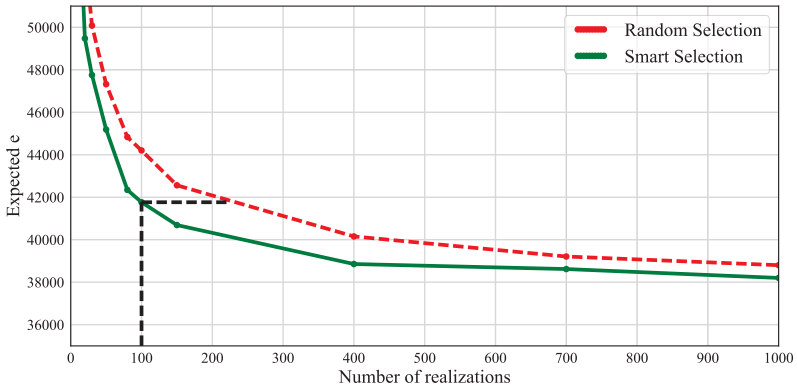

Figure 2.20: Comparing the distribution of ($OOIP$) for the two approaches against the reference case.

2.3 Multivariate Parameter Uncertainty for Continuous Variables

Geostatistical reservoir modelling provides subsurface characterization of multiple continuous petrophysical properties that can be used to inform technical tasks such as resource estimation, flow simulation and production forecasting. These tasks are often impacted by interactions between different properties. Geostatistical modelling aims to reproduce multivariate relationships that are often complex (Barnett and Deutsch, 2015a). Modelling of petrophysical properties relies on input statistical parameters. The most important parameter is the univariate distribution or histogram. In presence of sparse data, inferring this parameter is subject to uncertainty that can be quantified by statistical resampling similar to proportion uncertainty. However, in a multivariate modelling framework, the parameter uncertainty needs to reproduce the relationships between different properties. A methodology is proposed and checked for quantification of prior multivariate parameter uncertainty associated with multivariate distribution of continuous variables. This is done by multivariate transformation followed by univariate spatial bootstrap. A realistic model of histogram uncertainty is obtained in two steps. The

multivariate spatial bootstrap is the first step as it only accounts for data configuration and the spatial correlation. The second step is effective integration of the prior parameter uncertainty in the multivariate geostatistical reservoir modelling.

2.3.1 Quantifying Prior Multivariate Parameter Uncertainty

The first step is to quantify the prior joint multivariate parameter uncertainty by statistical resampling. This calls for unconditional multivariate simulation at data locations to generate multiple realizations of sampled data that respect the data configuration, multivariate relationships and the spatial model of continuity. One approach is co-simulation of multiple variables under an assumption of multivariate Gaussianity and using the linear model of coregionalization (LMC) (Goovaerts, 1997). This may be applied by Cholesky decomposition (Wilkinson, 1965) of the covariance matrix and implementing unconditional LU simulation (Khan and Deutsch, 2015; Tanabe and Sagae, 1992). Based on the conventional approach, variables are assumed to be multivariate Gaussian after univariate transformation that is not correct for most geological settings (Barnett, 2015). Being based on the assumption that the relationships between geological variables are linear, this approach is not capable of capturing complex relationships. In addition, developing a full LMC for more than three variables is tedious and quite challenging. Recent developments in multivariate geostatistical modelling motivate the idea of using multivariate transformation techniques to transfer data to a multivariate Gaussian framework (Barnett, 2015; Leuangthong and Deutsch, 2003; Silva and Deutsch, 2015a). The Gaussian space is mathematically tractable and can be fully parameterized by a mean vector and a covariance matrix.

In this research, multivariate statistical resampling is implemented by PPMT followed by independent univariate spatial bootstrap for each transformed variable. The homotopic observations of multiple continuous variables are transformed to an uncorrelated multivariate Gaussian distribution and the PPMT back-transformation information are recorded. Subsequently, the spatial bootstrap is done by unconditional sequential Gaussian simulation at data locations (Silva and Deutsch, 2015b). This only requires the data configuration (i.e., spatial coordinates) and a model of spatial variability that comes from independent variogram calculation and modelling for each variable. This is equivalent to unconditional LU simulation. The main advantage over LU is that it is capable of considering large data sets with high resolution sampling down wells. The variograms may be calculated and modeled based on PPMT transformed data; however, it is recommended to calculate and model the variograms after independent univariate normal score transformation because, this yields a better variogram reproduction after back-transformation (Barnett and Deutsch, 2015a). Finally, independently simulated Gaussian values at the data locations (i.e., spatial bootstrap realizations) are transformed to original units based on the same PPMT back-transformation information to get the prior multivariate parameter uncertainty. Since facies usually provide the stationary domains for modelling of continuous petrophysical properties, it is not likely required to quantify the join multivariate parameter uncertainty in presence of a trend. It should be noted that in case of unequally sampled reservoir properties, multivariate imputation needs to be considered prior to the

multivariate spatial bootstrap (Barnett and Deutsch, 2015b). This results in multiple imputed realizations of the data and each realization may be used as a reference multivariate distribution for the subsequent statistical resampling. The proposed methodology of multivariate spatial bootstrap can be summarized in three main steps:

1. Multivariate transformation using PPMT and storing the back-transformation table
2. Variogram calculation and modelling for the spatial model of variability
3. Univariate spatial bootstrap by unconditional sequential Gaussian simulation at the data locations
4. Back-transformation to the original units to reproduce the multivariate relationships inferred from data

The proposed methodology was checked by a predecessor approach based on LU simulation and full LMC (Khan and Deutsch, 2015) that is referred to as the conventional approach. The LMC yields the correct results in a multivariate Gaussian framework where the distributions are parameterized by the mean vector ($\boldsymbol{\mu}$) and covariance matrix (Σ) as is expressed in Equation 2.13.

$$\mathcal{N}(\mathrm{X};\boldsymbol{\mu},\Sigma) = \frac{1}{(\sqrt{2\pi})^d|\Sigma|^{\frac{1}{2}}}\exp[-\frac{1}{2}(\mathrm{X}-\boldsymbol{\mu})^T\Sigma^{-1}(\mathrm{X}-\boldsymbol{\mu})] \tag{2.13}$$

where d is the number of variables or the dimension of X and $|\Sigma|$ is the determinant of the covariance matrix. In a simple case study, a 2D bivariate Gaussian model is generated using sequential Gaussian simulation (SGS) (Manchuk and Deutsch, 2012) that provides a reference model to sample homotopic observations of two variables. This is necessary to assure that the conventional approach based on LMC provides the correct results. The two variables share the same model of spatial variability (i.e., the same direct omni-directional variogram) and the spatial bivariate relationship is characterized by a cross variogram as shown in Figure 2.21.

Figure 2.22 shows the sampled data along with the marginal and bivariate distributions. Note that with homotopic measurements of different variables, the amount of parameter uncertainty for one variable is not affected by the other ones. This can be explained in a simple bivariate estimation example. When the two variables are not highly correlated to each other the effect of one variable in estimation of the other ones is undermined due to the screening effect (Pyrcz and Deutsch, 2014) and if they are highly correlated they are somewhat redundant. In this context, the multivariate relationships are the mutual constraints for homotopic variables that need to be reproduced by the multivariate statistical resampling. Thus, univariate analytical solutions for uncertainty in mean and number of independent data is still a valid criteria in order to check the spatial bootstrap. Equation 2.13 shows the analytical solution to find the variance of the first order moment (i.e., mean) for the distribution of a regionalized random variable ($Z(\mathbf{u})$) that is characterized by n sampled data (Khan and Deutsch, 2015).

$$\begin{aligned}\bar{Z} &= E\{Z\} = \frac{1}{n}\sum_{\alpha=1}^{n} Z(\mathbf{u}_\alpha) \\ Var\bar{Z} &= \frac{1}{n^2}\sum_{\alpha=1}^{n}\sum_{\beta=1}^{n} C(\mathbf{u}_\alpha-\mathbf{u}_\beta) = \bar{C} = \frac{\sigma^2}{n_{eff}}\end{aligned} \tag{2.14}$$

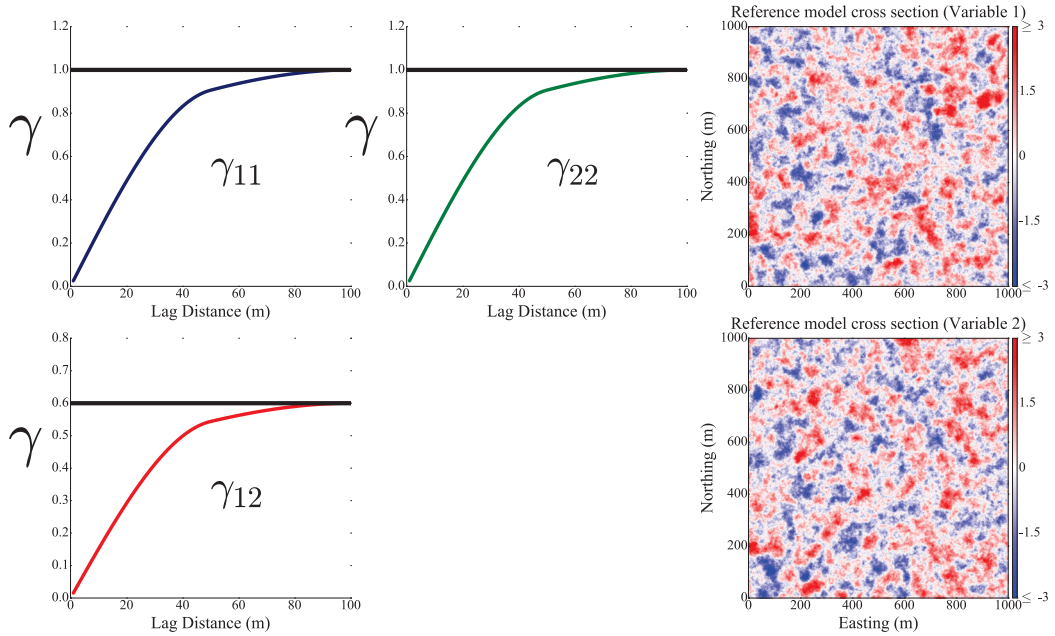

Figure 2.21: The reference bivariate Gaussian model and the corresponding variograms (model of spatial variability).

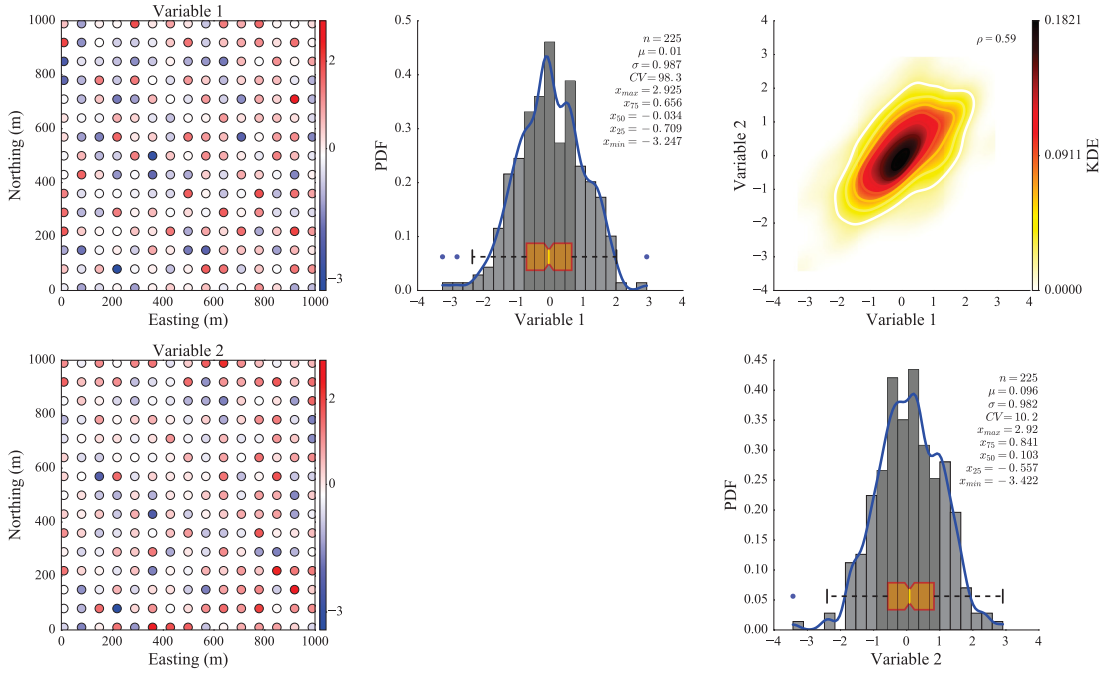

Figure 2.22: Sampled data from a bivariate Gaussian model.

where $\bar{Z}$ is the mean of the random variable Z, $C(\mathbf{u}_\alpha - \mathbf{u}_\beta)$ is the covariance between two data locations, $\bar{C}$ is the average covariance between data locations and σ is the standard deviation of the variable. Similar to proportion uncertainty, n_{eff} refers to the number of independent data that depends on the ranges of spatial continuity and data configuration.

$$n_{eff} = \frac{n^2}{\sum_{\alpha=1}^{n} \sum_{\beta=1}^{n} \rho(\mathbf{u}_\alpha - \mathbf{u}_\beta)} \tag{2.15}$$

where $\rho(\mathbf{u}_\alpha - \mathbf{u}_\beta)$ is the correlation coefficient between two data locations characterized by the variogram models. The proposed and the conventional spatial bootstrap approach can be checked against each other and also cross validated by the analytical solution. In this regard, each approach was used to generate a total number of 10000 spatial bootstrap realizations based on which the distribution of the mean was evaluated as a measure of the parameter uncertainty. Figure 2.23 compares the distribution of the mean for the two approaches and as can be seen, the distribution of the mean is the same for the two approaches.

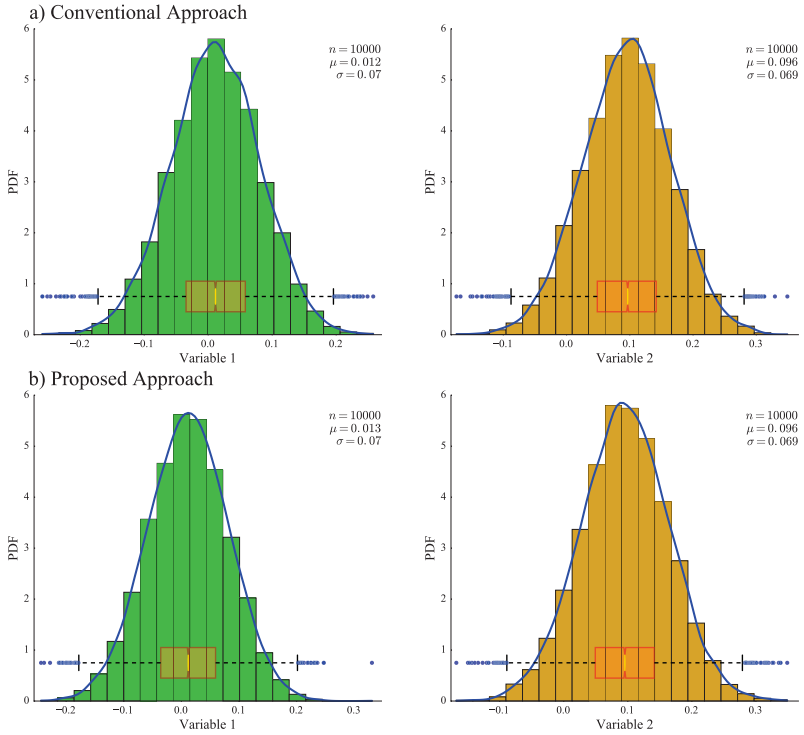

Figure 2.23: Parameter uncertainty represented as the distribution of the mean for the conventional and proposed approach.

Based on the analytical solution for this case study, the number of independent data is found to be 198.0 while the total number of sampled data is 225. Considering the range of the variograms (Figure 2.21), 100 m and the data spacing (Figure 2.22), 70 m the number of independent data is found to be lower than the total number of data due to the redundancy of the data. Table 2.1 compares the variance of the mean value based on the approaches against the analytical solution (Equation 2.14 and 2.15). The errors are related to the difference between the calculated variance and the one quantified by each method. The underestimation error is colored by shades of blue where the dark blue is the highest error. As can be seen in Table 2.1, both approaches match with the analytical solution with slight deviations.

Table 2.1: Comparing the variance for the mean values for the two methodologies and the analytical solution.

Variable	Analytical	Conventional	Proposed	Error_Conventional (%)	Error_Proposed (%)
Variable 1	0.0701	0.0696	0.0699	-0.782	-0.324
Variable 2	0.0697	0.0693	0.0687	-0.708	-1.499

2.3.2 Integration of Prior Multivariate Parameter Uncertainty to Geostatistical modelling

The prior multivariate parameter uncertainty is represented by multiple realizations of the sampled data that reproduce the same data configuration, model of spatial variability and multivariate relationships that are inferred from the original sampled data. Using a multivariate transformation technique like PPMT makes it possible to reproduce complex relationships between variables. Also, using PPMT makes the modelling easier because each variable can be modeled/simulated independently and in a Gaussian framework after the transformation. In this research, the prior multivariate parameter uncertainty is integrated into the geostatistical reservoir modelling as the reference multivariate distributions for PPMT transformation. The transformation is regraded as a pre-processing step for the subsequent geostatistical simulation of each transformed variable that is often done using SGS. When parameter uncertainty is not considered, the transformation (PPMT) is executed once for the original sampled data and all the SGS realizations are generated conditioned to the same transformed data. In order to integrate parameter uncertainty, for each SGS realization, the transformation is executed separately to transform the sampled data using a separate reference multivariate distribution that is a realization of sampled data from the joint prior multivariate uncertainty. This is followed by the back-transformation to the original units using the corresponding PPMT back-transformation table. In this way, each realization of SGS is conditioned to a multivariate spatial bootstrap realization.

2.4 Conclusions

Inferring input statistical parameters based on limited data is subject to uncertainty. Accounting for parameter uncertainty can improve the resource estimation and reservoir management. In this chapter, a methodology is introduced for accurate quantification of facies proportion uncertainty. The spatial bootstrap is implemented by unconditional indicator simulation at data locations and using two statistical parameters including model of spatial variability (i.e., indicator variograms) and a base-case trend model. This provides the prior proportion uncertainty that can be represented either by multiple realizations of global proportions or trend models. It should be noted that if there is uncertainty associated with inference of the variogram models or the trend model, it can be integrated into the spatial bootstrap. Rezvandehy (2016) proposed a workflow to quantify the variogram uncertainty that results in multiple realizations of the variogram model. In this context, each spatial bootstrap realizations is generated using a separate realization of the indicator variogram models. Also, if there are alternative geological frameworks that require different trend models, the same approach may be employed. The prior proportion uncertainty can be integrated into any geostatistical facies modelling technique to obtain

realistic posterior proportion uncertainty. Figure 2.24 summarizes the workflow for integration of proportion uncertainty in geostatistical modelling.

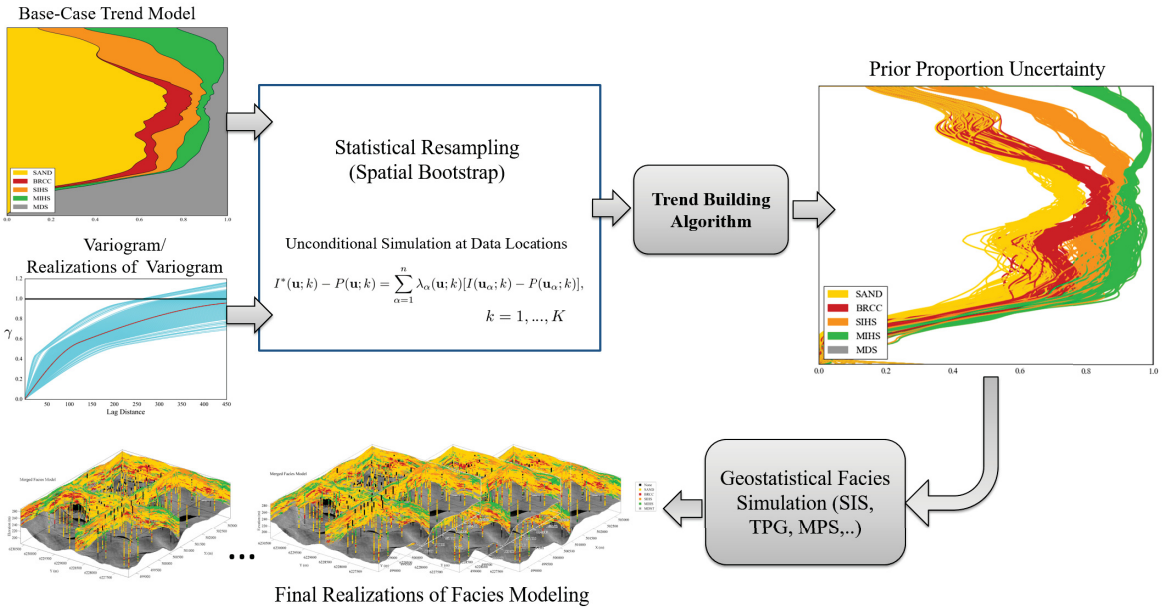

Figure 2.24: A flow chart to explain the proposed methodology for quantification and integration of proportion uncertainty.

The posterior proportion uncertainty depends on three main factors: spatial correlation (i.e., variogram), conditioning data and domain size. The prior proportion uncertainty that is quantified by the spatial bootstrap is not affected by the domain size or the conditioning effect of data. However, the subsequent geostatistical simulation accounts for these two factors. If the domain size increases while the others are fixed, the posterior uncertainty increases. If the number of conditioning data increases while the other factors are fixed, the posterior uncertainty goes down. The spatial continuity that is quantified by the range of the variograms has a mixed effect on proportion uncertainty. A large range of spatial continuity results in independent data that increases the prior proportion uncertainty. At the same time, the conditioning effect of data is increased due to the higher range of spatial continuity. Thus, depending on the size of the domain and the number of conditioning data, increasing the variogram range may increase or decrease the final posterior uncertainty. In practice, there is a complex interaction between all three factors and the proposed methodology provides a framework to account for all contributing factors.

The use of soft secondary data such as seismic is of great importance in facies modelling. Virtually all categorical variable simulation techniques allow for integration of secondary data. Thus, the final facies model would include such data by construction. As local conditioning to hard data updates the uncertainty of the spatial bootstrap, updating to local soft data would further update the uncertainty to account for more data. Thus, it is not required to include secondary data in the spatial bootstrap. There is, of course, a transition between soft and hard data that could be important. The technique presented in this chapter is aimed at a spatial bootstrap at hard

data locations. However, it could potentially be expanded to include soft data.

The experimental setup presented in this chapter validates the proposed methodology based on reference proportion uncertainty. In addition, a smart selection methodology is proposed for uniform sampling of the prior proportion uncertainty with a limited number of spatial bootstrap realizations. The multivariate modelling of petrophysical properties are often conducted within facies. A geostatistical tool is introduced for quantification of multivariate histogram uncertainty for continuous petrophysical properties within facies. In the next chapter, a case study is presented to demonstrate the practical implementation of the proposed methodology and geostatistical tools introduced in this chapter.

Chapter 3

Practical Integration of Facies Proportion Uncertainty in Modelling

Chapter 2 presents a methodology for integration of facies proportion uncertainty in geostatistical reservoir modelling. Figure 3.1 shows a flow chart that summarizes this methodology. The provided plots in Figure 3.1 are schematic and not intended to be readable. A case study is presented in this chapter to demonstrate the application of the proposed two-step methodology in facies modelling. The first step is the accurate quantification of prior proportion uncertainty in presence of a trend. This is followed by integrating the prior proportion uncertainty in geostatistical facies modelling to obtain a realistic model of proportion uncertainty. For this case study, real well data from a petroleum reservoir are used to generate an inventory of 100 vertical wells that sample facies and petrophysical properties including porosity, shale volume, permeability and water saturation. After integration of proportion uncertainty in facies modelling, the multivariate histogram uncertainty is quantified for petrophysical properties within facies and integrated in multivariate geostatistical modelling.

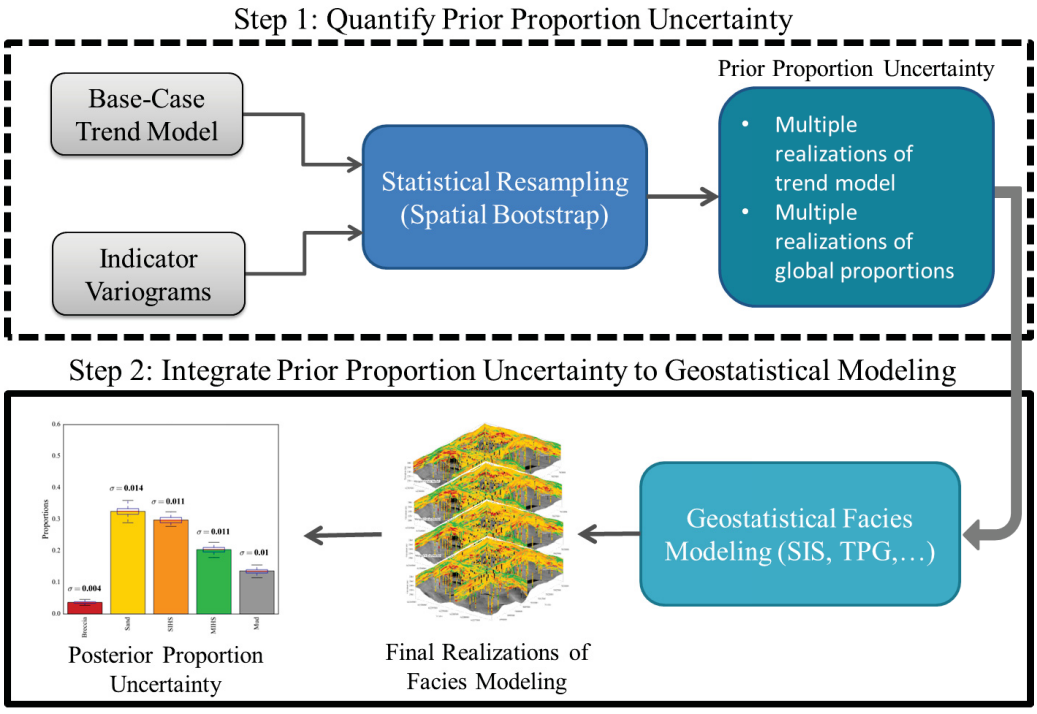

Figure 3.1: Workflow for integration of facies proportion uncertainty in geostatistical reservoir modelling (Hadavand and Deutsch, 2017).

3.1 Case Study

3.1.1 Well Data Inventory

A collection of 100 wells based on actual well data are used for this case study. There are five facies: Breccia, Sand, SIHS, MIHS and Mudstone that belong to a fluvial-estuarine deposit. Figure 3.2 shows the sampled well data.

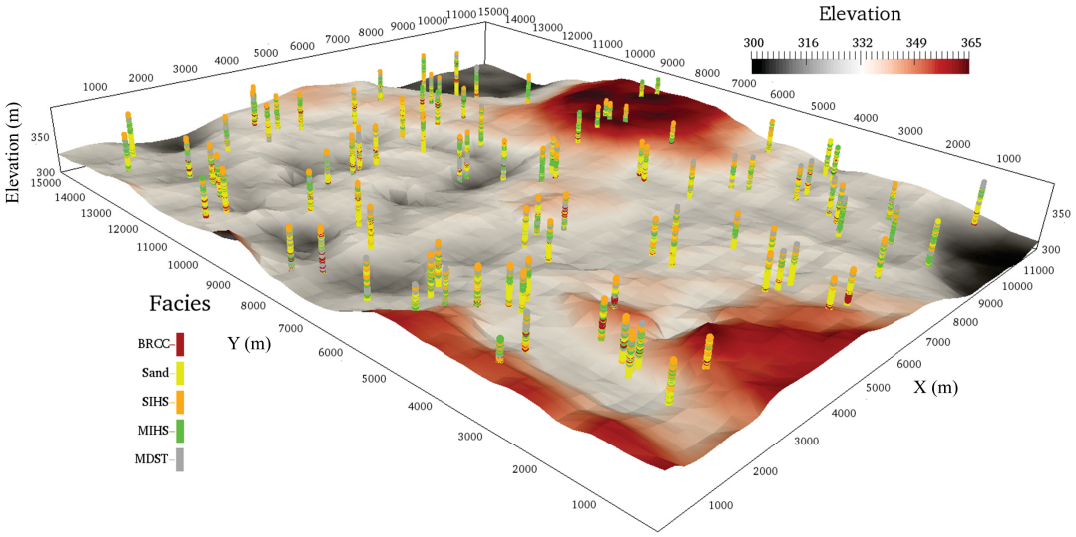

Figure 3.2: Sampled well data for facies.

The wells are sampled with high resolution in the vertical direction. For geomodelling, they are upscaled to $0.5\ m$ intervals. Figure 3.3 shows some examples of well logs at the original and geomodelling scale after stratigraphic transformation. The blue color highlights the bottom of the reservoir where the formation was deposited on top of the Devonian evaporates and carbonates.

Along with the sampled facies data there are well log measurements of four continuous petrophysical properties: porosity, shale volume, permeability and water saturation. Figure 3.4 shows two example well log plots.

3.1.2 Prior Facies Proportion Uncertainty

The first step is to quantify the prior proportion uncertainty in presence of a trend. This is automated using a computer program (SBS_Categorical, Appendix A) that implements the statistical resampling based on unconditional sequential indicator simulation at data locations. As described in Chapter 2, the statistical resampling follows the model of spatial variability quantified by the indicator variogram models. The local geological settings may be characterized by a base-case trend model that provides a locally varying model of proportions for the unconditional indicator simulation at data location. In this way, the prior proportion uncertainty is quantified in presence of a trend. The experimental indicator variograms are calculated based on sampled data in the three major directions. Figure 3.5 shows the calculated experimental indicator variogram and the fitted model for

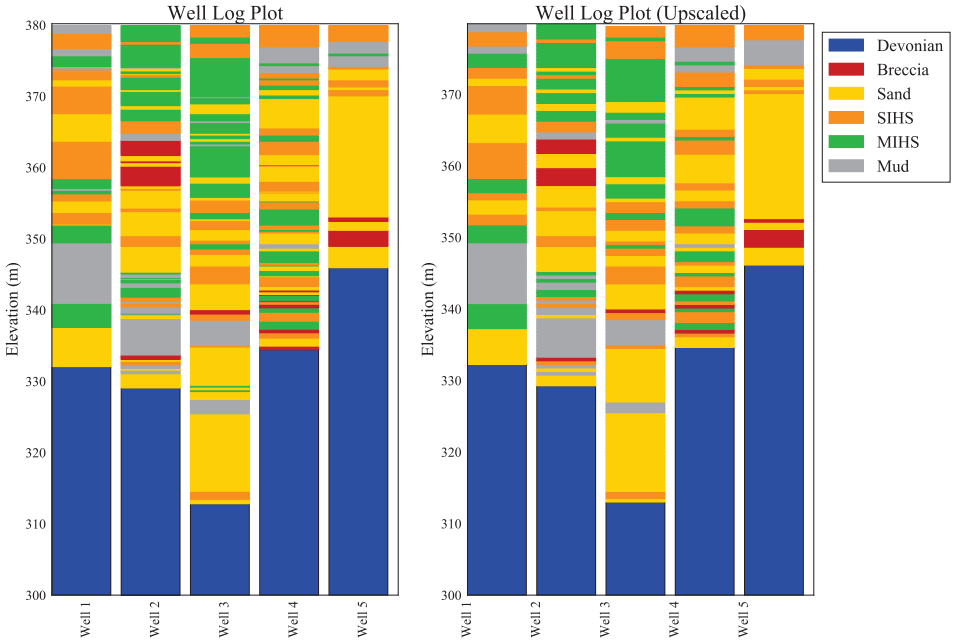

Figure 3.3: Well log plots after stratigraphic transformation.

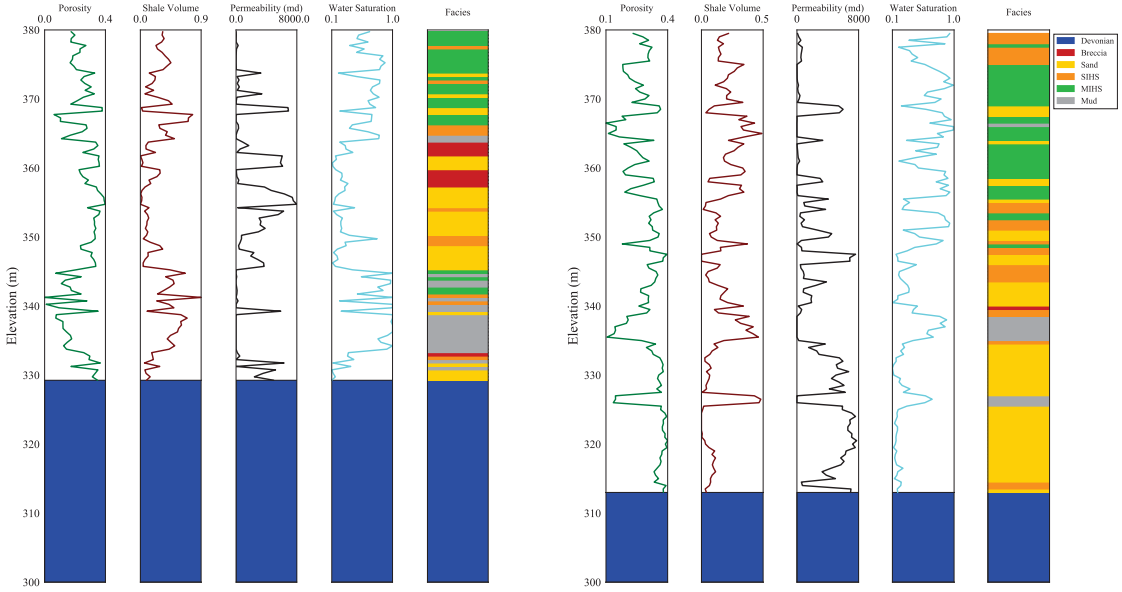

(a) Well 2 (b) Well 3

Figure 3.4: Two examples of well log plots for facies and petrophysical properties.

the Sand facies. Figure 3.6 shows the base-case 3D trend model and the corresponding VPC inferred based on sampled facies data and calculated using the TBA.

The spatial bootstrap is implemented to generate 100 realizations of the sampled data that respect the model of spatial variability and a base-case trend model. These realizations are processed by the TBA to generate multiple realizations of the trend model that represent the prior proportion uncertainty. Figure 3.7 shows 100 realizations

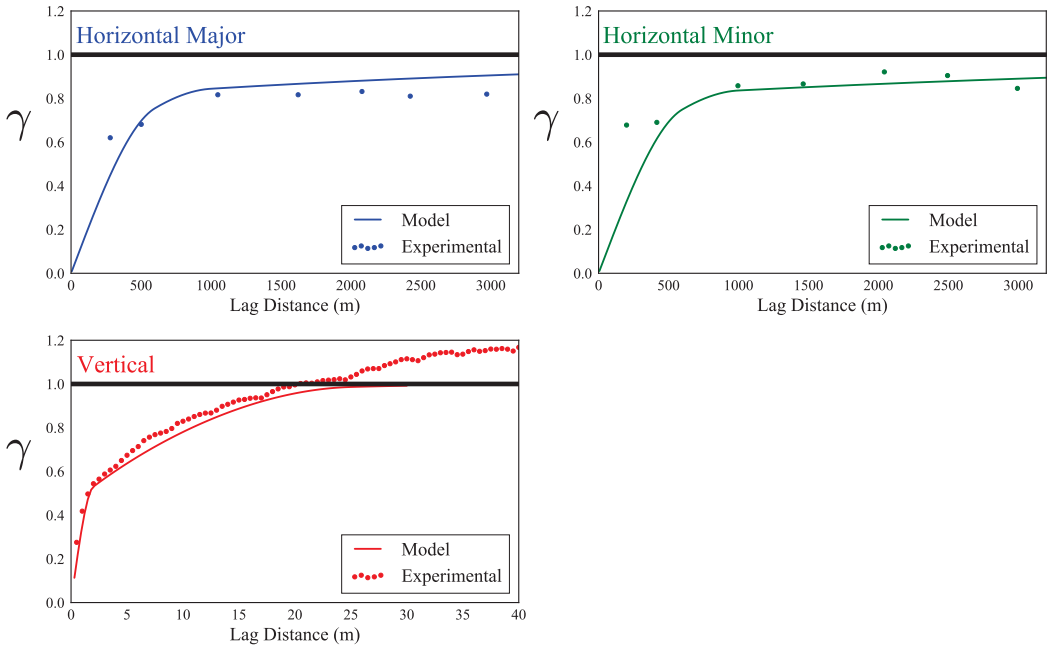

Figure 3.5: Experimental indicator variogram and its model for Sand facies.

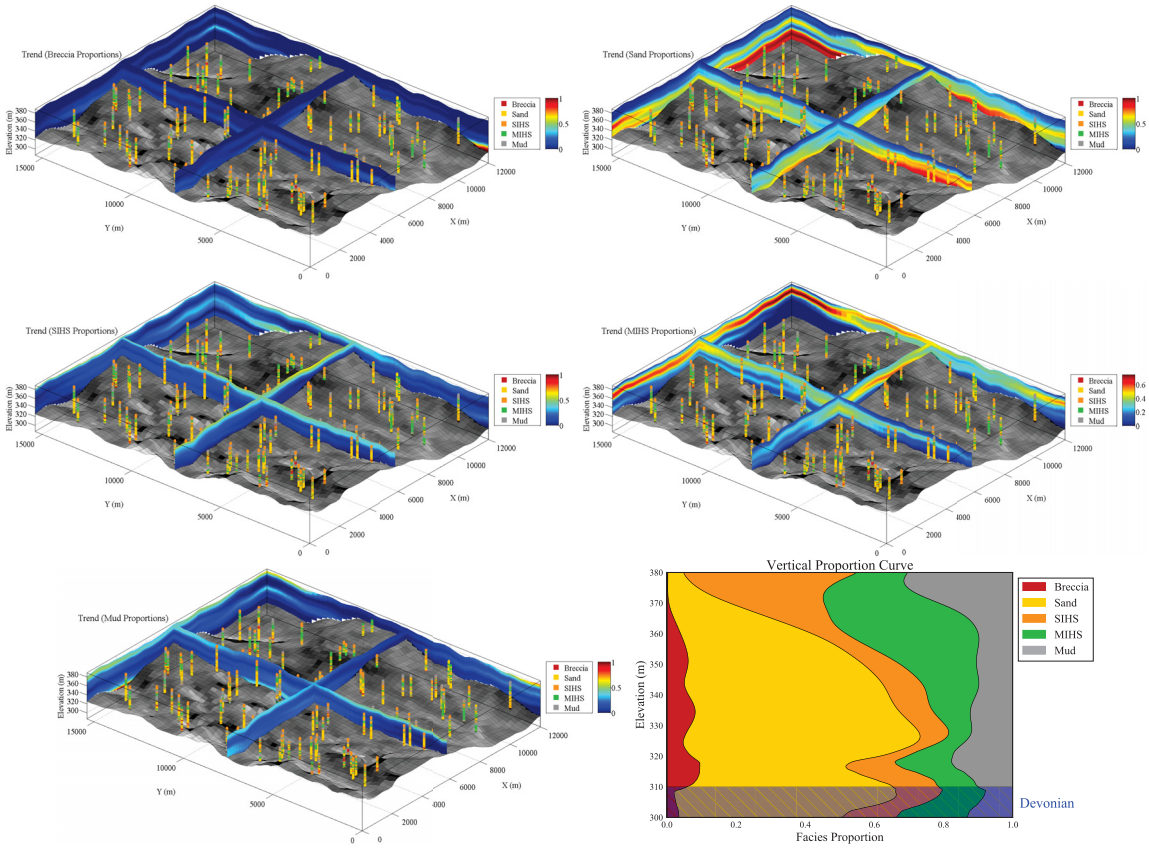

Figure 3.6: The base-case 3D trend models and the corresponding vertical proportion curve.

of the VPC to provide a better understanding of the prior uncertainty in the 3D trend model. The colored lines in Figure 3.7 represent the cumulative proportions and the space in between them determines the proportion of each category. In this context, the red line shows the proportion of Breccia while the yellow represents proportion of Sand plus Breccia. The P_{10} and P_{90} realizations of the trend model are highlighted based on the global proportion of Sand. Since the trend model accounts for both the declustering weights and also reservoir limits, the global proportion of facies are assessed through averaging the trend model. The realizations of the trend model are a means to transfer the prior proportion uncertainty to the subsequent geostatistical facies simulation.

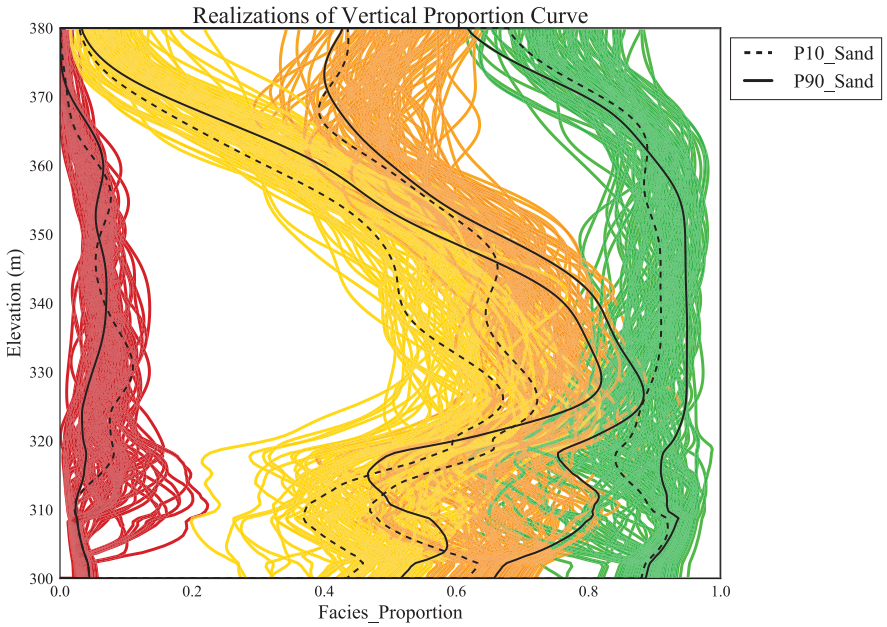

Figure 3.7: Realizations of the trend model (VPC).

3.1.3 Posterior Facies Proportion Uncertainty

The geostatistical modelling of facies is often performed by considering the same underlying global proportions or a trend model for all the realizations; however, as explained in Chapter 2, when this input statistical parameter is inferred from limited data, it is subject to uncertainty. In the first step, multiple realizations of the trend model are generated that represent the prior proportion uncertainty. The second step is to integrate this prior uncertainty in the geostatistical facies modelling to obtain a realistic model of proportion uncertainty. Each final geostatistical realization uses a different realization of the trend model. This approach can be implemented by different facies simulation techniques. In this case study, SIS is employed to simulate the spatial distribution of facies within the reservoir. Figure 3.8 shows some examples of final facies realizations for the case study. The reader is encouraged to zoom in on the electronic version of this document.

The realizations shown in Figure 3.8 are conditioned to the same original well data but, the input trend model is different for each realizations. While the indicator simulation accounts for local uncertainty conditioned to

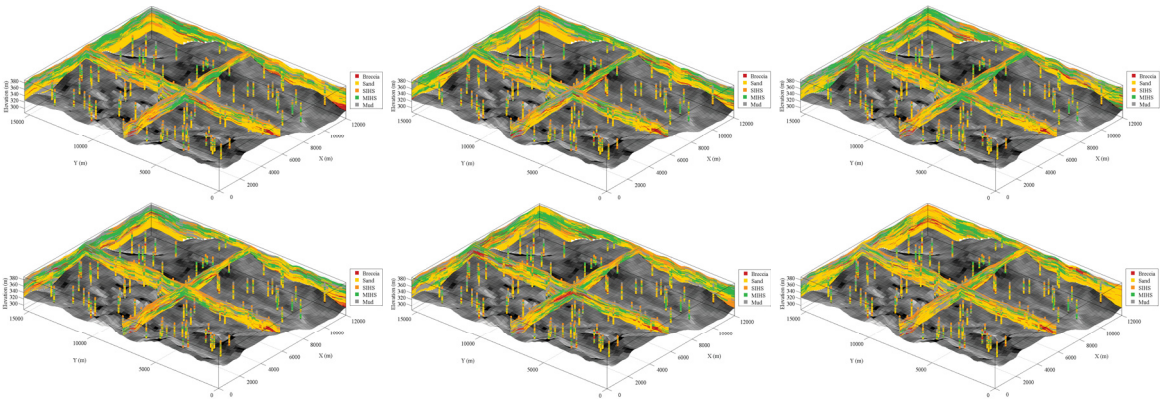

Figure 3.8: Some examples of final facies realizations for the case study.

sampled data and delineates the spatial heterogeneity, the integration of parameter uncertainty provides a better estimation of the global uncertainty. Subsequently, the posterior uncertainty can be quantified from the final realizations of the facies model. Figure 3.9 compares the prior and posterior uncertainty based on the global facies proportions. The proposed methodology provides a practical workflow for quantification and integration of proportion uncertainty into the geological modelling of categorical variables. For prior proportion uncertainty (Figure 3.9a), the colored bars are related to the mean of the global proportions calculated based on spatial bootstrap realizations. For the posterior uncertainty (Figure 3.9b), colored bars depict the mean of global proportions based on final realizations of the facies. As can be seen in Figure 3.9, the uncertainty in distribution of global proportions is reduced after post-processing and integration of prior proportion uncertainty into the geostatistical modelling workflow. The hatched bars in Figure 3.9b relate to the global proportions calculated from the base-case trend model. As explained in Chapter 2, the prior proportion uncertainty is overestimated because the spatial bootstrap is controlled by the spatial correlation between sampled data. The relatively large range of spatial continuity (i.e., variogram ranges) results in increased redundancy between data and overestimation of the prior uncertainty. In the second step, the same reason (i.e., spatial continuity) increases the conditioning effect of the data and results in considerable reduction of proportion uncertainty.

3.1.4 Multivariate Histogram Uncertainty for Petrophysical Properties

In a geostatistical reservoir modelling workflow, facies modelling is important because the petrophysical properties are different within each facies type. A prior model of facies can constrain the range of variability in porosity, permeability and fluid saturations (Pyrcz and Deutsch, 2014). Thus, facies simulation is often followed by modelling the spatial distribution of petrophysical properties within facies. This provides the stationary domains for the stochastic simulation of continuous reservoir properties in the Gaussian framework. Figure 3.10 shows the distribution of porosity and water saturation within Sand and Mud.

In this case study, porosity, shale volume, permeability and water saturation are simulated within each facies. The multivariate relationships between these petrophysical properties characterize the geological process and

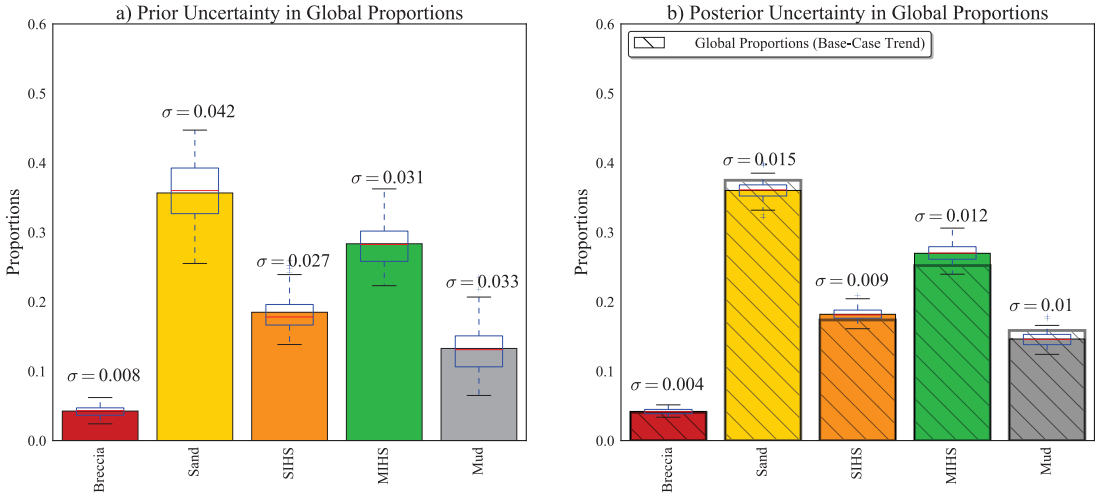

Figure 3.9: Prior and posterior proportion uncertainty for the case study.

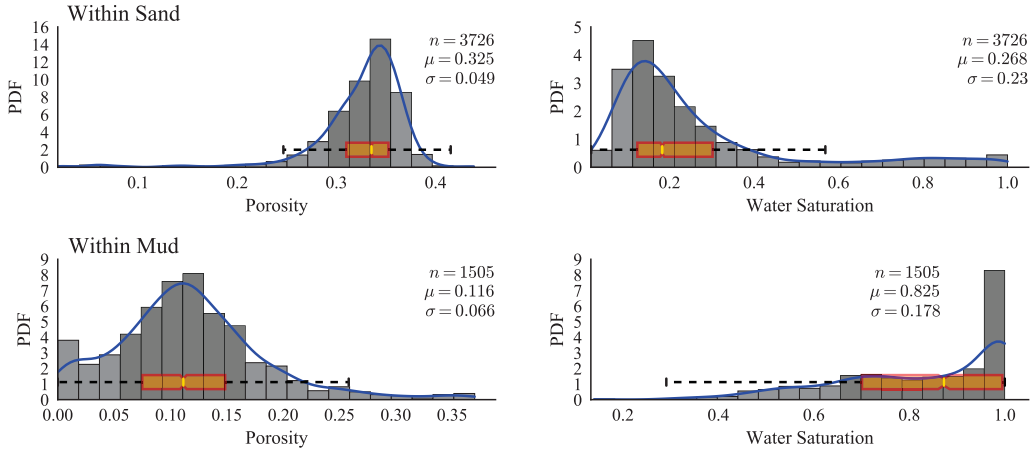

Figure 3.10: Distribution of porosity and water saturation within Sand and Mud.

must be reproduced by the geostatistical simulation. Figure 3.11 shows the multivariate relationships between sampled petrophysical properties within Sand facies.

The histogram is one of the main input statistics for modelling petrophysical properties. Inference of a histogram based on limited data is subject to uncertainty. In this case study, the joint multivariate histogram uncertainty is quantified and integrated in the multivariate geostatistical modelling of petrophysical properties. Similar to the facies proportion uncertainty, this is addressed in two steps. The first step is to quantify the prior multivariate histogram uncertainty by statistical resampling. This is automated by a computer program (SBS_MV, Appendix A) that implements multivariate spatial bootstrap and generates multiple realizations of sampled data within each facies. As described in Chapter 2, the spatial bootstrap realizations reproduce the complex multivariate relationships between different properties (Figure 3.11). Figure 3.12 shows the multivariate relationships reproduced by one of the spatial bootstrap realizations within Sand.

The prior multivariate histogram uncertainty is quantified by multiple realizations of sampled data. Each

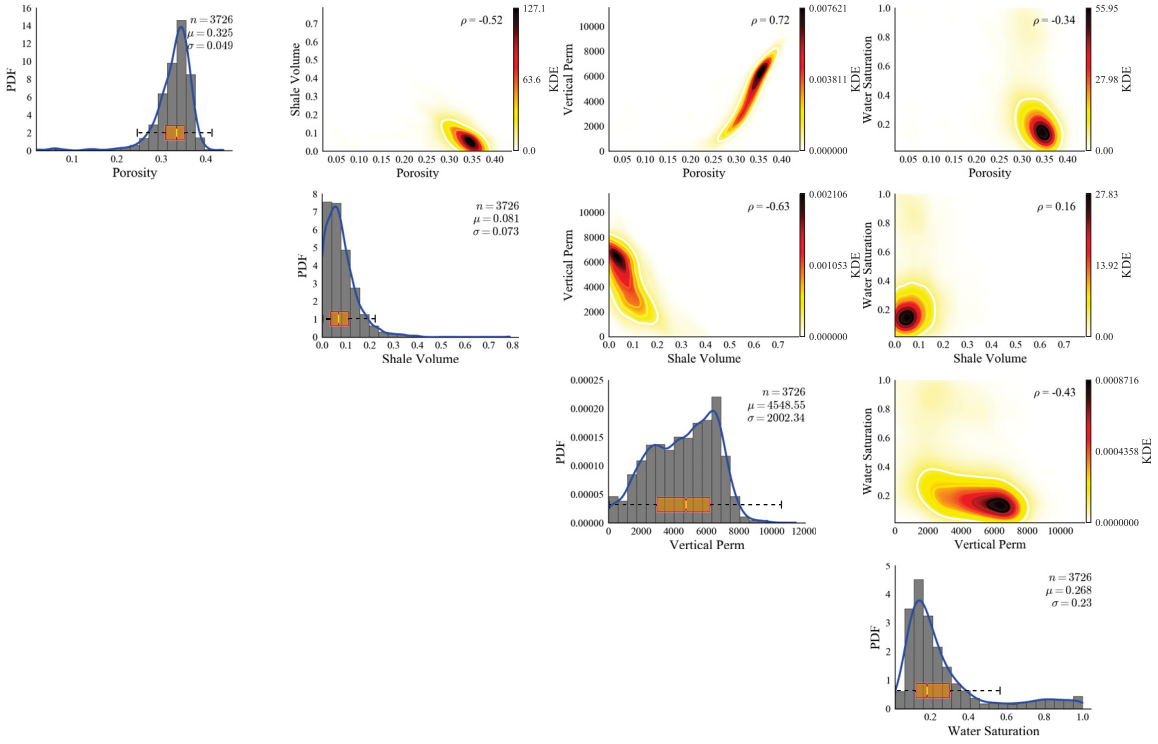

Figure 3.11: Multivariate analysis of sampled petrophysical properties based on well data.

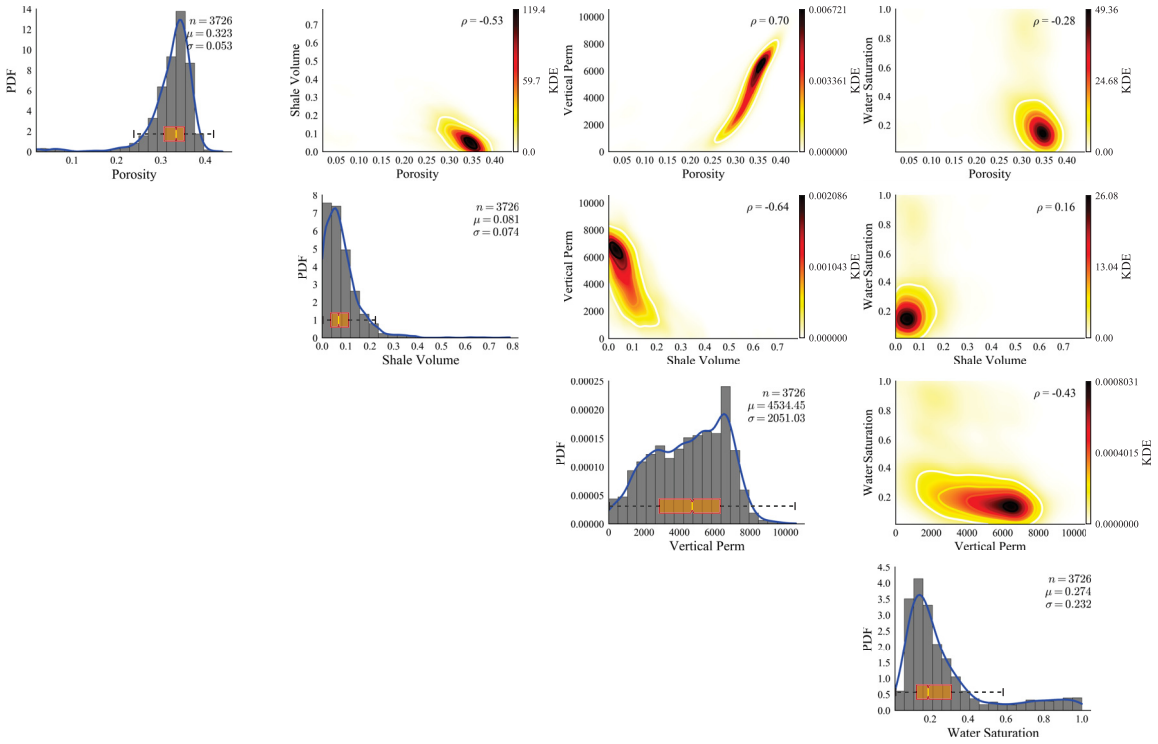

Figure 3.12: Multivariate relationships reproduced by a spatial bootstrap realization.

realization is considered as a reference distribution for the subsequent geostatistical simulation that gives the final spatial distribution of petrophysical properties in the reservoir. Figure 3.13 shows the prior uncertainty in statistical distribution of the four petrophysical properties within Sand and Breccia. The gray lines show the CDF plots for the spatial bootstrap realizations while the red line depicts the CDF inferred from original well data. As can be seen in Figure 3.13, less data within Breccia results in higher prior uncertainty in distribution of petrophysical properties.

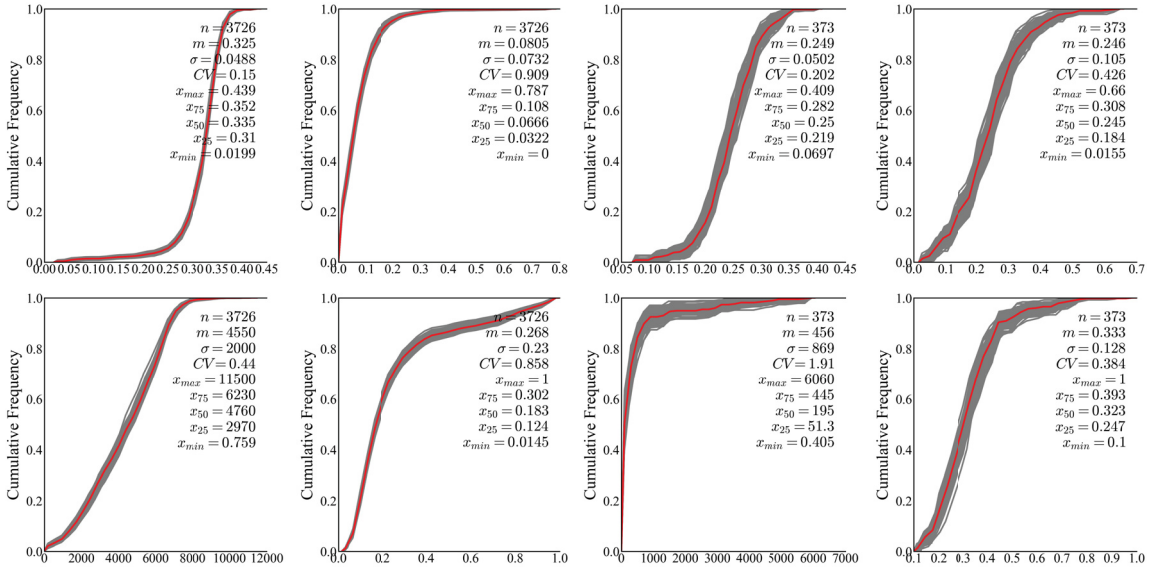

(a) Within Sand (b) within Breccia

Figure 3.13: Prior uncertainty in distribution of different petrophysical properties quantified by multivariate statistical resampling.

The second step is to integrate prior multivariate histogram uncertainty in the multivariate geostatistical simulation. PPMT is used to transfer petrophysical data to an uncorrelated multivariate Gaussian framework where each variable can be simulated independently using SGS. Spatial bootstrap realizations are used as reference distributions for PPMT transformation and the back-transformation information are recorded. In this way, multivariate histogram uncertainty quantified in the first step is integrated in multivariate geostatistical simulation. Since the simulation is performed in Gaussian framework, a back-transformation step is required to transfer petrophysical properties to the original units. The PPMT back-transformation is implemented for each realization separately using the corresponding back-transformation information. Figure 3.14 shows the posterior global uncertainty in distribution of petrophysical properties within Sand and Shale. This is calculated by considering the ensemble of final geostatistical realizations over the entire reservoir model.

The prior histogram uncertainty (Figure 3.13) is quantified by statistical resampling that does not account for conditioning effect of the data within the reservoir and the domain limits. These are included by integration of the prior parameter uncertainty in geostatistical modelling of the petrophysical properties within facies to obtain a realistic posterior uncertainty as shown in Figure 3.14. As mentioned in Chapter 2, there is a complex

interaction between range of spatial variability, domain size and number of conditioning data that affects the posterior uncertainty. If histogram uncertainty is not considered, all realizations more or less reproduce the same input distribution that comes from conditioning data. The objective here is to improve geostatistical reservoir modelling practices to obtain an accurate model of geological uncertainty that is essential for successful reservoir management decision making.

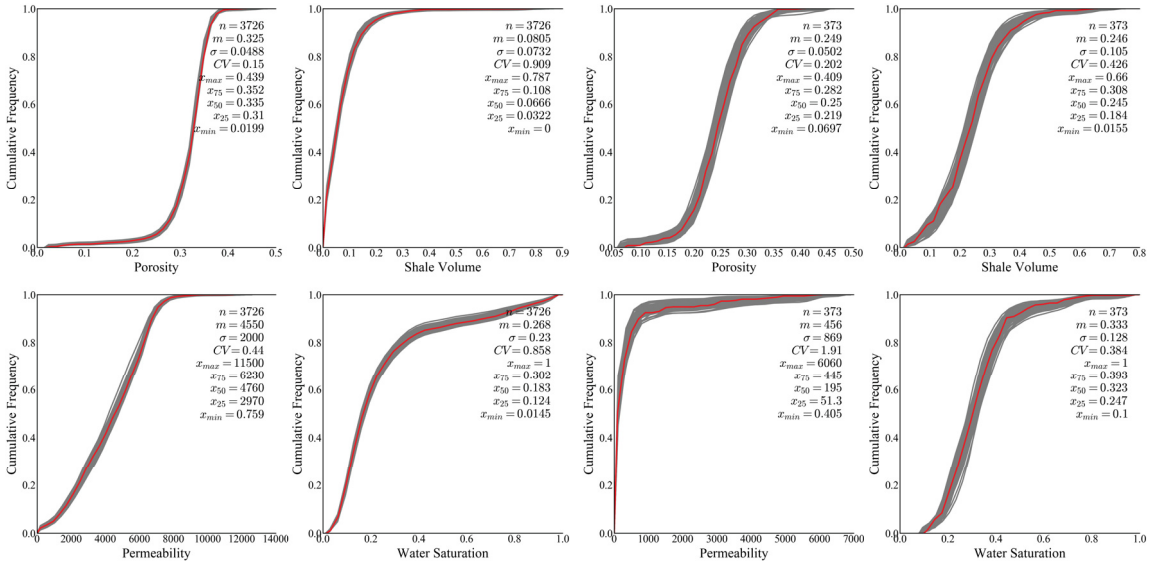

(a) Within Sand (b) within Breccia

Figure 3.14: Posterior global uncertainty in distribution of different petrophysical properties.

Finally, realizations of petrophysical properties for different facies are merged together based on final facies realizations. Figure 3.15 shows one final realization of merged petrophysical properties along with the facies model. The final merged realizations of petrophysical properties account for both the facies proportion uncertainty and the histogram uncertainty in the properties. These realizations can be used for resource estimation and reservoir management decision making as they provide a more realistic model of geological uncertainty. Figure 3.16 shows the distribution of different petrophysical properties based on final realizations of the reservoir. Figure 3.16a shows the CDF for all realizations while Figure 3.16b depicts the distribution of the mean for each property.

3.2 Comparative Study

In the case study, quantification and integration of facies proportion uncertainty along with multivariate histogram uncertainty is presented. A comparative study is conducted to evaluate the effect of integrating parameter uncertainty on resource estimation. In this context, four cases are considered:

- Case1 ● : Facies proportion uncertainty and multivariate histogram uncertainty are both considered

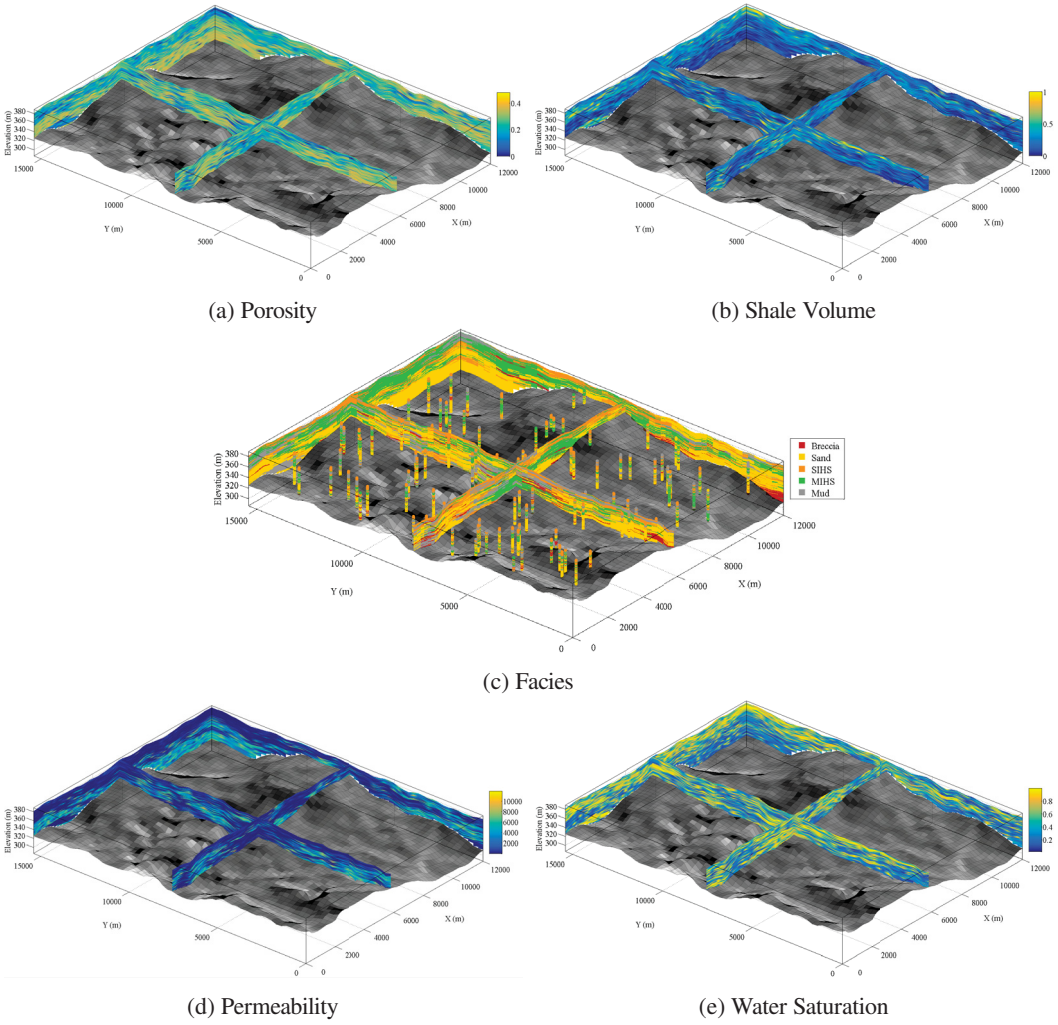

(a) Porosity

(b) Shale Volume

(c) Facies

(d) Permeability

(e) Water Saturation

Figure 3.15: One final realization of the reservoir after integration of proportion and histogram uncertainty.

- Case2 ● : Only multivariate histogram uncertainty is included
- Case3 ● : Only facies proportion uncertainty is integrated
- Case4 ● : No facies proportion uncertainty and no multivariate histogram uncertainty is considered

When facies proportion uncertainty is not considered, all realizations are simulated using the same base-case trend model inferred from the data. On the other hand, if multivariate histogram uncertainty is ignored, petrophysical properties are simulated based on the same distribution that is inferred based on the data within each facies. In order to evaluate resource estimation, Original Oil in Place (OOIP) is calculated for each case and over all realizations.

$$OOIP = \frac{1}{B_o} \sum_{i=1}^{n} V_i \phi_i (1 - S_{Wi}) \tag{3.1}$$

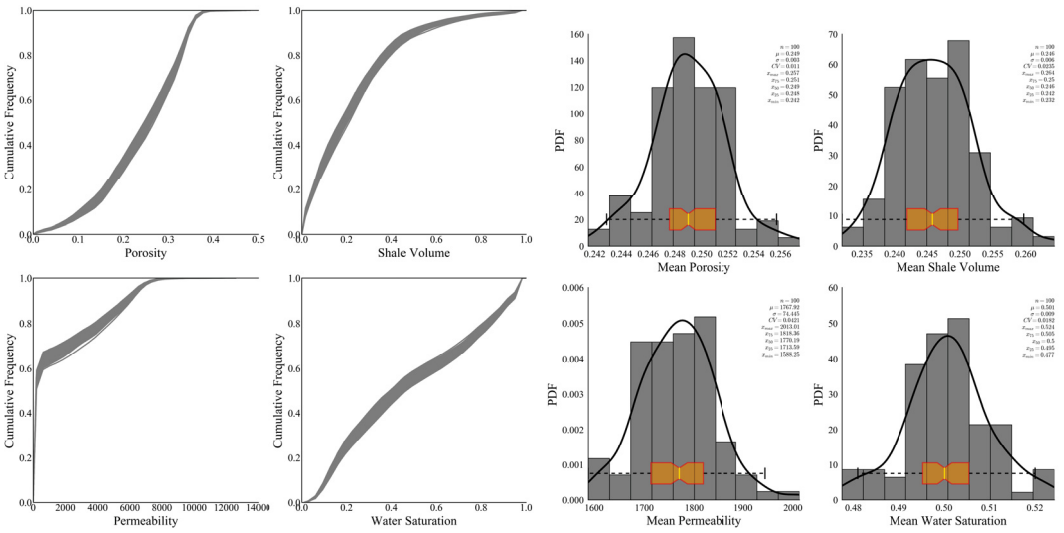

(a) CDF for all realizations (b) Distribution of Mean

Figure 3.16: Posterior uncertainty represneted by final merged realizations of petrophysical properties.

where n is number of grid cells within the reservoir, V_i denotes the volume of each grid cell, ϕ_i and $S_{W\,i}$ denote the porosity and water saturation for each cell respectively. Also, B_o is the oil formation volume factor that was considered to be 1.02. Figure 3.17 shows the distribution of OOIP for the different cases mentioned above. The range of variability may be judged based on standard deviation (σ) or the coefficient of variation (CV).

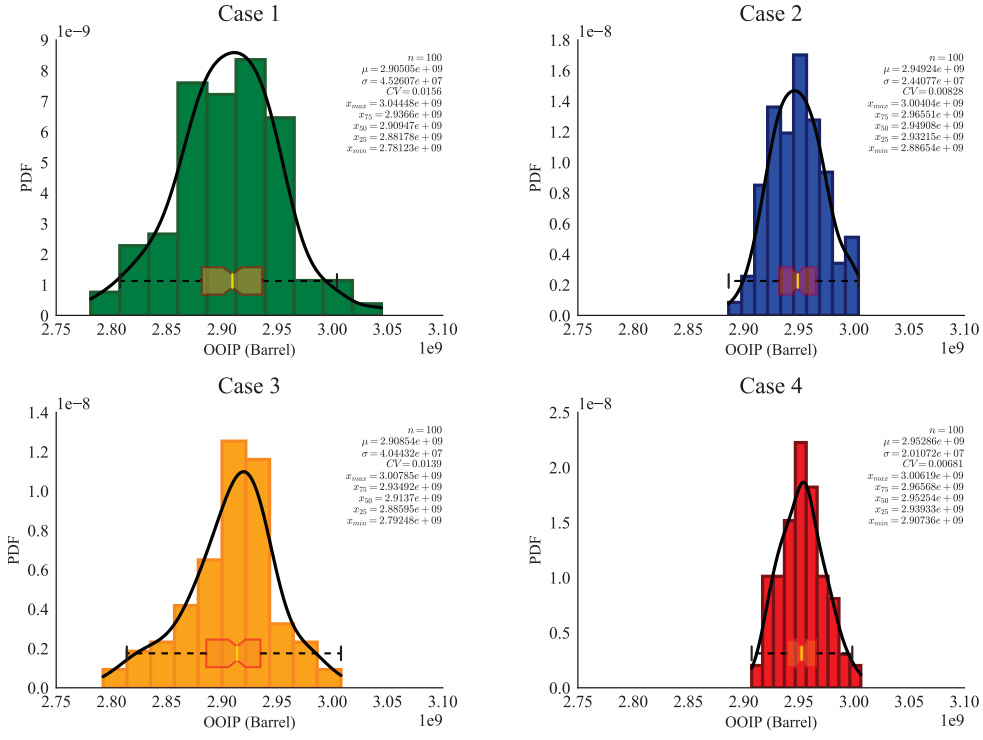

Figure 3.17: Distribution of OOIP related to the four cases considered in the comparative study.

Table 3.1: Result of the comparative study.

Case	Coefficient of Variation
Case 1	0.0156
Case 2	0.0083
Case 3	0.0139
Case 4	0.0068

As can be seen in Figure 3.17 and is summarized in Table 3.1, Case 1 has the highest range of variability because it accounts for both facies proportion uncertainty and multivariate histogram uncertainty within facies. On the other hand, comparison between distribution of OOIP for Case 2 and Case 3 reveals that facies proportion uncertainty has a more significant effect on resource estimation. Quantifying and integrating parameter uncertainty in geostatistical reservoir modeling results in a realistic model of geological uncertainty that is critical for resource estimation and decision making. Global uncertainty over ensemble of all realizations is considered for resource estimation.

3.3 Conclusions

In this chapter, a case study is presented to explain the practical integration of facies proportion uncertainty in a geostatistical modelling workflow. The multivariate modelling of petrophysical properties within facies and in presence of histogram uncertainty is another aspect of the case study. There are two main steps for integration of parameter uncertainty in geostatistical modelling. The first step is to quantify the prior parameter uncertainty based on statistical resampling. The second step is to integrate the prior parameter uncertainty to a typical geostatistical modelling workflow. In this context, the first step can be considered as a pre-processing step prior to the geostatistical modelling workflow. Parameter uncertainty essentially means that there is no single statistical input parameter for all realizations. Instead, each realization has its own input statistical parameter that is quantified in the first step. In the second step, each final geostatistical realization is generated separately with a corresponding input parameter. For instance, each facies realization has a separate trend model. Considering parameter uncertainty has a significant effect on resource estimation and should be considered in the geostatistical modelling. The following presents the workflow considered in the case study.

- Facies Modeling

  I Calculate and model experimental indicator variograms based on well data

  II Model a base-case trend model based on well data

  III Quantify prior proportion uncertainty using a geostatistical tool (SBS_Categorical, Chapter A). Multiple realizations of the trend model are generated

  IV Sequential indicator simulation of facies using a different trend model for each realization to generate the final model of facies

V Check prior and posterior facies proportion

- Multivariate Modeling of Petrophysical Properties

I Pool petrophysical data within different facies and consider steps II to VI for each of them

II Experimental variogram calculation and modelling for each variable after normal score transformation

III Quantify prior multivariate histogram uncertainty using a geostatistical tool (SBS_MV, Chapter A). This generates multiple spatial bootstrap realizations of sampled data.

IV Forward PPMT transformation of well data using spatial bootstrap realizations as reference distributions and record the back-transformation information

V Conditional sequential Gaussian simulation is conducted for each transformed variable separately. Note that each realization has its own conditioning Gaussian values.

VI PPMT back transformation of each realization using the corresponding back-transformation information.

VII Merge petrophysical realizations for different facies based on a corresponding facies realization generated in the facies modelling workflow

This chapter presents a practical workflow for effective integration of parameter uncertainty in geostatistical reservoir modelling. Computer programs facilitate the workflow and provide realizations of the input statistical parameters that are referred to as prior parameter uncertainty. The key idea is to simulate one final realization of the reservoir at a time based on a different realization of the input statistical parameter. This allows to integrate the prior parameter uncertainty in the subsequent geostatistical reservoir modelling to obtain an accurate model of geological uncertainty. Also, the effect of including parameter uncertainty on resource estimation is investigated by evaluating the distribution of OOIP. In presence of limited data, parameter uncertainty can play a significant role in resource estimation and needs to be included in reservoir modelling.

Chapter 4

Geostatistical Integration of 4D Seismic Data

4.1 Introduction

One objective in petroleum reservoir modeling is to predict the future performance of the reservoir under different recovery methods or production strategies. Uncertainty in reservoir modeling is inevitable and is due to our lack of knowledge about the truth. With limited data the modeling process is ill-posed and leads into non-unique realizations of reservoir properties. The uncertainty can be reduced by integration of all available sources of data including static and dynamic data.

Time-lapse or 4D seismic is a dynamic source of data that provides information about changes in reservoir rock and fluid properties over time (Chopra et al., 2010). Seismic attributes such as velocity and impedance are sensitive to variations in the fluid content, temperature and pressure distribution as a result of hydrocarbon production. Thus, the large-scale nature of fluid flow within the reservoir can be evaluated through information provided by 4D seismic data. As a recovery process proceeds, additional seismic surveys may become available. This provides incremental 4D seismic data that can be used for reservoir monitoring and management. Updating geostatistical realizations based on information inferred from 4D seismic images can reduce geological uncertainty and improve future reservoir management decisions. Considering the quality and scale of 4D seismic data, mathematical inverse modeling or automatic seismic history matching is not considered applicable in practice.

Perhaps the most reliable and important information that can be learned from 4D seismic data is related to anomalies in fluid flow within the reservoir. For instance, during SAGD, the steam chamber propagation is fairly clear from 4D seismic images mainly because of changes in reservoir conditions due to steam injection and bitumen production. Incremental 4D seismic data can be used to study the evolution of the steam chamber over time and identify anomalies in propagation of the steam chamber. Identified anomalies represent information extracted from 4D seismic data and should be reproduced by all realizations. Geostatistical anomaly enforcement is required in order to respect this information in the geological modeling workflow. The anomaly data is not left for history matching at the end. In this chapter, a practical methodology is introduced for consideration of anomalies identified from 4D seismic images in geostatistical reservoir models (Hadavand and Deutsch, 2016). The geostatistical realizations are updated to enforce missing anomalies and improve reservoir characterization. The updated models are suitable for reservoir decision making and management. In this thesis, SAGD is the focus of case studies and examples to demonstrate how geostatistical anomaly enforcement is implemented. However, the same concept could be extended to other recovery processes.

4.2 4D Seismic Data

Reflection seismology is a method of exploring subsurface geology. A seismic source generates sound waves at or near the earth's surface. These sound waves are reflected at geological boundaries and other discontinuities where there is a contrast in seismic impedance. Arrays of seismic receivers collect the reflected signals. Applying seismic signal processing results in a 3D seismic survey that is a snap shot of the subsurface geology (Veeken, 2006). 4D seismic analysis is the study of differences between repeated 3D seismic surveys such that the fourth dimension is time. The term 4D is usually considered for time-lapse 3D seismic surveys, as opposed to other time-lapse seismic techniques that do not cover a 3D volume (Lumley and Behrens, 1998). In this thesis, 4D seismic data refers to observations of differences in seismic attributes that are deemed to be significant considering the seismic signal quality and professional judgment. During a recovery process, fluid injection and hydrocarbon production results in changing dynamic properties such as fluid saturation, pore pressure and temperature. 4D seismic analysis provides a means of monitoring such changes during the recovery process. Figure 4.1 shows an example of incremental 4D seismic data for a SAGD drainage area. Figure 4.2 shows 4D seismic analysis for the Duri steamflood project in Indonesia. The time slice refers to the slices of seismic data with the same two-way travel time. Red and black colors highlight areas where the changes in seismic attributes are significant. The areal time slices can be used to monitor steam propagation over time and detect potential breakthrough of the steam front that can affect sweep efficiency.

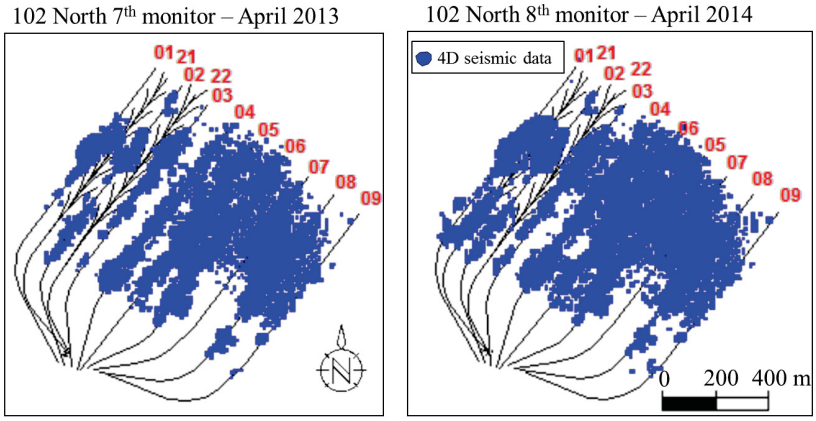

Figure 4.1: An example 4D seismic data for a SAGD drainage area at two different calendar times (obtained from in situ performance presentations archive, www.AER.com).

Seismic data are available at scales larger than typical geological modelling cells. 4D seismic analysis results in data at the larger scale of seismic. Although the areal resolution is often comparable, the vertical resolution is 10 to 100 times bigger than geological modelling cells (Pyrcz and Deutsch, 2014). The vertical resolution in a typical geostatistical model is between 1 to 3 feet which is supported by high resolution engineering data including well logs. In addition, 4D seismic data can be noisy and often mis-leading due to variations in acquisition and processing. The main limitations associated with 4D seismic are: inability to repeat precisely successive seismic

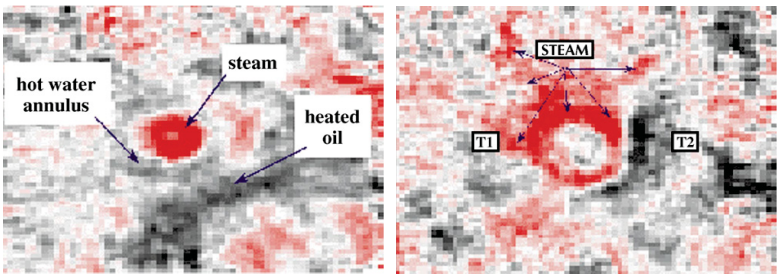

(a) 4D seismic areal time slice after 5 months.

(b) 4D seismic areal time slice after 19 months.

Figure 4.2: 4D seismic analysis for Duri steamflood project in Indonesia (obtained from (Lumley and Behrens, 1998). No scale is provided).

acquisitions, inconsistencies in processing time-lapse seismic data and 4D seismic interpretations that are not reconciled with geological settings and engineering production data (Lumley and Behrens, 1998). Figure 4.3 shows 4D seismic data related to a project with well designed seismic acquisition that is expected to be repeatable. The seismic sources and receivers are located in pre-drilled shot and receiver holes. Also, in order to obtain repeatable source waveform, small dynamite charges were used. However, as can be seen in Figure 4.3, the 4D seismic differences in non-reservoir part gets progressively noisier with time. Data processing can reduce the noise; however, not all 4D seismic changes are related to real changes in the reservoir during a recovery process. In other words, the seismic acquisition and processing should be done such that the seismic differences are due to changes in the reservoir condition and not influenced by seasonal changes near surface or signal processing algorithms. Professional judgment and corroboration with other engineering data including surveillance wells is required to infer reliable information from 4D seismic data.

SAGD is a common thermal recovery method in Canada and 4D seismic is one of the main dynamic data for monitoring this recovery process. During SAGD steam is injected to increase temperature and reduce bitumen viscosity. The propagation of the steam chamber results in temperature change and displacement of heated bitumen with steam. This results in significant changes of seismic attributes within parts of the reservoir affected by the steam chamber propagation. Thus, the evolution of the steam chamber can be monitored by incremental 4D seismic images over time. In this thesis, SAGD is considered to demonstrate the integration of 4D seismic data in geostatistical reservoir modeling. In Alberta, companies that operate SAGD publish plots of their 4D seismic data in annual reports they submit to Alberta Energy Regulator (AER). 4D seismic is often used to define the steam chamber thickness based on the amount/intensity of changes in seismic attributes. Figure 4.4 shows two examples of steam chamber thickness maps defined by 4D seismic data.

As can be seen in Figures 4.1 and 4.4, 4D seismic data can be used to identify large-scale flow patterns within the reservoir during SAGD. Geostatistical realizations conditioned to static well data and 3D seismic are not constrained to such time-varying data. Information obtained from a dynamic source of data such as 4D seismic complements hard and soft static data and its integration in geostatistical reservoir modeling can improve

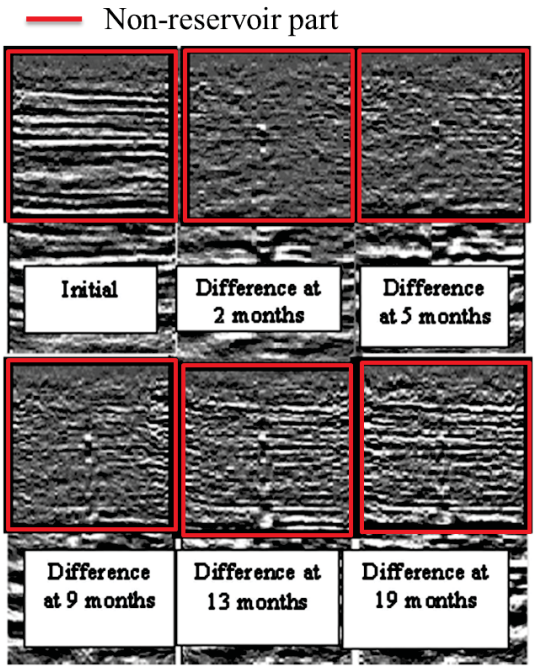

Figure 4.3: Cross sections of 4D seismic differences over time. The non-reservoir part is highlighted by the red frame. The 4D differences get noisier by time. The scale is not provided. (obtained from (Lumley and Behrens, 1998)).

the model of geological uncertainty. A practical methodology is proposed in this chapter for effective integration of information inferred from 4D seismic images.

4.3 Methodology

Quantitative inclusion of 4D seismic using inverse modeling is often referred to as seismic history matching and Figure 4.5 summarizes the main steps required for this approach. Inverse modeling requires a mathematical or forward model to generate synthetic 4D seismic data. It is required to couple a petro-elastic model by a flow simulation to reproduce 4D seismic responses based on changes in fluid saturation, temperature and pressure (Gosselin et al., 2001). A prior knowledge of rock-physics from lab data is needed that may not be always available and is subject to uncertainty.

Integration of additional information inferred from 4D seismic may constrain geological uncertainty but does not remove it. Thus, all geostatistical realizations need to be updated based on that information. The computational cost of implementing 4D seismic inversion along with concerns about the quality and scale of 4D seismic data pose a significant challenge that undermines the practicality of using this approach for integration of 4D seismic in geostatistical reservoir modelling. A practical approach is proposed that benefits from human judgment to infer reliable information from 4D seismic images. Such information may be described by anomalies in fluid flow that can be inferred from the unusual patterns in variations of a seismic attribute (i.e., travel time or acoustic impedance). The proposed methodology is based on geostatistical enforcement of anomalies that are

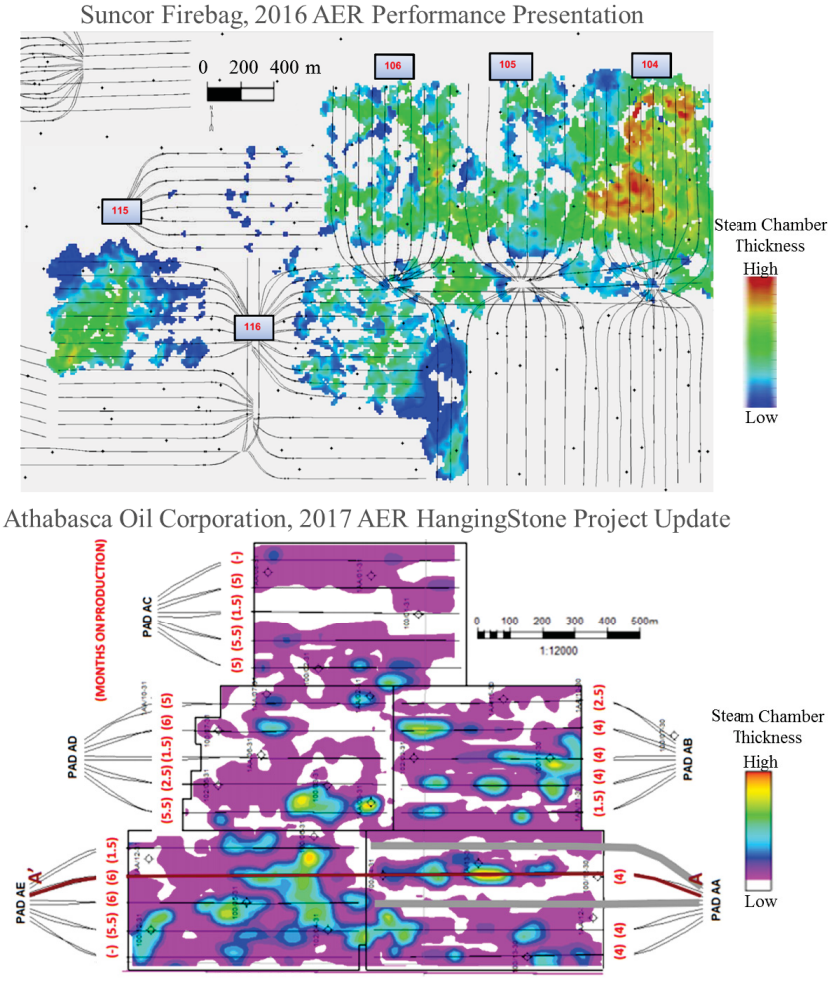

Figure 4.4: Steam chamber thickness defined based on 4D seismic data(obtained from in situ performance presentations archive, www.AER.com).

missing in the realizations constructed in the usual manner. There are three main steps in this methodology: 1) anomaly identification 2) anomaly fidelity analysis, and 3) anomaly enforcement. These steps are explained in detail in the following sections. Figure 4.6 shows a flow chart that summarizes the proposed methodology for the integration of 4D seismic data based on geostatistical anomaly enforcement.

4.3.1 Anomaly Identification

4D seismic images highlight areas in a reservoir where differences in seismic attributes are significant. During a recovery process, changes in pressure, temperature and fluid content can be monitored through 4D seismic images. Anomalies in large-scale flow patterns may be the most reliable source of information that can be inferred from 4D seismic data. Humans have a superb ability to detect irregular patterns and anomalies in an image. A professional with fair knowledge of the recovery process can identify anomalies in fluid flow through visual inspection of 4D seismic images. In SAGD, the identification is done by monitoring the steam chamber

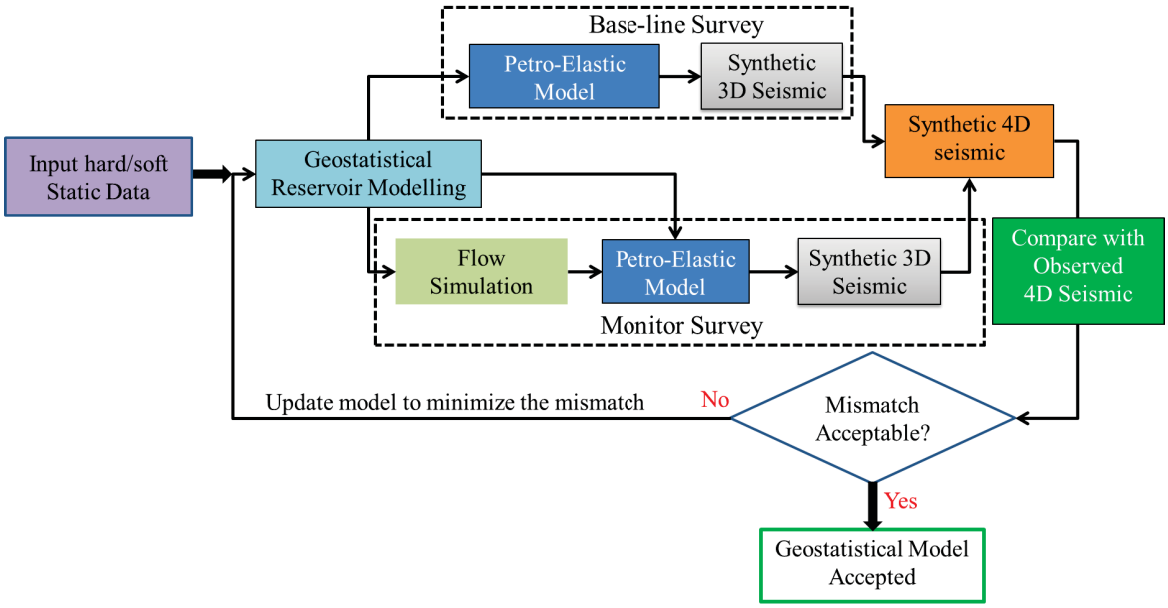

Figure 4.5: A flow chart summarizing 4D seismic history matching.

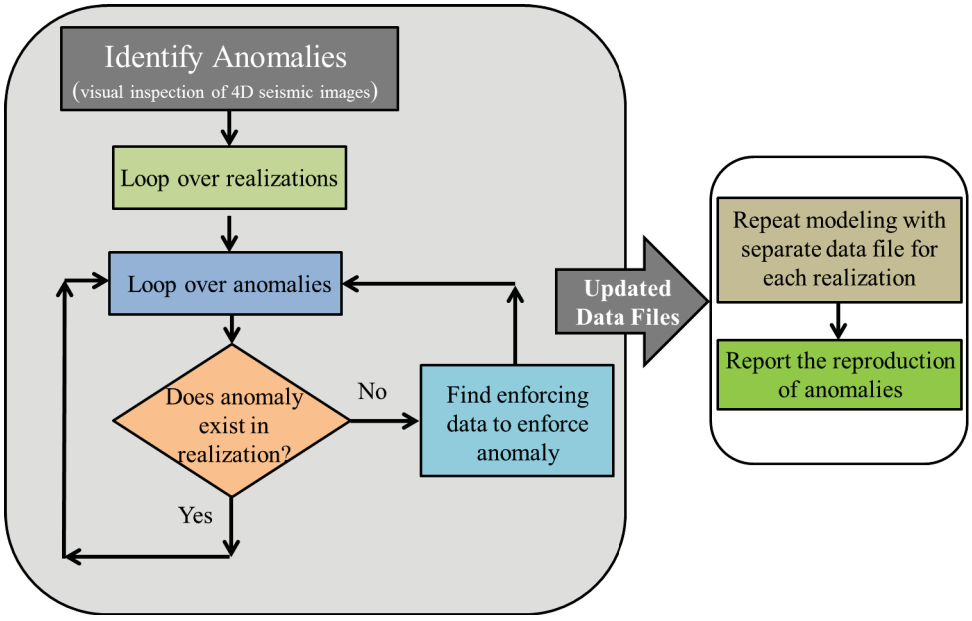

Figure 4.6: Flow chart of the proposed methodology for geostatistical anomaly enforcement.

evolution over time through incremental 4D seismic images and assessing it based on the expected steam chamber propagation for a specific drainage area. Thus, a successful identification process relies on professional judgment, knowledge of the recovery process, seismic interpretation, scheduling (timing) for each well pair, operating practices, reservoir height, water saturation and other factors. Anomaly identification is a subjective process. This is not regarded as a limitation but a positive feature because it employs human judgment and decision making to interpret the propagation of the steam chamber and identify anomalies. In addition, anomalies can be

cross-checked or even identified based on surveillance well data that monitor the changes in temperature.

There are two main types of anomalies: flow barrier/baffle (type -1) and flow conduit (type $+1$). The reservoir anomalies are not necessarily at the same location as the 4D seismic changes. The changes in the seismic attributes combined with our understanding of the flow process indicate where the anomalies must be located. In this regard, if there is no change in seismic attributes where it is expected, a flow barrier/baffle (type -1) can be identified. On the other hand, a flow conduit (type $+1$) is observed where the steam chamber is growing faster than expected indicating high permeability areas in the reservoir. In order to explain the proposed methodology, a simple synthetic example is presented. Consider a reference reservoir model that is a single well pair SAGD drainage area as shown in Figure 4.7. The black horizontal lines highlight the trajectory of the producer and injector wells. The grid sizes are $25,\ 1,\ 1\ m$ along the X, Y and Z directions respectively. The VPC (Figure 4.7d) characterizes the local geological setting.

As depicted in Figure 4.7, there are a limited number of vertical wells that sample facies and petrophysical properties from the reference model of the reservoir. Thermal flow simulation (STARS, Computer Modeling Group (CMG)) is considered to simulate SAGD for the reference model and get the distribution of temperature and also changes in fluid saturation as a result of the recovery process. Figure 4.8 shows the distribution of temperature within the reference reservoir model as a result of SAGD after 5 years. The orange isothermal surface in Figure 4.8 delineates the steam chamber based on a contour at $200\ C^{\circ}$.

A computer program (4D_PEM, Appendix A) is used to generate synthetic 4D seismic data based on Gassmann's fluid substitution model (Gassmann, 1951) and considering changes in fluid saturations provided by the thermal flow simulator. Figure 4.9a shows the changes in P-wave acoustic impedance between two synthetic seismic surveys based on the convention of subtracting the most recent survey from the earlier one. The blue area shows the reduction of acoustic impedance as a result of steam chamber propagation. The red areas around the steam chamber are due to condensate water that results in increased acoustic impedance. As can be seen in Figure 4.9, the steam chamber propagation is quite clear in the 4D seismic images mainly due to the changes in fluid content. Figure 4.9b depicts a contoured surfaces that delineates the 4D seismic defined steam chamber. Such visualization facilitates inference of the steam chamber profile and helps with the anomaly identification that is done by visual inspection of 4D seismic images. Monitoring the steam chamber propagation along the well pair provides a criteria for a professional to evaluate the local anomalies affecting steam chamber evolution. Also, if there are multiple well pairs in a drainage area and the timing of injection for each well pair is known, they can be used to cross-check the expected steam chamber propagation over time. Based on such criteria, a professional can review 4D seismic images, evaluate the steam chamber propagation and identify local anomalies. Figure 4.10 shows some examples of identified anomalies segmented in 2D slices of 4D seismic images. The green solid line highlights conduits (anomaly type $+1$) while red dashed line highlights barriers (anomaly type -1). As illustrated in Figure 4.10, a flow barrier is identified where the steam chamber propagation is hampered by low quality (i.e., low permeability) volumes within the reservoir. While flow

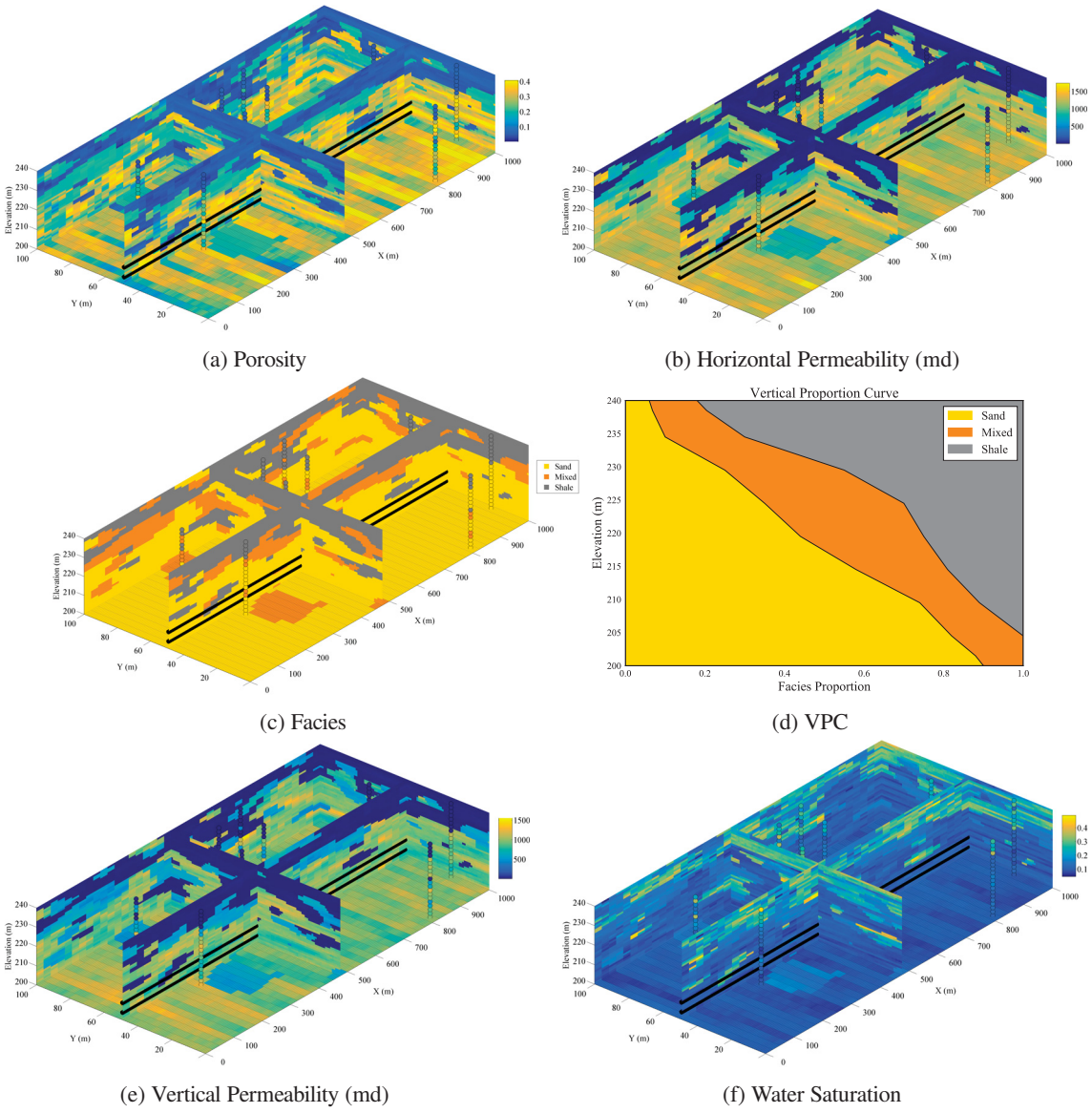

(a) Porosity

(b) Horizontal Permeability (md)

(c) Facies

(d) VPC

(e) Vertical Permeability (md)

(f) Water Saturation

Figure 4.7: A reference model for a single well-pair SAGD drainage area with a limited number of vertical wells.

conduits indicate volumes of the reservoir with relatively high effective permeability that allow the fast/normal propagation of steam chamber.

The final product of the identification process is an anomaly report that describes the location, type and spatial extent of each identified anomaly. There are two main options to describe an anomaly. The first option is a geometric shape like an ellipsoid. The second option is a cloud of points or grid addresses related to the grid specification for the geostatistical realizations. In the example presented here the first option is used. There are 11 parameters to characterize an anomaly using an ellipsoid: anomaly type (-1 or $+1$), X, Y, Z coordinates for the center of the ellipsoid, 3 principal diameters, 3 angles for the orientation (i.e., roll, pitch, yaw) and a confidence factor. The last parameter is in the range of 0 to 100% and expresses the quality of the identified

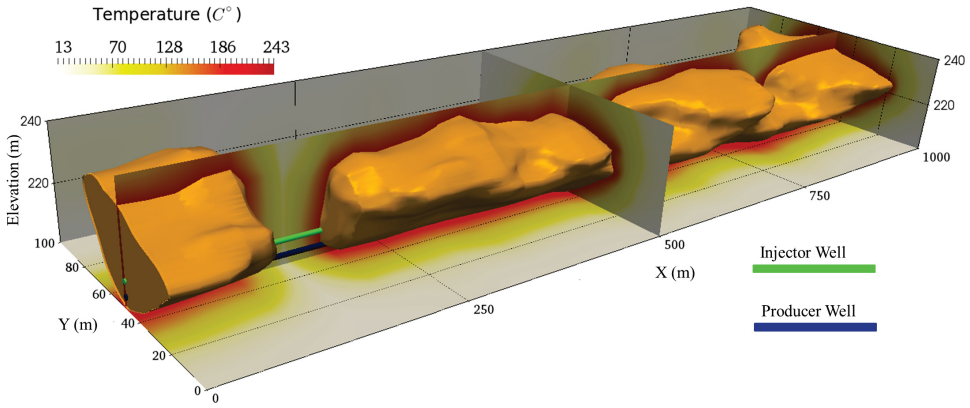

Figure 4.8: Distribution of temperature within the reservoir during SAGD.

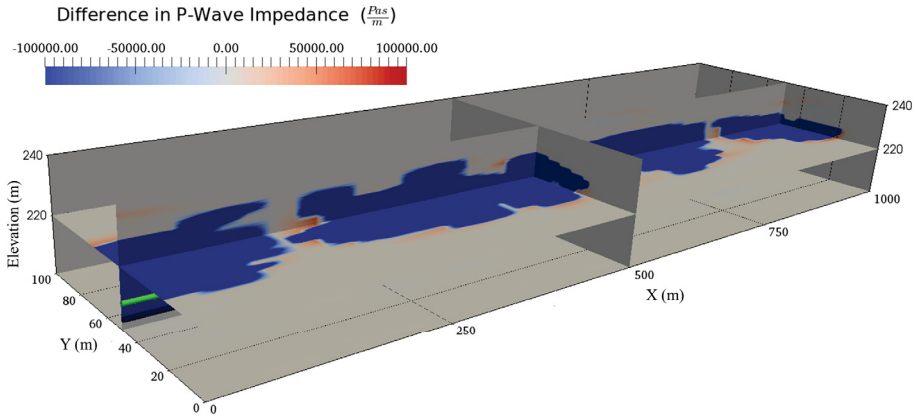

(a) Distribution of difference in P-wave impedance

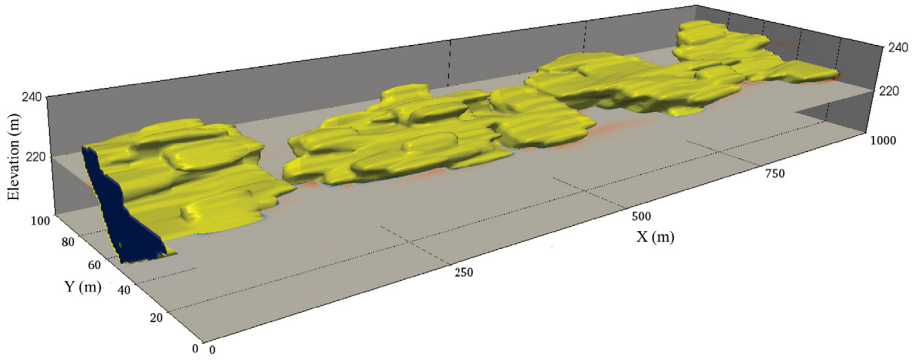

(b) Contoured surface representing 4D seismic defined steam chamber

Figure 4.9: Synthetic 4D seismic analysis for the reference model.

anomaly. For instance, consider two identified anomalies of type -1. One of them is a strong flow barrier while the other one acts like a baffle. The confidence parameter lets the user to differentiate between these two types of anomalies. This is explained in more detail in the next section. The anisotropy associated with the spatial extent of the anomaly can be captured by principal diameters of the ellipsoid. For this example, a total number of 10 anomalies including 7 type -1 and 3 type $+1$ are identified. Figure 4.11 shows the identified anomalies

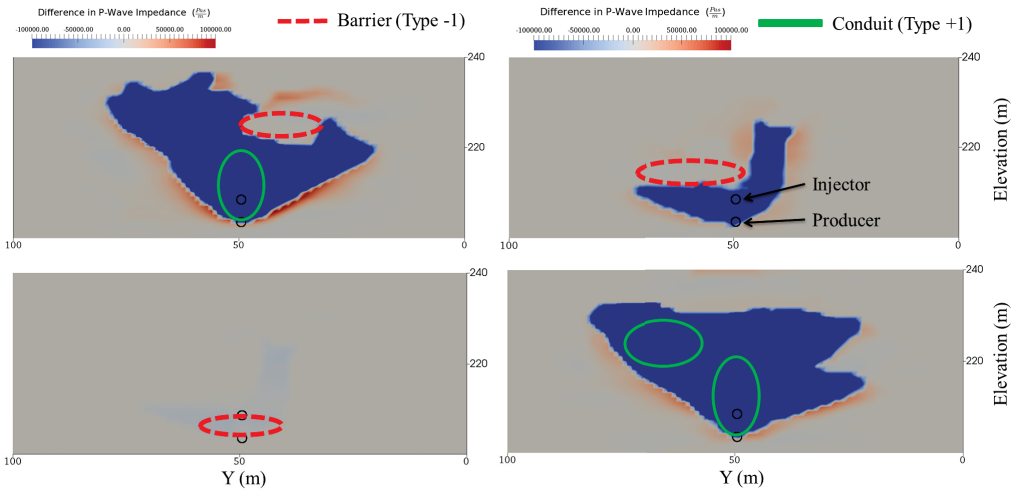

Figure 4.10: Some exampled of anomaly identification based on visual inspection of 4D seismic images.

along with the 4D seismic defined steam chamber represented by the transparent yellow surface.

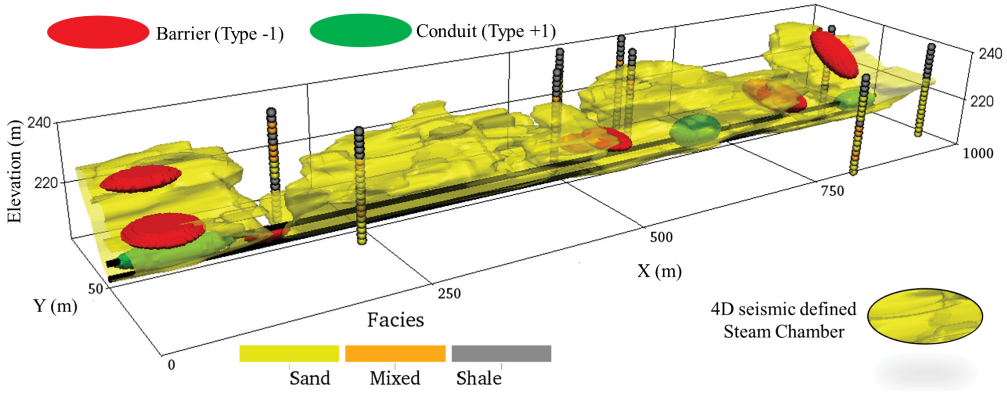

Figure 4.11: Identified anomalies based on visual inspection of 4D seismic images.

The anomaly identification is a critical step for the proposed methodology. In practice, this is a multidisciplinary task. A prior knowledge of the recovery process, local geology and seismic interpretation is required to identify true anomalies based on 4D seismic images. Incremental 4D seismic can be used to monitor the steam chamber evolution with time. This helps to ensure that the correct type and spatial extent is considered for an identified anomaly.

4.3.2 Fidelity Analysis

The initial geostatistical realizations are not informed by 4D seismic data. After anomaly identification, the next step is to assess the reproduction of identified anomalies by each realization. This is called fidelity analysis and determines the percentage of realizations that reproduce each anomaly. Since anomalies are mainly related to the quality of fluid flow, effective directional permeability is a suitable measure to check them. Although this

imposes more computational cost compared to a simple averaging scheme, it provides a more accurate measure of effective directional permeability that is representative of the anomaly being considered. In SAGD, effective vertical permeability is important. For instance, a flow barrier that hampers the propagation of the steam chamber is related to a volume of the reservoir with low effective vertical permeability. In this context, the fidelity of each anomaly is checked in each geostatistical realization by calculating the effective vertical permeability of the anomaly in that realization based on solving the pressure equation for single phase flow (Warren and Price, 1961).

The effective directional permeability for an anomaly is calculated by sampling horizontal and vertical permeability from a geostatistical realization. The anomaly report provides the location and spatial extent of each anomaly in the reservoir. In a gridded frame work, grid cells that are inside the anomaly are identified to sample the horizontal and vertical permeability. A gridded block that encompass the spatial extend of anomaly is populated by sampled horizontal and vertical permeabilities. Figure 4.12 shows an example block containing the anomaly geometry (i.e., an ellipsoid). As can be seen in Figure 4.12, parts of the block that are not within the anomaly geometry are filled by relevant extreme high and low permeability values to ensure that the effective permeability of this block represents the anomaly. This depends on the direction of effective permeability that is important for fidelity analysis. For SAGD, effective vertical permeability is important because the steam chamber rises upward. In this regard, the extreme high and low value permeabilities are added to the block to assure that effective vertical permeability of the block is defined by the anomaly. Solving the pressure equation will provide the effective vertical permeability of the anomaly geometry.

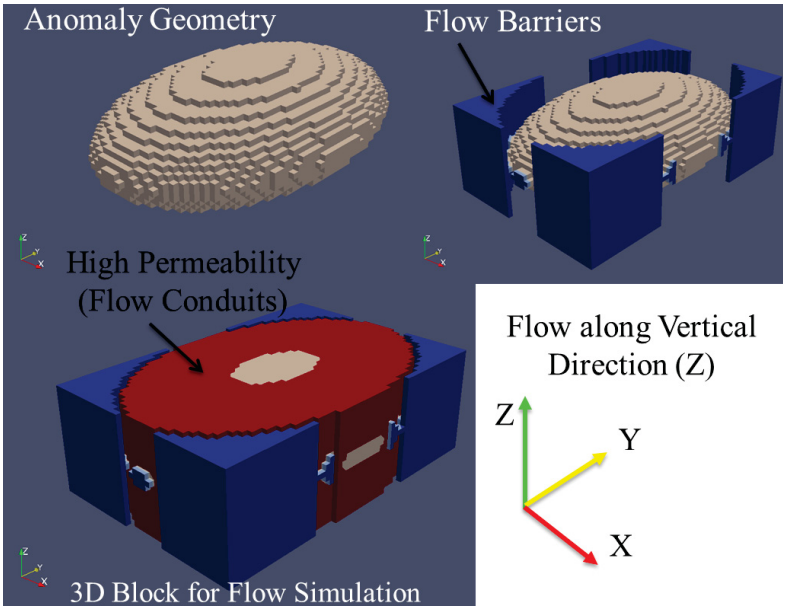

Figure 4.12: Populating a gridded block with sampled permeability within anomaly's geometry and relevant extreme permeability values to calculate the effective vertical permeability.

Anomalies are assessed based on reasonable permeability thresholds from professional discretion. Figure

4.13 explains how these threshold are defined for each type of anomaly. A flow barrier (type -1 anomaly) is reproduced by a realization if its effective vertical permeability in that realization is lower than the specified threshold (K_{-1}). Alternatively, a flow conduit exists in a realization if the effective permeability is higher than a specified threshold (K_{+1}). In practice, the permeability thresholds are assigned based on a flow simulation study that determines the effective permeability by which the steam chamber propagation is affected considering the type of anomaly. Also, thermal flow simulation results over a drainage area can be used to assess the thresholds of effective permeability based on steam chamber propagation. The confidence parameter introduced above can be used to modify the specified threshold for each anomaly. This provides more flexibility to account for quality of flow for each identified anomaly.

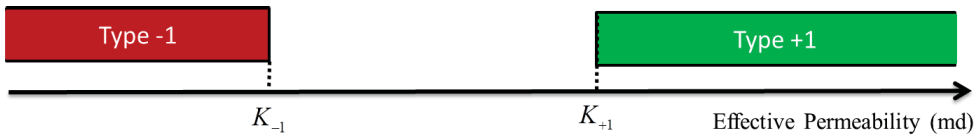

Figure 4.13: Considering permeability thresholds to evaluate the anomaly reproduction.

For this example, 20 realizations are generated conditioned to the limited well data (Figure 4.7). A computer program (Anomaly Recognition Tool (ART), Appendix A) is developed to implement fidelity analysis for geostatistical realizations using the anomaly identification report file. Figure 4.14 shows the fidelity analysis result for the initial conditional realizations in the example presented here. Figure 4.14a shows the fidelity percentage for each anomaly. Type -1 and $+1$ anomalies are highlighted by red and green bars respectively. Figure 4.14b depicts the range of effective vertical permeability for each anomaly over all realizations. The colored areas highlight the acceptable permeability range based on the user-defined thresholds.

The initial geostatistical realizations are conditioned to the well data and by the facies proportions model (i.e., VPC). The fidelity analysis determines which anomalies are missing in each realization. As can be seen in Figure 4.14, anomaly number 9 is reproduced by all realizations while anomalies number 5 and 6 do not exist in any of the realization. Geostatistical anomaly enforcement should be considered for the missing anomalies.

4.3.3 Geostatistical Anomaly Enforcement

The anomaly enforcement procedure is independent from the geostatistical modeling techniques so it can be added to any modeling workflow. In this regard, an effective and practical approach is proposed for anomaly enforcement based on adding enforcing data within the volume of missing anomalies. These additional data will be used along with the original conditioning data (i.e., well data) in order to assure the existence of identified anomalies. The enforcing data cannot be arbitrarily selected as they have to comply with the geological context of the reservoir model. Thus, the enforcing data for an anomaly are sampled from a realization where the properties of the target anomaly are found locally. This can be accomplished through a search algorithm that moves the volume of the anomaly within the geological model of the reservoir and calculates the effective

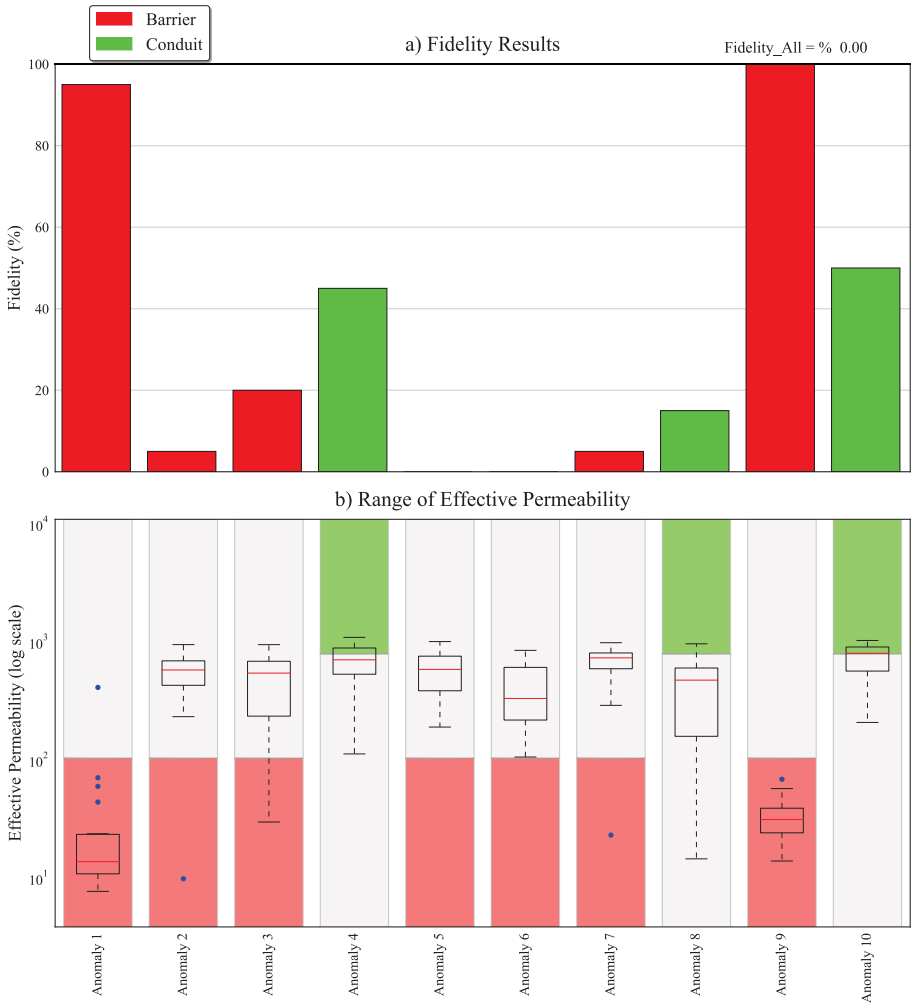

Figure 4.14: Fidelity analysis report before geostatistical anomaly enforcement. Panel a shows the fidelity percentage for each realization. Panel b shows the range of effective permeability for each anomaly over all realizations. Colored bars in panel b highlight the acceptable range of effective permeability for an anomaly to be reproduced.

directional permeability until reaching a location where the corresponding anomaly is honored, this location is a candidate sampling zone. For example, in order to find the enforcing data for a type -1 anomaly (flow barrier), it is required to search for a location where the effective permeability of the geological model within the anomaly geometry is low enough to be considered as a barrier. This process is done independently for each realization for all missing anomalies in the realization; in this way, it is possible to maintain realistic variability within realizations while enforcing the identified anomalies. This is achieved by choosing a random sequence of realizations and also searching randomly within each realization until finding the candidate sampling zone. Figure 4.15 schematically shows the concept of scanning within a realization of the reservoir in order to find a candidate sampling zone. The candidate zones are identified based on user-defined thresholds of effective directional permeability. For instance, a candidate sampling zone for a type -1 is found where the effective directional permeability is lower than the corresponding threshold.

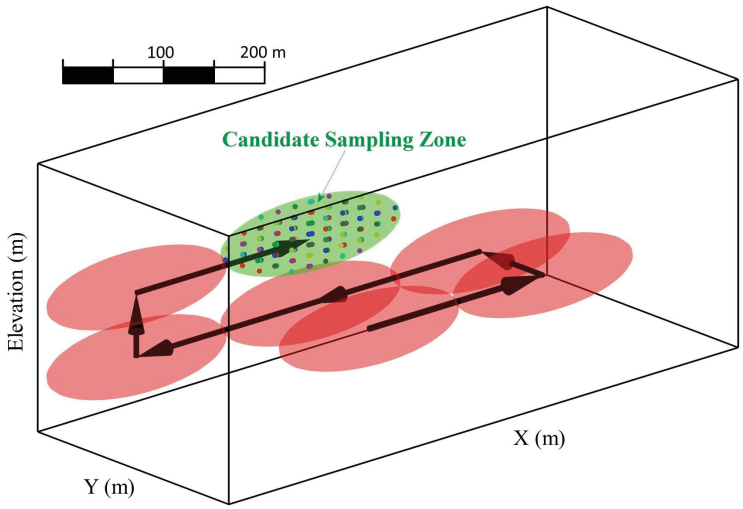

Figure 4.15: Schematic of finding a candidate-sampling zone.

There is a possibility that no candidate zone is found matching the specifications for an anomaly. This could indicate an issue with the available geostatistical realizations or the user-defined thresholds of effective permeability may need to be relaxed. Also, if the spatial extent of an identified anomaly is large compared to the size of the reservoir model, it is recommended to describe the anomaly as a combination of several small anomalies. This increases the chance of finding the candidate sampling zones within the ensemble of geostatistical realizations.

Note that according to the proposed enforcing methodology, each realization gets updated based on its unique conditioning data file that contains both the original well data and also the sampled enforcing data for that realization. The updating process amounts to repeating the same geostatistical modeling workflow using the new conditioning data files that are different for each realization. Consequently, the enforcement process is independent of the modeling workflow and can be integrated as a post/pre-processing tool in order to integrate the reliable information captured from 4D seismic images.

The developed software (ART, Appendix A) facilitates checking anomaly reproduction and extracting data to enforce anomalies if required. This geostatistical tool checks the identified anomalies for all the realizations and performs a fidelity analysis. Also, it samples the required enforcing data and generates separate data files for each realization that can be used to update the realizations and enforce the anomalies identified from 4D seismic images. Figure 4.16 shows one example of sampled enforcing data along with original well data for one realization related to the example presented above. As highlighted in Figure 4.16, there is no enforcing data for anomaly number 9 because it has a fidelity of 100% meaning that it is already reproduced by all realizations and does not need to be enforced. However, the software provides an option for the user to sample enforcing data for an anomaly that is not missing. Such enforcing data are collected from the same realization at the location of the anomaly to assure that it will be reproduced after repeating the geostatistical simulation. A user can control

the enforcing data by specifying the intervals along X, Y and Z coordinates for sampling the enforcing data. A very fine sampling resolution results in enforcing data at all grid locations withing the anomaly that corresponds to a strong anomaly enforcement.

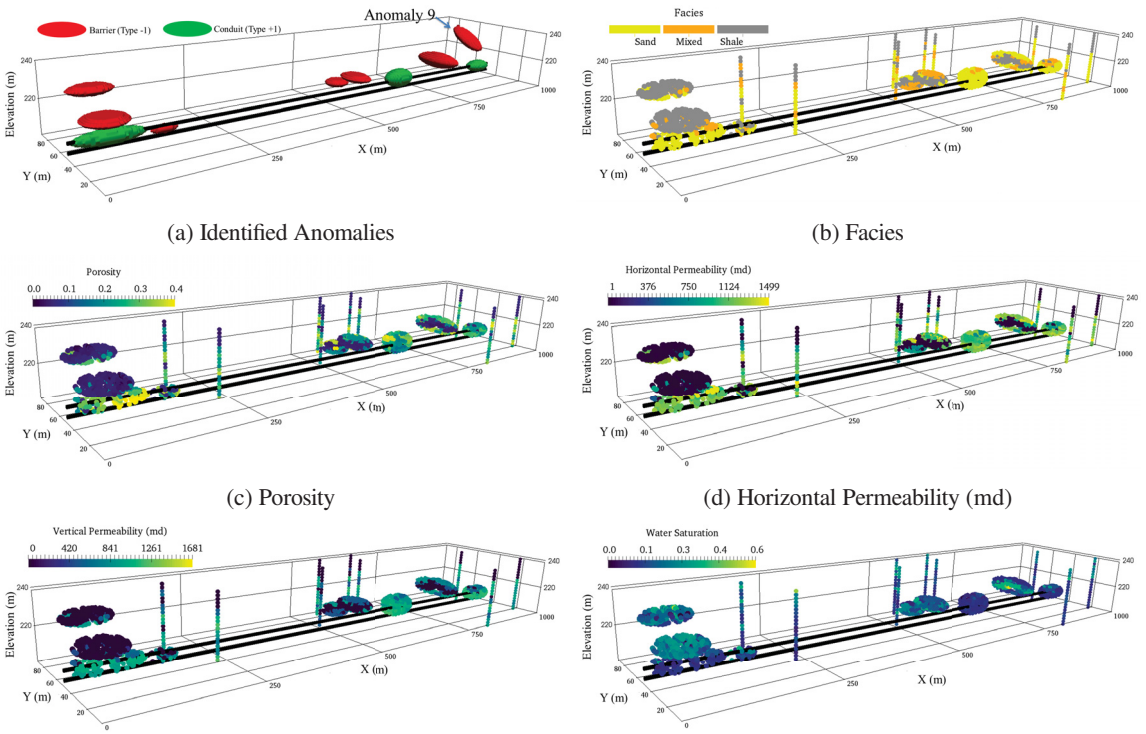

(a) Identified Anomalies

(b) Facies

(c) Porosity

(d) Horizontal Permeability (md)

(e) Vertical Permeability (md)

(f) Water Saturation

Figure 4.16: An example sampled enforcing data along with the original well data.

The final step is to repeat the geostatistical modelling for each realization separately with its own updated data file. Figure 4.17 shows the fidelity analysis report after geostatistical enforcement. As depicted in Figure 4.17, the fidelity of anomalies is improved and 60% of updated realizations (i.e., 12 out of 20) reproduced all identified anomalies.

4.3.4 Improved Steam Chamber Estimation for SAGD

The best way to study the effect of the proposed geostatistical anomaly enforcement on SAGD reservoir characterization is to check estimation of the steam chamber. The thermal flow simulation should be run for all initial and updated realizations to evaluate the effect of anomaly enforcement on steam chamber estimation. The main reason for considering only 20 realizations for this case study is the high computational cost associated with running thermal flow simulation (STARS, CMG) for all realizations. Figure 4.8 shows the steam chamber after 5 years for the reference model that is used as a criteria to assess local improvements in estimation of steam chamber propagation as a result of geostatistical anomaly enforcement.

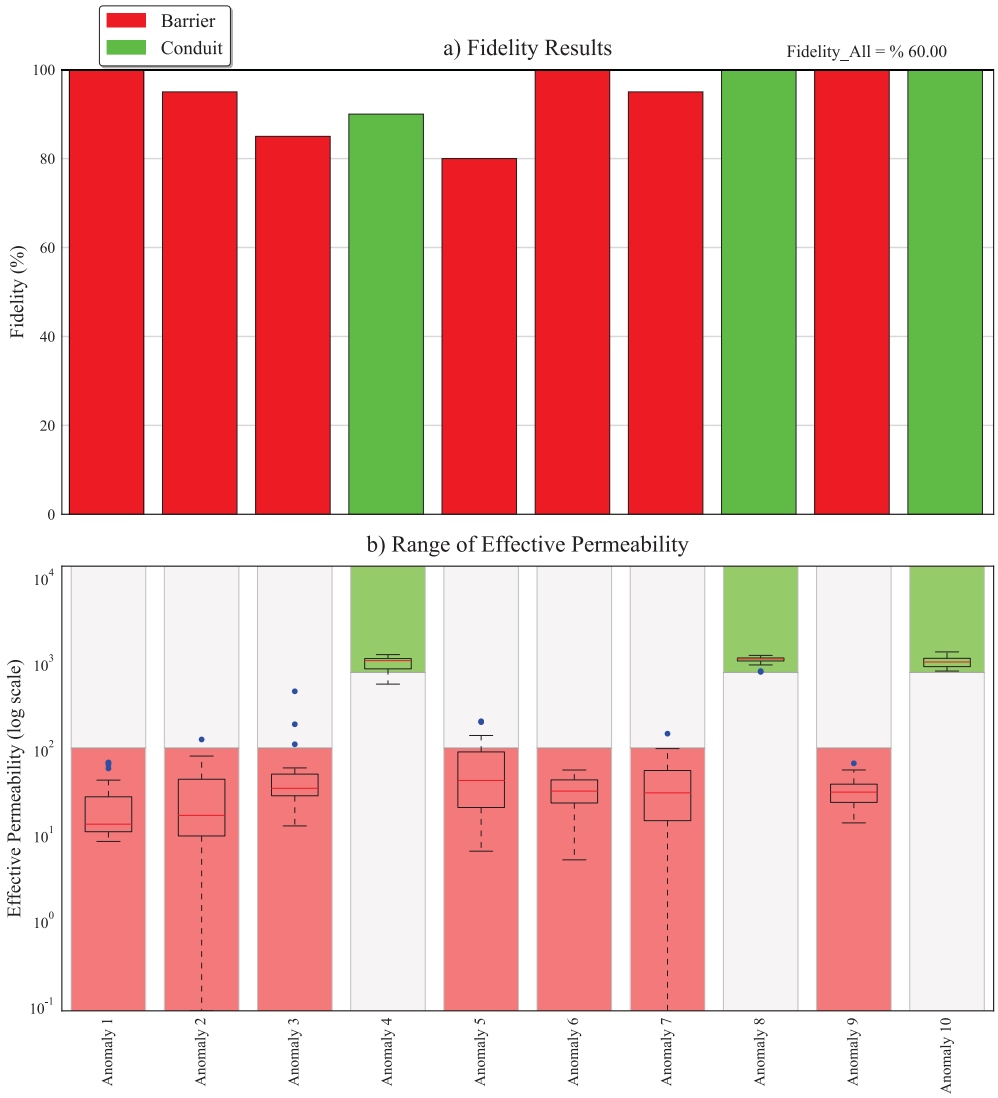

Figure 4.17: Fidelity analysis report after geostatistical anomaly enforcement. Panel a shows the fidelity percentage for each realization. Panel b shows the range of effective permeability for each anomaly over all realizations. Colored bars in panel b highlight the acceptable range of effective permeability for an anomaly to be reproduced.

Anomalies are enforced at specific locations identified from 4D seismic images; thus, it is expected to observe the effect of this enforcement as local improvements in estimation of the steam chamber. Figure 4.18 compares the steam chamber profile for all realizations with the reference model before and after anomaly enforcement. The top two panels in Figure 4.18 show top and cross-section views of the reference steam chamber (colored surface) based on an isothermal surface. Also, the location of the identified anomalies are highlighted. The bottom two panels show 2D cross-sections of steam chamber isothermal lines above the well pairs before and after anomaly enforcement. The red line highlights the reference steam chamber while the gray lines show its realizations. As can be seen in Figure 4.18, the steam chamber estimation is considerably improved at locations that anomalies are identified and enforced while there is no apparent improvement in areas that there

is no information available about the steam chamber and anomalies in its propagation. Note that the identified anomalies are reliable sources of information about the reality of steam chamber propagation in the reservoir.

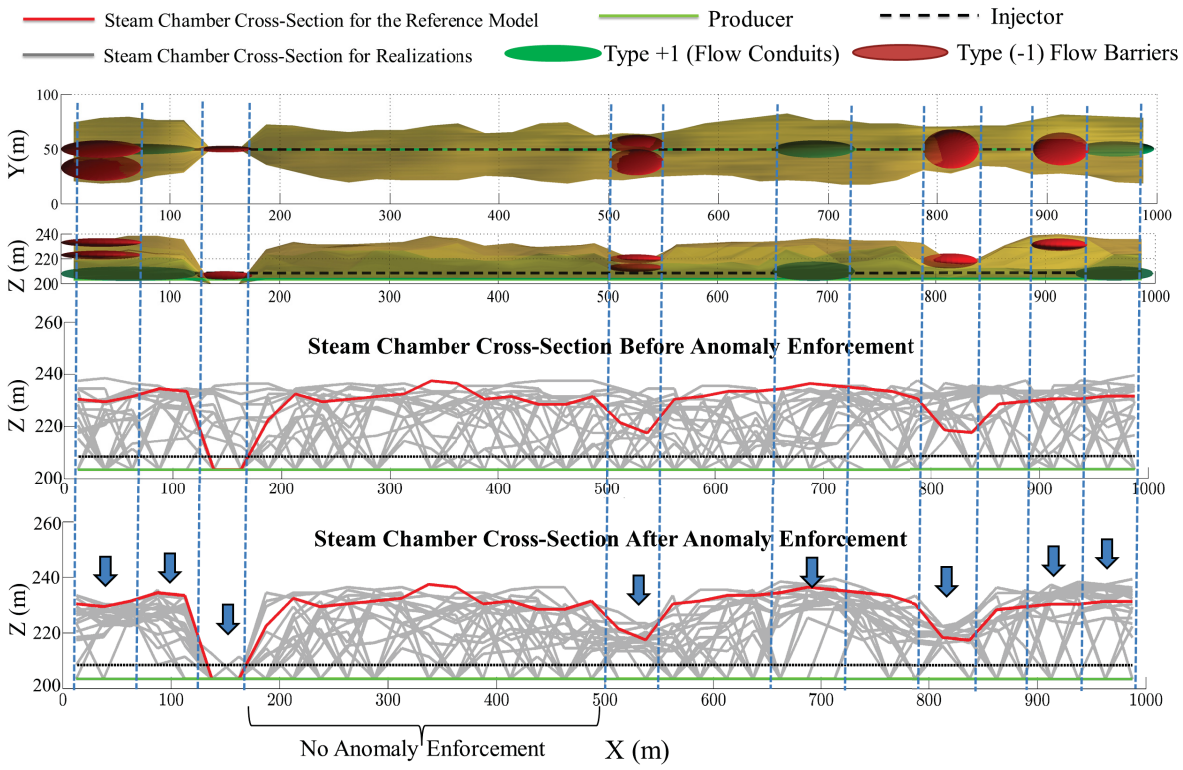

Figure 4.18: Effect of anomaly enforcement on local improvement of steam chamber estimation.

Considering the fact that anomaly enforcement is based on local updating of realizations, it is not necessarily expected to observe improvements in overall oil production. However, if there is a reasonable balance in identifying both flow barriers and conduits, improvements in estimation of overall oil production can also be achieved. Care is required to ensure that relative permeability, viscosity and other parameters are calibrated and reasonable. After geostatistical anomaly enforcement and updating all realizations, history matching and studies regarding the future performance of the reservoir can be carried out.

As can be seen in Figure 4.18, an area of the reservoir that has no identified anomaly is highlighted. Based on the synthetic 4D seismic data, another anomaly is considered for that area and the process of anomaly checking and enforcing is repeated using a total number of 11 anomalies. Figure 4.19 shows the effect of considering the additional anomaly on estimation of the steam chamber. By comparing Figure 4.18 and Figure 4.19, it can be realized that the additional anomaly is a flow conduit that explains the vertical growth of the steam chamber in this area. In practice, it is possible to get incremental 4D seismic data as more monitor surveys become available. Thus, the anomaly identification can be updated over time to provide more reliable information about the steam chamber propagation.

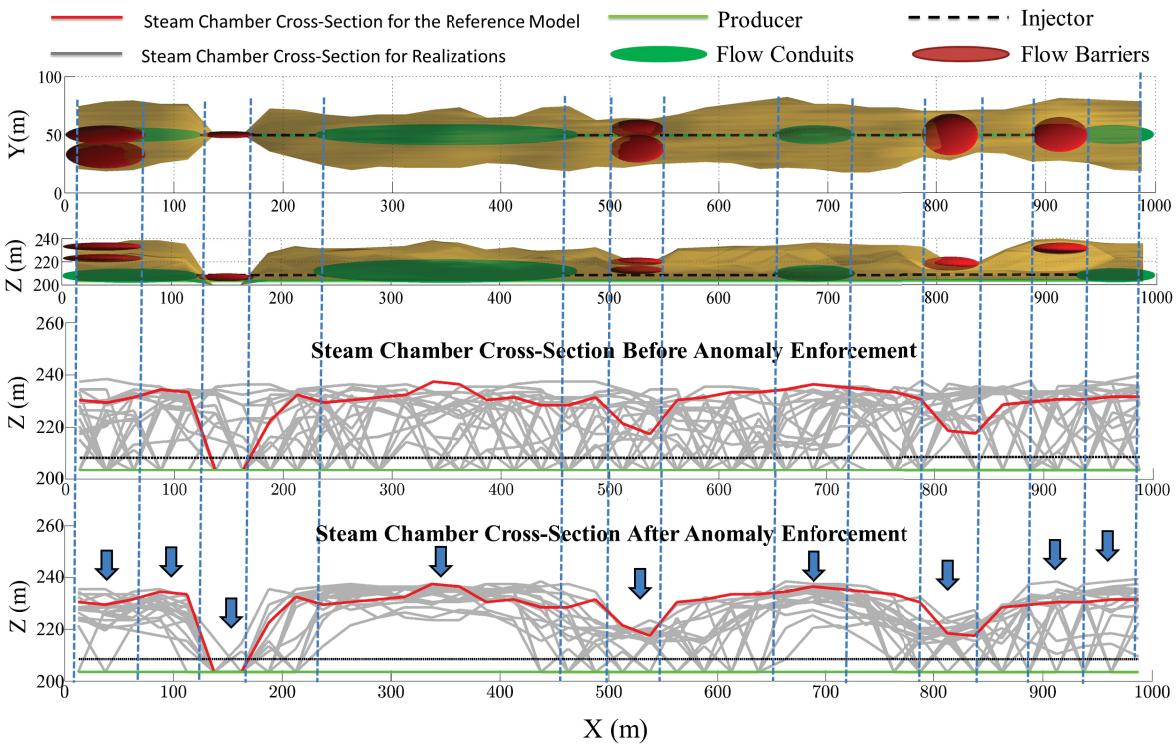

Figure 4.19: Effect of anomaly enforcement on local improvement of steam chamber estimation after considering an additional flow conduit.

4.3.5 Type 0 Anomaly (Normal Features)

In practice, it may be required to consider another type of anomaly apart from type $+1$ and -1. This additional type of anomaly highlights expected or neutral features (type 0) where the steam chamber is growing as expected. Defining the new type of anomaly allows to include more parts of the reservoir in the fidelity analysis. The permeability thresholds let the user specify how type 0 anomalies are evaluated compared to type $+1$ and -1. Figure 4.20 shows an example of considering the thresholds. K_{-1} and K_{+1} define the effective permeability thresholds for type $+1$ and -1 anomalies respectively. For type 0 anomaly a range $[K_{0-l},\ K_{0-h}]$ is considered to provide flexibility for the user to decide how these expected features are evaluated. The identification of type 0 anomaly can be facilitated through data analysis and automatic segmentation. In the next chapter, the details of identifying and including type 0 anomalies in geostatistical anomaly enforcement is explained by a case study.

4.4 Concluding Remarks

During a recovery process, incremental 4D seismic data becomes available that can be used to study the timing and quality of fluid flow within the reservoir. A practical methodology is proposed for the effective integration of information inferred from 4D seismic data in reservoir characterization. Anomalies in fluid flow are the most reliable information that can be inferred from 4D seismic data. The proposed methodology consists of four

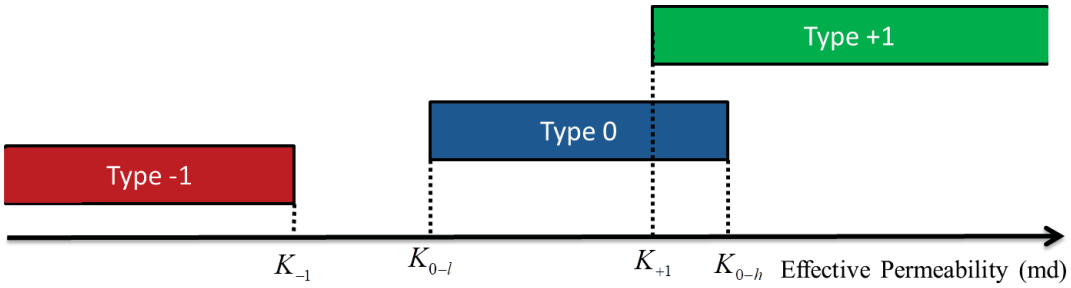

Figure 4.20: Considering permeability thresholds to evaluate different types of anomalies.

main steps: anomaly identification, fidelity analysis, sampling the enforcing data and repeating the geostatistical modeling workflow. The last three steps are automated. The success of this methodology depends on reliable anomaly identification. In this regard, professional judgment is employed to identify reservoir anomalies based on visual inspection of 4D seismic images. The output of anomaly identification is a report file containing the location and spatial extent of each identified anomaly. A large anomaly would be broken into several smaller anomalies with the same type. This improves the chance of finding candidate sampling zones for each anomaly within the ensemble of all realizations. Although ellipsoids can be used to describe the spatial extent of an anomaly, the proposed methodology is not confined to this approach and the anomalies can be also reported by grid addresses.

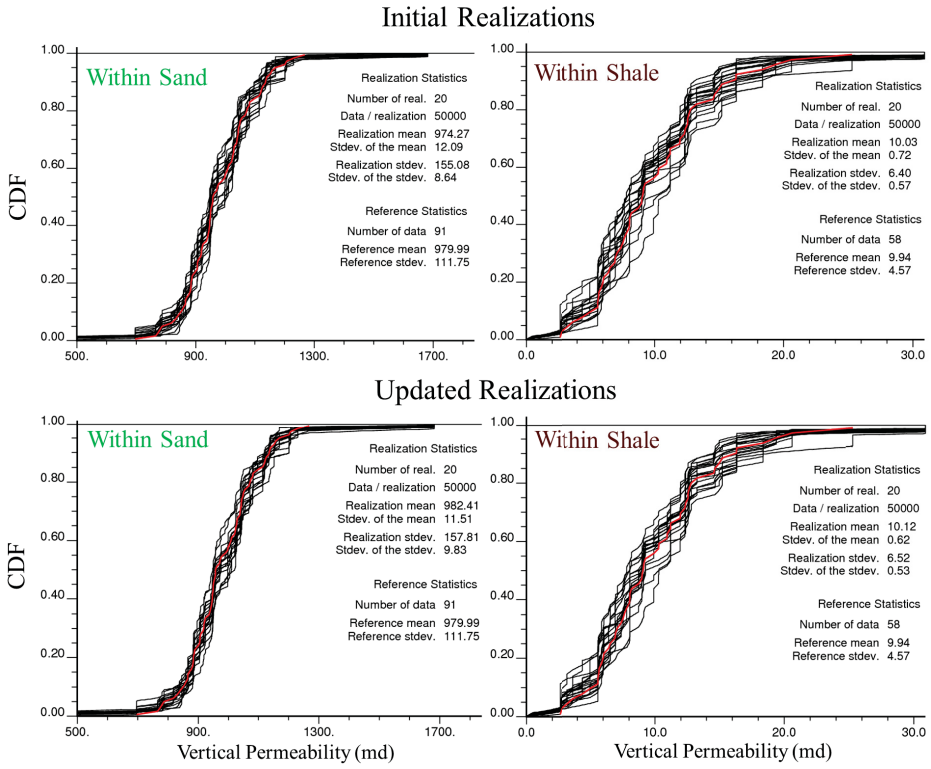

Figure 4.21: Histogram reproduction for realizations before and after anomaly enforcement.

The automated fidelity analysis determines what percentage of geostatistical realizations reproduce each anomaly. Also, the missing anomalies are identified and if the fidelity is not sufficient, automatic sampling of enforcing data can be considered. This results in a unique data file for each realization that contains the original well data and unique sampled enforcing data for the realization. The last step is to repeat the geostatistical modelling workflow with the same settings and input statistical parameters. The only difference is that each realization is conditioned to its own updated data file.

The anomaly enforcement is independent for each realization through a random process. In this way, the variability described by the ensemble of realizations will not be artificially reduced as a result of anomaly enforcement. Figure 4.21 shows the histogram reproduction and summary statistics for vertical permeability within two different rock types (Sand and Shale) before and after anomaly enforcement. The updated realizations are related to the case with 11 identified anomalies being considered. The anomaly enforcement may affect the proportion of facies because anomalies are related to relatively extreme flow regimes and adding the enforcing data and updating realizations can affect the proportions of different facies. This can be regarded as a desirable feature since the initial proportions are inferred based on limited static data and the integration of 4D seismic may contribute to better understanding of facies proportions. Checking the reproduction of statistical parameters including proportion and histograms before and after integration of 4D seismic should be considered.

Chapter 5

Case Study for Geostatistical Anomaly Enforcement

A practical methodology for effective integration of information obtained from 4D seismic data is proposed and explained in Chapter 4. This methodology is based on three main steps: anomaly identification, fidelity analysis and geostatistical anomaly enforcement. In this chapter, a case study is presented to demonstrate the implementation of the proposed methodology based on real 4D seismic data from a SAGD Drainage Area (DA) in the Surmont project (Hadavand et al., 2017). Figure 5.1 shows an example of 4D seismic data and inferred steam chamber thickness for the DA. 4D seismic data are often represented as a cloud of points that highlight areas in the reservoir where the changes in seismic attributes are higher than a certain threshold (Figure 5.1a). As shown in Figure 5.1b, 4D seismic data can be used to infer a 2D map of the steam camber thickness for SAGD. In this case study, initial geostatistical realizations of the DA that are conditioned to well data get updated based on information inferred from incremental 4D seismic data. In addition, best practices and guidelines for anomaly identification are presented and implemented.

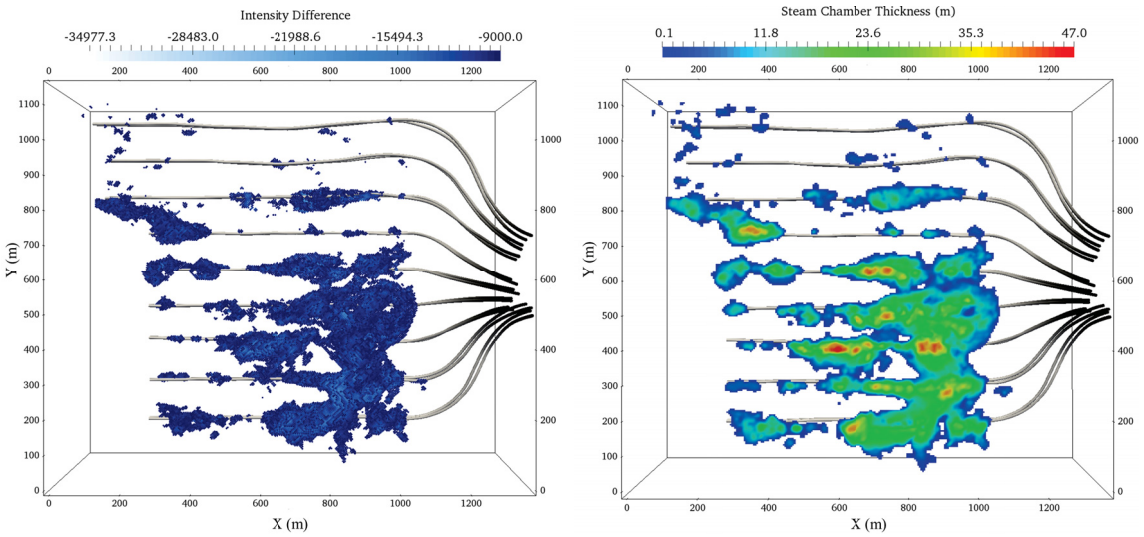

(a) 4D seismic data points

(b) Steam chamber thickness map

Figure 5.1: 4D seismic data obtained from a SAGD drainage area in Surmont Project (Hadavand et al., 2017).

Fidelity analysis determines what percentage of initial geostatistical realizations reproduce each identified anomaly. Also, it reveals the missing anomalies in each realization. The enforcing data are sampled to provide unique updated data files for each realizations. Repeating the geostatistical modelling workflow using new data files results in updated realizations that are informed by 4D seismic anomalies. Another fidelity analysis may be considered to compare updated and initial geostatistical realizations.

5.1 Case Study

Surmont is a SAGD recovery project located in the Athabasca Region of northeastern Alberta. In this chapter, 4D seismic data from one of the drainage areas in Phase 1 of the Surmont project are considered to identify anomalies in propagation of the steam chamber. Figure 5.2 shows the Surmont area and highlights the drainage areas in this project.

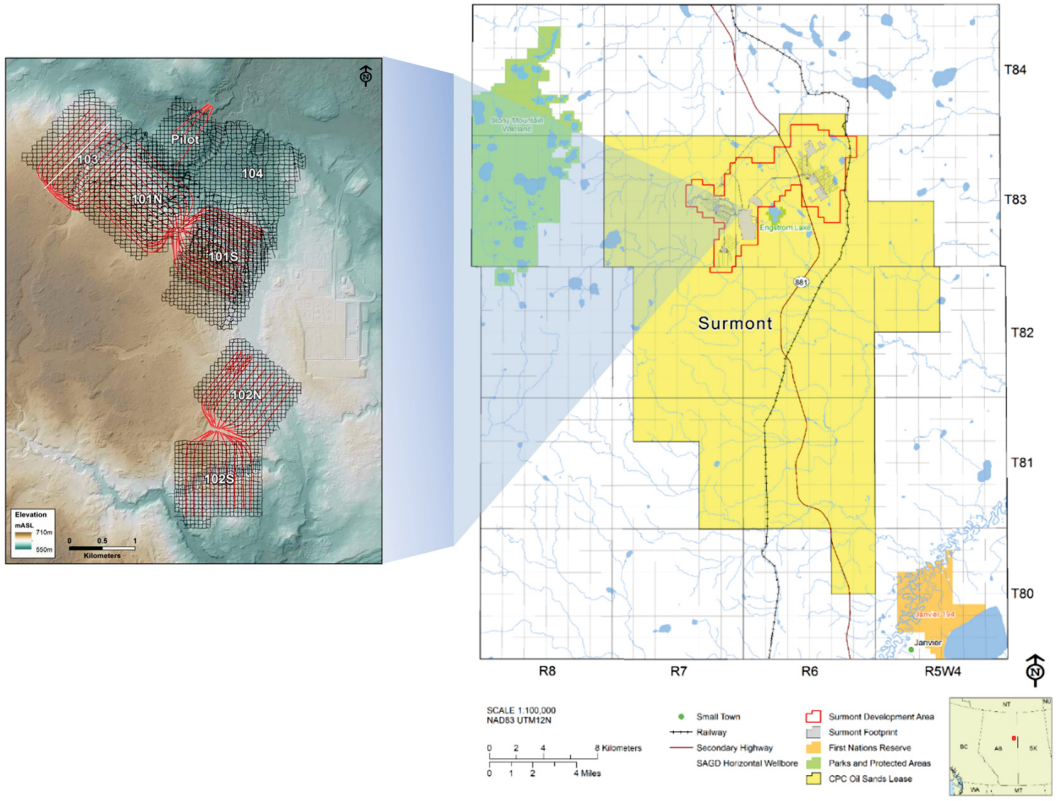

Figure 5.2: The target drainage area from Surmont SAGD project (obtained from AER in situ performance presentations (www.aer.ca)).

5.1.1 Data Inventory

Figure 5.3 shows the DA considered in the case study. There are 9 SAGD well pairs with average length of 1000 m and separation distance of 100 m. As shown in Figure 5.3a, a limited number of wells provide data for facies. Also, petrophysical properties including shale volume, porosity, permeability and fluid saturations are sampled. There are five facies of Sand, Breccia (BRCC), SIHS, MIHS and Mud stone (MDST) that explain rock quality. Steam injection and production of heated bitumen changes the observed seismic attributes. Figure 5.3b shows an example of 4D seismic data that highlights areas in the DA that are deemed to be affected by the steam chamber propagation.

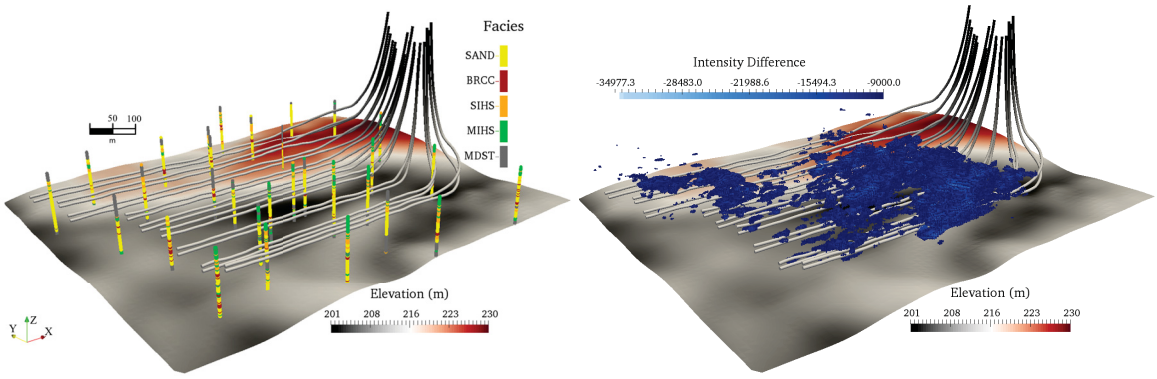

(a) Drainage area and sampled well data for facies. (b) 4D seismic data points.

Figure 5.3: 4D seismic data obtained from the drainage area in Surmont Project.

Geostatistical realizations are often conditioned to available static data including well logs. Study of incremental 4D seismic data are considered in this case study to infer some information about steam chamber propagation around each well pair within the DA. Geostatistical realizations are then updated based on such information to constrain the geological uncertainty.

5.1.2 Initial Geostatistical Realizations

The sampled well data are considered to generate the initial geostatistical realizations. Seismic horizons along with geological interpretations determine different zones in the DA (Figure 5.4a). Each zone has a different geostatistical modelling framework. Hierarchical truncated pluri-Gaussian (HTPG) is employed for geostatistical facies modelling within different zones (Silva and Deutsch, 2016). HTPG is an implementation of truncated pluri-Gaussian technique that yields a better reproduction of transition probabilities while enforcing the geological ordering between facies. HTPG provides a hierarchical workflow to define often complex relationships and ordering between facies. In this case study, HTPG is employed as an alternative for facies modelling to emphasize that the proposed geostatistical anomaly enforcement can be implemented with different modelling techniques. Figure 5.4b shows one initial geostatistical realization of facies conditioned to the well data.

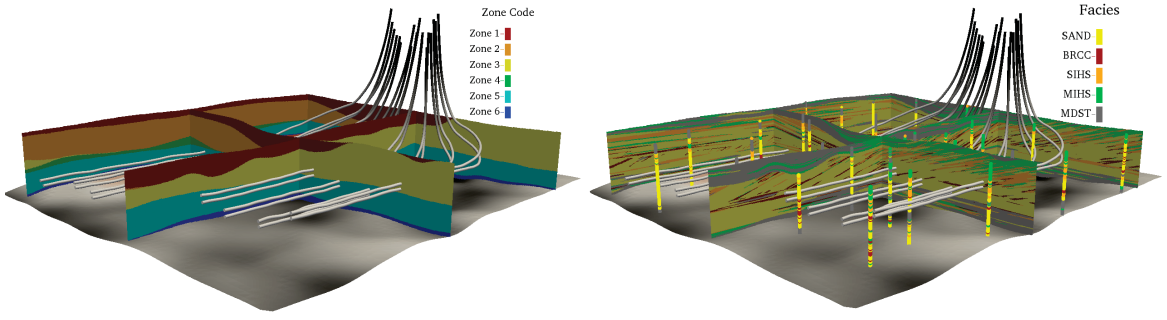

(a) Identified zones within the DA. (b) One initial realization of facies model.

Figure 5.4: Initial geostatistical facies modeling.

Petrophysical properties are modeled within each facies using multivariate Gaussian framework provided by PPMT (Barnett et al., 2014). PPMT transforms the continuous petrophysical properties into an uncorrelated multivariate Gaussian framework where each variable is simulated independently. This is followed by PPMT back-transformation into original units. This allows to reproduce the complex multivariate relationships observed in the sampled data. Figure 5.5 summarizes the multivariate relationships between different petrophysical properties inferred from sampled well data within Sand facies.

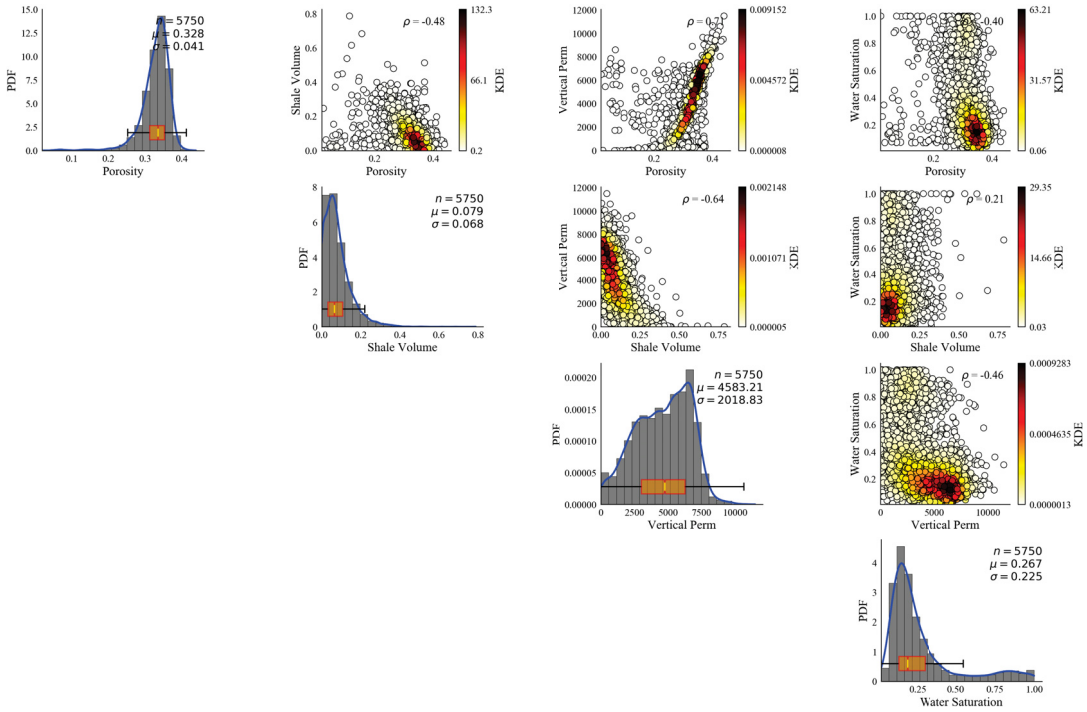

Figure 5.5: Univariate and bivariate analysis for petrophysical properties within SAND facies.

Figure 5.6 shows one realization of petrophysical properties modeled within facies based on the explained multivariate modeling framework. The next step is to study 4D seismic data to evaluate the steam chamber propagation and identify anomalies.

5.1.3 4D Seismic and Steam Chamber

Variations in temperature, fluid saturation, pore pressure and temperature during SAGD makes it possible to monitor the steam chamber propagation using 4D seismic data. As explained in Chapter 4, the key idea is to identify anomalies in propagation of the steam chamber. This is done by visual inspection of 4D seismic data. As was mentioned above, 4D seismic data are often represented by a cloud of points. In order to have a better visualization, surfaces surrounding the cloud of points are constructed. This can be obtained by applying a kernel weighting function where there is a 4D seismic data point to get a smooth 3D location map. Applying a contour function on the 3D model gives the surfaces surrounding the available 4D seismic data that is referred

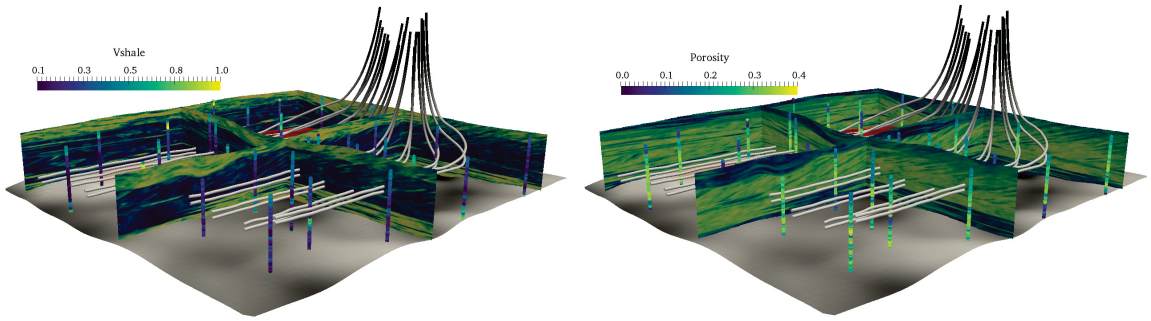

(a) Shale volume (b) Porosity

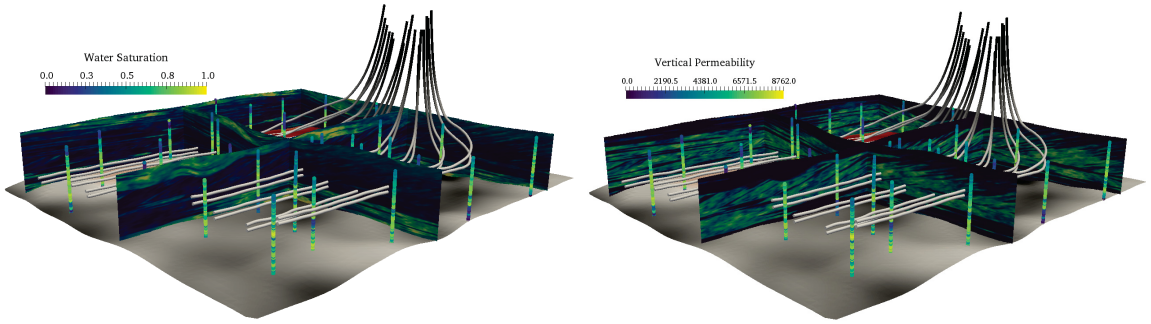

(c) Water saturation (d) Vertical permeability (md)

Figure 5.6: One realization of petrophysical properties modeled within facies.

to as 4D seismic defined steam chamber. Figure 5.7 shows the improved visualization that facilitate anomaly identification. Also, an example flow barrier (anomaly type -1) is highlighted in Figure 5.7.

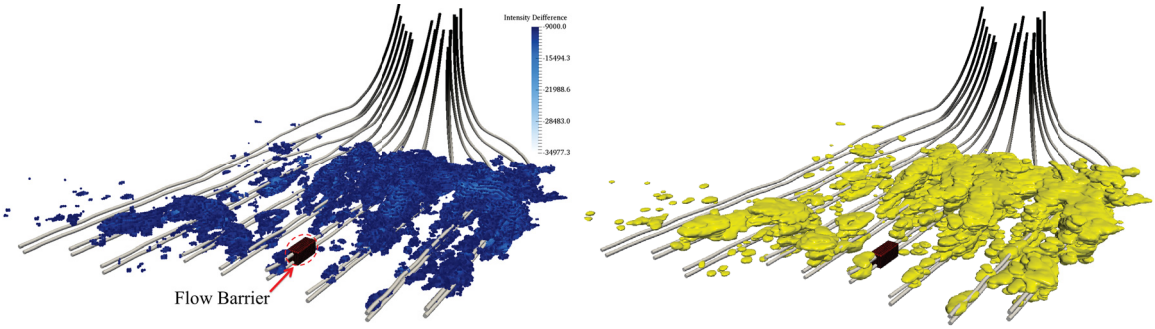

(a) 4D seismic data as a cloud of points (b) 4D seismic data as surfaces

Figure 5.7: 4D seismic data and the steam chamber.

During this SAGD project, several 3D seismic surveys were obtained. Time lapse analysis is used to provide incremental 4D seismic data that can be used to study the propagation of steam chamber over time. Figure 5.8 shows the incremental 4D seismic data for the DA considered in this case study. The evolution of 4D seismic defined steam chamber helps with anomaly identification.

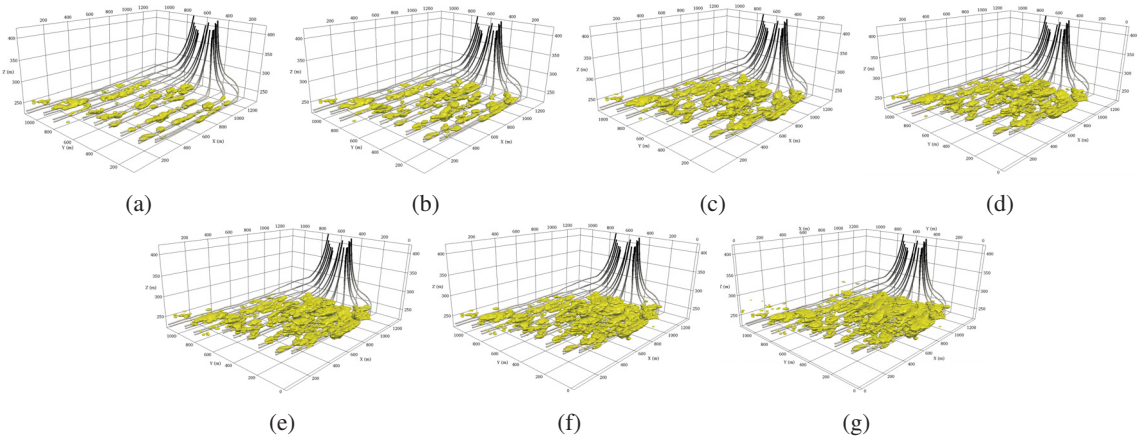

(a) (b) (c) (d)

(e) (f) (g)

Figure 5.8: Incremental 4D seismic data for the DA.

5.1.4 Anomaly Identification

Anomaly identification is based on visual inspection of 4D seismic data and professional judgment. In practice, this may be regarded as a multi-disciplinary task that can be accomplished through collaboration between a reservoir engineer and a geophysicist. In this chapter, some guidelines are presented for successful identification of each type of anomaly.

5.1.4.1 Identifying Anomaly Type -1 (Barrier)

A flow barrier is a volume within the reservoir where the effective permeability is not sufficient for the steam chamber to grow as expected. A review of incremental 4D seismic data helps to understand how steam chamber is growing around a well pair. The identification of this type of anomaly is related to volumes of the reservoir where the steam chamber is missing. Production details such as the timing of injections for different well pairs and the variation in steam injection along the well pair should be considered. The steam chamber may grow faster around the heel of the well pair due to higher injection rate and steam quality. This may be mitigated with flow control devices that provide a more uniform distribution of pressure along the wells (Stalder, 2013). Having a detailed knowledge of the recovery process and operating conditions for each well pair is critical for confident anomaly identification. Figure 5.9 shows isolated incremental 4D seismic images for a single well pair from the DA. As can be seen in Figure 5.9, a type -1 anomaly (flow barrier) is identified for this well pair because there is steam chamber growth along the well pair before and after the identified anomaly. In other words, the steam chamber is expected to start growing at that location, but it is missing.

When there is no steam chamber growth at a location along the well pair, the barrier is most likely close to the wells and between the producer and injector. Such barrier hampers the hot connection between the two wells and does not allow the steam chamber to form. Figure 5.10 shows another type -1 anomaly identified along the same well pair. This barrier is identified in an area where the steam chamber is formed but, the lack of steam

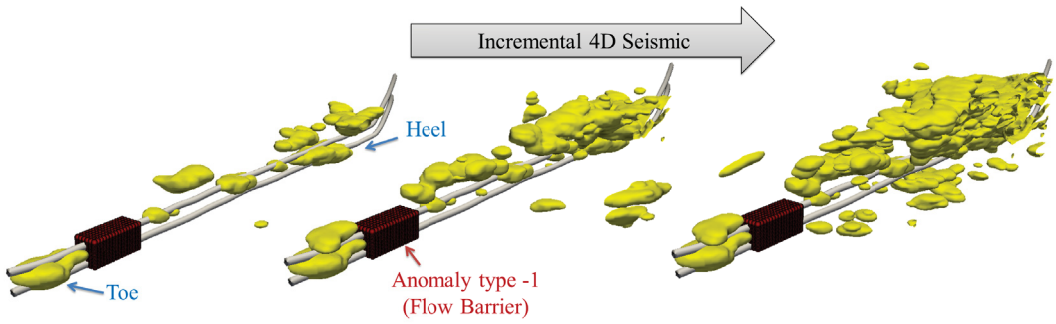

Figure 5.9: An example identification of a flow barrier based on visual inspection of 4D seismic images along a single well pair.

injection in that area caused a hole in steam chamber profile that can be confirmed by inspection of incremental 4D seismic data.

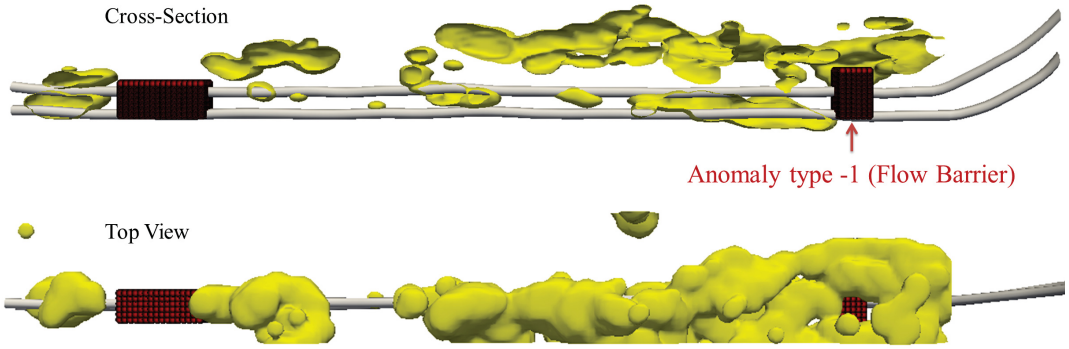

Figure 5.10: Another example of an identified flow barrier.

A list of guidelines on identifying anomaly type -1 (barrier) for SAGD are provided below. Considering these guidelines help to infer reliable information from 4D seismic defined steam chamber.

- A flow barrier/baffle is associated with a volume in the reservoir with relatively low effective permeability.
- A barrier hampers the propagation of steam chamber during SAGD.
- Barriers are identified where the steam chamber is expected to exist, but it is missing or growing slower than expected.
- In general, each well pair may be considered independently to understand the expected steam chamber propagation over time.
- If the timing of steam injection and the operation strategy are known for different well pairs, the steam chamber propagation can be compared between wells.
- The pressure gradient along the well affects the timing of the steam chamber propagation.

- If there is no significant differences in seismic attribute (no 4D seismic data points), it is likely the interconnection between the producer and injector is blocked by a barrier.

5.1.4.2 Identifying Anomaly Type +1 (Conduit)

Identifying a type +1 (flow conduit) is also based on how the steam chamber evolves over time. However, a flow conduit is where the steam chamber is growing faster than expected due to high flow quality. Thus, a flow conduit is an area in the reservoir with relatively high effective permeability that lets the steam chamber grow quickly. Figure 5.11 shows example flow conduits that are identified where the steam chamber is growing relatively fast. Reviewing incremental 4D seismic data is very helpful to better understand the location and spatial extent of a flow conduit.

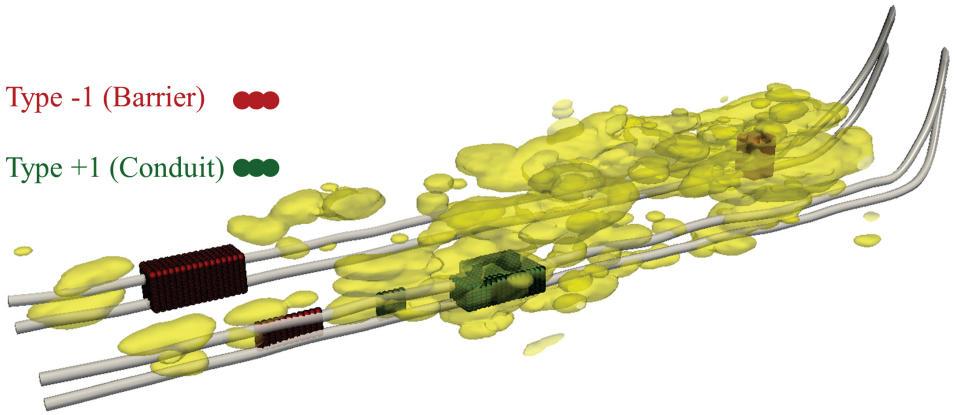

Figure 5.11: Flow conduits identified where steam chamber is growing faster than expected.

The overlap or coalescence between adjacent steam chambers is also an indicator of relatively high effective permeability. Thus, a flow conduit can be identified to ensure that all realizations reproduce this feature. Note that the identified anomalies describe the quality of fluid flow at certain locations based on 4D seismic data. Thus, it is critical that all realizations reproduce the identified anomalies. Figure 5.12 shows a flow conduit related to the interconnection between the steam chambers of two adjacent well pairs.

A list of guidelines are provided below the should be considered for identification of anomaly type +1 (conduit).

- A flow conduit is associated with a volume in the reservoir with relatively high effective permeability.
- A flow conduit is where the steam chamber is growing faster than expected.
- Steam chamber propagation is inferred based on visual inspection of 4D seismic images.
- Using surface visualization of 4D seismic data facilitates the identification of flow conduits.
- The overlap or coalescence between to adjacent steam chamber is identified as a flow conduit.

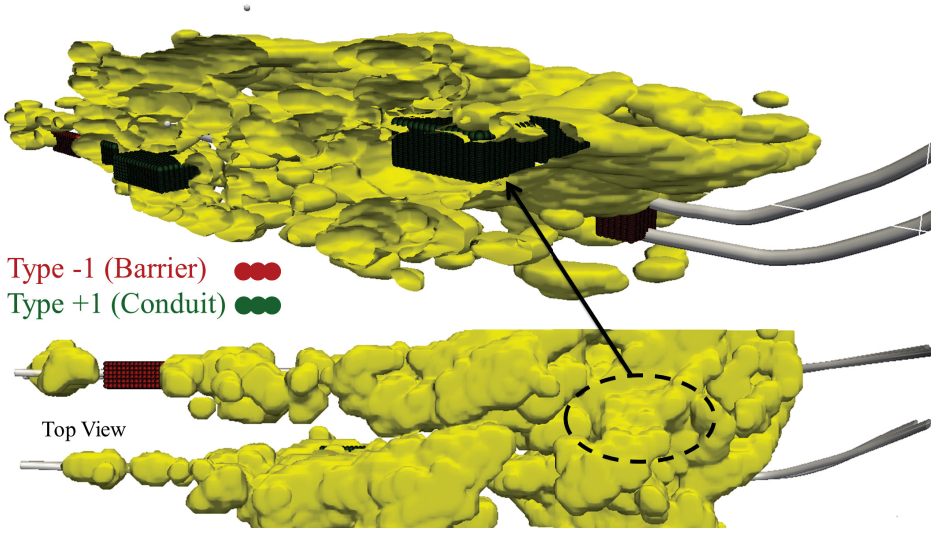

Figure 5.12: A cross-section through 4D seismic surfaces that shows the coalescence between to adjacent steam chamber and also the identified flow conduit.

- Comparison between different well pairs helps to understand how the steam chamber grows over time.
- Positive anomalies are more likely to be reproduced by the geostatistical realizations because, usually the well trajectories are optimized based on an ensemble of all realizations to be in regions of high quality.

5.1.4.3 Identifying Anomaly Type 0 (Expected Feature)

Anomaly type 0 refers to a volume in the reservoir where the steam chamber is growing as expected. Thus, any volume of the reservoir inside the 4D seismic defined steam chamber is potentially a type 0 feature. A data analysis algorithm can be employed to process 4D seismic data and identify type 0 features. This is done based on finding grid addresses that correspond to volumes inside the 4D seismic defined steam chamber. The grid address is related to the grid specification for the geostatistical realizations. In this context, a grid pattern may be considered that highlights the center of grid cells based on the grid specification. Then, grid cells that are inside the steam chamber can be identified. This process is schematically demonstrated in Figure 5.13. Figure 5.13-I shows a part of 4D seismic surfaces along with the grid pattern. The first step for the algorithm is to scan the 4D seismic data and assign each 4D seismic data point to the nearest grid cell. 4D seismic data highlight locations where the difference in the seismic attribute(s) is higher than a threshold. For SAGD, this difference may be considered as a measure of changes in the reservoir due to steam chamber propagation and bitumen production. The difference for each point is normalized by the maximum difference over the entire 4D seismic data set and this process can be implemented for all incremental 4D seismic data used for anomaly identification. The objective is to provide a measure of 4D seismic difference that corresponds to timing of steam chamber propagation within the reservoir. During SAGD, volumes closer to the center of the steam chamber have higher temperature and in turn stronger changes in reservoir properties due to bitumen production. Incremental 4D

seismic analysis compares different monitor surveys with the base seismic survey. The algorithm keeps track of the number of 4D seismic data points assigned to each grid cell and the number of incremental surveys that affect each grid cell. As a result, a parameter (normalized difference factor (NDF)) is defined that is normalized to be in the range 0 to 1 providing a measure to assess the level of difference in seismic attributes. Note that the algorithm provides an initial automated identification for type 0 features that needs to be evaluated based on professional judgment to determine which identifies features should be included in the subsequent fidelity analysis.

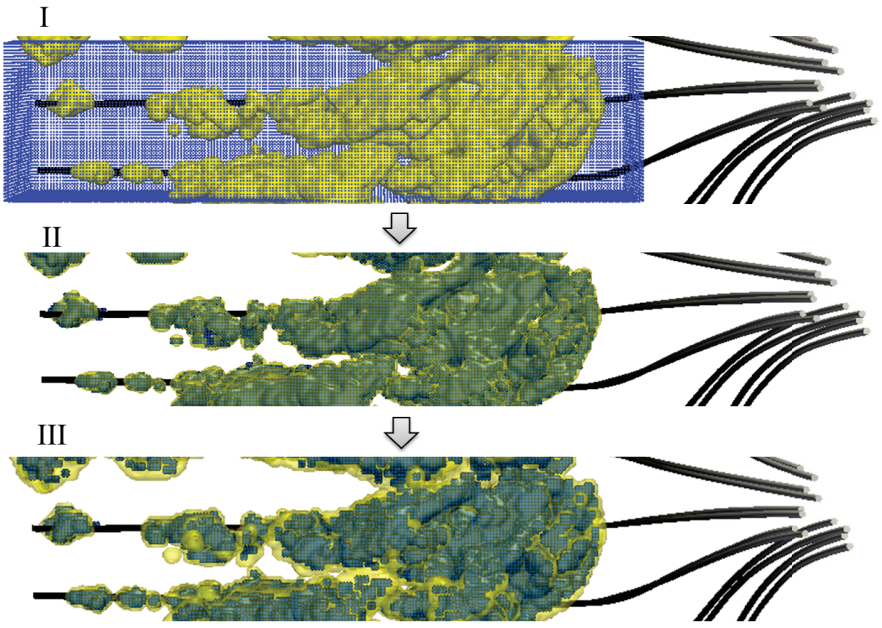

Figure 5.13: Processing 4D seismic data to get the grid addresses associated with points inside the steam chamber.

Figure 5.13-II shows the collection of grid addresses with NDF larger than 0. Large NDF values indicate a large difference in the seismic attributes. Figure 5.13-III shows the collection of grid addresses with NDF bigger than a threshold (i.e., 0.1). This provides more flexibility to select grid addresses with higher seismic differences as the potential type 0 anomalies. The second step of the algorithm is to break the selected grid addresses to separate features with reasonable spatial extent. This makes it possible to process an identified feature by a flow simulation unit in order to get the effective directional permeability. The spatial extent and NDF threshold may be defined based professional discretion, considering the recovery process and 4D seismic data. The well trajectories are considered and the identified grid addresses are divided to type 0 features based on a user defined distance around the well pair and a desired spatial extent for each feature. The data analysis facilitates the identification of expected features and professional judgment may be considered to check them.

In this case study, a total number of 110 anomalies including: 10 type -1 (flow barriers) and 19 type $+1$ (flow conduits) and 81 type 0 anomalies are identified for the drainage area. Figure 5.14 shows the identified anomalies. Type -1 and $+1$ are highlighted by red and green points respectively. Type 0 anomalies are presented

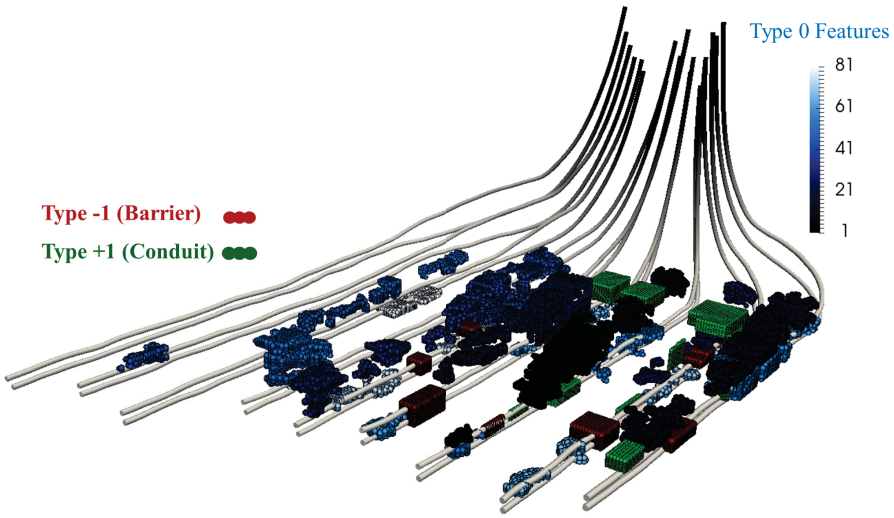

Figure 5.14: A total number of 110 anomalies identified for the drainage area.

by a spectrum of blue color. If an anomaly with considerably large spatial extent is identified, it is recommend to break such anomaly into two or more smaller anomalies. This helps to assure that enforcing data can be found for the anomaly within the ensemble of geostatistical realizations. Considering the size of the reservoir, one can decide what is a large spatial extent that reduces the possibility of finding a candidate sampling zone. Also, the random search algorithm that finds candidate sampling zone for each anomaly (Chapter 4 and Appendix A) notifies the user if a sampling zone cannot be found within the ensemble of realizations.The identified anomalies represent the information inferred from 4D seismic data. A fidelity analysis is carried out to evaluate reproduction of such information by the initial realizations.

5.1.5 Fidelity Analysis

The fidelity analysis is automated by the software ART (Appendix A). As explained in Chapter 4, the effective directional permeability is the measure to check the fidelity of an anomaly. In case of SAGD, effective vertical permeability is calculated by sampling horizontal and vertical permeability from each realization and within the anomaly for which the fidelity analysis is performed. Then, the fidelity analysis is conducted by considering thresholds of permeability that are determined based on professional discretion and the local geological and flow properties. For this case study, flow simulation studies and feedback from reservoir engineers are considered to determine the thresholds. Figure 5.15 demonstrate how the permeability thresholds are defined. The thresholds are assigned as: $K_{-1} = 150\ md$, $K_{0-l} = 500\ md$, $K_{0-h} = 3000\ md$ and $K_{+1} = 2500\ md$. Also, it is possible to consider separate thresholds for each anomaly. In Figure 5.15, the acceptable range of effective permeability for each type of anomaly is highlighted by the color bars.

Figure 5.16 demonstrates the fidelity analysis results for anomalies type -1 and $+1$ considering the initial geostatistical realizations. The initial realizations are conditioned to available sampled well data and do not

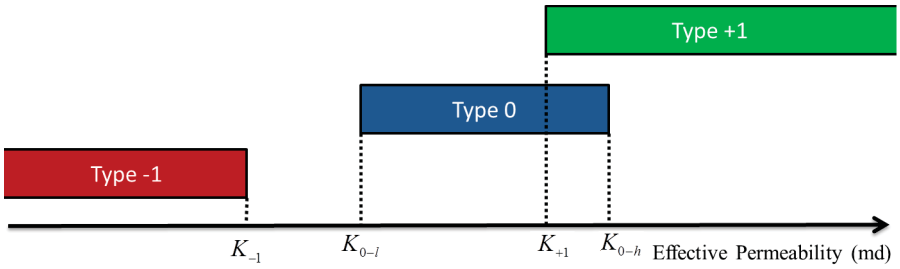

Figure 5.15: Considering permeability thresholds to evaluate the anomaly reproduction.

consider the anomalies identified from 4D seismic images. The fidelity analysis is conducted to determine what percentage of initial geostatistical realizations reproduce each anomaly. The top graph (Figure 5.16-a) shows the fidelity percentage for each anomaly. The colored bars depict the percentage of realizations that reproduce each anomaly. Red highlights anomaly type -1 while green highlights anomaly type $+1$. Also, the average shale volume for each anomaly and across all realizations are plotted by orange points. Apart from permeability, the shale volume is another petrophysical property that can be used to monitor the fidelity analysis. Because, the average shale volume is correlated with the type of anomaly. For example, a flow barrier is expected to have a higher average shale volume compared to a flow conduit.

In Figure 5.16-b, the box plot shows the range of effective vertical permeability for each anomaly and across all initial realizations. The colored area highlights the range of effective permeability within which the anomaly is reproduced or satisfies the fidelity test (based on the specified thresholds). For instance, for an anomaly type -1, the effective permeability is supposed to be lower than $K_{-1} = 150\ md$ threshold that is highlighted by the red area.

Figure 5.16-c summarizes the range of variability of average shale volume within each anomaly and across all realizations. The fidelity analysis is automated and provides an evaluation of anomaly reproduction for the geostatistical realizations. The same fidelity analysis for anomaly type 0 is presented separately in Figure 5.17. This helps to have a better visual evaluation of fidelity analysis for different types of anomalies.

As can be seen in Figure 5.16-a and 5.16-b, the low fidelity percentage for anomalies corresponds with the range of effective permeability calculated for each anomaly and across all realizations. For instance, consider anomaly number 5 that is a flow barrier and its range of effective permeability across all initial realizations is shown by the box plot in 5.16-b. The effective permeability of this anomaly in all realizations is higher than the corresponding threshold resulting in %0 fidelity. In Figure 5.16, the fidelity for all anomalies (i.e., Fidelity_All) is reported to be $\%0$ meaning that none of the initial realizations reproduces all the identified anomalies type -1 and $+1$. Also, Figure 5.17 shows that the fidelity for all identified expected features (type 0) is $\%0$. After the fidelity analysis, the missing anomalies for each realization are specified and if the initial realizations do not provide sufficient fidelity, geostatistical anomaly enforcement can be implemented.

5.1.6 Geostatistical Anomaly Enforcement

The geostatistical anomaly enforcement is based on sampling enforcing data for the missing anomalies that is automated by the software ART (Appendix A). As explained in Chapter 4, the sampled data have to comply with the geostatistical modeling and geological framework. This is done by sampling enforcing data from the ensemble of initial realizations resulting in a separate updated data file for each realization. The data file contains the original well data and the unique enforcing data for the corresponding realization. As mentioned above, the geostatistical modeling of a reservoir is often done separately for each geological zone. Each zone may have different rock properties, anisotropy angles and geological framework. There is an option for zone-wise sampling in order to assure the enforcing sampled data come from a plausible geological framework.

In the case study, the geostatistical enforcement is conducted based on sampling the enforcing data for facies and all other simulated petrophysical properties. Figure 5.18 shows an example updated data file for two realizations. In Fig. 5.18, only facies and vertical permeability data are presented; however, the updated data file contain all petrophysical properties. As seen in Figure 5.18, the updated data file contain the original well data (vertical wells) along with sampled enforcing data. There is a potential concern about anomalies/features that are located immediately adjacent to one another. Although the sampled enforcing data are sampled from the same geological zone, there is a risk of spatial discontinuity being introduced due to contradictory conditioning data next to each other. There are two solutions to this. As mentioned in Chapter 4, the enforcing data are sampled from a candidate sampling zone based on a user-defined spatial resolution. Thus, the first option is to choose sufficiently large sampling resolution that allows the simulation engine to introduce a natural blending between the conditioning data. The second option is to introduce a buffer region with no enforcing data between two immediately adjacent anomalies. The buffer zone may be determined based on the range of spatial continuity (i.,e variogram ranges). As a result, the geostatistical simulation provides the spatial continuity between adjacent anomalies.

After sampling the enforcing data, all geostatistical realizations are updated to integrate the information inferred from 4D seismic data. This is done by repeating the geostatistical modeling workflow using the updated data files. The key idea is that each realization is updated independently using its own unique data file. Afterwards, a fidelity analysis is conducted to evaluate the effect of anomaly enforcement. Figure 5.19 shows the result of the fidelity analysis after geostatistical anomaly enforcement. As can be seen in Figure 5.19, the fidelity of anomalies are significantly improved after the geostatistical enforcement. The average shale volume also corresponds with the improved fidelity as there is a higher shale volume associated with the barriers(type -1) and lower with the conduits (type $+1$).

The fidelity analysis demonstrates that the geostatistical enforcement results in improved reproduction of anomalies considering the acceptable range of effective permeability. The effect of anomaly enforcement may be evaluated based on the flow responses and the local improvements in the estimation of steam chamber propagation. However, the computational cost often does not allow to run flow simulation for the entire drainage area

and all realizations. One practical approach is to consider a limited volume of the reservoir that is affected by an identified anomaly and run flow simulation for that isolated volume. Figure 5.20 shows the spatial distribution of vertical permeability for one realization of the reservoir and highlights a segmented volume that is affected by an identified type -1 anomaly (a flow barrier). This allows to execute thermal flow simulation for multiple realizations in a manageable time in order to study the effect of local anomaly enforcement on estimation of the steam chamber propagation.

Figure 5.21 shows the result of running thermal flow simulation STARS, (CMG) for the segmented volume to evaluate the effect of enforcing the flow barrier highlighted in Figure 5.20. The spatial distribution of temperature and vertical permeability is compared for three realizations before and after geostatistical anomaly enforcement. As can be seen in Figure 5.21, the anomaly enforcement creates a flow barrier in between the producer and injector at the location of the identified anomaly. This limits the propagation of the steam chamber in the updated realizations. The integration of 4D seismic data in geological modeling results in local improvement in estimation of the steam chamber.

5.2 Facies Proportion Calibration

Updating realizations based on geostatistical anomaly enforcement can result in slight changes of realization statistics due to inclusion of sampled enforcing data. Facies proportions are one of the main statistics that can be changed after integration of 4D seismic data. These changes are often minimal because as mentioned above and also explained in Chapter 4, the anomaly enforcement is implemented through repeating the geostatistical modelling workflow and using the same input statistical parameters inferred from original well data. Integration of a new source of information can improve the realization statistics.

However, one potential concern is that the geostatistical realizations of the DA are updated based on information that does not cover the entire DA. 4D seismic data is available in areas affected by the recovery process. This is an inherent limitation of this dynamic data because it monitors large-scale changes in the reservoir conditions induced by the recovery process. In case of SAGD, areas with sufficient effective permeability are affected by the steam chamber and the identified anomalies provide information about these areas in the reservoir. One can argue that such areas include the recoverable parts of the reservoir that are important for reserve evaluation and decision making. However, updated realizations of the DA may be used for planning new well pairs in order to produce bypassed oil or other purposes. Thus, in practice, it may be necessary to review changes in realization statistics after geostatistical anomaly enforcement. In the Surmont project, the inferred facies proportions are of significant importance because they can drastically affect the overall resource assessment. This motivated the idea of developing a facies proportion calibration algorithm with minimal interference on geostatistical anomaly enforcement.

5.2.1 Calibration Algorithm

The algorithm works based on calculating the facies proportions for a realization and minimizing the mismatch between the calculated ones and provided target proportions. The target proportion is inferred from well data or geological interpretations. This algorithm is implemented for one realization at a time:

- Calculate the facies proportions by averaging across the realization.
- Calculate the proportion mismatch for all facies ($mismatch = P_k^{Target} - P_k^{Current} \ \ for \ \ k = 1, .., K$) where K is the number of facies.
- Note that if there is a mismatch between proportions, there are negative and positive instances because the proportions sum up to 1. If a facies code has a negative mismatch, then another facies code must be added to the realization.
- Consider the facies with the smallest mismatch (most negative one) and minimize its mismatch. This is referred to as target facies and the mismatch is minimized by modifying the realization and adding the required number of additional instances of the target facies to the realization. For instance, consider the case study above, if Breccia has the smallest mismatch, a ranking system specifies locations within the realization where their facies can be changed to Breccia without changing the conditioning data.
- A ranking measure is assigned to each location based on considering a user specified window around it. In a gridded framework, each grid cell within the reservoir model is processed to assign a ranking measure. A kernel weighting function is used to calculate facies proportion around the location and within the window. This allows to have a weighting system based on distance from the location being processed. Figure 5.22 shows how distances within an example window around a location are translated to kernel weights that are considered in proportion calculation.
- Facies proportion is important to assess a location for being a candidate to be changed in order to minimize the mismatch. For example, if Breccia is the target facies to minimize its mismatch by adding more of its code to the realization, a location with facies code different from Breccia and high proportion of Breccia within the local window is considered as a candidate location to be changed to Breccia. Also, being close to conditioning data affects the ranking measure depending on whether it is the same facies code or a different one from the target facies. For instance, if a location is evaluated to be changed to the target facies, lets say Breccia, and within the local window there are conditioning data of Breccia, that location is highly ranked as a candidate to be changed. On the other hand, if there are conditioning data different from Breccia, it is less likely to be changed to Breccia. Equation 5.1 summarizes the calculation of the ranking measure (i.e., RM) for a location/grid cell within a facies realization.

$$I_{i,k} = \begin{cases} 1, & \text{if } Z(i) = k \\ 0, & \text{otherwise} \end{cases}, \forall\, i \in Local\ Window \tag{5.1}$$

$$RM_k = \frac{\sum_{i=1}^{n} w_i I_{k,i} D_i}{\sum_{i=1}^{n} w_i D_i}$$

where RM is the ranking measure for a grid cell, $i = 1, ..., n$ denotes the grid cells or locations within the local window, $I_{i,k}$ is the indicator variable for the target facies (k), w_i is the weight based on kernel function and Z denoted the categorical variable (facies) for the realization. Note that if a grid cell contains conditioning data, it is not included in the ranking process as it cannot be changed.

- After ranking all potential grid cells, candidate locations are changed to the target facies in a sequential fashion based on their rank until the mismatch is minimized. Then, this process is repeated by finding the next facies with smallest mismatch. After a location has been changed once is not included in the ranking process. Figure 5.23 shows the implementation of the algorithm using a computer program (proportion calibration tool (PCT)) for a facies realization of the entire DA in the Surmont project.

As can be seen in Figure 5.23 and also expected from the algorithm, as the mismatch is minimized for one facies, the overall mismatch is reduced. In practice, there are only slight deviations from the target proportions and applying the algorithm does not significantly affect the reproduction of geostatistical parameters within the realizations. This algorithm may be implemented when the inferred facies proportions are reliable and expected to remain unchanged for the entire DA. Figure 5.24 shows one example of 2D slices related to a facies realization for the DA before and after implementing proportion calibration. The conditioning data including original vertical wells and enforcing data are highlighted.

As can be seen in Figure 5.24, the conditioning data are not affected by the calibration algorithm and depending on specified local window in the algorithm, the changes in facies are affected by the conditioning data. The proposed algorithm can be implemented in other cases where a target facies proportion needs to be enforced after facies modelling. A practitioner should be cautious about the effect of using this algorithm on reproduction of geostatistical modelling parameters (i.e., variograms) if there is a considerable deviation from the target proportions. In this chapter, the proportion calibration algorithm is presented to demonstrate an engineering solution for specific requirements in geological modelling. However, slight changes in realization statistics after integration of 4D seismic data is expected and it can improve the geological model.

5.3 Concluding Remarks

A case study is presented to demonstrate the implementation of the proposed methodology for practical integration of information inferred from 4D seismic data. This is done by considering 4D seismic data from a DA in

the Surmont project. Anomalies in propagation of the steam chamber represent the information obtained from 4D seismic data. Anomaly identification is a critical step that can be accomplished through a collaborative effort of professionals from different disciplines. In this chapter, some guidelines are presented for visual study of 4D seismic-driven steam chamber and reliable identification of anomalies. A total of 110 anomalies were identified for the DA considered in the case study. A data analysis algorithm can be implemented to facilitate the identification of type 0 or expected features. However, professional judgment is necessary to check and confirm the identified features. Fidelity analysis provides a through evaluation of anomaly reproduction by the initial geostatistical realizations. This is followed by sampling the enforcing data for the missing anomalies and repeating the geostatistical modelling workflow using the updated data files. The proposed methodology is implemented as a pre/post processing step and does not interfere with the modelling workflow.

Fidelity analysis before and after anomaly enforcement can be used to evaluate the performance of the proposed methodology. Local improvements in estimation of the steam chamber are expected and can be checked by running flow simulation. However, the associated computational cost is the bottleneck for fast evaluation of anomaly enforcement. A SAGD proxy model that provides a fast simulation of steam chamber propagation as a function of time is a potential solution for this limitation. The updated geostatistical realizations are constrained by the 4D seismic anomalies and provide a more accurate model of geological uncertainty that can be used for history matching and transfer of geological uncertainty to production uncertainty.

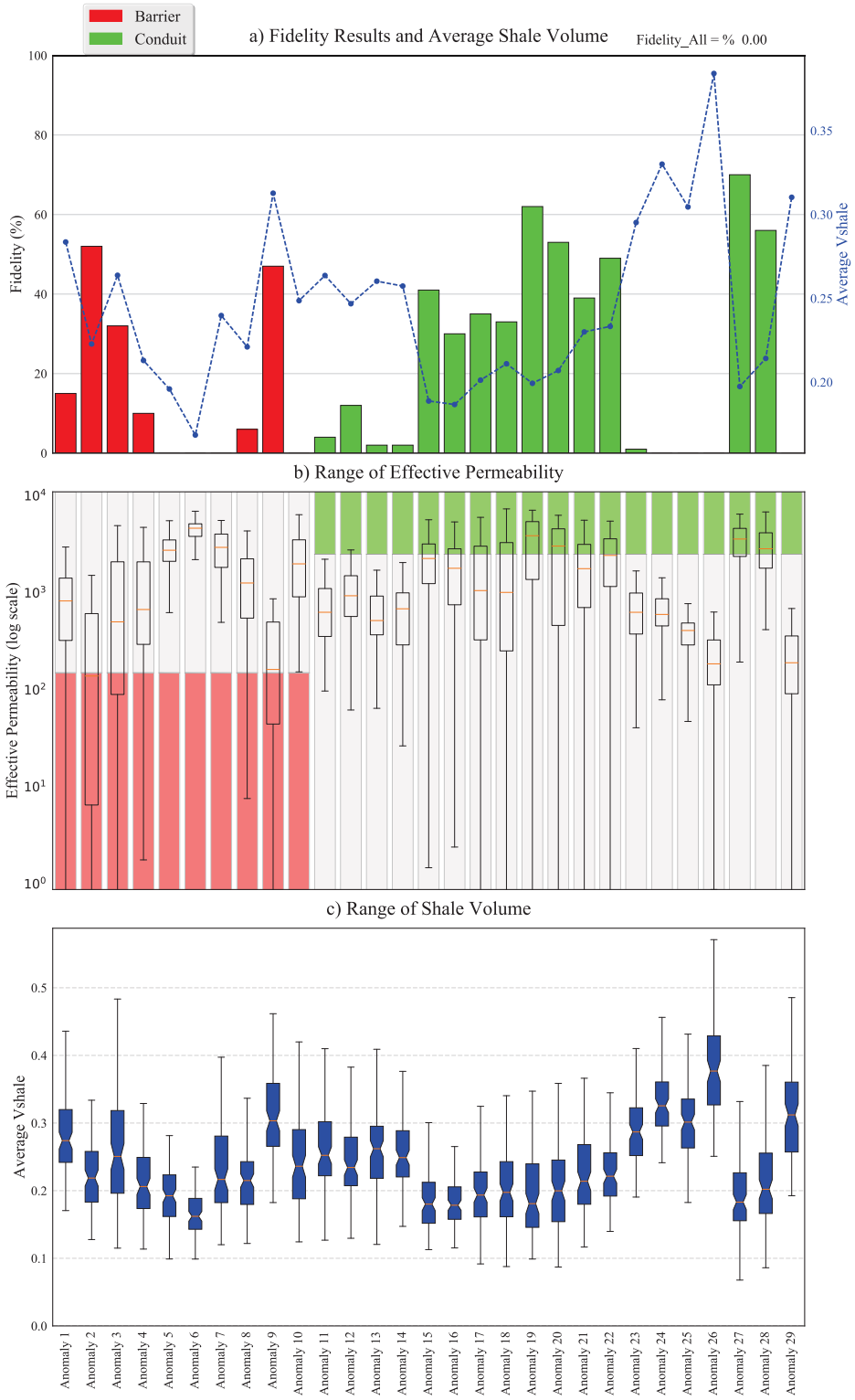

Figure 5.16: Fidelity analysis considering the initial conditional realizations (before anomaly enforcement) and for type $+1$ and -1 anomalies. Panel a shows the fidelity percentage for each anomaly along with average shale volume. Panel b and c show the range of variability for effective permeability and shale volume respectively.

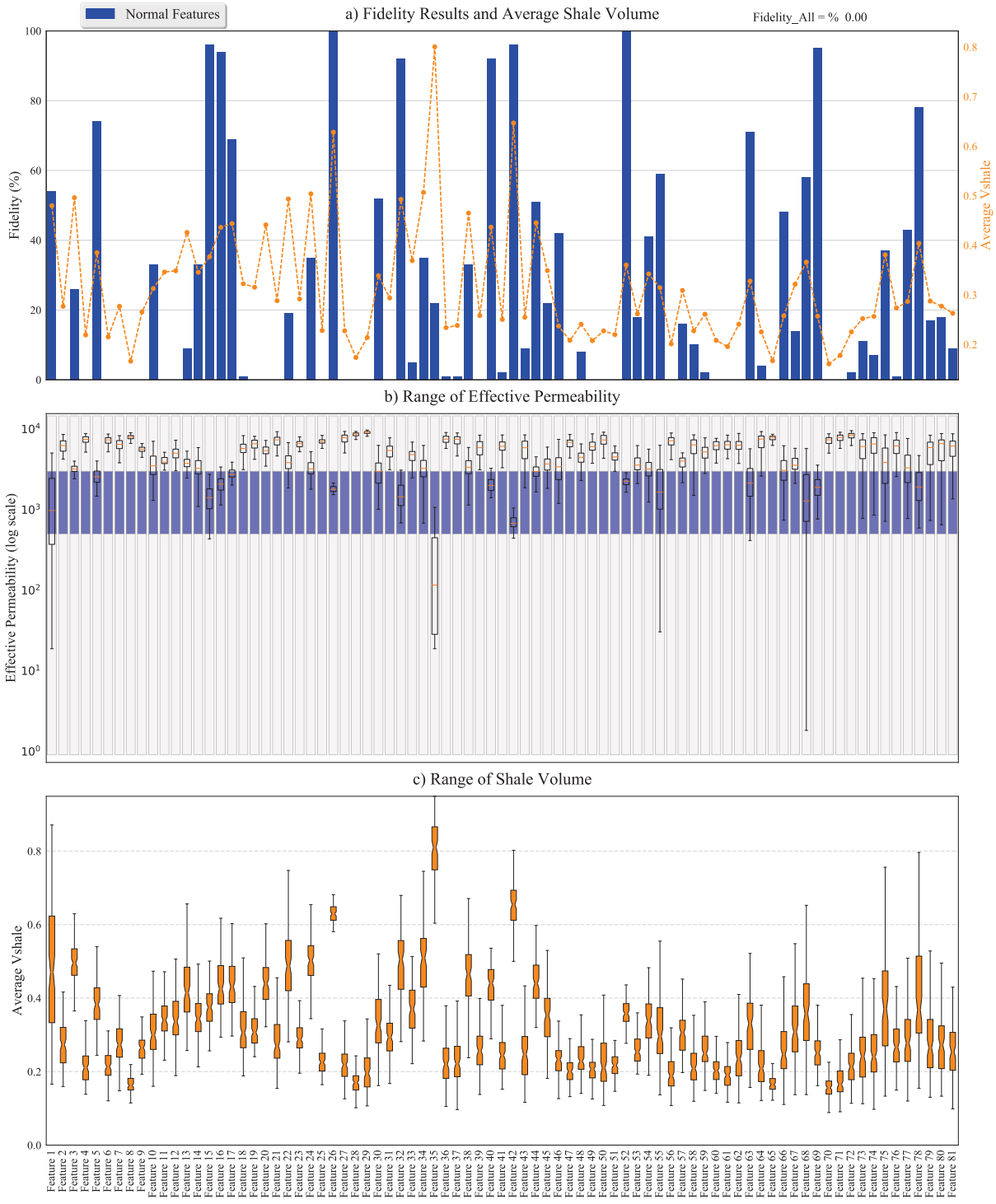

Figure 5.17: Fidelity analysis considering the initial conditional realizations (before anomaly enforcement) and for type 0 anomalies.

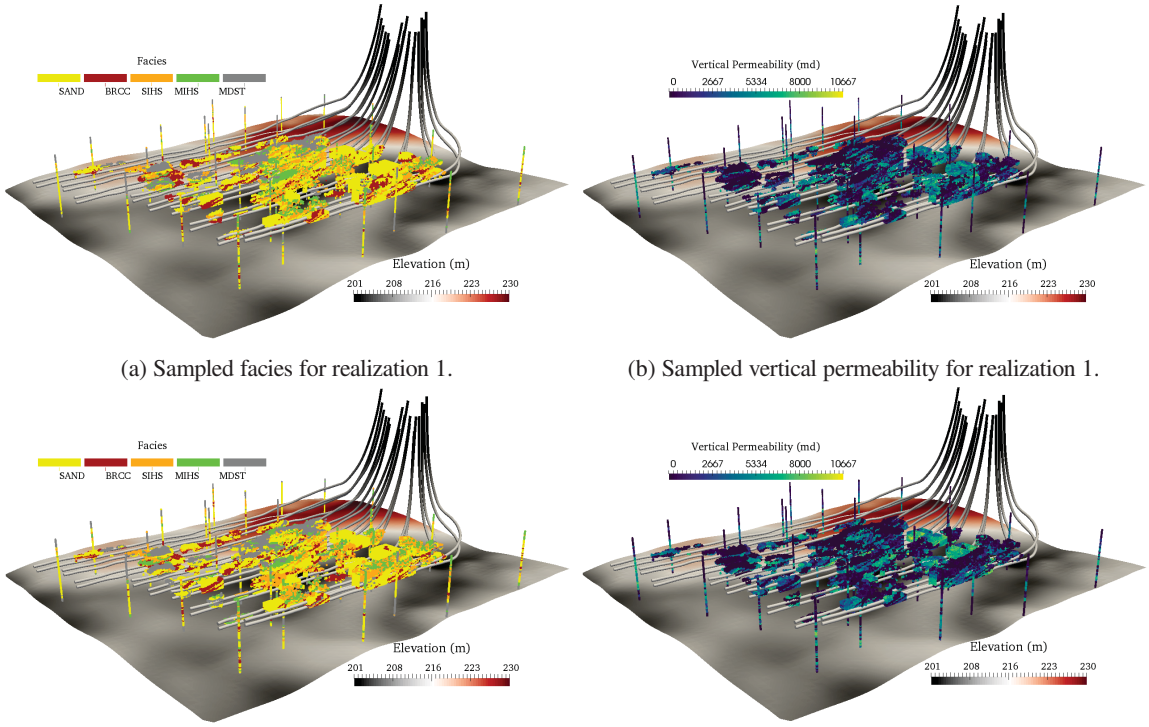

(a) Sampled facies for realization 1.

(b) Sampled vertical permeability for realization 1.

(c) Sampled facies for realization 2.

(d) Sampled vertical permeability for realization 2.

Figure 5.18: Updated data files containing the original well data and sampled enforcing data for two realizations.

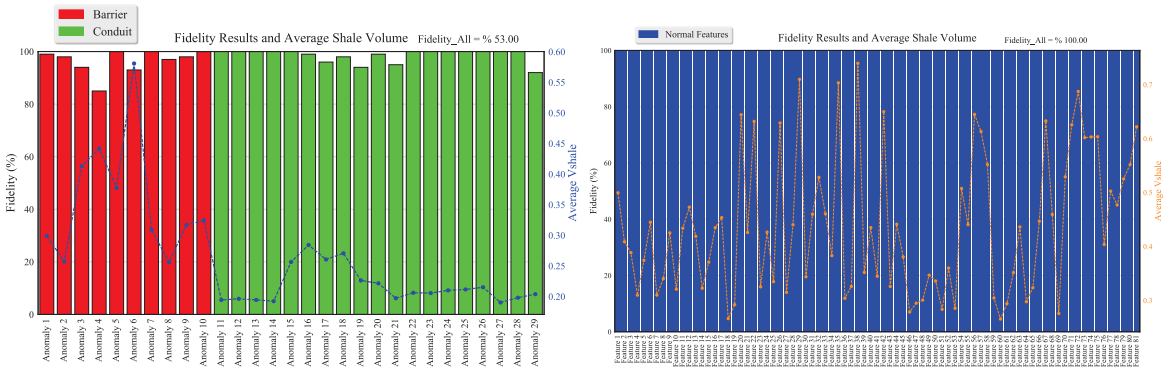

(a) Fidelity analysis for anomaly type -1 and $+1$ after geostatistical enforcement.

(b) Fidelity analysis for anomaly type 0 after geostatistical enforcement.

Figure 5.19: Results of the fidelity analysis for the updated geostatistical realizations.

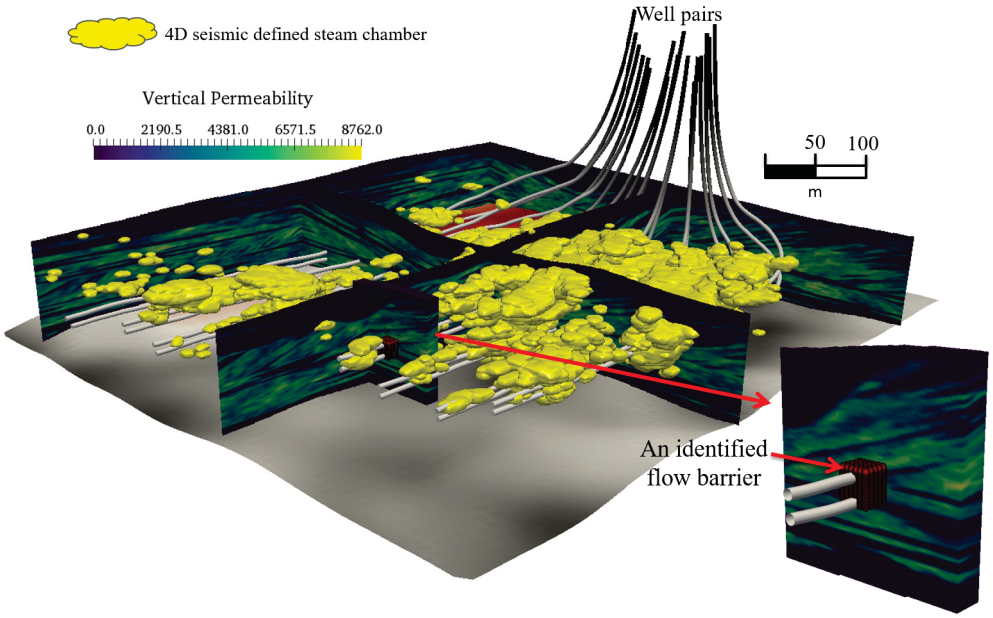

Figure 5.20: Considering a limited volume of the reservoir affected by an identified anomaly for flow simulation.

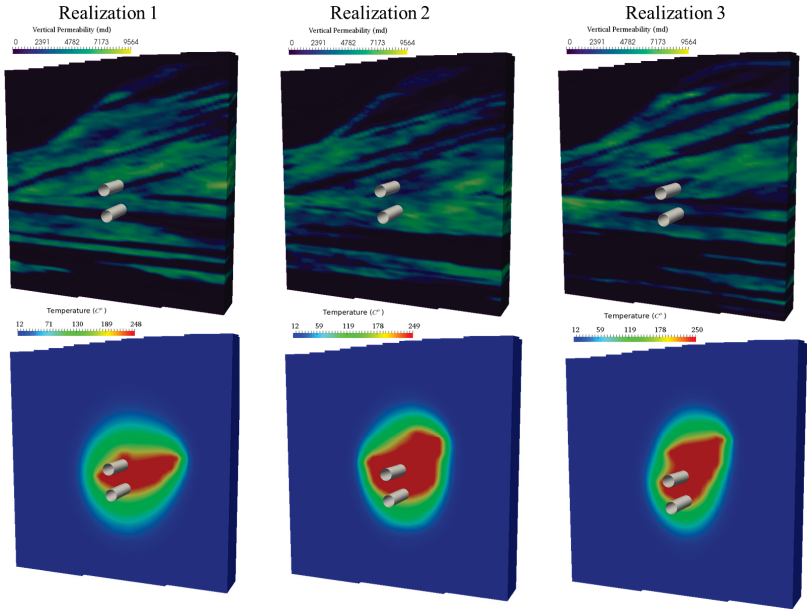

(a) Before geostatistical anomaly enforcement.

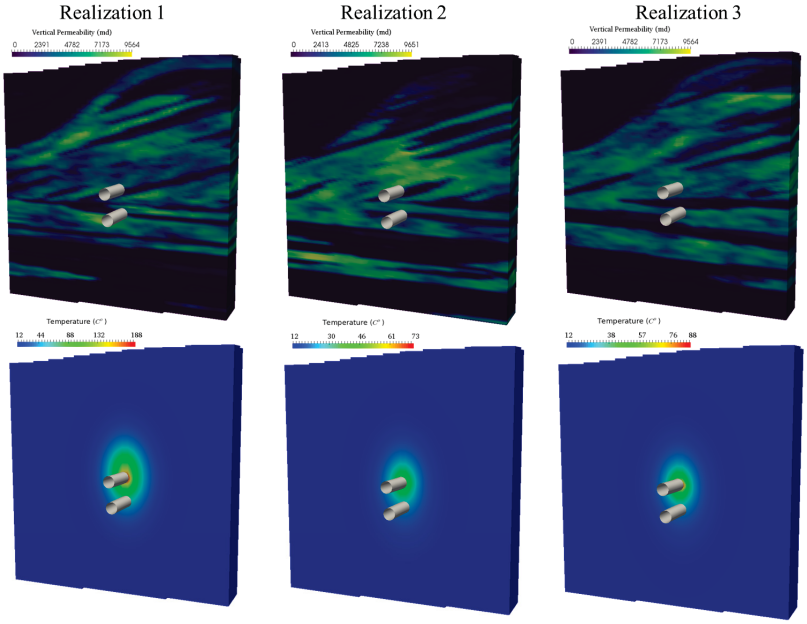

(b) After geostatistical anomaly enforcement.

Figure 5.21: Flow simulation results for three realizations.

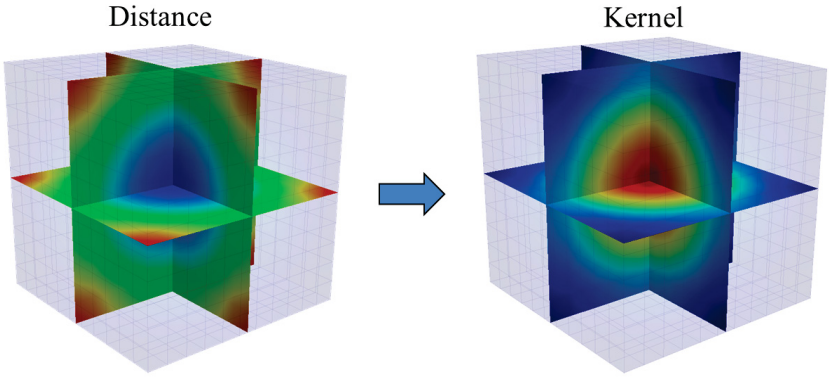

Figure 5.22: Kernel weighting function to account for distance in calculation of the ranking measure.

```
**Process started to minimize the missmatch...

 Categorical Codes:        1       2       3       4       5

  Initial Mismatch:    -0.0127  0.0218 -0.0303 -0.0133  0.0345

  Reduce mismatch for Code:   3
  100% of grid addresses Considered
  Updated Mismatch:    -0.0244  0.0182 -0.0000 -0.0221  0.0283
  Reduce mismatch for Code:   1
  100% of grid addresses Considered
  Updated Mismatch:    -0.0000  0.0086 -0.0000 -0.0269  0.0184
  Reduce mismatch for Code:   4
  100% of grid addresses Considered
  Updated Mismatch:    -0.0000  0.0052 -0.0000 -0.0000 -0.0051
  Reduce mismatch for Code:   5
  100% of grid addresses Considered
  Updated Mismatch:    -0.0000  0.0000 -0.0000 -0.0000 -0.0000
  Final Mismatch:    -0.0000  0.0000 -0.0000 -0.0000 -0.0000

 Initial Proportions:     0.4873  0.0708  0.0887  0.1067  0.2465

  Final Proportions:     0.5000  0.0490  0.1190  0.1200  0.2120


Total time= 0 hours and 4 minutes and 19 seconds
```

Figure 5.23: An example of running the computer program that implements the proposed facies proportion calibration for one realization of the DA from Surmont project.

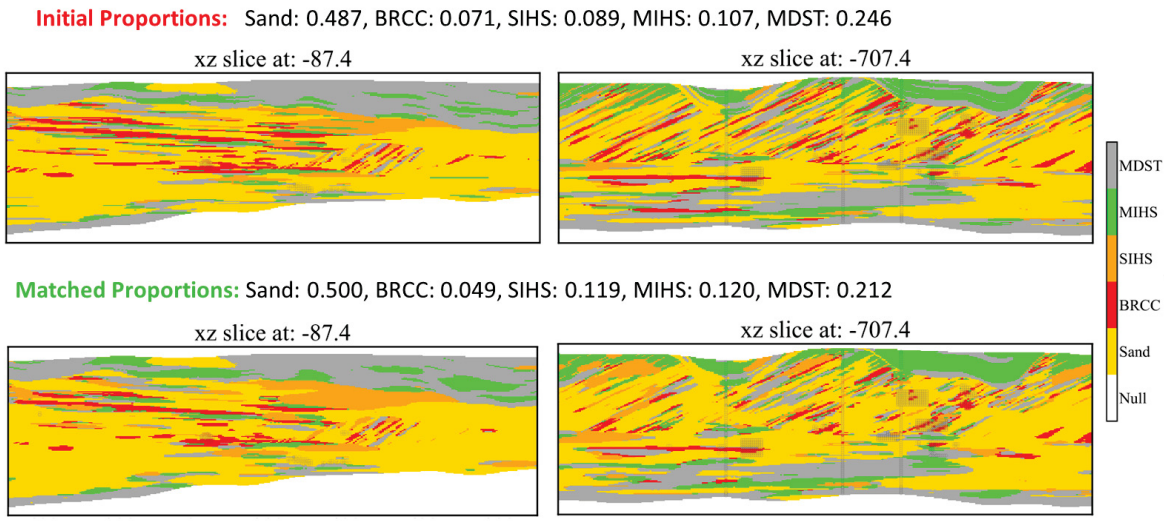

Figure 5.24: Facies calibration implemented for one facies realization of the DA.

Chapter 6

Comprehensive Case Study

There are two main contributions in this thesis. The first one is a methodology for accurate quantification of facies proportion uncertainty in presence of a trend followed by integration in geostatistical facies modelling. The second contribution is a methodology for practical integration of 4D seismic in geostatistical reservoir modelling. These methodologies are explained and evaluated in Chapters 2 and 4. In addition, real case studies are presented in Chapters 3 and 5 to demonstrate implementation of the proposed methodologies in practice. In this chapter, a comprehensive case study is presented that implements both proposed methodologies in geostatistical reservoir modelling. The main objective of this chapter is to provide a workflow for practitioners to implement the proposed methodologies in geostatistical reservoir modelling.

A synthetic yet realistic reference model is generated to sample a limited number of wells. This model also provides a criteria to assess the geostatistical anomaly enforcement. Accounting for parameter uncertainty becomes important when limited data is available. Both facies proportion uncertainty and multivariate histogram uncertainty within facies are considered and the workflow is explained in detail. Synthetic 4D seismic data are generated based on running thermal flow simulation for the reference model. Guidelines presented in Chapter 5 are used to identify anomalies in the propagation of the steam chamber defined by 4D seismic. The initial geostatistical realizations conditioned to the limited well data do not consider the anomalies. These realizations are evaluated through the proposed fidelity analysis. Geostatistical anomaly enforcement improves local estimation of the steam chamber and also the fidelity results. Finally, the effects of 4D seismic integration on facies proportions and distributions of petrophysical properties are studied.

6.1 Modelling Workflow

Geostatistical reservoir modelling provides a quantitative numerical representation of subsurface geology that can be used for resource estimation and predicting reservoir performance under a recovery process. However, incomplete data results in uncertainty that is quantified by stochastic simulation and represneted by multiple realizations of the reservoir model. A geostatistical modelling workflow is presented here to provide a realistic model of geological uncertainty. Including model parameter uncertainty and reproducing all available sources of data are two essential components for accurate assessment of geological uncertainty. The key concept is that in each step of the workflow, relevant sources of uncertainty are quantified by multiple realizations and carried forward throughout the modelling process. The workflow presented below is based on quantifying overall geological uncertainty with an ensemble of 100 realizations.

1. Define the reservoir structure including stratigraphic top, base and additional surfaces that identify different zones. 3D seismic data along with structural picks from well data are used. In this case study, it is assumed that the reservoir structure is well-defined. However, the structural uncertainty can be integrated in the modelling process by using different realizations of stratigraphic surfaces for each final realization of geological properties.

2. Use facies data to quantify the prior proportion uncertainty based on statistical resampling (i.e., categorical spatial bootstrap) methodology proposed in Chapter 2. This is important for assessment of global proportion uncertainty especially when limited data is available. Indicator variograms are calculated and modeled to provide the model of spatial variability for the resampling. Based on this practice, 100 realizations of global proportions or trend models are generated that can be used as input for subsequent facies modelling within the reservoir. If there is variogram uncertainty, it can be integrated in the spatial bootstrap process. As a result, each realization of global proportions/trend model are generated a separate realization of indicator variogram. This process is applied within each modelling zone separately.

3. Use indicator variogram models and realizations of the global proportions/trend model to simulate facies within the reservoir or different modelling zones. SIS, TPG are some of facies modelling technique that can be used to simulate one realization of facies at a time using a different realization of input statistical parameters. In this case study, SIS is used. Then, the global posterior proportion uncertainty is evaluated by averaging over the entire reservoir model and for all realizations.

4. Pool petrophysical data within each facies to constrain the range of variability and provide stationary domains. In general, for 3D reservoir modeling, modelling facies based on a inferred trend models remove the need for considering a trend model for petrophysical properties.

5. Quantify multivariate histogram uncertainty for petrophysical properties within each facies. A geostatistical tool (i.e., software) is introduced in Chapter 2 that can be used to implement multivariate spatial bootstrap. Realizations of data are generated that can be used as reference distribution for subsequent geostatistical multivariate modelling of properties within facies.

6. Use a multivariate transformation technique (i.e., PPMT) to transfer petrophysical data into an uncorrelated multivariate Gaussian framework. Spatial realization of data is used as reference distribution for the transformation,

7. Use SGS to simulate each property independently in Gaussian units. This is followed by back-transformation to original units using the same reference distributions that was used in the previous step. Merge petrophysical realizations for all facies and then for each zone to get the final realizations of the reservoir for facies and petrophysical properties. Evaluate the posterior histogram uncertainty compared to the prior

one. Note that the final realizations could account for facies proportion uncertainty, histogram uncertainty, variogram and structural uncertainty.

8. As time passes and a dynamic source of data becomes available, update the model of geological uncertainty. In case of 4D seismic, the proposed methodology in Chapter 4 can be used to update all realizations based on geostatistical anomaly enforcement. Note that the enforcing data do not affect the input statistical parameters since they are inferred based on hard data/measurements. However, the parameter uncertainty is included in the updating process as enforcing data are included in geostatistical modelling as conditioning data.

The following case study is focused on demonstrating the workflow for geostatistical reservoir modelling in presence of proportion and histogram uncertainty. Also, the effect of integrating 4D seismic on the model of geological uncertainty is studied.

6.2 Reference Reservoir Model

A single well pair SAGD DA is considered as the reference model for the case study. The reservoir is 1000 m along the wells (X direction), 100 m perpendicular to the wells (Y direction) and with average thickness of 50 m. In a typical SAGD project, well pairs are separated by an average distance of 100 m. Facies modeling is done using SIS for three categories of Sand, Shale and Mixed. This is done in presence of a trend model that controls facies proportion in the vertical direction (VPC). Petrophysical properties including porosity, permeability and fluid saturation are modeled using SGS within facies. Figure 6.1 shows the reference reservoir model and limited sampled well data that are used to generate initial conditional realizations. Higher shale proportion on top of the reservoir provides an impermeable seal. On the other hand, sand proportion increases by depth to obtain high quality reservoir around the well pairs. The reference model represents a typical SAGD reservoir and is used to assess geostatistical realizations. The trajectories for the injector and producer wells are highlighted by solid and dashed black lines as shown in Figure 6.1. The grid size is 25 m for X direction (along the wells) and 1 m for Y and Z directions. For flow simulation, it is required to have finer resolution perpendicular to well pairs because in SAGD vertical flow is dominant.

The reference model is required to evaluate the effect of anomaly enforcement on SAGD characterization before an after integration of information inferred from 4D seismic. Because, after anomaly enforcement and updating all realizations, local improvements in estimation of steam chamber profile is expected. Thermal flow simulation (STARS CMG) is used to simulate SAGD for the reference model during the first three years of operation. Figure 6.2 shows the distribution of temperature and oil saturation within the reservoir after operating SAGD for three years. A uniform injection and production rate is considered along the well pair. As can be seen in Figure 6.2, the heated bitumen inside the steam chamber is displaced by steam. The oil production is in direct

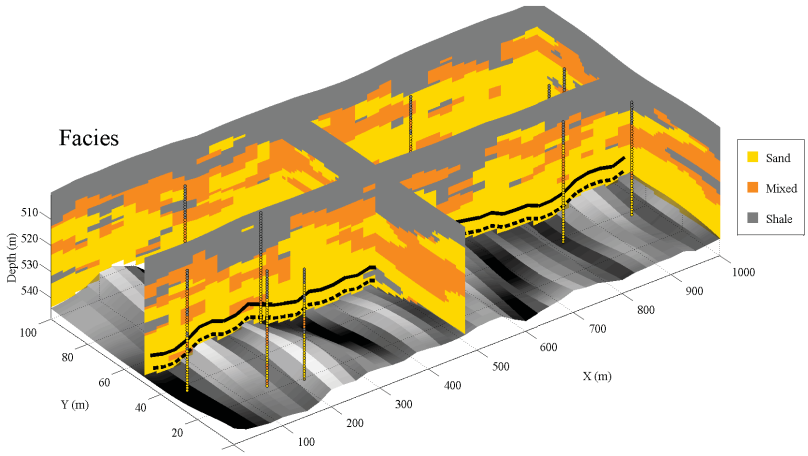

(a) Reference facies model and sampled wells.

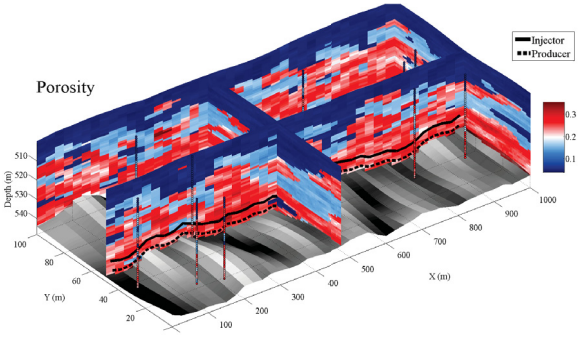

(b) Reference porosity model and sampled wells.

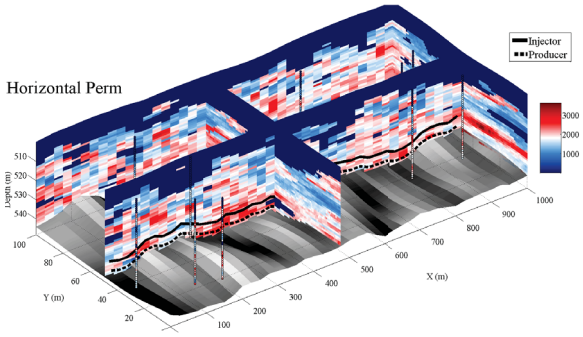

(c) Reference horizontal permeability model and sampled wells.

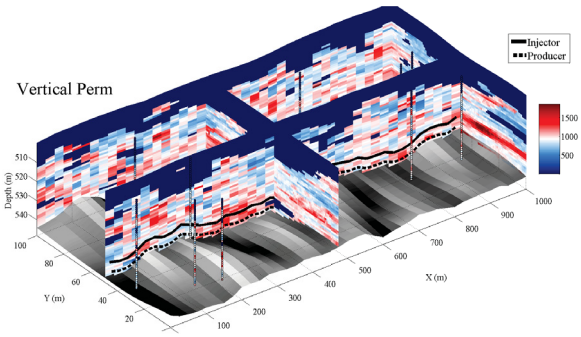

(d) Reference vertical permeability model and sampled wells.

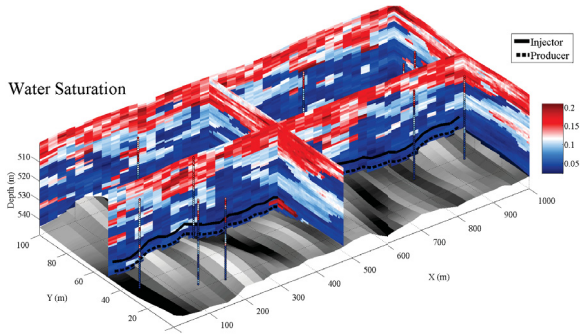

(e) Reference water saturation model and sampled wells.

Figure 6.1: Reference reservoir model and 10 vertical wells that provide limited data for facies and petrophysical properties.

relation with propagation of the steam chamber. Integration of 4D seismic data can improve the estimation of the steam chamber and constraint the geological and in turn production uncertainty.

6.3 Initial Conditional Realizations

100 initial realizations are simulated conditioned to the data sampled by 10 vertical wells shown in Figure 6.1. An example log plot for one of the wells is shown in Figure 6.3. SIS is used to generate the conditional facies

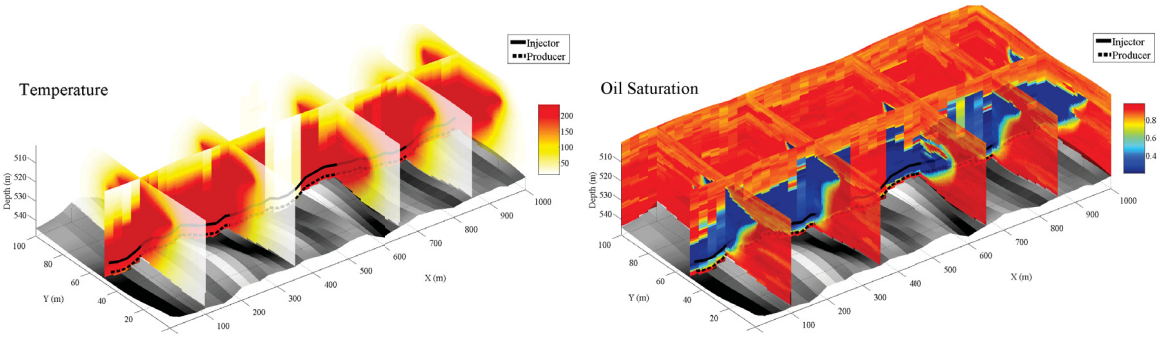

(a) Spatial distribution of temperature.

(b) Changes in oil saturation.

Figure 6.2: Steam chamber propagation for the reference model after 3 years of SAGD.

realizations and SGS along with PPMT are employed for multivariate simulation of petrophysical properties within facies. In practice, some preprocessing steps including multivariate imputation (Barnett and Deutsch, 2015b) may be required to prepare the data for geostatistical modelling.

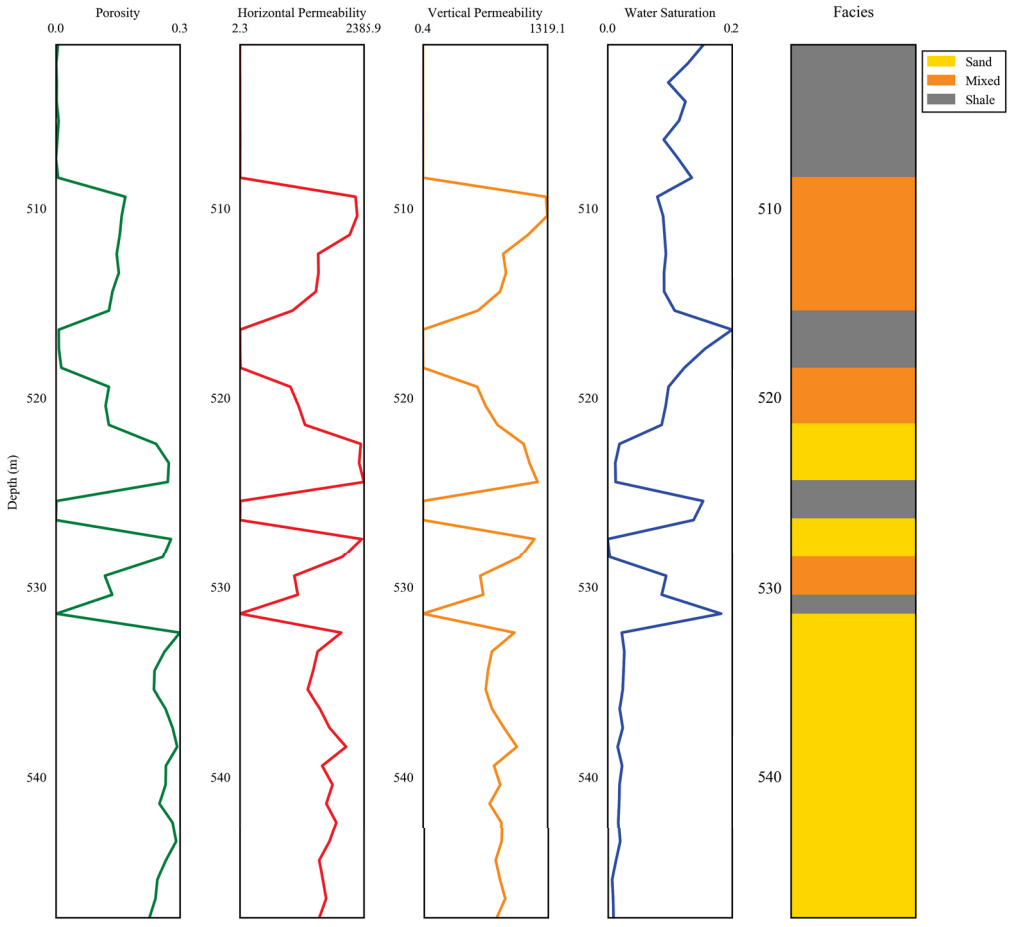

Figure 6.3: An example well log plot sampled from the reference model.

Figure 6.4 summarizes the multivariate relationships between petrophysical properties within Sand. The

geostatistical realizations should reproduce such relationships as they are inferred from data and explain geological setting. Geostatistical modelling of both facies and petrophysical properties rely on input statistical parameters including the VPC and histograms. Inferring these parameters based on limited data is subject to uncertainty. In practice, economical and environmental limitations do not allow to sample many data especially in the exploration step and beginning of the reservoir life cycle. Thus, the proposed methodologies in Chapter 2 are implemented to quantify and integrate parameter uncertainty in geostatistical reservoir modelling. This provides a more accurate model of geological uncertainty that is critical for successful reservoir management decision making.

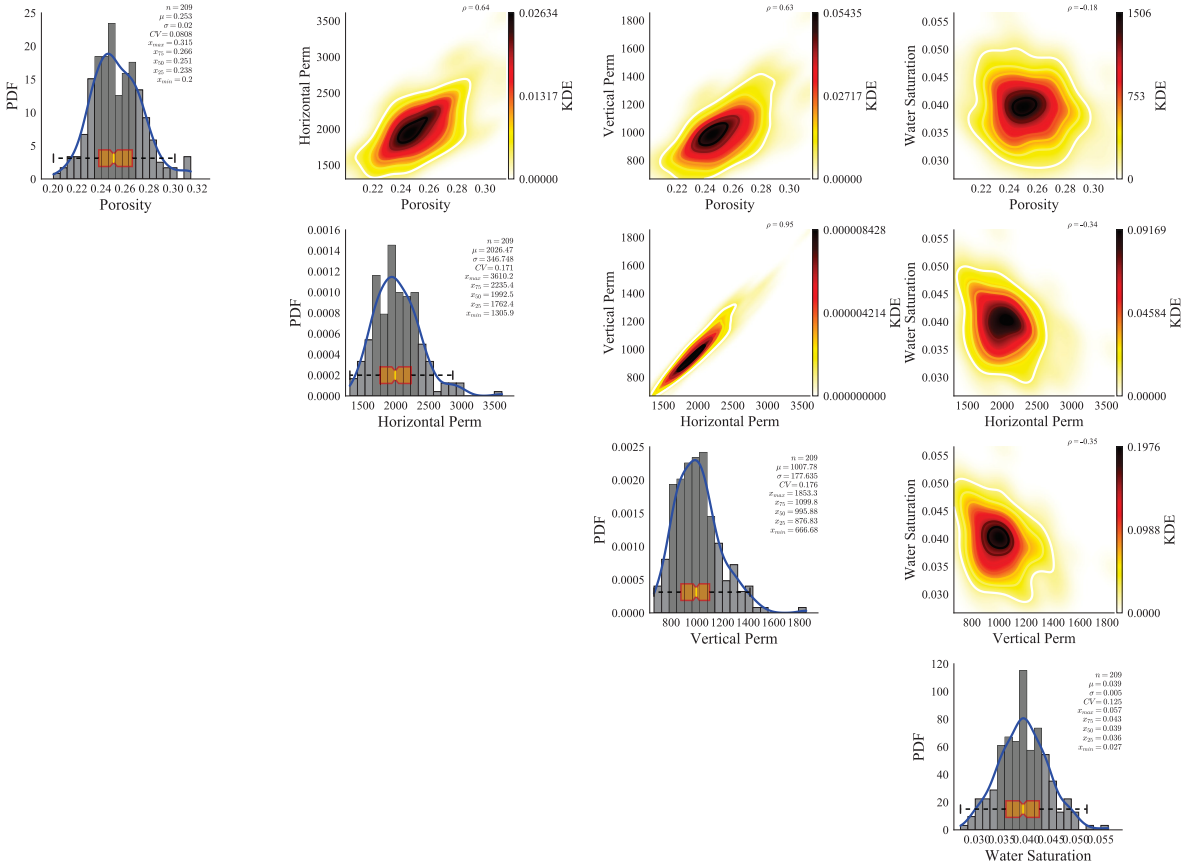

Figure 6.4: Multivariate relationships between petrophysical properties within Sand.

6.3.1 Facies Simulation

SIS is used to simulate facies within the reservoir based on the well data. In order to improve facies modelling, prior proportion uncertainty is quantified in presence of a trend model (i.e., VPC). This is followed by inclusion of the prior uncertainty in SIS for the reservoir.

6.3.1.1 Facies Proportion Uncertainty

SBS_Categorical (Appendix A) is employed to implement spatial bootstrap for facies data using the indicator variograms and the base-case trend model inferred form the facies data (Figure 6.5). In order to remove variogram uncertainty, the indicator variogram models used to generate the reference model are used for the spatial bootstrap. The variogram ranges correspond to spatial continuity for each facies along horizontal and vertical direction. The software asks for facies data file, indicator variogram models, grid specification and trend modelling parameters when the prior proportion uncertainty is quantified in presence of a trend model. The grid specification is used for facies simulation over the entire reservoir model. In this case study, the trend model is a VPC and as shown in Figure 6.6, the prior proportion uncertainty is represneted by 100 realizations of the VPC. Indicator variogram modelling is often required for geostatistical facies simulation. Thus, there is no significant overhead effort needed to quantify prior proportion uncertainty using the software. The trend model accounts for declustering weights and also the domain limits. Thus, the uncertainty in global proportions is provided by SBS_Categorical in a report file and based on averaging over the entire trend models. The result is summarized in Figure 6.6b where the colored bars show the average proportion for each facies while the box plots delineate the range of variability.

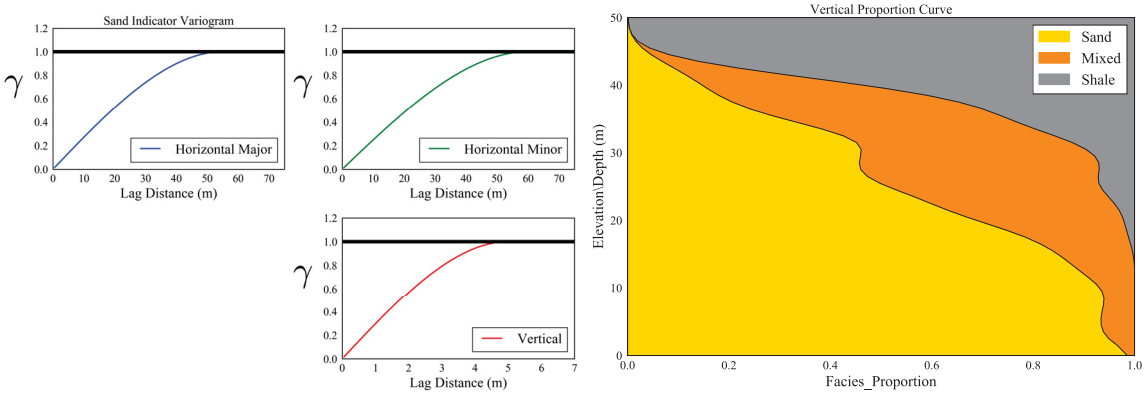

(a) Indicator variogram model for Sand facies.

(b) Base-case trend model inferred from data.

Figure 6.5: Spatial bootstrap for facies.

The final facies realizations of the reservoir are simulated one at a time using a different realization of the VPC. This allows to integrate prior proportion uncertainty in facies simulation. Figure 6.7 shows five final facies realizations for the reservoir. Note that all realizations are conditioned to the same facies data (from vertical wells) but the input trend model is different for each realization. The reader is encouraged to zoom in on the electronic version of this document.

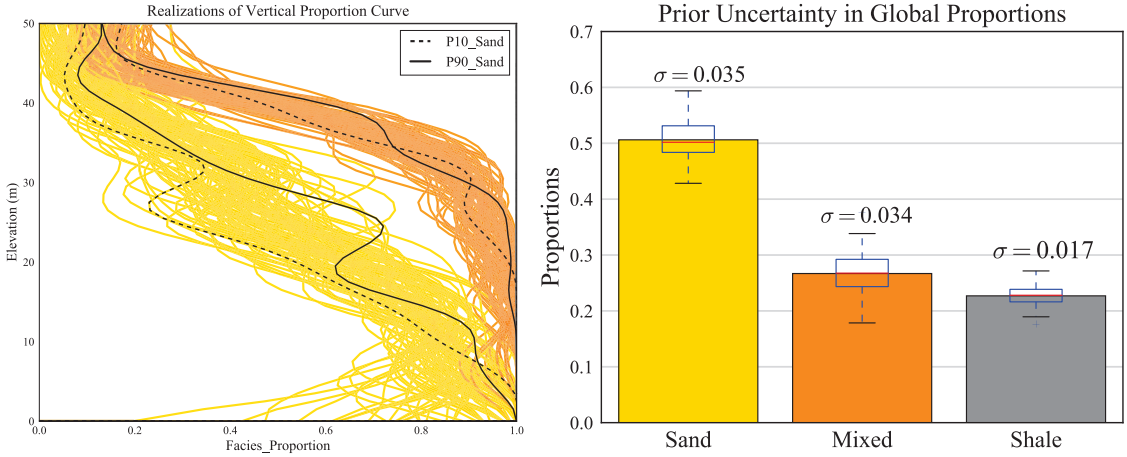

(a) 100 realizations of the trend model.

(b) Prior uncertainty in global proportions (average over the entire trend model).

Figure 6.6: Prior proportion uncertainty quantified based on statistical resampling.

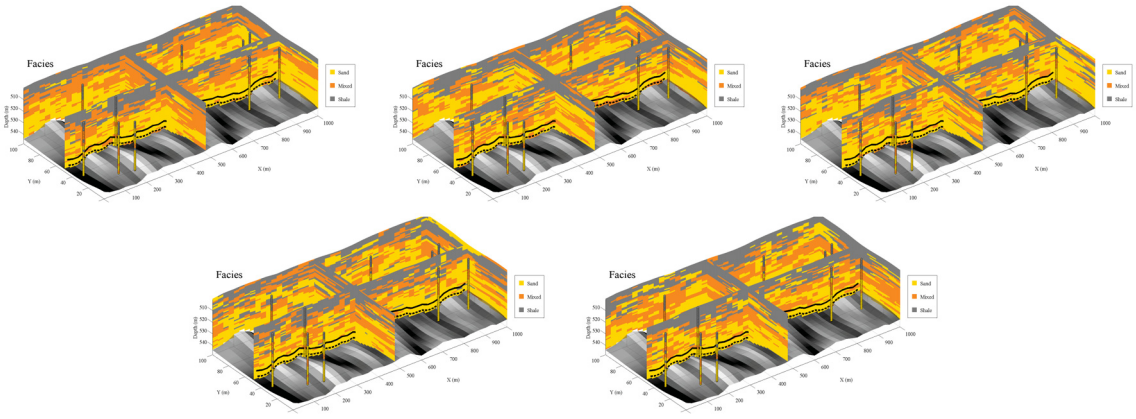

Figure 6.7: Some examples of initial facies realizations with effective integration of proportion uncertainty.

6.3.2 Simulation of Petrophysical Properties within Facies

Facies modelling is followed by simulation of petrophysical properties within facies to provide stationary domains for property modeling with lower range of variability. Accounting for the trend in facies proportions often removes the need to consider a trend in modelling of petrophysical properties. The decision of stationarity is implicit in all statistics and allows defining a pool of data over which inferred statistical parameters including histogram and variogram are assumed to be representative (Journel, 1989). In this context, petrophysical data are pooled within each facies (i.e., Sand, Mixed and Shale) and the following modelling steps are implemented for each facies. The same variogram models as the reference model are considered for the realizations. This removes the variogram uncertainty form the case study. However, multivariate parameter uncertainty associated with the histogram of petrophysical properties are quantified and included in the geostatistical simulation.

6.3.2.1 Multivariate Histogram Uncertainty

SBS_MV (Appendix A) is employed to implement multivariate spatial bootstrap for petrophysical properties. This is done within each facies separately to generate 100 realizations of petrophysical properties that respect the spatial model of variability (i.e., variogram) and reproduce the multivariate relationships between different properties. Figure 6.8 shows the prior histogram uncertainty after merging spatial bootstrap realizations of all facies. The red line highlights the distribution inferred from well data while the gray lines highlight the distribution of spatial bootstrap realizations. In addition, Figure 6.9 summarizes the multivariate relationships between different petrophysical properties based on considering all spatial bootstrap realizations within Sand. Comparing Figures 6.4 and 6.9 reveals that the multivariate statistical resampling implemented by SBS_MV reproduces the relationships observed from original data. As explained in the user manual of SBS_MV (Appendix A), it is required to provide data locations and variogram model for each property. Thus, there is no considerable professional effort required for the quantification of prior histogram uncertainty.

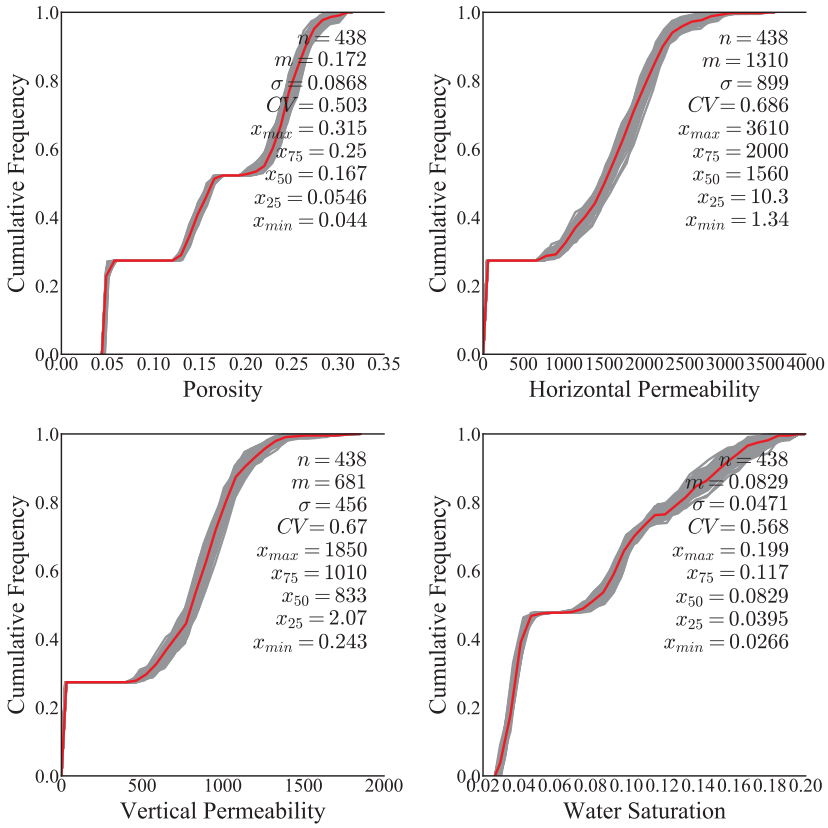

Figure 6.8: Prior uncertainty in distribution of petrophysical properties quantified by the multivariate spatial bootstrap.

The petrophysical well data (Figure 6.1) are transformed to an uncorrelated multivariate Gaussian framework using PPMT. This provides the conditioning data in Gaussian units for the independent simulation of each property within the reservoir using SGS to obtain 100 final realizations of petrophysical properties. In presence of histogram uncertainty, the PPMT transformation is done for each final realization independently and by con-

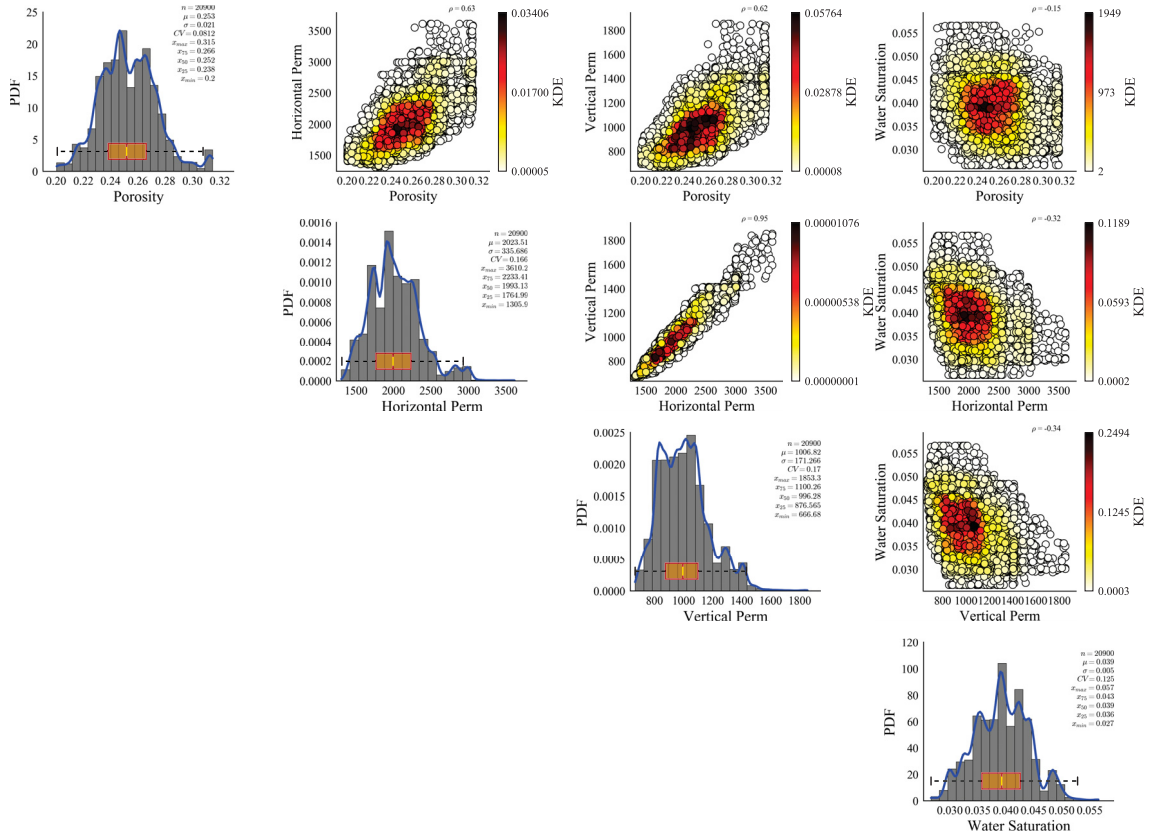

Figure 6.9: Reproduction of multivariate relationships by the ensemble of spatial bootstrap realizations of petrophysical data within Sand.

sidering a separate spatial bootstrap realization as the reference distribution. In other word, the conditioning data is always the same in original units but the representative distribution that is used for PPMT transformation is different due to the parameter uncertainty. As a result, there are 100 realizations of data in Gaussian units after PPMT transformation. SGS simulation of each property is performed using a separate realization of data in Gaussian units to integrate prior histogram uncertainty in geostatistical multivariate modelling. After SGS, final Gaussian realizations are back transformed to original units where all of them reproduce the same conditioning data. Modelling within different facies requires to repeat multivariate forward and back transformation that adds more steps to a typical modelling workflow. However, using a multivariate transformation allows to model each property independently. Figure 6.10 shows one final realization of the reservoir after merging petrophysical models from different facies.

The posterior uncertainty in facies proportion can be evaluated through averaging over all final facies realizations. In a modelling workflow, it is recommended to assess the posterior global proportion uncertainty against the quantified prior proportion uncertainty. Figure 6.11 compares the prior and posterior proportion uncertainty. The colored bars show the average proportion while the box plots delineate the range of variability. The hatched bar represent the proportions from the base-case trend model that is inferred from the well data.

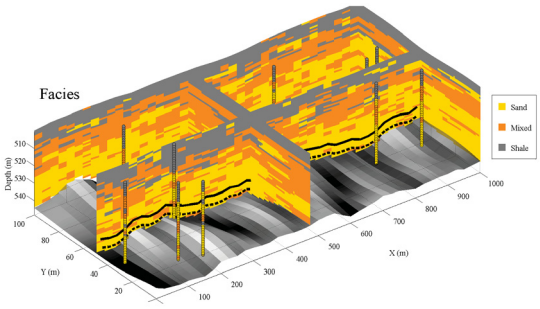

(a) Facies realization and well data.

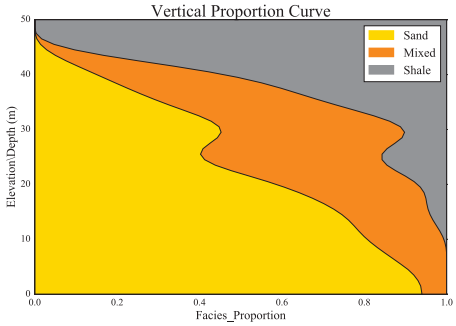

(b) Base-case vertical proportion curve.

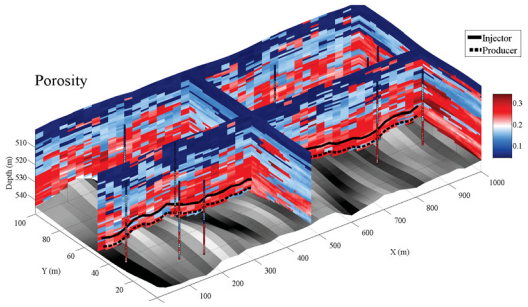

(c) Porosity realization and well data.

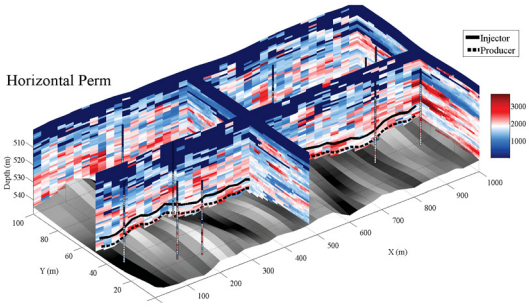

(d) Horizontal permeability realization and well data.

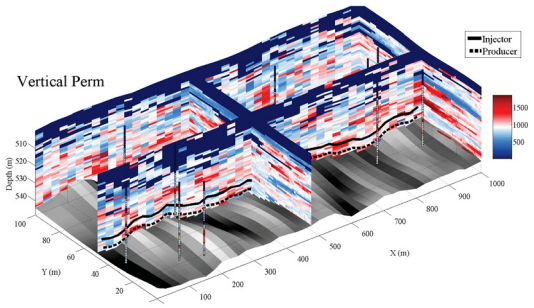

(e) Vertical permeability realization and well data.

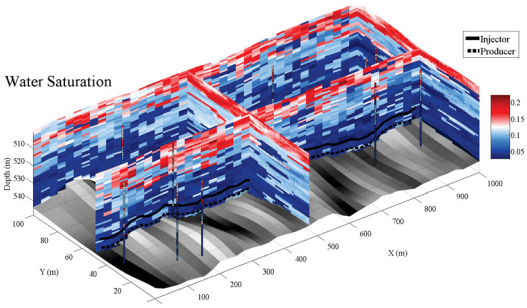

(f) Water saturation realization and well data.

Figure 6.10: One final realization of the reservoir conditioned to well data. Both facies proportion uncertainty and multivariate histogram uncertainty are included.

As can be seen in Figure 6.11, the posterior proportion uncertainty is reduced due to the inclusion of reservoir limits and conditioning effect of the data within the reservoir.

Integration of multivariate histogram uncertainty in geostatistical modelling of petrophysical properties result in a more realistic estimation of global uncertainty in their statistical distribution. Figure 6.12 shows the distribution of different properties (i.e., CDF) for the final realizations of the reservoir. Panels 6.12a, 6.12b and 6.12c depict the CDF within each facies. The red line is related to the CDF inferred from well data while the gray lines highlight the CDF for different realizations. On the other hand, panel 6.12d shows the distribution of petrophysical properties over the entire reservoir after merging facies. Note that distributions shown in Figure 6.12d are influenced by both facies proportion uncertainty and multivariate histogram uncertainty. This can be realized through a comparison between Figures 6.12d and 6.8. Checking realization statistics is recommended

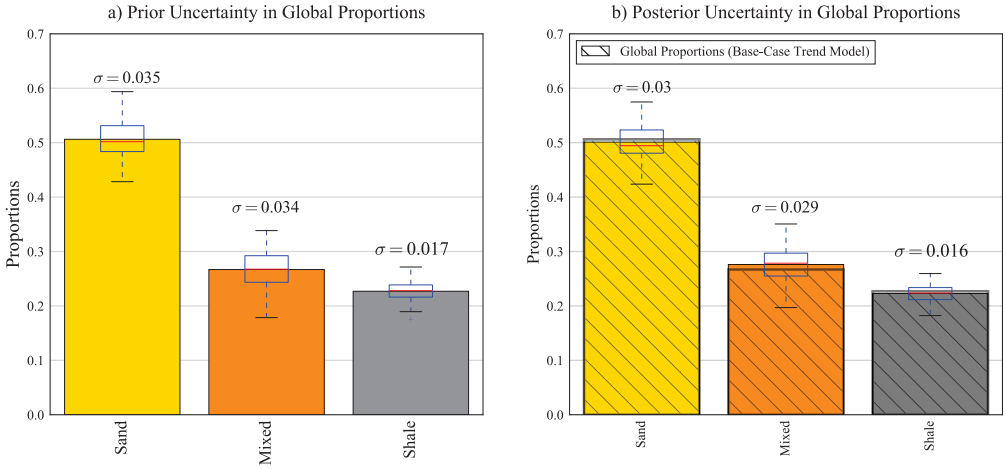

Figure 6.11: Prior and posterior uncertainty in global facies proportions.

to evaluate the proposed geostatistical modelling workflow.

An accurate model of geological uncertainty is provided by including model parameter uncertainty that can be used for resource assessment and reservoir management. A workflow for integration of parameter uncertainty in geostatistical reservoir modelling is presented above. Other sources of parameter uncertainty may be included in the modelling process based on the same concept of simulating one realization at a time using a separate set of modelling parameters. The next step is to constrain the uncertainty by integration of information inferred from 4D seismic data. The geostatistical realizations should get updated as more information become available or when an unaccounted source of uncertainty is discovered. This results in a dynamic model of geological uncertainty that gets updated during the reservoir life cycle to support management decision making.

6.4 Integration of 4D Seismic

After 3 years of SAGD operation, synthetic 4D seismic data is generated for the reference reservoir model. This is done by implementing Gassmann's fluid substitution model (Gassmann, 1951) and considering changes in fluid saturations provided by the thermal flow simulation (STARS, CMG). Figure 6.13 shows the result of synthetic 4D seismic analysis for the reference model. As shown in Chapter 5, in practice, real 4D seismic data results in a similar evaluation of the steam chamber.

6.4.1 Anomaly Identification

Th first step is to extract reliable information from 4D seismic data. As explained in Chapter 4, differences in acquired seismic surveys are not always related to the steam chamber growth. Professional judgment is employed to assess the 4D seismic defined steam chamber and infer reliable information that are represented by anomalies in large scale flow patterns. This is a critical step for successful integration of 4D seismic. A collection of guidelines provided in Chapter 5 are used to identify the anomalies based on visual inspection of the 4D seismic

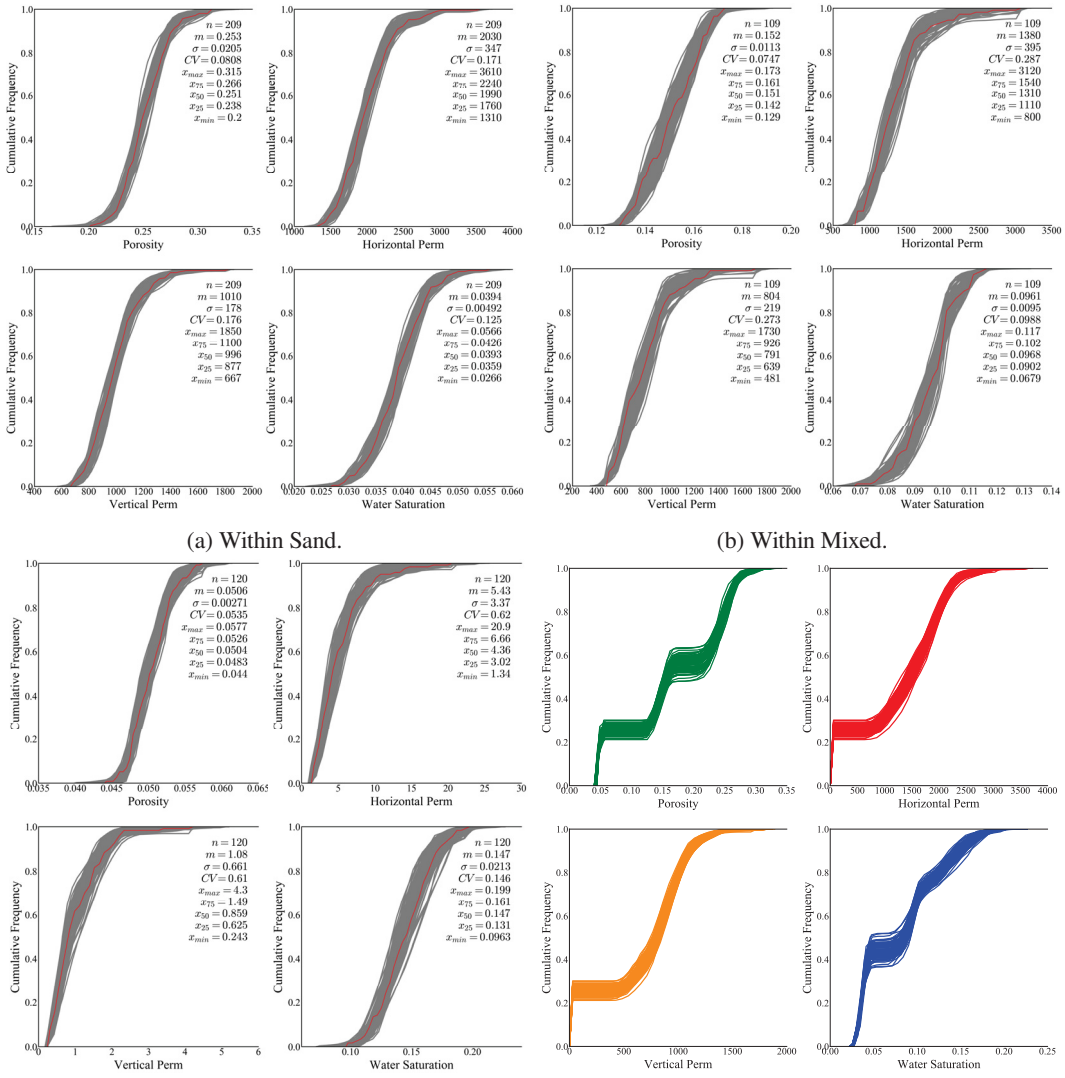

(a) Within Sand.

(b) Within Mixed.

(c) Within Shale.

(d) Merged for all facies (entire reservoir).

Figure 6.12: Posterior uncertainty in distribution of petrophysical properties before integration of 4D seismic data.

derived steam chamber. Figure 6.14 shows four identified anomalies including three flow barriers (type -1) and one flow conduit (type $+1$). No type 0 anomaly is considered for the case study.

As mentioned in Chapter 4, there are two options for describing an anomaly including ellipsoid and cloud of points with grid addresses related to the geostatistical modelling. As depicted in Figure 6.14, the later is implemented for the case study. An anomaly report file is the final result of the identification process. This report includes type of each anomaly (i.e., -1, +1, 0) and the corresponding grid addresses. The next step is to assess the reproduction of the identified anomalies by initial geostatistical realizations.

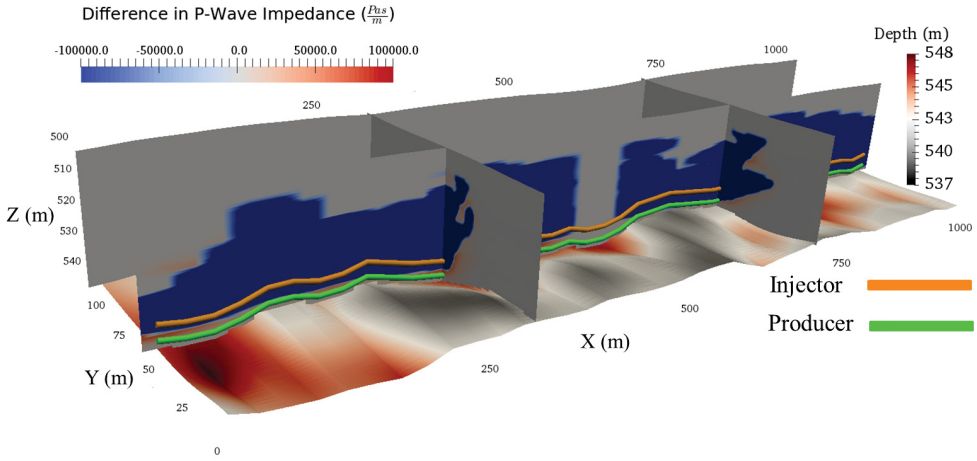

(a) Synthetic 4D seismic data for the reference model represented as the distribution of difference in P-wave impedance.

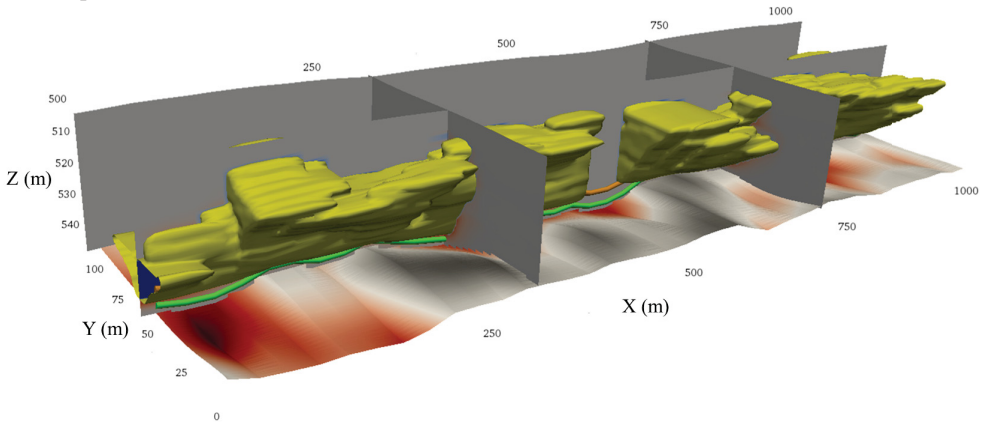

(b) Contoured surface that represents 4D seismic defined steam chamber.

Figure 6.13: Synthetic 4D seismic analysis for the reference model.

6.4.2 Fidelity Analysis

ART (Appendix A) can be used to automate the fidelity analysis for ensemble of all initial geostatistical realizations. This is based on calculating and assessing the effective permeability for each identified anomaly in all realizations. In this context, it is required to specify thresholds of effective permeability to determine if an anomaly is reproduced in a realization. Flow simulation results and knowledge of local geology can be used to assign these thresholds. In this case study, thresholds for type -1 and $+1$ anomalies are 100 and 800 md respectively (i.e., $K_{-1} = 100\ md$ and $K_{+1} = 800\ md$). The anomaly report file and thresholds are the main required parameters for execution of the fidelity analysis using ART. The initial realizations are simulated based on sparse well data and statistical parameters inferred from them. Thus, the low fidelity in reproduction of an identified anomaly is often expected especially if the anomaly is far from conditioning data.

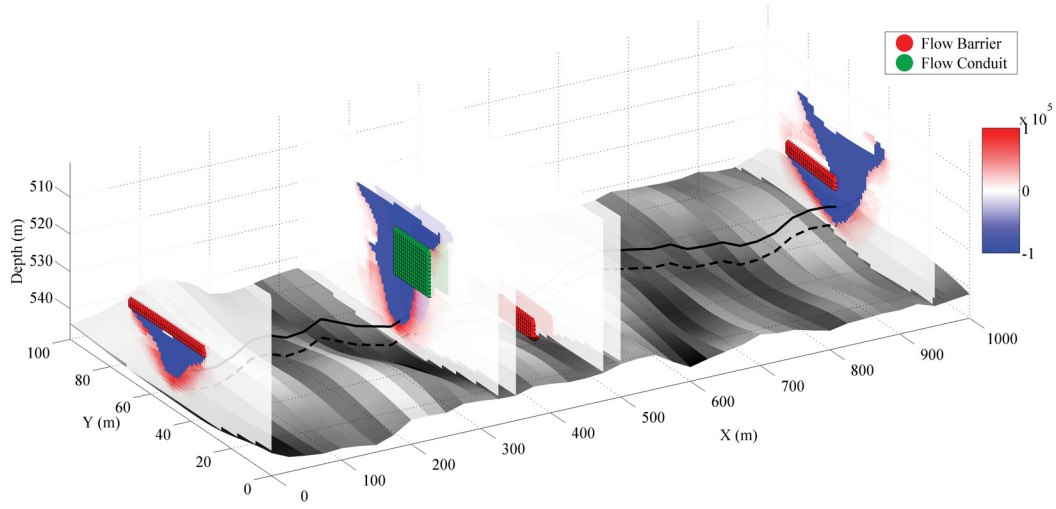

Figure 6.14: Identified anomalies and slices of the synthetic 4D seismic data. The color bar shows delineates difference in P-Wave impedance $\frac{Pas}{m}$. The flow barriers and conduit are highlighted by red and green points respectively.

6.4.3 Sampling the Enforcing Data

In order to honor information obtained from 4D seismic, all realizations should reproduce the identified anomalies. The fidelity analysis determines which anomaly(s) are missing in each realization. The large scale spatial arrangement of facies and distribution of flow properties (i.e., vertical and horizontal permeability) controls the flow quality of an anomaly. The initial realizations that do not reproduce the identified anomalies are updated through geostatistical anomaly enforcement. This is done by considering unique enforcing data for the missing anomalies in each realization. ART is used to search through ensemble of all initial realizations and sample the enforcing data. Figure 6.16 shows one example of sampled enforcing data for one realization along with the original well data. In practice, facies may be regarded as the primary enforcing data because the variability of permeability in between different facies is dominant compared to variability within them. In addition to facies, all simulated properties including porosity, water saturation, vertical and horizontal permeability are sampled. As can be seen in Figure 6.16, the enforcing data are consistent with the type of anomaly and also respect the relationship between different petrophysical properties within facies.

6.4.4 Updating Geostatistical Realizations

The last step for integration of 4D seismic is straightforward. The same geostatistical modelling workflow that was used to generate the initial realizations is repeated. The only difference is that each realization is conditioned to its own updated data file that contains the required enforcing data to reproduce the missing anomalies. Figure 6.17 shows one final updated realization of the reservoir. In Figure 6.17c, location of an identified type -1

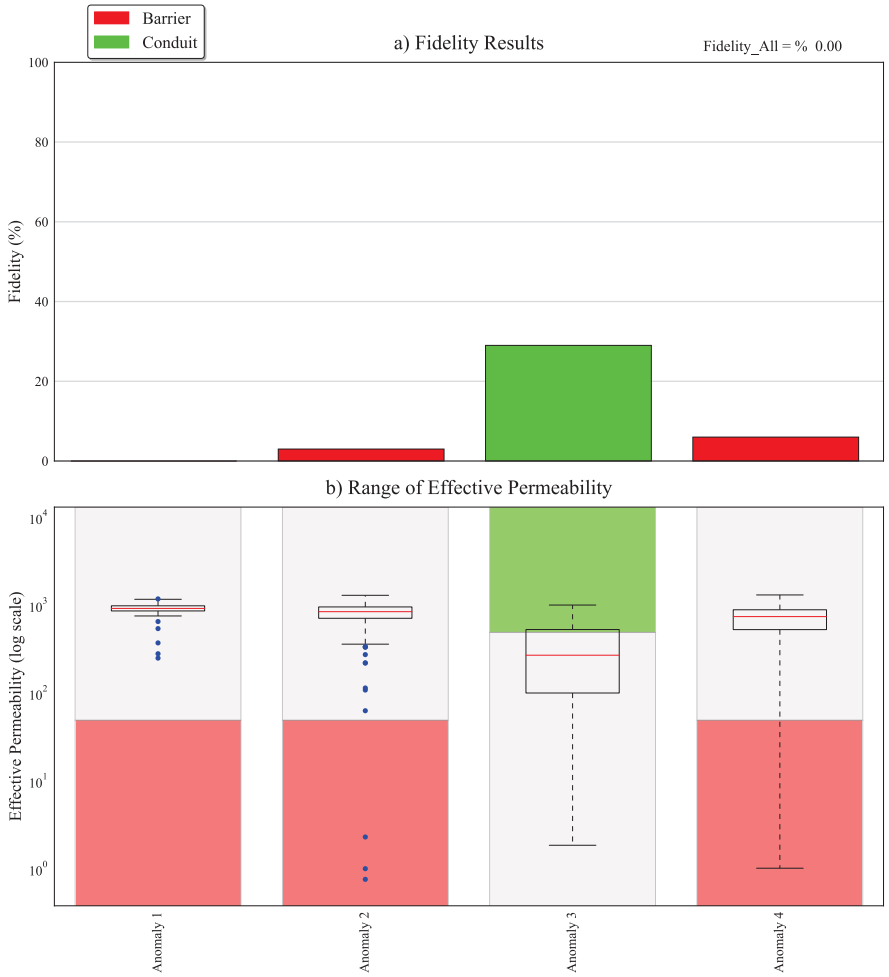

Figure 6.15: Fidelity analysis result for the case study considering initial realizations. Panel a depicts the percentage of realizations that reproduce each anomaly while panel b high lights the acceptable range of effective permeability.

anomaly (a flow barrier) is highlighted. A comparison between Figure 6.17 and 6.10 reveals that the identified flow barrier is reproduced.

Note that the input statistical parameters are not changed because there is no change in available hard well data. In other words, the same quantified prior parameter uncertainty including realizations of VPC and histograms are used for facies modelling and simulation of petrophysical properties. In practice, if additional well data become available, the parameter uncertainty needs to be updated. In this case study, the prior parameter uncertainty is not changed; however, including additional conditioning data may affect the posterior global uncertainty. In this regard, global facies proportion uncertainty before and after integration of 4D seismic are calculated and compared as shown in Figure 6.18. The hatched bars highlight the facies proportion inferred from the bas-case trend model that is calculated based on well data. As can be seen in Figure 6.18, apart from slight reduction of uncertainty in Shale proportion, the inclusion of enforcing data does not considerably affect distribution of global facies proportions. This is often expected since the enforcing data are sampled from the initial realizations. Also,

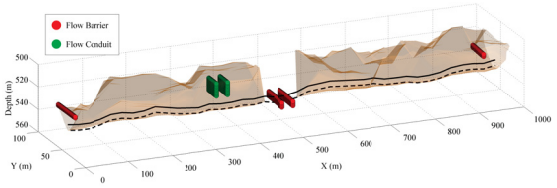

(a) Identified anomalies along with the steam chamber profile interpreted based on temperature threshold of 200 degree Celsius (transparent surface).

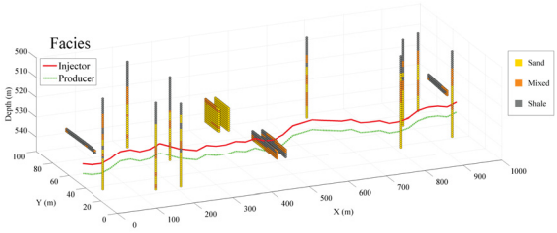

(b) Sampled enforcing data for facies.

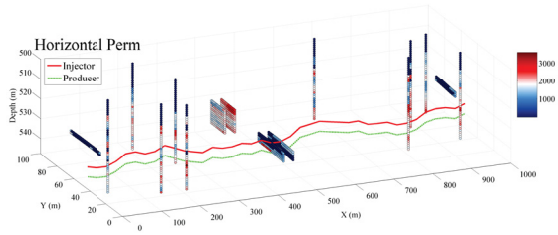

(c) Sampled enforcing data for horizontal permeability.

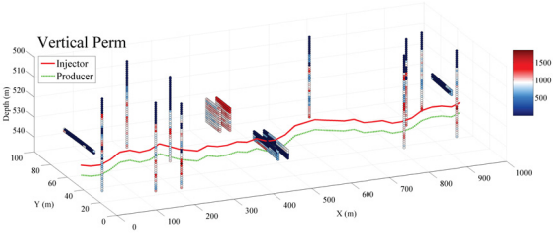

(d) Sampled enforcing data for vertical permeability.

Figure 6.16: Posterior uncertainty in distribution of petrophysical properties before integration of 4D seismic data.

the updating process is done with the same input statistical parameters. As discussed in Chapter 5, in practice, if there are a considerable amount of enforcing data some changes may be introduced to the posterior global uncertainty. Integration of a new source of information updates the model of geological uncertainty.

In addition, Figure 6.19 shows the posterior uncertainty in distribution of petrophysical properties after updating all realizations and integrating 4D seismic anomalies. In Figure 6.19a, the CDF for all updated realizations are highlighted in gray while the red line depicts the CDF inferred from the well data. Figure 6.19b shows the uncertainty in distribution of different properties for the entire reservoir model that includes facies proportion uncertainty, multivariate histogram uncertainty and also effect of geostatistical anomaly enforcement. In practice, reproduction of facies proportions and histograms should be checked before and after integration of 4D seismic to assess the effect of anomaly enforcement on geological uncertainty.

After updating realizations, ART is to provide a second fidelity analysis after anomaly enforcement. Figure 6.20 shows the fidelity results after integration of 4D seismic anomalies. As can be seen in Figure 6.20, almost all updated realizations reproduce the acceptable effective permeability for the identified anomalies. The reader is encouraged to consider a comparison between Figures 6.15 and 6.20 to study the improvement in fidelity results after anomaly enforcement. As mentioned above, identifying anomalies is a critical step in the proposed methodology for integration of 4D seismic. In addition, this step demands for considerable professional effort and judgment. However, the other steps are either automated using the software (ART) or can be easily added to any geostatistical modelling workflow.

The effect of geostatistical anomaly enforcement on SAGD reservoir characterization should be studied based on local improvements in propagation of the steam chamber. In this case study, there is a reference model that

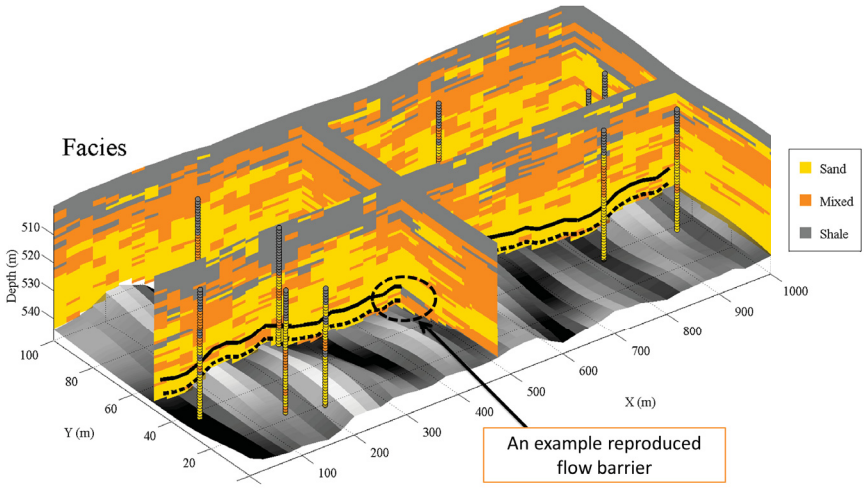

(a) Updated facies realization and well data.

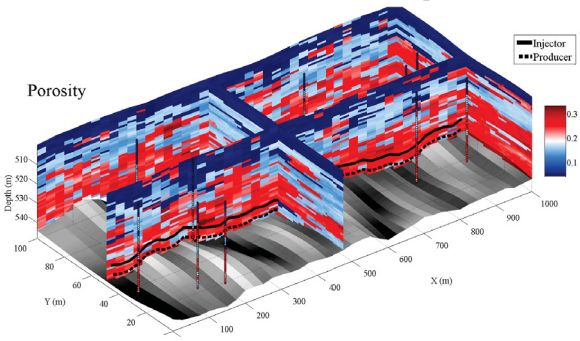

(b) Updated porosity realization and well data.

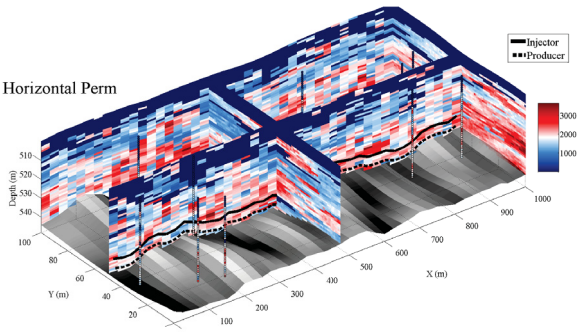

(c) Updated horizontal permeability realization and well data.

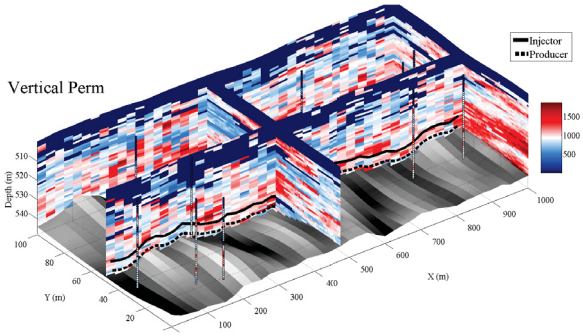

(d) Updated vertical permeability realization and well data.

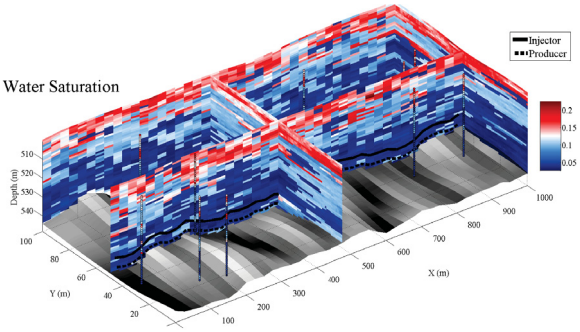

(e) Updated water saturation realization and well data.

Figure 6.17: One final updated realization of the reservoir after integration of 4D seismic data via geostatistical anomaly enforcement.

can be used as a benchmark to assess the steam chamber propagation estimated by geostatistical realizations. Figure 6.21 shows how the proposed anomaly enforcement approach can improve the local estimation of the steam chamber. Thermal flow simulation (STARS. CMG) is used to simulate SAGD for initial and updated geostatistical realizations. Then, the steam chamber is inferred based on considering areas with temperature higher than a specified threshold (i.e., 200° C). In Figures 6.21a and 6.21b, the steam chamber related to the

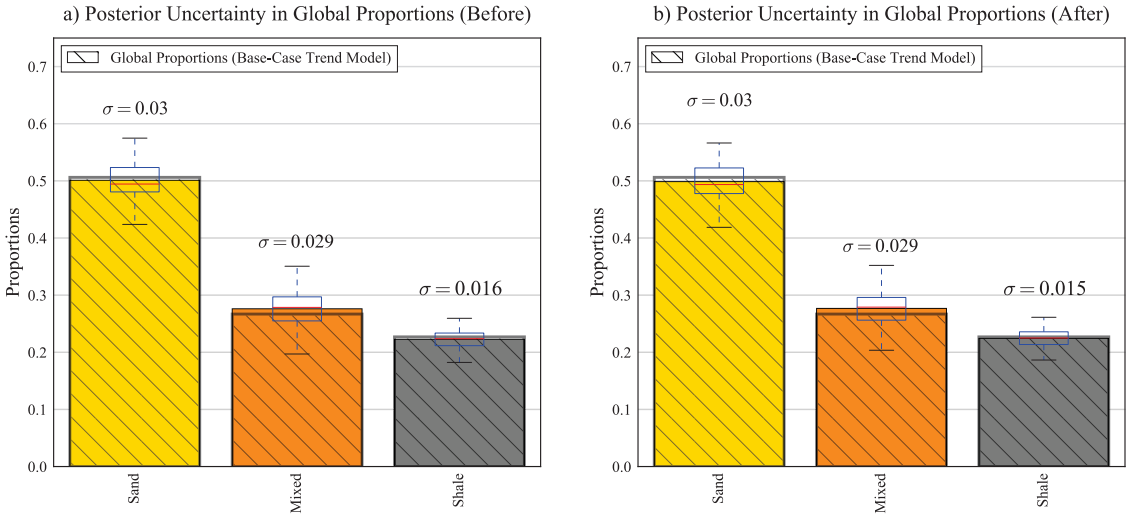

Figure 6.18: A comparison of posterior global proportion uncertainty before and after geostatistical anomaly enforcement.

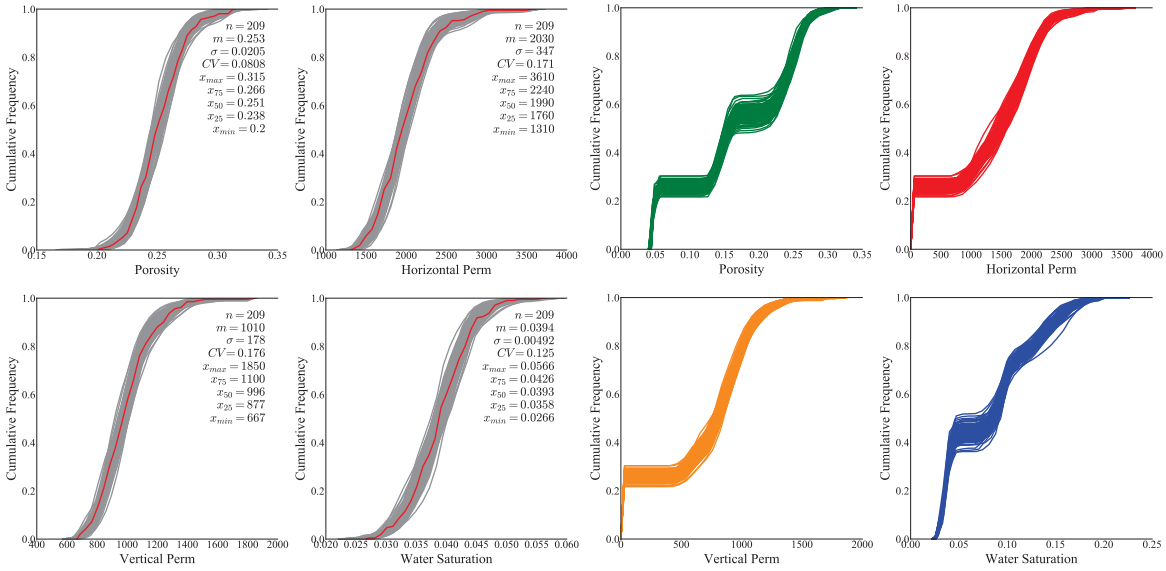

(a) Within Sand.

(b) Merged for all facies (entire reservoir).

Figure 6.19: Posterior histogram uncertainty for updated realizations after inclusion of parameter uncertainty and integration of 4D seismic data.

reference model is represented by the transparent surface. Figures 6.21c and 6.21d show cross sections of the steam chamber above the well pair for the reference model (blue line) and realizations (gray line) before and after anomaly enforcement respectively. In these figures, the top of steam chamber based on the temperature threshold is highlighted along the well pair. As can be seen in Figure 6.21, one of the anomalies (a flow barrier) is highlighted with a black rectangle. Because, the cross section view of the steam chamber above the well pair shows the improvement in estimation of steam chamber propagation at the location of this anomaly. Due to the computational cost associated with running thermal flow simulation for the reservoir, only twenty realizations

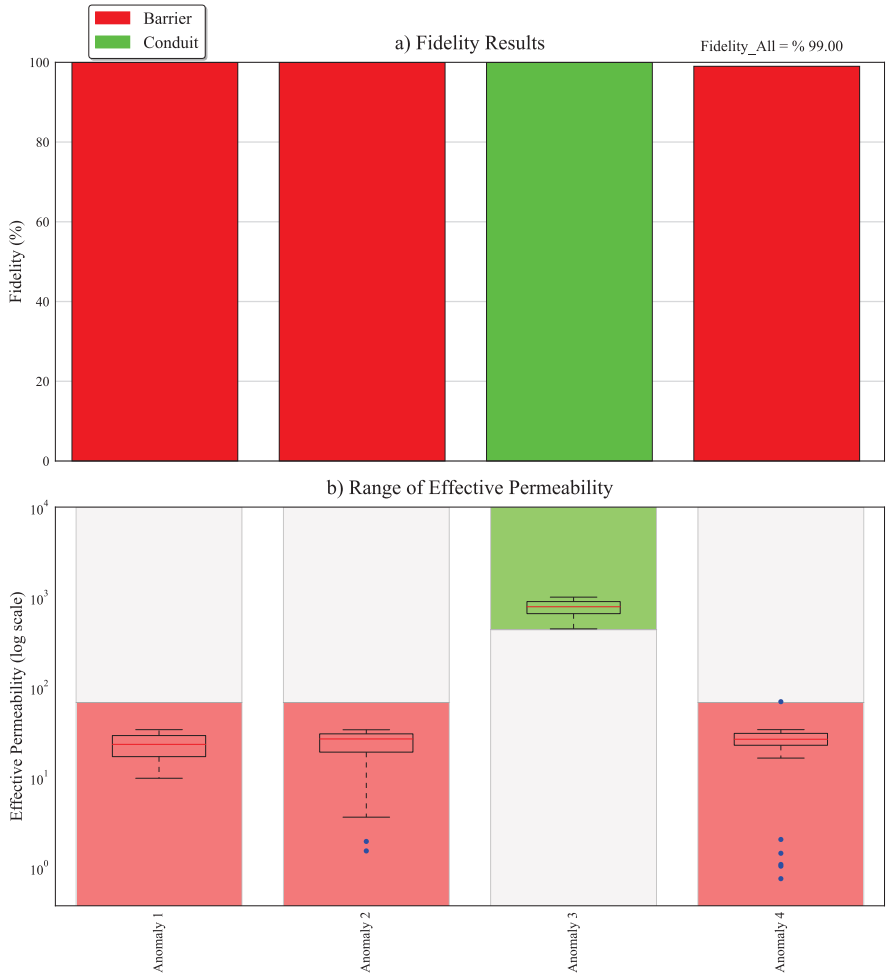

Figure 6.20: Fidelity analysis result after geostatistical anomaly enforcement. Panel a depicts the percentage of realizations that reproduce each anomaly while panel b high lights the acceptable range of effective permeability.

are considered and presented in Figure 6.21.

6.5 Conclusion Remarks

A comprehensive case study is presented in this chapter that provides a practical workflow for implementation of methodologies that are proposed and developed in this thesis. Geostatistical modelling is often done in presence of limited data due to inevitable economic and environmental constraints. As a result, input statistical parameters are subject to uncertainty that should be included in geostatistical reservoir modelling. A computer program (SBS_Categorical, Appendix A) is developed to quantify prior facies proportion uncertainty in presence of a trend. There is no additional professional effort required since the software only needs indicator variogram models and spatial facies data to generate multiple realizations of the trend model (i.e., VPC). Different facies modelling techniques including SIS and TPG can be used to simulate one final facies realization at a time using a separate trend model to get the posterior proportion uncertainty. Facies modelling is often followed by modelling

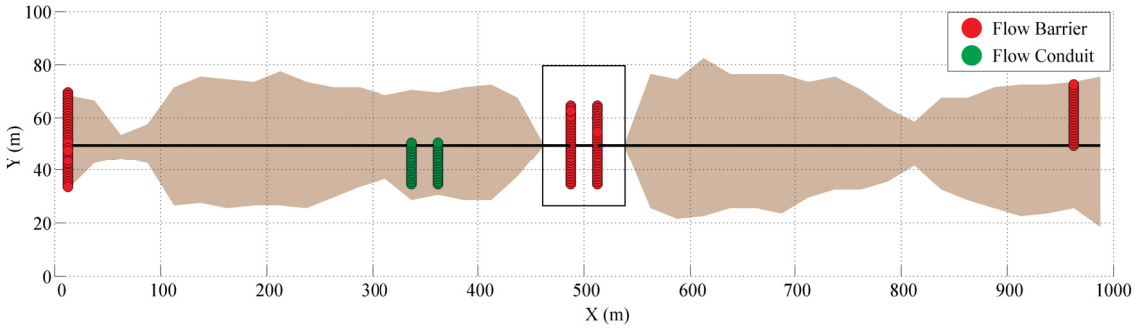

(a) Top view of the identified anomalies and steam chamber for the reference model.

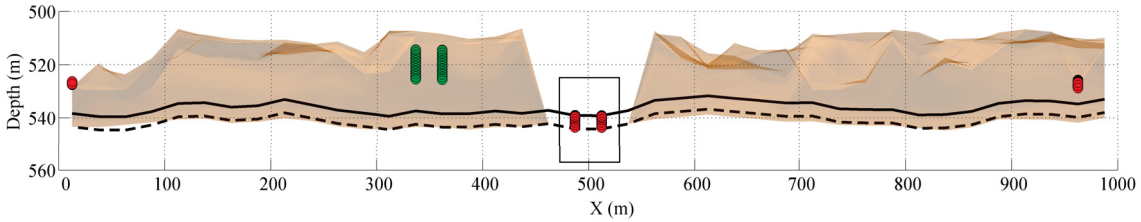

(b) Side view of the identified anomalies and steam chamber for the reference model.

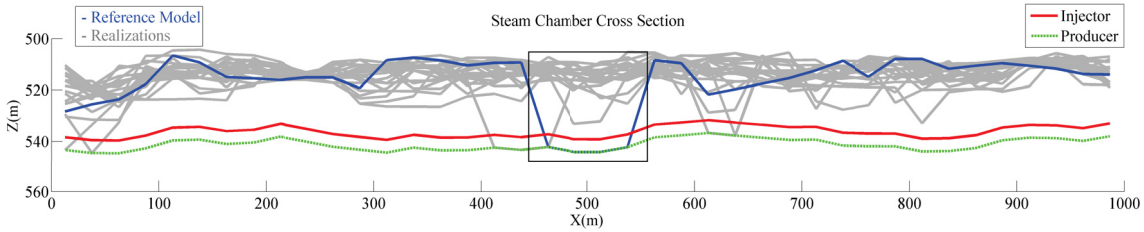

(c) Cross section above the well pair before Anomaly enforcement. Gray line highlight realizations while the red line shows the reference steam chamber cross section.

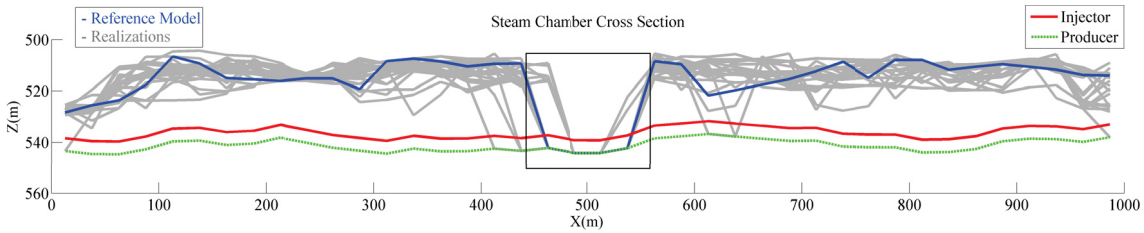

(d) Cross section above the well pair after Anomaly enforcement.Gray line highlight realizations while the red line shows the reference steam chamber cross section.

Figure 6.21: Effect of geostatistical anomaly enforcement on estimation of the steam chamber propagation.

of petrophysical properties within facies. Another computer program (SBS_MV, Appendix A) is used to quantify multivariate histogram uncertainty within facies. This provides multiple realizations of the reference distribution for each property that are considered in multivariate transformation prior to implement SGS to simulate each property within the reservoir. The proposed workflow provides an accurate estimation of geological uncertainty as it accounts for inevitable parameter uncertainty in presence of limited data.

4D seismic is a dynamic source of information and its integration can constraint the geological uncertainty.

In the case study, when 4D seismic data becomes available there is no additional well data. Therefore, the prior parameter uncertain is still considerable and should be included in geostatistical reservoir modelling. All realizations are updated based on the identified 4D seismic anomalies. The sampled enforcing data do not affect the input statistical parameters and are included in the modelling process as conditioning data. This may affect the global uncertainty for facies and distribution of petrophysical properties. As demonstrated in the case study, the posterior uncertainty for facies and petrophysical properties can be evaluate before and after geostatistical anomaly enforcement. It should be noted that 4D seismic provides information about large scale flow patterns. Thus, the main effect of integrating 4D seismic is the influence on local flow estimation. In case of SAGD, local improvements in estimation of the steam chamber propagation is expected. The computational cost of running flow simulation for the entire reservoir is a limitation that hampers fast evaluation of geostatistical anomaly enforcement. In this context, semi-analytical and geometry-based flow simulation approaches can be considered as a proxy for thermal flow simulation of SAGD (Gallardo and Deutsch, 2016).

Chapter 7

Summary and Conclusions

This final chapter summarizes the main contributions of the thesis and discusses limitations of the proposed methodologies. In addition, future work is proposed to build on what is achieved in this thesis. The motivation of this thesis is improved geostatistical reservoir modelling based on considering different sources of uncertainty and effective integration of dynamic sources of data.

7.1 Summary of Contributions

In general, the uncertainty associated with input statistical parameters is referred to as model parameter uncertainty. The current practice of geostatistical reservoir modelling often ignores the effect of parameter uncertainty. The main reason is lack of a practical workflow to quantify and integrate parameter uncertainty in geostatistical reservoir characterization. In this thesis, a collection of methodologies are proposed, developed and checked to provide a practical framework for integration of two important sources of parameter uncertainty: (1) facies proportions, and (2) multivariate histogram uncertainty. When limited well data are available, the parameter uncertainty is considerable and should be included in reservoir characterization. This improves the model of geological uncertainty that is used for resource assessment and reservoir management decision making.

At the same time, integration of dynamic data can constrain the geological uncertainty and provide a better estimation of reservoir performance under a recovery process. 4D seismic is one of the main dynamic data that can be used for reservoir monitoring and management. However, in practice, qualitative evaluation of 4D seismic data is preferred over quantitative integration using mathematical methods such as inverse modelling. The computational cost of inverse modeling methods and the complexity of real data undermine their practicality. Professional judgment is employed to infer reliable information about certain large-scale features within the reservoir. In this thesis, a novel methodology is proposed for practical integration of the reliable information obtained from 4D seismic in geostatistical reservoir modelling. Including 4D seismic data can improve the model of geologic uncertainty and provides a better estimation of flow response that is critical for reservoir management. The following provides a summary of each of the contributions in a greater detail.

7.1.1 Facies Proportion Uncertainty in Presence of Trends

Proportions are one of the main input parameters for geostatistical facies modeling techniques. Limited data does not allow unambiguous inference of proportions. Thus, using the same input target proportions for all geostatistical facies realizations results in underestimation of the global proportion uncertainty that can impact

resource estimation. Also, the spatial arrangement of facies has a determining effect on flow patterns and oil production. Facies are often modeled in presence of a trend that is a model of locally varying proportions. In Chapter 2, a methodology is proposed and developed for statistical resampling of facies data in presence of a trend model. This is done by the spatial bootstrap that is implemented via unconditional sequential indicator simulation at data locations. Indicator variogram models along with a base-case trend model inferred from data are used in the spatial bootstrap to generate multiple realizations of the facies data (resampling). Then, a trend building algorithm generates multiple realizations of the trend model that represent the prior proportion uncertainty. A computer program (SBS_Categorical, Appendix A) is developed that can be used to quantify the prior proportion uncertainty. A user manual is provided in Appendix A.

Indicator variogram models and facies data (i.e., coordinates plus categories) are the main required parameters for SBS_Categorical. A user can assign relevant trend modelling parameters if the prior proportion uncertainty is quantified in presence of a trend. In Chapter 2, an algorithm was proposed to improve uniform sampling of the multivariate space of proportion uncertainty. This algorithm can be implemented by SBS_Categorical to improve the assessment of prior proportion uncertainty. Integration of prior parameter uncertainty in geostatistical facies modelling is based on simulating one final facies realization for each realization of the trend model. This provides the posterior proportion uncertainty that is quantified by averaging over the entire reservoir for all realizations. An experimental setup is designed and presented in Chapter 2 to check the posterior proportion uncertainty quantified by the proposed methodology. In addition, a case study is presented in Chapter 3 to demonstrate and evaluate practical application of the methodology along with integration of multivariate histogram uncertainty.

7.1.2 Integration of Multivariate Histogram Uncertainty

Histograms are the main input statistical parameter for geostatistical modelling of continuous variables (i.e., petrophysical properties). Histogram uncertainty should be quantified and integrated in multivariate geostatistical reservoir modelling. Another contribution of this thesis is a geostatistical tool (SBS_MV , Appendix A) to facilitate quantification of multivariate histogram uncertainty using a multivariate transformation technique (i.e., PPMT) followed by unconditional and independent sequential Gaussian simulation at data locations for each property. Also, a workflow is presented to integrate histogram uncertainty in multivariate Gaussian simulation of petrophysical properties within facies. A case study based on real well data is presented in Chapter 3 to provide a workflow for effective integration of facies proportion uncertainty and multivariate histogram uncertainty. Also, the effect of considering these sources of parameter uncertainty on a final model of geological uncertainty is studied.

It should be noted that other sources of parameter uncertainty including variogram and structural uncertainty can be included in the modelling workflow. The key idea is to process one realization at a time based on its corresponding realization of input parameters. There is no branching and multiple realizations (often 100 to

200) that are generated to represent/sample each space of uncertainty are carried forward through the work flow. More complex forms of uncertainty may also be included by defining different modelling scenarios.

7.1.3 A Practical Methodology for Integration of 4D Seismic

Ou model of geological uncertainty is a numerical representation of our lack of knowledge about the subsurface geology. While including parameter uncertainty provides a more realistic assessment of geological uncertainty, accounting for additional information obtained from dynamic sources of data can constrains and perhaps reduce the uncertainty. 4D seismic is a valuable source of information that becomes available during a recovery process. It is fairly expensive to acquire and process time-lapse seismic surveys. Also, there is a limited time to benefit from 4D seismic in order to improve the geological models and make changes to reservoir operations. In Chapter 4, a methodology is proposed, developed and checked for effective integration of 4D seismic in geostatistical reservoir modelling. The key idea is to benefit from professional judgment to infer reliable information about large scale changes in reservoir conditions due to the recovery process. Such information may be best represented as anomalies in large scale flow patterns.

A combination of professional judgment, knowledge of the recovery process and seismic interpretation is employed to identify anomalies based on visual inspection. This is the first step and plays a key role in the success of the proposed methodology. Best practices and guidelines for anomaly identification are documented in Chapter 5. The main objective is to update geostatistical realizations that are not informed by 4D seismic anomalies. In this context, the next step is to evaluate reproduction of identified anomalies in each realization. This is referred to as fidelity analysis and determines what percentage of realizations reproduce each anomaly and also pinpoints the missing anomalies in each realization. Effective directional permeability is used to evaluate anomalies since they are associated with large scale quality of flow. A computer program (ART, Appendix A) is developed to automate the fidelity analysis by processing all realizations. Also, ART can be used to sample enforcing data for the missing anomalies by a random search through the ensemble of all realizations. This provides a unique updated data file for each realization that contains the original well data plus the enforcing data for anomaly(s) missing in the realization. Finally, the same geostatistical modelling work flow is repeated to update one realization at a time using a separate updated data file. A detailed user manual is provided for ART in Appendix A. The proposed methodology can be added to any geostatistical modelling workflow as a pre/post processing step. In Chapter 5, a case study is presented that demonstrates the application of the proposed methodology in practice where real 4D seismic data from a DA in Surmont project are used to update initial geostatistical realizations. Also, in Chapter 6 a comprehensive case study provides a workflow for integration of 4D seismic in presence of parameter uncertainty.

Improving the practice of geostatistical reservoir modelling is the main motivation for this thesis. Different case studies and flow charts are provided to establish a practical workflow for integration of 4D seismic and facies proportion uncertainty in geostatistical reservoir characterization. The methodologies summarized above are to

address some of the current challenges in geostatistical reservoir modelling. A collection of computer programs facilitate the implementation of methodologies and solutions proposed in this thesis. During the course of this research, the proposed methodologies were tested and improved through practical application, peer reviewed publication and getting feedback from reservoir engineers and geologists.

7.2 Limitations

The developed methodologies and geostatistical tools have been implemented and checked in real case studies. However, there are some conceptual and computational limitations that are discussed here. The prior facies proportion uncertainty is represented by multiple realizations of global proportions or the trend model. Facies modeling techniques like SIS, truncated Gaussian (TG), and TPG use the trend model directly in the simulation at the data locations to obtain the posterior uncertainty. However, for facies modeling techniques like MPS, additional steps may be required to integrate realizations of the trend model in the simulation process. One suggested approach is to use realizations of the trend model to modify/generate multiple realizations of training images that are used in MPS.

Success of the proposed methodology for integration of 4D seismic data depends on reliable anomaly identification. Anomalies are associated with large scale features within the reservoir. However, an observed anomaly in 4D seismic data is not always related to the geology. For instance, technical issues associated with well completion can block steam injection and in turn hamper the propagation of the steam chamber during SAGD. Thus, what is interpreted as a flow barrier may not correlate with large scale flow properties within the reservoir. Recent developments in remote sensing technology along the wells combined with improved seismic acquisition and processing techniques can help practitioners to overcome this limitation.

It is required to run flow simulation for all realizations before and after geostatistical anomaly enforcement to study changes in local flow patterns and also assess production uncertainty. In this regard, obtaining flow responses provides a closed-loop system for integration and evaluation of identified 4D seismic anomalies. However, the computational cost is a bottleneck for fast evaluation of 4D seismic integration. Also, flow responses can be used to quantify the value of information as incremental 4D seismic data become available and more anomalies are identified. A potential solution to address this limitation is a semi-analytical or approximate flow simulation for the recovery process (i.e., proxy). In case of SAGD, such proxy should be capable of estimating the steam chamber propagation over time.

Geostatistical anomaly enforcement is based on sampling enforcing data that are consistent with modelling workflow and geological setting. This is accomplished by a random search through ensemble of all realizations. In order to achieve a fast search, the computer program (ART) is designed to load all realizations into memory and scan through them. However, this can be memory intensive for a large reservoir model. For instance, loading 100 realizations of different geological properties for a DA with multiple well pairs can cause memory issues for a typical computer. In general, there is a trade off between making a computational algorithm fast and memory

efficient. A potential solution is to provide an option to load realization on the fly when they are required by the algorithm. This approach make the algorithm considerably slower that can be mitigated through the use of binary files to store realizations. This was not an issue for the case studies presented in this thesis because the computer used to run the algorithm had sufficient memory. Thus, the computer program was developed in favor of having a fast search algorithm.

7.3 Future Work

There are a number of suggestions to improve methodologies and geostatistical tools developed in this thesis.

The facies proportion uncertainty is quantified in presence of a trend model that is calculated based on the hard data. The trend building algorithm could be improved by considering 2D/3D seismic data. Also, there are well established geostatistical techniques to integrate soft seismic data in facies simulation process which is another approach to update the uncertainty using seismic data. The case studies presented in Chapter 3 and Chapter 6 provide a workflow for practical integration of proportion uncertainty in geostatistical facies modelling using SIS. In this regard, integration of prior proportion uncertainty in other geostatistical techniques such as TPG could be considered through additional case studies.

The proposed methodology for practical integration of 4D seismic and the computer program that implements it have been improved through application in real industrial case studies. Additional case studies are required to further improve the methodology and enhance the efficiency of the computer program. During a recovery process, seismic surveys are often obtained periodically to perform time-lapse analysis and get incremental 4D seismic data that can be used to evaluate the reservoir performance over time. However, the information obtained from each incremental 4D seismic analysis is different depending on the timing and details of the recovery process. Quantifying the value of information for each set of incremental 4D seismic data can help to make better decisions about future monitoring seismic surveys. In practice, it is challenging to quantify the value of information based on complex reservoir recovery.

Integration of 4D seismic results in updating geological model. It is required to evaluate the effect of such modifications on production results. The qualitative assessment of 4D seismic often is considered to change reservoir operations. Additional case studies are reacquired to study how the updated geological model can support and improve such decisions. Although the proposed methodology for integration of 4D seismic is a practical alternative, additional studies are required to assess it performance compared to conventional history matching and inverse modelling.

References

Abdollahzadeh, A., Christie, M., Corne, D., Davies, B. J., and Elliott, M. T. (2013). An adaptive evolutionary algorithm for history-matching. In EAGE Annual Conference and Exhibition incorporating SPE Europec. Society of Petroleum Engineers.

Alfi, M. and Hosseini, S. A. (2016). Integration of reservoir simulation, history matching, and 4d seismic for co 2-eor and storage at cranfield, mississippi, usa. Fuel, 175:116–128.

Alshehri, N. (2009). Quantification of reservoir uncertainty for optimal decision making. PhD thesis, University of Alberta.

Amudo, C., Graf, T., Dandekar, R. R., and Randle, J. M. (2009). The pains and gains of experimental design and response surface applications in reservoir simulation studies. In SPE Reservoir Simulation Symposium. Society of Petroleum Engineers.

Andersen, T., Zachariassen, E., Otterlei, C., Hatland, K., and Liestolt, F. (2006). Method for conditioning the reservoir model on 3D and 4D elastic inversion data applied to a fluvial reservoir in the north sea. SPE, 100190:6.

Arenas, E., van Kruijsdijk, C., and Oldenziel, T. (2001). Semi-automatic history matching using the pilot point method including time-lapse seismic data. In SPE Annual Technical Conference and Exhibition. Society of Petroleum Engineers.

Armstrong, M., Galli, G., Le Loch, R., Geffroy, F., and Eschard, R. (2003). Plurigaussian Simulations in Geosciences, volume Berlin.

Arnold, D., Demyanov, V., Christie, M., Bakay, A., and Gopa, K. (2016). Optimisation of decision making under uncertainty throughout field lifetime: A fractured reservoir example. Computers & Geosciences, 95:123–139.

Avansi, G. and Schiozer, D. (2015). A new approach to history matching using reservoir characterization and reservoir simulation integrated studies. In Offshore Technology Conference. Offshore Technology Conference.

Babak, O. and Deutsch, C. V. (2009). Accounting for parameter uncertainty in reservoir uncertainty assessment: The conditional finite-domain approach. Natural Resources Research, 18(1):7–17.

Babin, V., Vashevnik, A., Ushmaev, O., Gruzdev, A., Pozdneev, A., Semenikhin, A., Quinones, M. P., Flach, B., and Ciaurri, D. E. (2016). A methodology for the refinement of well locations during operational drilling in presence of geological uncertainty. In SPE Russian Petroleum Technology Conference and Exhibition. Society of Petroleum Engineers.

Barnett, R. M. (2015). Managing Complex Multivariate Relations in the Presence of Incomplete Spatial Data. PhD thesis, University of Alberta.

Barnett, R. M. and Deutsch, C. V. (2015a). Guide to Multivariate Modeling with the PPMT. Centre for

Computational Geostatistics (CCG).

Barnett, R. M. and Deutsch, C. V. (2015b). Multivariate imputation of unequally sampled geological variables. Mathematical Geosciences, 47(7):791–817.

Barnett, R. M., Manchuk, J. G., and Deutsch, C. V. (2014). Projection pursuit multivariate transform. Mathematical Geosciences, 46(3):337–359.

Begg, S., Bratvold, R., and Campbell, J. (2001). Improving investment decisions using a stochastic integrated asset model. In SPE Annual Technical Conference and Exhibition. Society of Petroleum Engineers.

Begg, S., Bratvold, R., and Campbell, J. (2002). The value of flexibility in managing uncertainty in oil and gas investments. In SPE Annual Technical Conference and Exhibition. Society of Petroleum Engineers.

Bhakta, T., Luo, X., and Nævdal, G. (2016). Ensemble based 4d seismic history matching using a sparse representation of ava data. In SEG Technical Program Expanded Abstracts 2016, pages 2961–2966. Society of Exploration Geophysicists.

Bickel, E. and Bratvold, R. (2008). From uncertainty quantification to decision making in the oil and gas industry. Energy, Exploration & Exploitation, 26(5):311–325.

Bratvold, R. B. and Begg, S. H. (2006). Education for the real world: equipping petroleum engineers to manage uncertainty. In SPE Annual Technical Conference and Exhibition. Society of Petroleum Engineers.

Butler, R. (1985). A new approach to the modelling of steam-assisted gravity drainage. Journal of Canadian Petroleum Technology, 24(03).

Butler, R. (1998). Sagd comes of age! Journal of Canadian Petroleum Technology, 37(07).

Castro, S., Caers, J. K., Otterlei, C., Andersen, T., Hoye, T., and Gomel, P. (2006). A probabilistic integration of well log, geological information, 3D/4D seismic, and production data: application to the oseberg field. In SPE Annual Technical Conference and Exhibition. Society of Petroleum Engineers.

Chakra, N. C. and Saraf, D. N. (2015). History matching of petroleum reservoirs employing adaptive genetic algorithm. Journal of Petroleum Exploration and Production Technology, pages 1–22.

Chakra, N. C. and Saraf, D. N. (2016). History matching of petroleum reservoirs employing adaptive genetic algorithm. Journal of Petroleum Exploration and Production Technology, 6(4):653–674.

Chen, Y. and Oliver, D. S. (2010). Ensemble-based closed-loop optimization applied to brugge field. SPE Reservoir Evaluation and Engineering, 13(01):56–71.

Chopra, S., Lines, L. R., Schmitt, D. R., and Batzle, M. L. (2010). Heavy oils: reservoir characterization and production monitoring. Society of Exploration Geophysicists.

da Cruz, P. S. (2000). Reservoir Management Decision-Making in the Presence of Geological Uncertainty. PhD thesis, Stanford University, Stanford, CA.

Damsleth, E., Hage, A., and Volden, R. (1992). Maximum information at minimum cost. Journal of Petroleum Technology.

Deutsch, C. V. (2006). A sequential indicator simulation program for categorical variables with point and block

data: Blocksis. Computers & Geosciences, 32(10):1669–1681.

Deutsch, C. V. and Journel, A. G. (1994). The application of simulated annealing to stochastic reservoir modeling. SPE Advanced Technology Series, 2(02):222–227.

Deutsch, J. L. and Deutsch, C. V. (2010). Some geostatistical software implementation details. Centre for Computational Geostatistics (CCG), Annual Report 12.

Deutsch, J. L. and Deutsch, C. V. (2012). Latin hypercube sampling with multidimensional uniformity. Journal of Statistical Planning and Inference, 142(3):763–772.

Dowd, P. and Pardo-Igúzquiza, E. (2002). The incorporation of model uncertainty in geostatistical simulation. Geographical and Environmental Modelling, 6(2):147–169.

Efron, B. and Tibshirani, R. (1986). Bootstrap methods for standard errors, confidence intervals, and other measures of statistical accuracy. Statistical science, pages 54–75.

Ehinola, O. A. and Akinbodewa, O. (2014). Uncertainty in quantification and ranking of stock tank oil initially in place (stoiip) in oa field, niger delta. In Unconventional Resources Technology Conference, Denver, Colorado, 25-27 August 2014, pages 2524–2533. Society of Exploration Geophysicists, American Association of Petroleum Geologists, Society of Petroleum Engineers.

Evensen, G. (1994). Sequential data assimilation with a nonlinear quasi-geostrophic model using monte carlo methods to forecast error statistics. Journal of Geophysical Research: Oceans (1978–2012), 99(C5):10143–10162.

Falivene, O., Arbus, P., Gardiner, A., Pickup, G., Muoz, J. A., and Cabrera, L. (2006). Best practice stochastic facies modeling from a channel-fill turbidite sandstone analog (the quarry outcrop, eocene ainsa basin, northeast spain). AAPG bulletin, 90(7):1003–1029.

Fenik, D., Nouri, A., and Deutsch, C. (2009). Criteria for ranking realizations in the investigation of SAGD reservoir performance. In Canadian International Petroleum Conference. Petroleum Society of Canada.

Friedman, M. and Savage, L. J. (1952). The expected-utility hypothesis and the measurability of utility. The Journal of Political Economy, pages 463–474.

Gallardo, E. and Deutsch, C. V. (2016). A new proxy for modeling the evolution of the steam chamber in SAGD. Centre for Computational Geostatistics (CCG), Annual Report 18.

Gassmann, F. (1951). Elasticity of porous media: Über die elastizität poröser medien: Vierteljahrsschrift der naturforschenden gesselschaft in zurich.

Geman, S. and Geman, D. (1984). Stochastic relaxation, gibbs distributions, and the bayesian restoration of images. Pattern Analysis and Machine Intelligence, IEEE Transactions on, (6):721–741.

Gohari, K., Jutila, H., Mascagnini, C., Gryaznov, A., Goodwin, N., Howell, M., Kidd, P. J., and Bijani, B. (2015). Novel workflow for the development of a flow control strategy with consideration of reservoir uncertainties. In Abu Dhabi International Petroleum Exhibition and Conference. Society of Petroleum Engineers.

Gómez-Hernánez, J. J., Sahuquillo, A., and Capilla, J. E. (1997). Stochastic simulation of transmissivity fields conditional to both transmissivity and piezometric data–1. theory. Journal of Hydrology(Amsterdam), 203(1):167–174.

Goovaerts, P. (1997). Geostatistics for natural resources evaluation. Oxford University Press on Demand.

Gosselin, O., van den Berg, S., and Cominelli, A. (2001). Integrated history-matching of production and 4D seismic data. In SPE Annual Technical Conference and Exhibition. Society of Petroleum Engineers.

Gu, Y. and Oliver, D. S. (2005). History matching of the PUNQ-S3 reservoir model using the ensemble kalman filter. SPE journal, 10(02):217–224.

Guardiano, F. B. and Srivastava, R. M. (1993). Multivariate geostatistics: beyond bivariate moments. In Geostatistics Troia'92, pages 133–144. Springer.

Hadavand, M., Carmichael, P., Dali, A., Rodriguez, M., Silva, D., and Deutsch, C. V. (2017). Integration of 4D seismic in sagd reservoir characterization. submitted to SPE Reservoir Evaluation & Engineering.

Hadavand, M. and Deutsch, C. V. (2014). An example application of EnKF with flow-based pressure data. Centre for Computational Geostatistics (CCG), Annual Report 16.

Hadavand, M. and Deutsch, C. V. (2016). A practical methodology for integration of 4D seismic in steam-assisted-gravity-drainage reservoir characterization. SPE Reservoir Evaluation & Engineering.

Hadavand, M. and Deutsch, C. V. (2017). Facies proportion uncertainty in presence of a trend. Journal of Petroleum Science and Engineering, 153:59 – 69.

Hanea, R., Evensen, G., Hustoft, L., Ek, T., Chitu, A., and Wilschut, F. (2015). Reservoir management under geological uncertainty using fast model update. SPE Reservoir Simulation Symposium.

Hein, F. J. (2006). Heavy oil and oil (tar) sands in north america: an overview & summary of contributions. Natural Resources Research, 15(2):67–84.

Hotelling, H. (1933). Analysis of a complex of statistical variables into principal components. Journal of educational psychology, 24(6):417.

Isaaks, E. H. (1991). The application of Monte Carlo methods to the analysis of spatially correlated data. PhD thesis, Stanford University Dissertation.

Jiménez, S., Mariethoz, G., Brauchler, R., and Bayer, P. (2016). Smart pilot points using reversible-jump markov-chain monte carlo. Water Resources Research.

Johnson, R. A. and Wichern, D. W. (2002). Applied multivariate statistical analysis, volume 5. Prentice hall Upper Saddle River, NJ.

Journel, A. (1989). Fundamentals of geostatistics in five lessons, volume 8. American Geophysical Union Washington, DC.

Journel, A. (2002). Combining knowledge from diverse sources: an alternative to traditional data independence hypotheses. Mathematical geology, 34(5):573–596.

Journel, A. and Alabert, F. (1989). Focusing on spatial connectivity of extreme-valued attributes: Stochastic

indicator models of reservoir heterogeneities. AAPG Bull.;(United States), 73(CONF-890404-).

Journel, A. and Isaaks, E. (1984). Conditional indicator simulation: application to a saskatchewan uranium deposit. Journal of the International Association for Mathematical Geology, 16(7):685–718.

Journel, A. G. (1983). Nonparametric estimation of spatial distributions. Mathematical Geology, 15(3):445–468.

Journel, A. G. and Huijbregts, C. J. (1978). Mining geostatistics. Academic press.

Khan, K. D. and Deutsch, C. V. (2015). Practical incorporation of multivariate parameter uncertainty in geostatistical resource modeling. Natural Resources Research, pages 1–20.

Khan, K. D., Deutsch, J. L., and Deutsch, C. V. (2014). A refresher on large scale uncertainty for resource estimation. Centre for Computational Geostatistics (CCG), Annual Report 16.

Kokal, S. and Al-Kaabi, A. (2010). Enhanced oil recovery: challenges & opportunities. World Petroleum Council: Official Publication, pages 64–68.

Kulahci, M. (2015). Technology focus: History matching and forecasting (april 2015). Journal of Petroleum Technology, page 170945.

LaVenue, A. M., RamaRao, B. S., De Marsily, G., and Marietta, M. G. (1995). Pilot point methodology for automated calibration of an ensemble of conditionally simulated transmissivity fields: 2. application. Water Resources Research, 31(3):495–516.

Le Ravalec, M., Morlot, C., Marmier, R., and Foulon, D. (2009). Heterogeneity impact on sagd process performance in mobile heavy oil reservoirs. Oil & Gas Science and Technology-Revue de l'IFP, 64(4):469–476.

Leuangthong, O. and Deutsch, C. V. (2003). Stepwise conditional transformation for simulation of multiple variables. Mathematical Geology, 35(2):155–173.

Likanapaisal, P. and Tchelepi, H. A. (2015). Quantification of prediction uncertainty: What does it mean and how does it evolve with history matching. In SPE Reservoir Simulation Symposium. Society of Petroleum Engineers.

Lumley, D., Adams, D. C., Meadows, M., Cole, S., and Wright, R. (2003). 4D seismic data processing issues and examples. In 2003 SEG Annual Meeting. Society of Exploration Geophysicists.

Lumley, D. and Behrens, R. (1998). Practical issues of 4d seismic reservoir monitoring: What an engineer needs to know. SPE Reservoir Evaluation & Engineering, 1(06):528–538.

MacBeth, C., Floricich, M., and Soldo, J. (2006). Going quantitative with 4D seismic analysis. Geophysical Prospecting, 54(3):303–317.

Manchuk, J. G. and Deutsch, C. V. (2012). A flexible sequential gaussian simulation program: Usgsim. Computers & Geosciences, 41:208–216.

McKay, M. D. (1992). Latin hypercube sampling as a tool in uncertainty analysis of computer models. In Proceedings of the 24th conference on Winter simulation, pages 557–564. ACM.

McLennan, J. and Deutsch, C. V. (2005). Selecting geostatistical realizations by measures of discounted

connected bitumen. In SPE International Thermal Operations and Heavy Oil Symposium. Society of Petroleum Engineers.

Mezghani, M., Fornel, A., Langlais, V., and Lucet, N. (2004). History matching and quantitative use of 4D seismic data for an improved reservoir characterization. paper SPE, 90420:26–29.

Negash, B., Ayoub, M. A., Jufar, S. R., and Robert, A. J. (2017). History matching using proxy modeling and multiobjective optimizations. In ICIPEG 2016, pages 3–16. Springer.

Oliver, D. S. and Chen, Y. (2011). Recent progress on reservoir history matching: a review. Computational Geosciences, 15(1):185–221.

Ouenes, A. and Bhagavan, S. (1994). Application of simulated annealing and other global optimization methods to reservoir description: myths and realities. In SPE Annual Technical Conference and Exhibition. Society of Petroleum Engineers.

Pyrcz, M. J. and Deutsch, C. V. (2014). Geostatistical reservoir modeling. Oxford university press.

Qu, J. and Deutsch, C. V. (2015). Optimal/automatic trend modeling parameter selection. Centre for Computational Geostatistics (CCG), Annual Report 17.

Rajput, S., Yin, K. Y., Pathak, R. K., Kandau, F., Agrawal, P., Ring, M., Garun, L. L., Bertoldi, L., Amat, H. B., and Ismail, S. A. B. (2016). Seismic inversion driven improved reservoir characterisation and production optimisation in a mature field. In Offshore Technology Conference Asia. Offshore Technology Conference.

RamaRao, B. S., LaVenue, A. M., De Marsily, G., and Marietta, M. G. (1995). Pilot point methodology for automated calibration of an ensemble of conditionally simulated transmissivity fields: 1. theory and computational experiments. Water Resources Research, 31(3):475–493.

Rezvandehy, M. (2016). Geostatistical Reservoir Modeling with Parameter Uncertainty in Presence of Limited Data. PhD thesis, University of Alberta.

Rose, P. R. (2007). Measuring what we think we have found: Advantages of probabilistic over deterministic methods for estimating oil and gas reserves and resources in exploration and production. AAPG Bulletin, 91(1):21–29.

Rwechungura, R. W., Dadashpour, M., and Kleppe, J. (2011). Advanced history matching techniques reviewed. In SPE Middle East Oil and Gas Show and Conference. Society of Petroleum Engineers.

Sazonov, E., Nugaeva, A., Muryzhnikov, A., and Eydinov, D. (2015). Risks and uncertainties evaluation of reservoir models as a way to optimal decisions. In SPE Russian Petroleum Technology Conference. Society of Petroleum Engineers.

Shuai, Y., White, C., Sun, T., and Feng, Y. (2016). A gathered enkf for continuous reservoir model updating. Journal of Petroleum Science and Engineering, 139:205–218.

Silva, D. S. and Deutsch, C. V. (2016). Hierarchical approach to truncated plurigaussian simulation. Centre for Computational Geostatistics (CCG), Annual Report 18.

Silva, D. S. F. and Deutsch, C. V. (2015a). Transformation for multivariate modeling using gaussian mixtures with exhaustive secondary data. CCG Anual Report 17 105, University of Alberta.

Silva, D. S. F. and Deutsch, C. V. (2015b). Well/drill hole prediction tool. CCG Anual Report 17 204, University of Alberta.

Solow, A. R. (1985). Bootstrapping correlated data. Mathematical Geology, 17(7):769–775.

Srivastava, R. (1990). An application of geostatistical methods for risk analysis in reservoir management. SPE Annual Technical Conference and Exhibition.

Srivastava, R. M. (1987). Minimum variance or maximum profitability?. CIM Bulletin, 80(901):63–68.

Stalder, J. (2013). Test of sagd flow-distribution-control liner system in the surmont field, alberta, canada. Journal of Canadian Petroleum Technology, 52(02):95–100.

Tanabe, K. and Sagae, M. (1992). An exact cholesky decomposition and the generalized inverse of the variance-covariance matrix of the multinomial distribution, with applications. Journal of the Royal Statistical Society. Series B (Methodological), pages 211–219.

Tolstukhin, E., Lyngnes, B., and Sudan, H. H. (2012). Ekofisk 4D seismic-seismic history matching workflow. In SPE Europec/EAGE Annual Conference. Society of Petroleum Engineers.

Vasco, D. and Datta-Gupta, A. (1997). Integrating field production history in stochastic reservoir characterization. SPE Formation Evaluation, 12(03):149–156.

Veeken, P. C. (2006). Seismic stratigraphy, basin analysis and reservoir characterisation, volume 37. Elsevier.

Wang, F. and Wall, M. M. (2003). Incorporating parameter uncertainty into prediction intervals for spatial data modeled via a parametric variogram. Journal of agricultural, biological, and environmental statistics, 8(3):296–309.

Warren, J. and Price, H. (1961). Flow in heterogeneous porous media. Society of Petroleum Engineers Journal, 1(03):153–169.

Wen, X., Deutsch, C., Cullick, A., and Reza, Z. (2005). Integration of production data in generating reservoir models. Centre for Computational Geostatistics (CCG), Volume 1.

Wen, X.-H., Tran, T., Behrens, R., and Gomez-Hernandez, J. (2000). Production data integration in sand/shale reservoirs using sequential self-calibration and geomorphing: A comparison. In SPE annual technical conference.

Wen, X.-H., Tran, T., Behrens, R., and Gomez-Hernandez, J. (2002). Production data integration in sand/shale reservoirs using sequential self-calibration and geomorphing: Acomparison. SPE Reservoir Evaluation & Engineering, 5(03):255–265.

Wilkinson, J. H. (1965). The algebraic eigenvalue problem, volume 87. Clarendon Press Oxford.

Appendix A

Computer Programs

Methodologies proposed in this thesis are implemented by a collection of computer programs. In this appendix, each computer program is introduced and a user manual is provided for practitioners. All programs are developed in Fortran (formerly FORTRAN[1], derived from Formula Translation) that is a scientific programming language. The user interface is a keyword based parameter file that is a simple ASCII text file. The keywords do not have to follow a certain sequence; however, it is more intuitive to use the sequence of the default parameter file that is generated by the software. If a keyword is not required for the application selected by the user, it will be excluded and does not need to be provided. Note that data files and geostatistical realizations are in GeoEAS/Geostatistical Software Library (GSLIB) format. Thus, for each property, the user must provide the data file director plus the corresponding column number. If its is desired to exclude a variable (i.e., the clustering weight) set the corresponding column number to be 0.

A.1 Spatial Bootstrap for Categorical Variables (SBS_Categorical)

The prior proportion uncertainty for a categorical variable (i.e., facies) can be quantified using SBS_Categorical. The user can choose to quantify the prior proportion uncertainty in presence of a trend model. The main inputs are facies data and indicator variogram models. The parameter file of SBS_Categorical is presented below. Each keyword is used to provide information or specify a parameter that is used by the software.

```
 1 ****************************************
 2 ** Section1: Input Files and Parameters
 3 ****************************************
 4
 5 REFDIST          Sampled.out       ** File with reference...
 6 REFCOL           4   0             ** Column for variable...
 7 CATNUM           3                 ** Number of categories
 8 CATCODE          1 2 3             ** Categorical Codes
 9 TRIMLIM          -1.0e21   1.0e21  ** Trimming limit
10 LOCFILE          Sampled.out       ** File with locations...
11 LOCCOL           1 2 3             ** Columns for X, Y and Z...
12 TRENDTYPE        1                 ** 0:Vertical Trend,1:Aerial...
```

[1] http://www.thefreedictionary.com/FORTRAN

```
13 TRENDCALIB       0  10              ** Calibrate 3D trend with...
14 KERNELBW         120.0 105.0 10.0   ** Bandwidth along principal...
15 ROTANG           0.0 0.0            ** Azimuth and Dip angles
16 TKERNEL          1                  ** 1: Quartic Spline...
17 XGRID            40 12.5 25         ** Nx, Xmn, Xsiz
18 YGRID            100 0.5 1.0        ** Ny, Ymn, Ysiz
19 ZGRID            40 0.5 1.0         ** Nz, Zmn, Zsiz
20 SEED             69069              ** Random number seed
21 NREAL            100                ** Number of Realizations
22 EFFSAMPLE        1  5               ** Option for uniform sampling...
23
24 ****************************************
25 ** Section2: Model of Spatial Variability
26 ****************************************
27
28 VAR_CAT1       ** Category 1: Variogram
29 2    0.0                        -nst, nugget effect
30 1    0.4  0.0   0.0   0.0       -it,cc,ang1,ang2,ang3
31           200.0  200.0  2.0     -a_hmax, a_hmin, a_vert
32 1    0.6  0.0   0.0   0.0       -it,cc,ang1,ang2,ang3
33           400.0  400.0  4.0     -a_hmax, a_hmin, a_vert
34
35 VAR_CAT2       ** Category 2: Variogram
36 2    0.0                        -nst, nugget effect
37 1    0.4  0.0   0.0   0.0       -it,cc,ang1,ang2,ang3
38           200.0  200.0  2.0     -a_hmax, a_hmin, a_vert
39 1    0.6  0.0   0.0   0.0       -it,cc,ang1,ang2,ang3
40           400.0  400.0  4.0     -a_hmax, a_hmin, a_vert
41
42 VAR_CAT3      ** Category 3: Variogram
43 2    0.0                        -nst, nugget effect
44 1    0.4  0.0   0.0   0.0       -it,cc,ang1,ang2,ang3
45           200.0  200.0  2.0     -a_hmax, a_hmin, a_vert
46 1    0.6  0.0   0.0   0.0       -it,cc,ang1,ang2,ang3
47           400.0  400.0  4.0     -a_hmax, a_hmin, a_vert
```

```
48
49
50 ****************************************
51 ** Section3: Output Files
52 ****************************************
53
54 OutOption        1           ** Output options 1: Global
      Proportions 2: Global Proportion and Trend
```

The first keyword in the above parameter file is REFDIST that specifies the directory of data file that contains hard measurements of facies. REFCOL is the keyword that needs to parameters including the column numbers for the facies and declustering weights respectively. It is reacquired to specify the number of categories/facies codes and the corresponding numerical codes using the keywords CATNUM and CATCODE respectively. There is an option to trim the missing data or Null values using the keyword TRIMLIM that gets the lower and higher limits. The file that contains the coordinates of facies data along with column numbers for X, Y an Z coordinates are provides by the keywords LOCFILE and LOCCOL respectively. If there is no need for trend modelling, REFDIST and LOCFILE can be different. In this way, the global proportion for unconditional indicator simulation at data locations is provided by REFDIST while the coordinate information comes from LOCFILE.

There are three option for trend modelling that can be assigned through the keyword TRENDTYPE. The option are 0: VPC, 1: areal trend 2: 3D trend model. If the 3D trend model is chosen, it can be calibrated by the VPC if TRENDCALIB option is set to 1 followed by the kernel bandwidth along the vertical direction. The keyword KERNELBW gets maximum of three bandwidth value along the three Cartesian axes depending on type of the trend model. The anisotropy angles (azimuth and dip) can also be defined by the keyword ROTANG. There are two option for the type of kernel used in trend calculation including 1: Quartic Spline, 2: Epanechnikov that can be determined using the keyword TKERNEL. In order to used the trend model in geostatistical facies simulation it is required to provide a gridded trend model based on the grid specifications used for facies simulation. The keywords XGRID, YGRID and ZGRID are used to specify the grid settings based on GSLIB format.

The spatial bootstrap is implemented by stochastic facies simulation at data location based on Monte Carlo sampling. The keyword SEED is used to specify the seed number for the random number generator used in the program. This allows to repeat the results. Total number of spatial bootstrap realizations is specified by the keyword NREAL. Effective sampling of the multivariate proportion uncertainty (see Chapter 2) can be implemented if the keyword EFFSAMPLE is set to 1 followed by specifying the multiplication factor. This improves uniform sampling of proportion uncertainty with limited number of realizations. Indicator variogram models for

each facies is provided using the keyword VAR_CAT. The reader is motivated to study GSLIB documentation[2] to learn about variogram models. Finally, the type of output is specified using the keyword OutOption with two options: 1) only global proportion for each bootstrap realizations 2) realizations of global proportions plus corresponding trend models.

A.2 Multivariate Spatial Bootstrap for Petrophysical Properties (SBS_MV)

The prior multivariate histogram uncertainty for multiple continuous variables is quantified using the computer program SBS_MV. The result is multiple realizations of sampled data that are used as reference distributions for multivariate transformation during geostatistical reservoir modelling. The parameter file for SBS_MV is shown below.

```
 1 ***************************************
 2 ** Section1: Input Files and Parameters
 3 ***************************************
 4
 5 PMODE            1                ** Program mode 1:
       Transformation...
 6 TRANS            1                ** Transformation Type...
 7 VARNUM           2                ** Number of continuous variables
 8 REFDIST          Sampled.out      ** File with reference...
 9 REFCOL           4  5  0          ** Column for variable(s)...
10 RTCODE           1  1             ** Number of rocktype(s)...
11 TRIMLIM          -1.0e21   1.0e21 ** Trimming limit...
12 LOCFILE          Sampled.out      ** File with locations to...
13 LOCCOL           1 2 3            ** Columns for X, Y and Z...
14 REALALL          1                ** Save separate realizations?...
15 LOCREP           1                ** Report location for each...
16 OutFILE          SBS_MV.out       ** File for all simulated
17 SEED             69069            ** Random number seed
18 NREAL            100              ** Number of Realization
19
20 ***************************************
21 ** Section2: Model of Spatial Variability
22 ***************************************
```

[2] www.gslib.com

```
23
24 VARMODEL1                          ** Variogram for variable 1
25 1    0.0                          -nst, nugget effect
26 3    1.0  0.0   0.0   0.0          -it,cc,ang1,ang2,ang3
27           200.0  200.0  4.0       -a_hmax, a_hmin, a_vert
28 VARMODEL2                          ** Variogram for variable 2
29 1    0.0                          -nst, nugget effect
30 3    1.0  0.0   0.0   0.0          -it,cc,ang1,ang2,ang3
31           300.0  300.0  4.0       -a_hmax, a_hmin, a_vert
```

The program can be used for two applications: 1) transform data to Gaussian units 2) quantify the multivariate histogram uncertainty. Use the keyword PMODE to specify the desired application. The variogram models in Gaussian units for each variables is required. If the program is used to implement transformation there are two option including 1: normal score and 2: PPMT that can be chosen using the keyword TRANS. The transformed data are used for experimental variogram calculation and modelling. Use the keyword VARNUM to specify the number of continuous variables passed to the program. REFDIST and REFCOL are the keywords to provide the data file directory plus the corresponding column numbers for each petrophysical property, facies/rock type if applicable and the declustering weights. SBS_MV enables the user to quantify histogram uncertainty within a specified single or multiple facies. Use the keyword RTCODE to specify number of facies and the corresponding numerical code. Facies are ignored if the first number after the keyword RTCODE is set to 0. Specify the trimming limits using the keyword TRIMLIM.

The keywords LOCFILE and LOCCOL to introduce the file containing X, Y and Z coordinates and the corresponding columns. The spatial bootstrap is implemented by sequential Gaussian simulation at these location. By default, all the spatial bootstrap realizations are written in one single output file that is specified by the keyword OutFile. If it is desired to have a separate file for each spatial bootstrap realization set the keyword REALALL to be 1. For plotting purposes, it may be required to include the X, Y and Z coordinates. This is achieved by choosing the keyword LOCREP to be 1. The keywords SEED and NREAL are used to specify the random seed number for the spatial bootstrap and number of realizations respectively. Finally, the keyword VARMODEL is used to provide variogram models for each property in Gaussian units.

A.3 Anomaly Recognition Tool (ART)

ART is exclusively developed to implement the proposed methodology for practical integration of 4D seismic data (see Chapter 4). ART has two main applications: 1) anomaly assessment that is used for fidelity analysis and 2) anomaly enforcement. ART's parameter file is provided below. Each keyword and its application is introduced to provide a comprehensive user manual.

```
 1 *************************
 2 ** Program Mode
 3 *************************
 4
 5 ARTMODE      1          **1:Anomaly Assessment, 2:Enforcement
 6
 7 ***************************
 8 ** Anomaly Information
 9 ***************************
10
11 ANOMALYFL          Report.dat ** File containing...
12 REPTYPE            2          ** Report Type(1: Ellipsoids...
13 ANOMALYNUM         19         ** Total number of anomalies
14 CONDUITLIMIT       800        ** Limit for effective...
15 BARRIERLIMIT       100        ** Limit for effective...
16 NormalRange        200 1000   ** Range for normal...
17
18 ***********************************
19 ** Input Realizations(Permeability)
20 ***********************************
21
22 VERTICALPERMFL     Reals.out  ** File with vertical...
23 KVCOL              5          ** Column number for...
24 HORIZONTALPERMFL   Reals.out  ** File with horizontal...
25 KHCOL              4          ** Column number for...
26 NR                 100        ** Number of relizations...
27 NX                 50         ** Number of grids...
28 XSIZ               5          ** Size of grids in...
29 XMN                2.5        ** X coordinate of...
30 NY                 100        ** Number of grids...
31 YSIZ               1          ** Size of grids...
32 YMN                0.5        ** Y coordinate...
33 NZ                 50         ** Number of grids...
34 ZSIZ               1          ** Size of grids...
35 ZMN                0.5        ** Z coordinate...
```

```
36
37 ************************************
38 ** Anomaly Enforcement
39 ************************************
40 XINTERVAL         5.0                ** Interval of sampling...
41 YINTERVAL         5.0                ** Interval of sampling...
42 ZINTERVAL         1.0                ** Interval of sampling...
43 FACIESFL          Reals.out          ** File containing...
44 RTCOL             1                  ** Column number...
45 POROSITYFL        Reals.out          ** File containing...
46 PORCOL            3                  ** Column number...
47 VSHFL             Reals.out          ** File containing...
48 VSHCOL            2                  ** Column number...
49 SWFL              Reals.out          ** File containing...
50 SWCOL             6                  ** Column number...
51 DATAFL            Data.dat           ** File containing...
52 DATACOL           2 3 4 11 5 7 9 8 6  ** Column for X, Y, Z,...
53 OTHER             4                  ** Number of column(s)...
54 OTHERCOL          14 15 16 17        ** Column(s) for other...
55 SAMPLEOTHER       1                  ** Option to Sample...
56 OTHERFL           Reals.out          ** File for other...
57 THEIRCOL          7 8 9 10           ** The corresponding...
58 SEED              69069              ** Random number seed...
59 LEVEL             1                  ** Enforcement Level
60 KEEP              0                  ** Option too keep...
61
62 ************************************
63 ** Considering Zones for Enforcement
64 ************************************
65 ZONES             1               ** Sample within zones...
66 ZONEFL            Zone.out        ** File containing...
67 ZONECOL           1               ** Column number...
68 ZONECODES         6 1 2 3 4 5 6   ** Number of zone...
69
70 ************************************
```

```
71 ** Output Files
72 ************************************
73
74 PREFIX            ART               ** Prefix for Anomaly...
75 PREFIX_Data       Well_Data         ** Prefix for new data...
76 NULL              -999.0            ** Null value
```

The first keyword is ARTMODE that specifies the application. There are two options: 1) anomaly assessment (fidelity analysis results) and 2) Geostatistical anomaly enforcement. The first option provides report files in ASCII format that can be used to study the distribution of effective permeability or average shale for each anomaly and over all realizations. The second option performs anomaly assessment to identify missing anomalies and samples the enforcing data for each realization. Use ANOMALYFL keyword to specify the anomaly report file that summarizes results of anomaly identification. This file is essential for the software as it contains information about type, location and spatial extent of identified anomalies. There are two main option to describe anomalies: 1) ellipsoid-based 2) grid address-based use REPTYPE keyword to determine which type of anomaly report file is provided. ANOMALYNUM is used to specify total number of anomalies. CONDUITLIMIT, BARIERLIMIT and NormalRange are three keywords that specify threshold(s) of effective permeability for type $+1$, -1 and 0 anomalies respectively.

Realizations of vertical and horizontal permeability are required to calculated the effective directional permeability for each anomaly over all realizations. VERTICALPERMFL and HORIZONTALPERMFL keywords provide files for vertical and horizontal permeability receptively. Also, KVCOL and KHCOL keywords are used to introduce the corresponding columns in each file. The software is designed to check if different properties are provided in a single file or multiple files to achieve efficient and fast loading of data into the memory. NX, Xsiz, XMN, NY, YSIZ, YMN, NZ, ZSIZ, ZMN and NR keywords are used to specify grid specifications and number of realizations.

For geostatistical anomaly enforcement additional parameters are required. One important set of parameters that determines the level of geostatistical enforcement are the spatial intervals based on which the enforcing data are sampled. XINTERVAL, YINTERVAL and ZINTERVAL are the keywords to specify sampling intervals along X, Y and Z direction. Apart from permeability, some important geological properties including facies, shale volume, porosity, and water saturation can be included in enforcing data. However, they are not necessary to execute the program. Thus, the user may choose to provide files that contain realizations of some or all of these properties. Use the following keywords to specify the file and column number for geological properties listed above.

- FACIESFL and RTCOL GeoEAS format file for facies and the corresponding column number.
- POROSITYFL and PORCOL GeoEAS format file for porosity and the corresponding column number.

- VSHFL and VSHCOL GeoEAS format file for shale volume and the corresponding column number.
- SWFL and SWCOL GeoEAS format file for water saturation and the corresponding column number.

ART samples the enforcing data for each realizations and generates separate data file for each realization. If the user wants to include the original well data in all the updated data files, the keyword DATAFL and DATACOL should be used to specify the original data file and column numbers for coordinates and main geological properties. Advanced users may need to sample other variables including properties in Gaussian units. In this context, keywords associated with the word OTHER are preserved for such needs.

The search algorithm uses a pseudo random number generator and the user can specify the seed number using the keyword SEED in order to get repeatability. The keyword LEVEL controls the level of enforcement based on a hard coded modification of effective permeability thresholds. The user has three main including 1: Light, 2: Moderate and 3: Heavy. Along with sampling intervals, this keyword can be used to control the sampling of enforcing data. For each realization, the search algorithm samples enforcing data for missing anomaly(s); however, if the keyword KEEP is set to be 1 (0 by default), the enforcing data for the reproduced anomaly(s) are also sampled and added to the data file for that realization. The difference is that, for an anomaly that is reproduced the enforcing data are sampled from the same realization and same location. This may be considered to ensure that after updating the realization, the enforcement of misusing anomalies will not result in loosing the reproduced anomalies.

As mentioned in Chapter 4, the enforcing data should be sampled from the same geological zone where the anomaly is identified. If the keyword ZONES is 0 the enforcing data are sampled form the entire reservoir model; otherwise, the user needs to provide a file containing the zone codes and the corresponding column number using the keywords ZONEFL and ZONECOL respectively. The keyword ZONECODES are used to specify the zone codes for sampling the enforcing data.

The last section of the parameter files is used to specific the settings for output formats. The user may choose to have a specific prefix for output report files using the keyword PREFIX. One example is shown in the parameter file. The same can be considered for the enforcing data using the keyword PREFIX_Data. Finally, the user should define the null values for the missing entities in output files.

A.4 PCT (Proportion Calibration Tool)

The proportion calibration tool is used to modify a facies realization to match a target proportion. The parameter file is provided below.

```
1 ******************************
2 ** Input Files and Parameters
3 ******************************
```

```
 4
 5 INPUTFILE  Facies.out     ** File for input model
 6 CATCOL     1              ** Column for facies
 7 GRIDX      275 2.5 5.0    ** Nx, Xmn, Xsiz
 8 GRIDY      255 2.5 5.0    ** Ny, Ymn, Ysiz
 9 GRIDZ      175 0.25 0.5   ** Zx, Zmn, Zsiz
10 CATNUM     3              ** Number of facies
11 CODES      1 2 3          ** Facies Codes
12 TARGETP    0.5 0.3 0.2    ** Target Facies Proportions
13 DATAFL     ./data.dat     ** Data file
14 XYZCOL     1 2 3          ** Columns for X, Y and Z
15 WINDOWR    5 5 2          ** Search window
16 OUTFL      ./Matched.out  ** Output file
```

Use the keywords INPUTFILE and CATCOL to provide the facies realization file and the column number. The grid settings are specified using the keywords GRIDX, GRIDY and GRIDZ. Number of facies and the corresponding codes are defined using the keywords CATNUM and CODES respectively. The user must provide the target facies proportions using the keyword TARGETP. In order to preserve the conditioning data file, the user may choose to provide the data file and the corresponding columns for X, Y and Z coordinates. Use the keyword WINDOWR to assign the local search window along different directions which is defined based on number of grid cells. Finally, the keyword OUTFL determine the output file after proportion calibration.

A.5 Synthetic 4D Seismic (4D_PEM)

4D_PEM is used to generate synthetic 4D seismic data based on Gassmann's fluid substitution model and considering changes in fluid saturations. The parameter file for 4D_PEM is presented below.

```
1 ******************************************
2 ** Section1: Program Mode and Data Files
3 ******************************************
4
5 PEMMODE   2     ** Type of synthetic data required...
6 Nx        40    ** Number of grids in X direction
7 Ny        100   ** Number of grids in Y direction
8 Nz        40    ** Number of grids in Z direction
9
```

```
10  ** Base Survey:
11
12 RT_1       ./Facies.out  ** File containing rock type (Facies)
13 RTCOL_1    1             ** Column number for rock type (Facies)
14 POR_1      ./Phi.out     ** File containing Porosity
15 PORCOL_1   1             ** Column number for Porosity
16 SW_1       ./SW1.out     ** File containing Water Saturation
17 SWCOL_1    1             ** Column number for Water Saturation
18 SO_1       ./SO1.out     ** File containing Oil Saturation
19 SOCOL_1    1             ** Column number for Oil Saturation
20
21  ** Time-Laspe Survey (if 4D seismic is desired):
22
23 RT_2       ./Facies.out  ** File containing rock type (Facies)
24 RTCOL_2    1             ** Column number for rock type (Facies)
25 POR_2      ./Phi.out     ** File containing Porosity
26 PORCOL_2   1             ** Column number for Porosity
27 SW_2       ./SW2.out     ** File containing Water Saturation
28 SWCOL_2    1             ** Column number for Water Saturation
29 SO_2       ./SO2.out     ** File containing Oil Saturation
30 SOCOL_2    1             ** Column number for Oil Saturation
31
32 ******************************************
33 ** Section2: Petro-Elastic Model Settings
34 ******************************************
35
36 CATNUM    3               ** Number of categories
37 CATCODE   1   2   3       ** Categorical codes
38 CLAYFRAC  0.2   0.4   0.6 ** Fraction of Clay for each category
```

Use the PEMMODE keyword to determine the objective of running the program. There are two options: 1) generating synthetic 3D seismic data and 2) providing synthetic 4D seismic data based on calculating differences in seismic attributes between two surveys. Nx , Ny and Nz are the keywords to assign number of grids along X, Y and Z directions respectively. If 3D seismic data is required only provide information for one seismic survey that is refereed to as base survey. Otherwise, information on two surveys (i.e., base and time-lapse/monitor

surveys) are required as shown in the parameter file above. It is required to provide facies, porosity, water and oil saturation using the following keywords. The suffix _1 is related to the base survey while _2 highlights the monitor survey.

- RT and RTCOL GeoEAS format file for facies and the corresponding column number.
- POR and PORCOL GeoEAS format file for porosity and the corresponding column number.
- SW and SWCOL GeoEAS format file for water saturation and the corresponding column number.
- SOFL and SOCOL GeoEAS format file for oil saturation and the corresponding column number.

The final section of the parameter file determines the number of facies the corresponding numerical codes and the fraction of clay for each facies. This information is important to assess the seismic attributes.